1988

The transition state of the cyclopropylidene to allene ring opening

Robert Jude Sutherland
Iowa State University

Order Number 8825455

The transition state of the cyclopropylidene to allene ring opening

Sutherland, Robert Jude, Ph.D.

Iowa State University, 1988

U·M·I
300 N. Zeeb Rd.
Ann Arbor, MI 48106

PLEASE NOTE:

In all cases this material has been filmed in the best possible way from the available copy. Problems encountered with this document have been identified here with a check mark __✓__.

1. Glossy photographs or pages _____
2. Colored illustrations, paper or print _____
3. Photographs with dark background __✓__
4. Illustrations are poor copy _____
5. Pages with black marks, not original copy _____
6. Print shows through as there is text on both sides of page _____
7. Indistinct, broken or small print on several pages __✓__
8. Print exceeds margin requirements _____
9. Tightly bound copy with print lost in spine _____
10. Computer printout pages with indistinct print _____
11. Page(s) _____ lacking when material received, and not available from school or author.
12. Page(s) _____ seem to be missing in numbering only as text follows.
13. Two pages numbered _____. Text follows.
14. Curling and wrinkled pages _____
15. Dissertation contains pages with print at a slant, filmed as received _____
16. Other _____

_____

_____

The transition state of the cyclopropylidene to allene ring opening

by

Robert Jude Sutherland

A Dissertation Submitted to the
Graduate Faculty in Partial Fulfillment of the
Requirements for the Degree of
DOCTOR OF PHILOSOPHY

Department: Chemistry
Major: Organic Chemistry

Approved:

Signature was redacted for privacy.

In Charge of Major Work

Signature was redacted for privacy.

For the Major Department

Signature was redacted for privacy.

For the Graduate College

Iowa State University
Ames, Iowa

1988

TABLE OF CONTENTS

INTRODUCTION

In 1958, Doering and LaFlamme (1) demonstrated that olefins 1 may be transformed into allenes 4 in a convenient two step synthesis. A possible intermediate in this work, cyclopropylidene 3, has since been the subject of experimental (2,3) and theoretical (4) efforts. Experimental investigations have probed the stereochemical course of the ring opening, while theoretical efforts have focused on the mapping of the energy surface of the transformation.

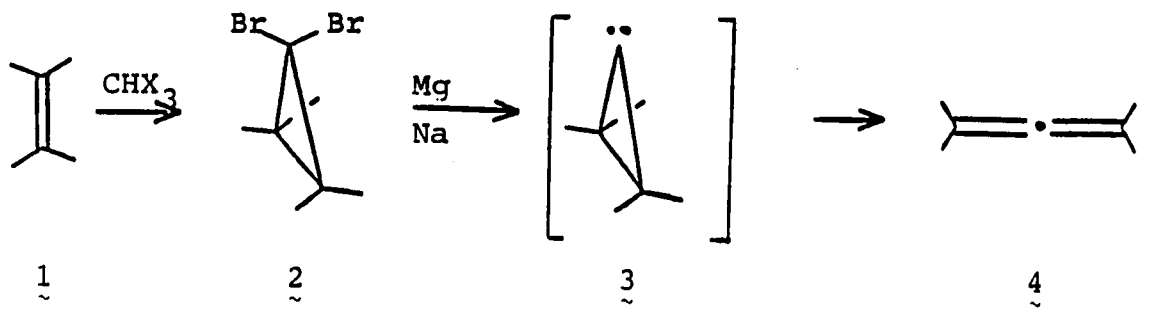

1 2 3 4

In 1954, Doering and Hoffmann (5) reported a synthesis of cyclopropyl geminal dihalides from alkenes, via the reaction of alkoxide ion with a haloform. Later, Doering and LaFlamme (1) converted 1,1-dibromocyclopropanes 2 into allenes by reduction with sodium or magnesium, although sodium was preferred. Sodium was dispersed on alumina and the reaction carried out at reduced pressure, without a solvent. Using this technique, 1,1-dibromo-2-n-propylcyclopropane was converted to 1,2-hexadiene in 64 percent yield.

The reaction was predicted to occur via the free carbene, although the authors considered and dismissed several possibilities (Scheme 1). The prediction of a carbene intermediate stems from the stereospecific addition of methylene iodide, reduced with zinc-copper couple, to cis and trans 2-butene.

Scheme 1

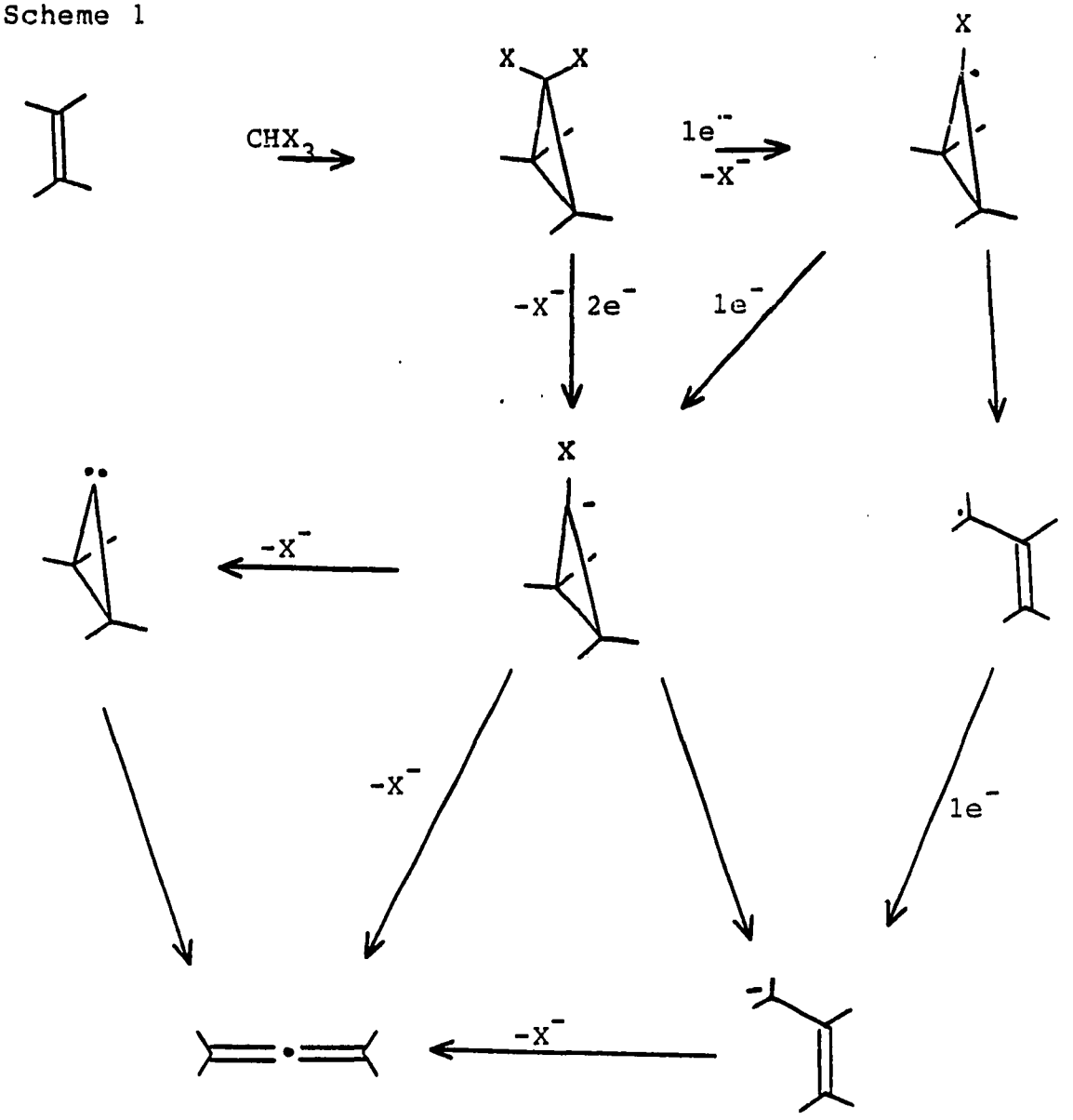

Skattebøl (6) used this technique to synthesize both acyclic and cyclic allenes in good yield. The appropriate olefins were cyclopropanated and subsequently decomposed with alkyl lithium compounds. In the case of 1,1-dibromo-2,3-tetramethylcyclopropane the expected allene was only a trace product (7). Instead, the carbon-hydrogen insertion product predominated (Scheme 2).

Scheme 2

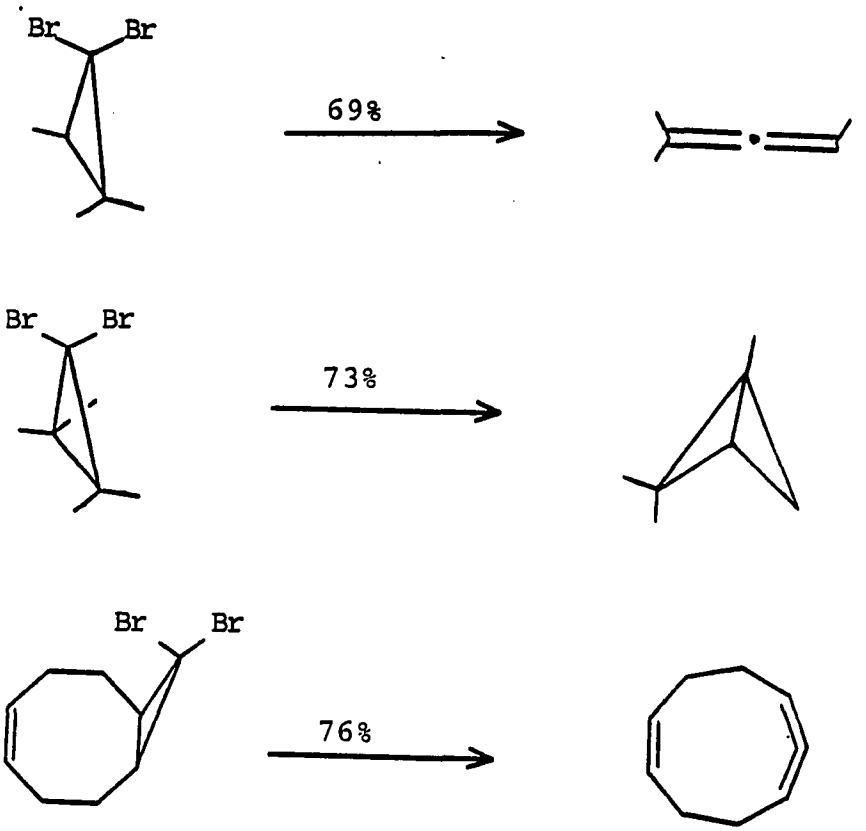

Moore and Hill (8) reported that the ratio of bicyclobutane to allene was dependent upon the ability of the substituents to stabilize the intermediate. They also noted that insertion into a methylene was highly preferred over a methyl carbon-hydrogen insertion (Scheme 3). The product ratios in reactions 2-4 can be rationalized as arising from steric control of insertion over ring opening. Comparison of reactions 3 and 5 demonstrates that stabilization by the anisyl groups favors ring opening.

Jones et al. (9) have generated cyclopropylidenes via diazocyclopropane intermediates. They prepared 2,2-diphenylcyclopropanecarboxylic acid from diphenyldiazomethane and methacrylate, a procedure developed by Walborsky and Hornyak (10). The acid was then converted to the N-nitroso urea, which is the precursor of the diazocyclopropane and ultimately cyclopropylidene (Scheme 4). The N-nitroso urea was then decomposed with a lithium ethoxide in hydrocarbon solvent to give 1,1-diphenylallene in 90 percent yield. When cyclohexene was present they obtained 18-22 percent yields of the spiropentane product shown in Scheme 4.

Scheme 3

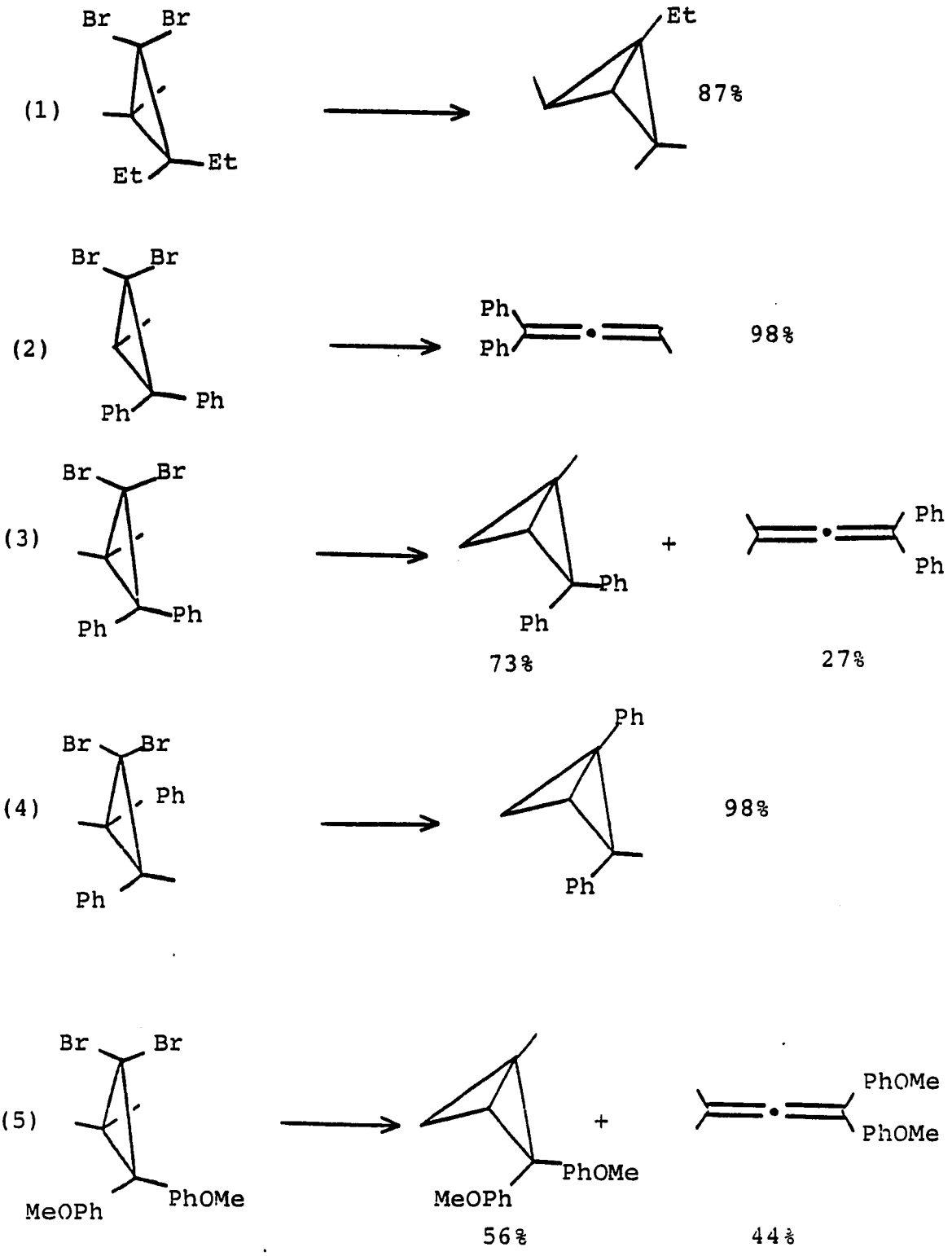
(1)
Br
Br
Et
Et
Et
87%
(2)
Br
Br
Ph
Ph
Ph
Ph
98%
(3)
Br
Br
Ph
Ph
Ph
Ph
+
Ph
Ph
73%
27%
(4)
Br
Br
Ph
Ph
Ph
98%
(5)
Br
Br
MeOPh
PhOMe
MeOPh
PhOMe
+
PhOMe
PhOMe
56%
44%

Scheme 4

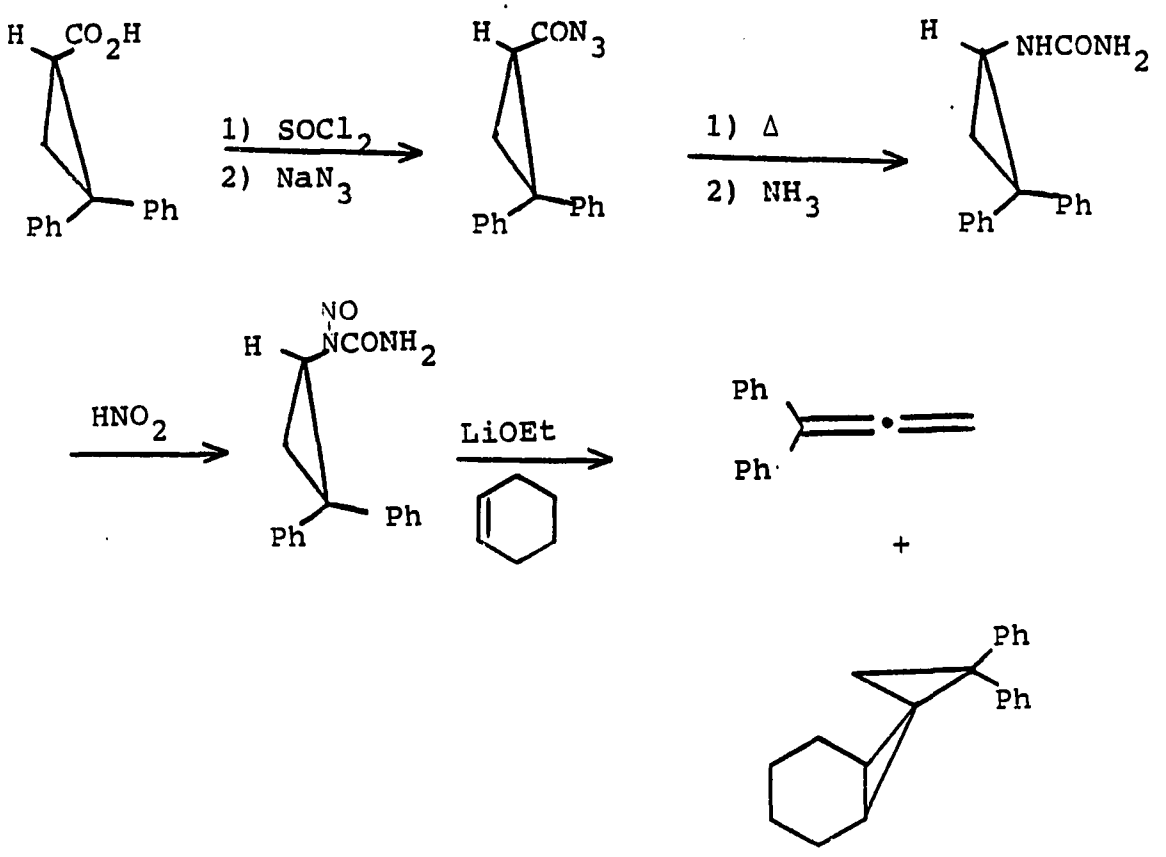

In 1963, Jones et al. (11) demonstrated the stereospecifity of the ring opening. Using the method of D'yakonov et al. (12) they prepared trans-2,3-diphenylcyclopropanecarboxylic acid. After resolving the enantiomeric mixture of acids, they transformed the (-)-trans-2,3-diphenylcyclopropanecarboxylic acid into the N-nitroso urea as before. The N-nitroso urea provided, when decomposed at 0°C, a 79 percent yield of (+)-1,3-diphenylallene. This finding demands that the transition structure be asymmetric,

but it does not require that free cyclopropylidene be its source.

In order to determine the nature of the allene precursor, Jones et al. (13) sought to elucidate the mechanism, of the decomposition, of the N-nitroso urea. By a study of the expected side products and/or their stability to the reaction conditions, they were able to identify a very probable mechanism, which is shown in Scheme 5. Base

Scheme 5

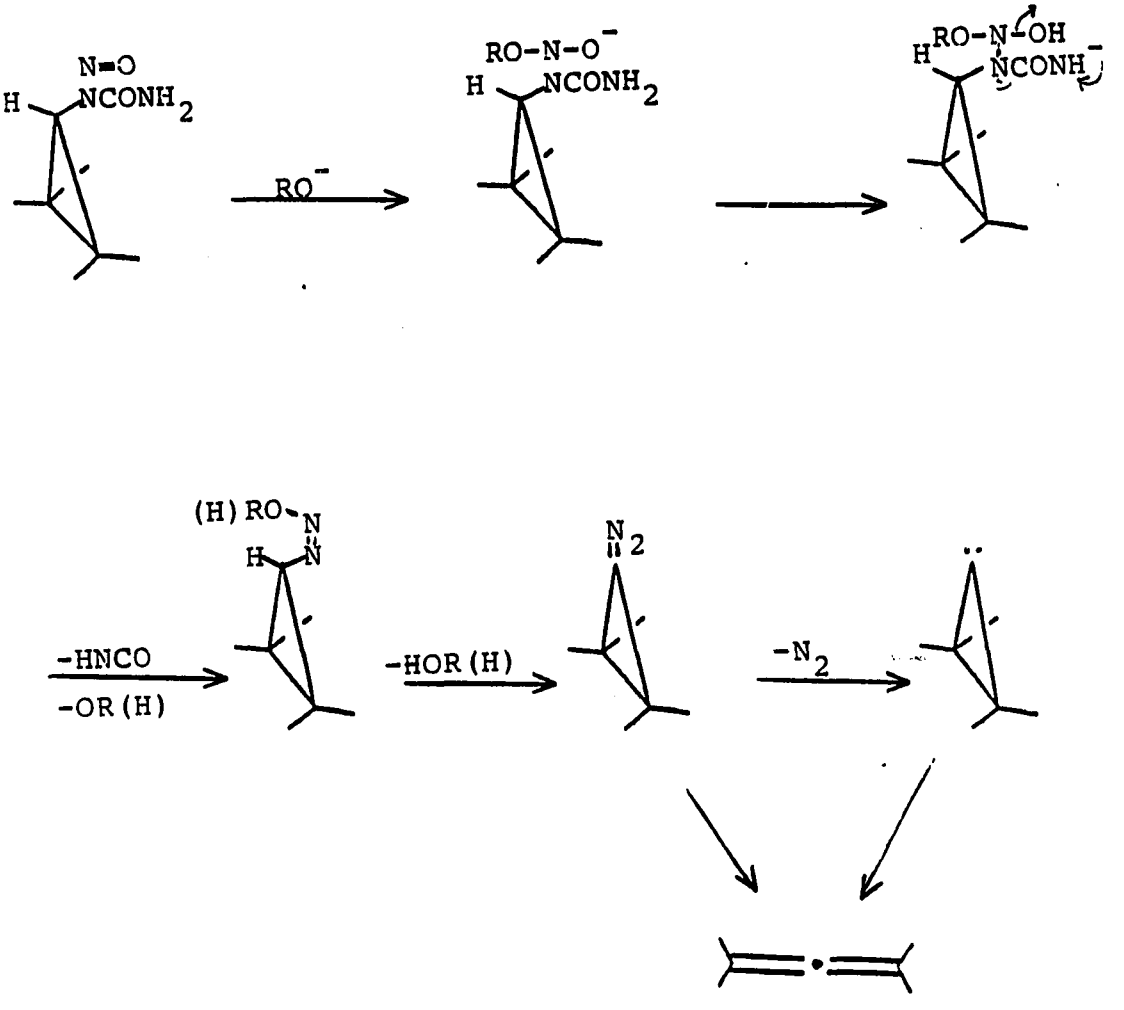

first attacks the N-nitroso nitrogen, whose basic oxygen then deprotonates the amide nitrogen. Isocyanic acid is then generated, followed by loss of either hydroxide or alkoxide ion to give the diazotate. Finally, loss of water or alcohol gives the diazocyclopropane which can decompose to give allene directly or via cyclopropylidene.

This mechanism is complementary to the thermal mode of decomposition, which was studied by Muck and Jones (14). Here they propose that the oxygen, of the N-nitroso nitrogen, abstracts a proton from the amide nitrogen. Loss of isocyanic acid then gives the diazotic acid, which loses water to give the diazo compound (Scheme 6).

Scheme 6

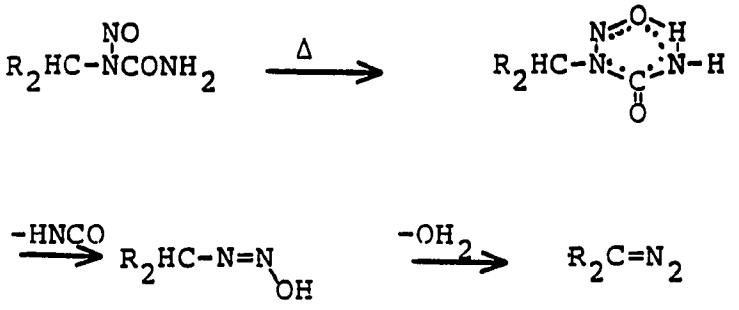

Jones and Walbrick (15) next looked at the stereochemistry of the allene which was generated in the presence of a cyclopropylidene trap. They found that allene generated in the presence of cyclohexene was of the same optical purity as allene generated without a trapping agent. They argued that it was very unlikely that two different

intermediates would produce allene of the same optical purity. They conclude from this that both the spiropentane and allene have a common intermediate, namely cyclopropylidene.

In perhaps their most interesting discovery, Jones and Krause (16) have shown that the ring opening of cyclopropylidene is affected by the electronic nature of the substituents. They studied para substituted cis-2,3-diarylcyclopropylidenes in order to demonstrate this effect. It is reasonable to assume that para substituted phenyl rings are of equal steric bulk; therefore, any optical activity in the products must arise from electronic controls on the mode of ring opening. To minimize any steric effects, they chose to study cis-2-phenyl-3-p-chlorophenylcyclopropylidene, cis-2-p-methylphenyl-3-phenylcyclopropylidene and cis-2-p-bromophenyl-3-p-methylphenylcyclopropylidene (Scheme 7). Compound 5a, whose acid had a rotation of -5.73°, gave allene with a rotation of +5.95°; compound 5b, whose acid had a rotation of -1.00°, gave allene with a rotation of -8.26°; and compound 5c, whose acid had a rotation of -8.24°, gave allene with a rotation of +101.0°. All of these rotations were collected at 22-23°C, at 436 nanometers. Although the optical yields were low, it is clear that some difference in energy exists between path a and path b for the ring openings.

Scheme 7

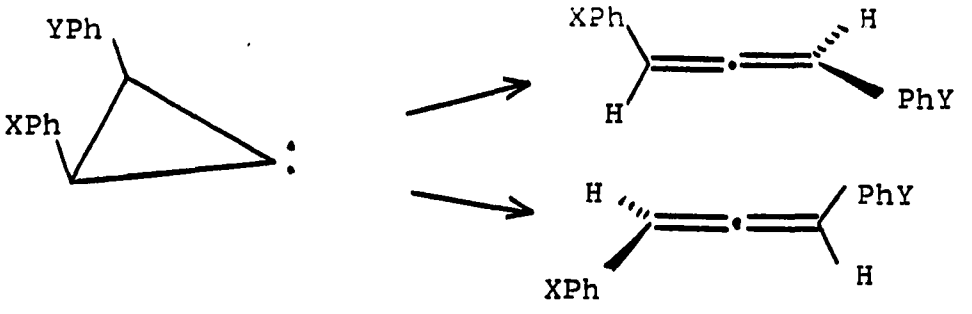

5

5a X=H, Y=Cl

5b X=Me, Y=H

5c X=Me, Y=Br

Miller and Shechter (17) have studied the electronic effects on the rate of decomposition of diaryldiazomethanes. A series of mono and disubstituted diphenyldiazomethanes were studied at 70°C, in a temperature regulated spectraphotometer. Interestingly, all substituents gave rate accelerations over the unsubstituted diphenyldiazomethane. The linear free energy plot showed a parabolic curve, which is usually indicative of a change in mechanism or complex kinetic behavior. Symmetrically disubstituted compounds show a rate reduction compared to the monosubstituted ones, and unsymmetrically disubstituted compounds show a large rate increase over either of monosubstituted ones. These results may be explained by

consideration of the orbital interactions as the transition state is approached (Scheme 8). The results suggest that

Scheme 8

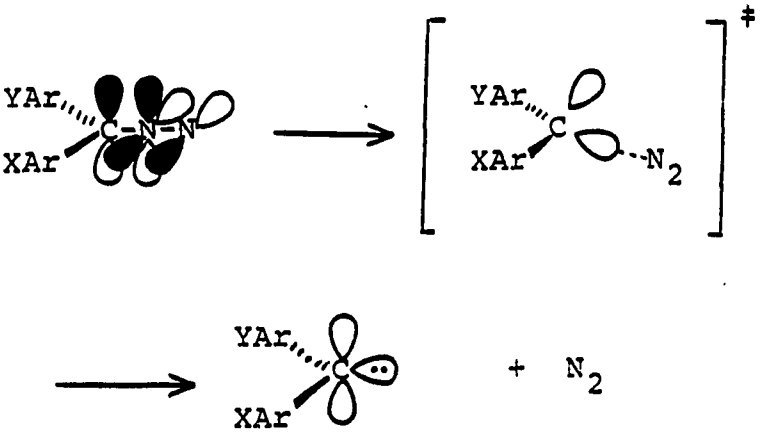

each aryl ring may align itself with a different carbene orbital. Electron donors would align with the empty orbital and electron acceptors would line up with the filled carbene orbital, such that both groups would stabilize the transition state. Rate reduction occurs when a molecule bears two donors or two acceptors; one may align itself so as to lower the energy of the transition state, but the other is forced into a destabilizing orientation.

A reaction which is analogous to the cyclopropylidene to allene ring opening is the cyclopropyl cation to allyl cation ring opening, both are two pi electrocyclic ring openings, and as such are governed by the same orbital symmetry considerations (18).

Cyclopropanol was first synthesized by Magrane and Cottle (19) in 1942. They reacted 3-chloropropylene oxide

with magnesium bromide, followed by ethylmagnesium bromide and iron chloride. Since then, many authors have noted the reluctance with which cyclopropanol derivates under solvolysis (20,21). In 1966, DePuy et al. (21) reported a detailed investigation of the relative solvolysis rates of arylcyclopropyl tosylates. The solvolysis of trans-2-aryl-cyclopropyl tosylates were run in buffered acetic acid solutions at 108°C. They studied the phenyl, para chloro-, para methyl- and trifluoromethylphenyl cases, and correlated the data to standard sigma values. They obtained a rho value of -2.4±.2 for the trans systems. The evidence points to a transition state in which partial solvolysis and ring opening have begun (Figure 1).

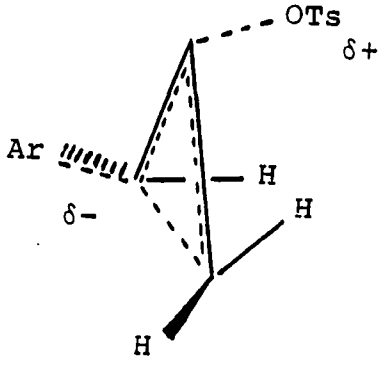

Figure 1. The transition state for the solvolysis of arylcyclopropyl tosylates

Kirmse and Schütte (22) investigated the cyclopropyl cation problem via the diazonium ion precursor. They used sodium formate to decompose N-(2-phenylcyclopropyl)-N-

nitroso urea in deuterated methanol. After studying both cis and trans substituted compounds, they concluded that the ring opening was not in concert with nitrogen loss, and that the free cation was a common intermediate. This work is not, in principle, contrary to the solvolysis of cyclopropyl tosylates.

The thermal (23) and solvolytic (24) behavior of cyclopropyl halides has also been investigated. Parham and Yong (25) studied the solvolysis of trans-1,1-dichloro-2,3-dipropylcyclopropane, in ethanol, at 80.8°C. The reactions were carried out in the dark with a silver nitrate catalyst. The product, trans ether 9, supports the idea that ring opening and solvolysis occur in concert (Scheme 9).

Scheme 9

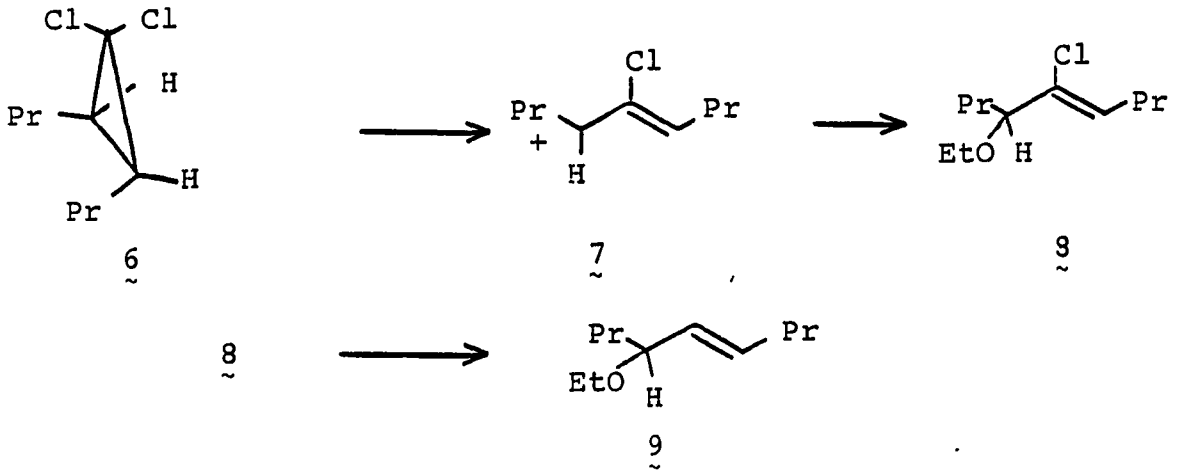

The formation of a single bond between the termini of a linear n-pi electron system, and the reverse process, was defined as an electrocyclic transformation, by Woodward and

Hoffmann (18). For such a reaction to occur, the termini must rotate in either a conrotatory or a disrotatory sense (Figure 2). The rotatory pathway that is followed by a

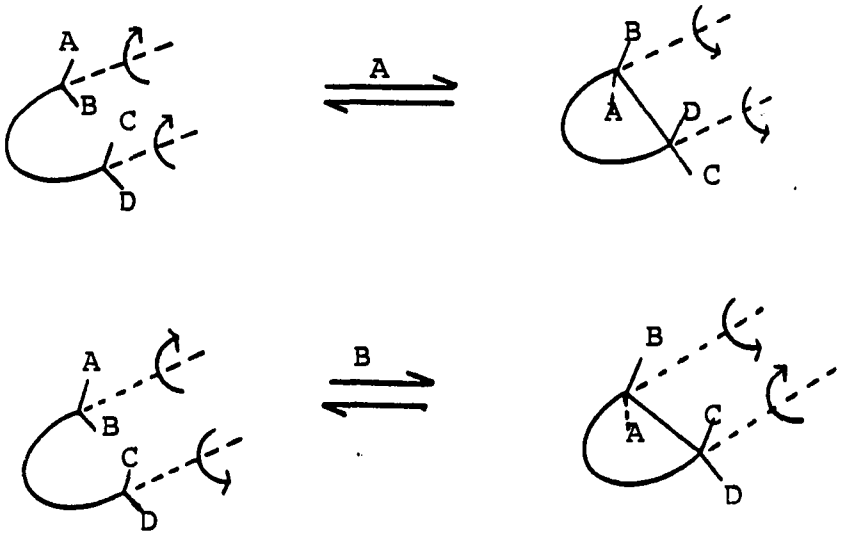

Figure 2. Modes of ring opening and closing; (A) conrotatory, (B) disrotatory

given molecule is dependent upon the number of pi electrons and the mode of activation, i.e., thermal or photochemical. The conservation of orbital symmetry is the guiding principle for these reactions. In a conrotatory process, a two fold axis of rotation (C_2) is maintained, whereas a mirror plane (σ) is maintained in a disrotatory process. Some predicted modes of ring opening are shown in Figure 3 (26). The generalized rule is that a thermal $(4n+2)\pi$ electrocyclic ring opening will be thermally disrotatory and photolytically conrotatory. A $(4n)\pi$ electrocyclic ring

opening will be thermally conrotatory and photolytically disrotatory. Odd electron species will behave as the even electron species containing one more electron, and charged species will behave as the neutral ones, with the same number of electrons. Note that cyclopropylidene, in its ground singlet state, should behave as cyclopropyl cation, and, in its lowest triplet state, as a cyclopropyl anion.

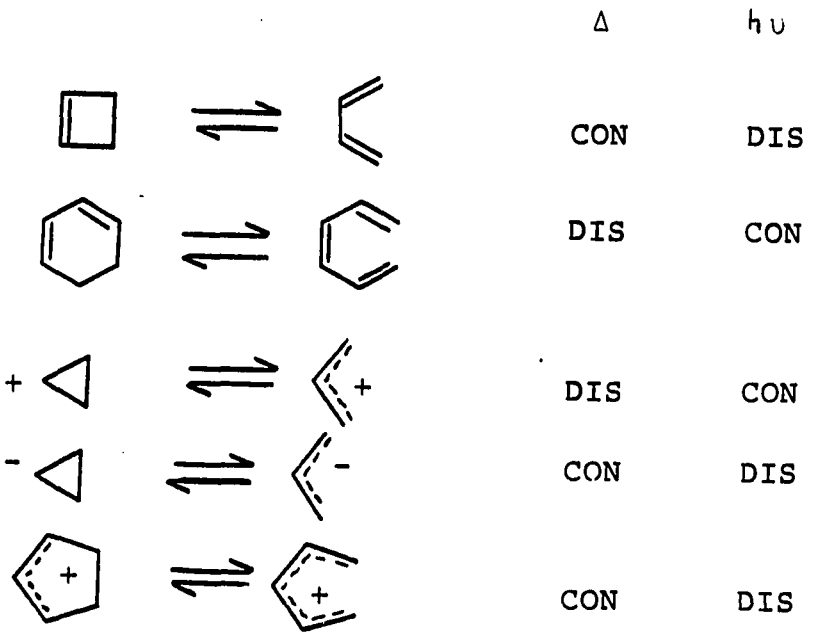

Figure 3. Examples of electrocyclic reactions for thermal (Δ) and photochemical (hν) modes

The C_3H_4 systems in general, and cyclopropylidene in specific, undergo a variety of rearrangements which encompass a great deal of chemistry (27). These include: ring opening and closing, hydrogen shifts, carbon-hydrogen

bond insertions, additions to olefins, etc. Some of these are depicted in Figure 4. The first problem in computing

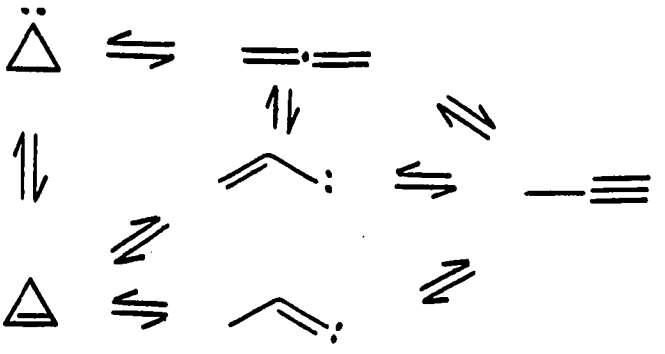

Figure 4. Representative species on the C_3H_4 energy surface

the cyclopropylidene to allene energy surface was to determine the ground state multiplicity and geometry for cyclopropylidene.

In 1978, Pasto et al. (28) reported that the triplet state was 8.4 kcal/mol lower in energy than the lowest singlet. Pasto's calculations employed a restricted Hartree-Fock (RHF) wave function, for the singlet, and an unrestricted Hartree-Fock (UFH) wave function for the triplet. The geometries were optimized with STO-3G and 4-31G basis sets. Baird and Taylor (29), on the other hand, determined that the triplet was 6.4 kcal/mol above the lowest singlet. This work was based on STO-3G basis sets, but used RHF wave functions for both the singlet and triplet energies.

Honjou et al. (27,30) have published the results of their investigation of the C_3H_4 energy surface. In this study the structures and paths were determined by self-consistent-field (SCF) wave functions, with double zeta plus polarization (DZP) functions used to determine the geometrical parameters. Energies were determined with either one-reference single and double-excitation configuration-interaction (SDCI) with a DZP basis, or a multi-reference SDCI wave function. They found that the singlet lies approximately 12 kcal/mol below the triplet, with an estimated error of $\pm$ 2 kcal/mole. The resultant relative energies of some C_3H_4 species are shown in Figure 5.

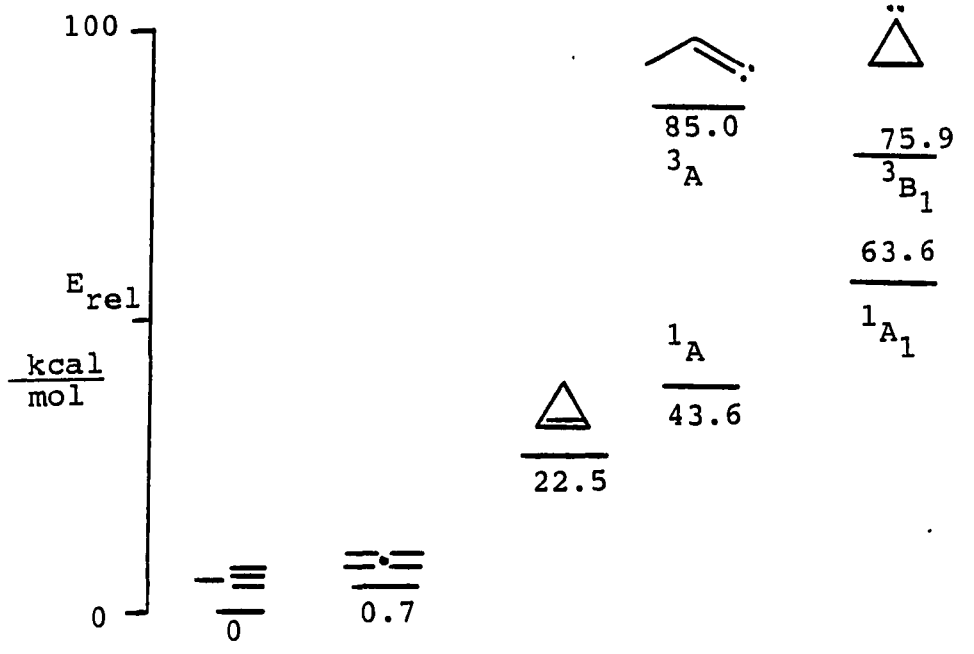

Figure 5. Relative energies for some C_3H_4 species

The energy surface that contains the transition state of the cyclopropylidene to allene ring opening has received separate attention. Several authors (31-33) have done extensive mapping of the surface for cyclopropylidene to allene, and for the cyclopropyl cation to allyl cation as well (34).

Dillon and Underwood (31) were among the first to attempt to map the cyclopropylidene to allene ring opening surface. Their calculations imposed severe restrictions on the cyclopropylidene geometry, so much so that no minimum could be found. The calculation suggests that an initially disrotatory ring opening leads to a nonrotated transition state, which yields a conrotated product. Dewar et al. (33) have explored the surface using MINDO/2 calculations, from which they find a nonrotatory ring opening to give a planar allene. This, of course, is not consistent with the experimental work of Jones et al. (11).

In 1985, Rauk et al. (35) published a detailed account of the cyclopropyliden to allene ring opening. Geometries were optimized at the Hartree-Fock level with analytical gradient procedures and a split valence 3-21G basis set. The 3-21G structures were then reoptimized at the 6-31G and 6-31G** levels. They found that the transition state occurs when the CCC angle is 96.2°, with an activation barrier of 11.5 kcal/mol. AT 95° of opening and 35° of disrotation,

the molecule begins to enter the conrotatory phase as the transition state nears. Although Rauk et al.'s computations are more exact and detailed than are those of Dillon and Underwood, they provide qualitatively the same picture of the energy surface. They both suggest a transition structure which resembles the one depicted in Figure 6.

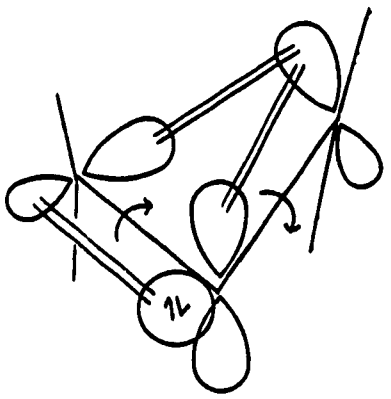

Figure 6. Transition state structure for the cyclopropylidene to allene ring opening, as obtained by Rauk et al. (35)

Ruedenberg et al. (36) have also mapped this energy surface in great detail. They used the Fully Optimized Reaction Space (FORS) model, which was introduced by Ruedenberg and Sundberg (37). MCSCF energies were calculated using a minimal basis set (STO-3G). In order to calculate the ground state energy of cyclopropylidene, one would need to optimize the 15 internal coordinates in a 16 dimensional space. In order to simplify the calculation,

Ruedenberg et al. fixed all but three of these variables. The three key coordinates, ϕ, δ_1 and δ_2 (Figure 7), were varied in order to find important geometries on the energy surface. Then, at each geometry, all 15 coordinates were reoptimized, to provide the best structure. Calculations were performed to test the validity of these approximations, and no discontinuities were found.

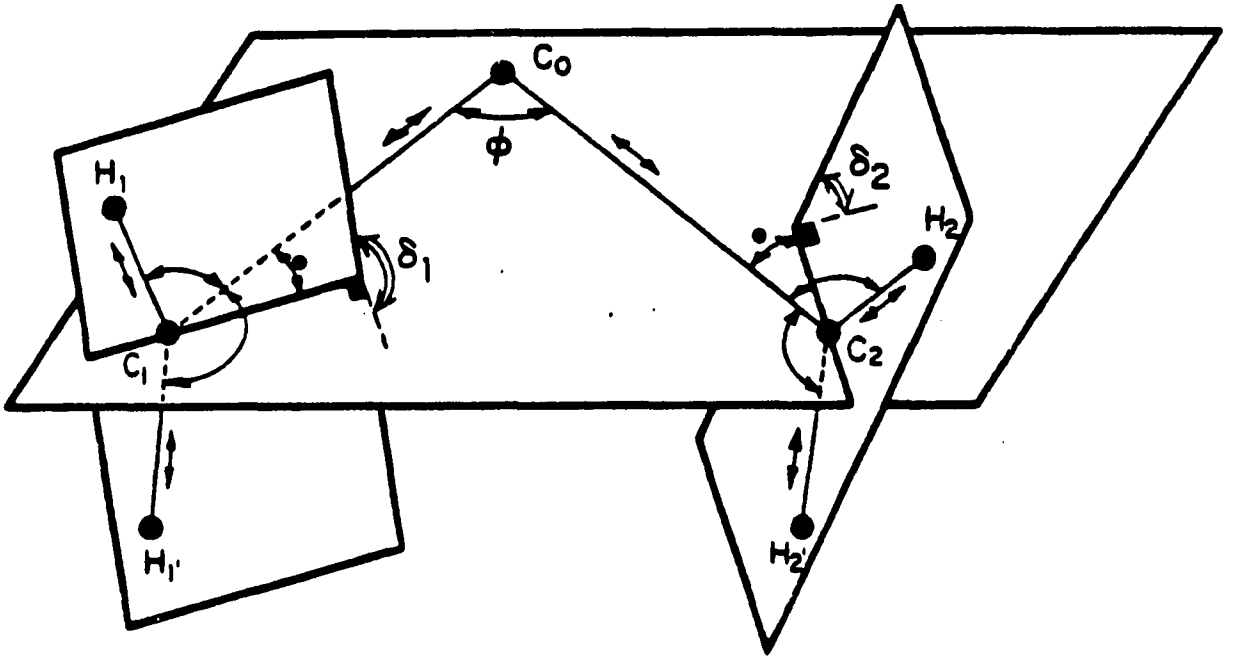

Figure 7. The fifteen internal coordinates for cyclopropylidene, as defined by Ruedenberg et al.

The angle ϕ was investigated in 5° steps from 50° to 100° and in 1° steps from 82° to 86° (the transition region). At a CCC angle of 80° the first bifurcation was reached. This corresponds to the choice between two degenerate,

disrotatory paths that the molecule may take. As the ring continues to open, the transition region was found to lie between 84° and 85°. At 85° a second bifurcation was revealed, which provides a path to each of two enantiomeric geometries. A detailed examination of the transition region gave ϕ = 84.24°, δ_+ = 5.94° and δ_- = 38.85° at the transition state ($\delta_+ = (\delta_1+\delta_2)/2-90$ and $\delta_- = \delta_1-\delta_2$). This is shown in Figure 8. A barrier of approximately 40 kcal/mol was found with these minimal basis calculations. Ruedenberg et al. describe the "transition region," containing the second bifurcation, as relatively flat. With the energy surface calculated in detail, via a minimal basis function, they recalculated key species with an expanded basis set.

These new calculations by Ruedenberg et al. (36) serve the purpose of more carefully defining the activation barrier. The changes made include the use of the Dunning-Hay (38) basis plus polarization functions, and an even-tempered Gaussian basis (39) of double-zeta quality. These changes result in a lowering of the ring opening barrier to

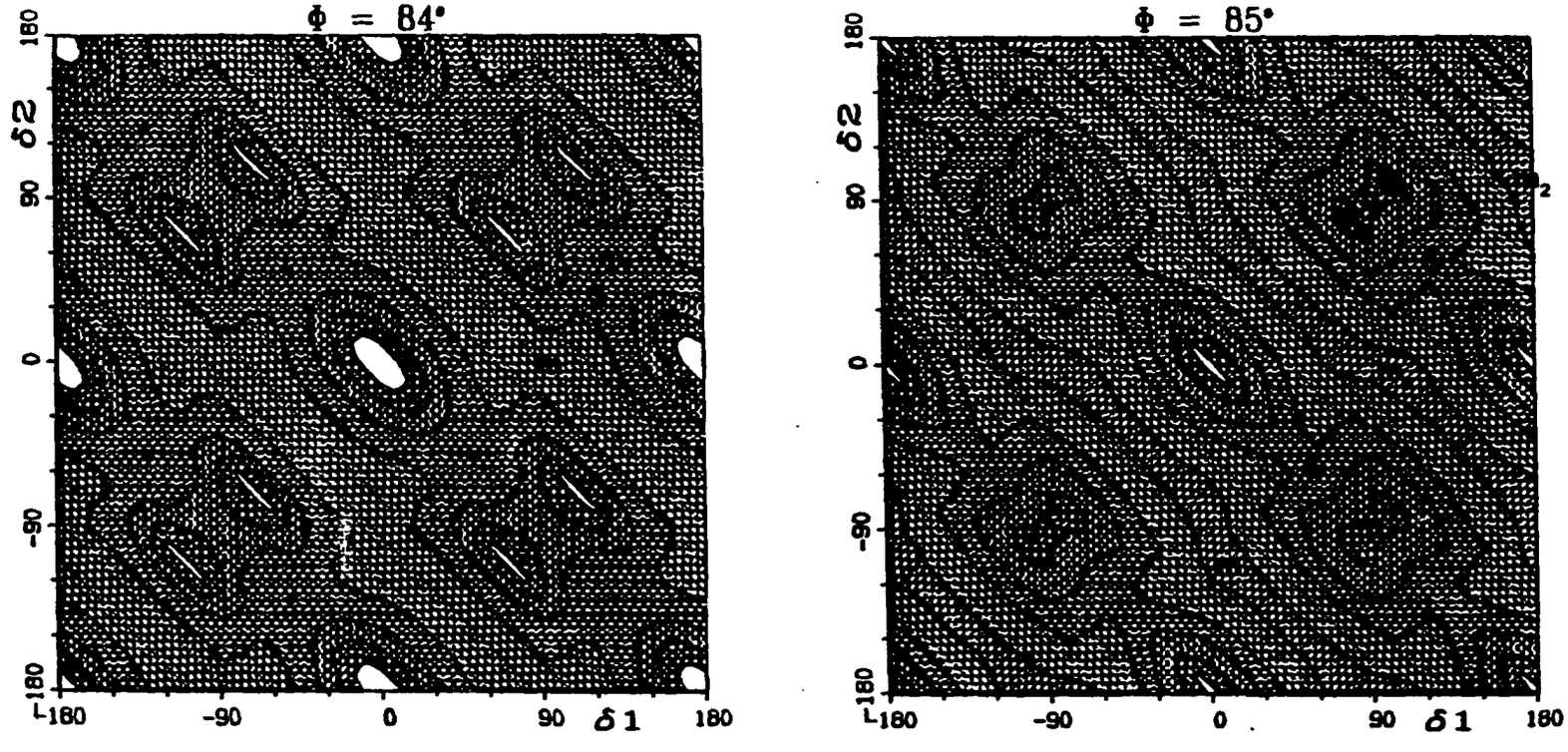

Figure 8. Contour plots of cyclopropylidene before (left) and after (right) the transition state, as calculated by Ruedenberg et al.

13 kcal/mol leaving other features of the surface almost unchanged (Figure 9). A notable change is that the extended basis calculation finds only one transition structure. The second bifurcation comes after the transition state at a valley ridge inflection point; the walls of the valley gradually lower, flatten and invert (the inflection point) as the molecule descends from the transition state. In a further calculation they employed the extended basis set with single and double excitation configuration interactions (SDCI) to yield a value of 7.4 kcal/mol for the ring opening barrier. This value is not corrected for zero point energy differences.

In order to shed some light on the work of Jones and Krause (16) on electronic influences on allene stereochemistry, Ruedenberg et al. (36) calculated some substituted cyclopropylidene to allene surfaces. Due to the overly complex nature of such calculations, they modeled substituent effects by adding long range electrostatic and steric effects to the unsubstituted case. The molecules thus modeled were 2-methylcyclopropylidene, 2,3-dimethyl-cyclopropylidene and 2-bromo-3-methylcyclopropylidene. The computations indicate that short-range covalent interactions are not involved, and that stereospecificity is determined by long range dipole-dipole interactions as well as by

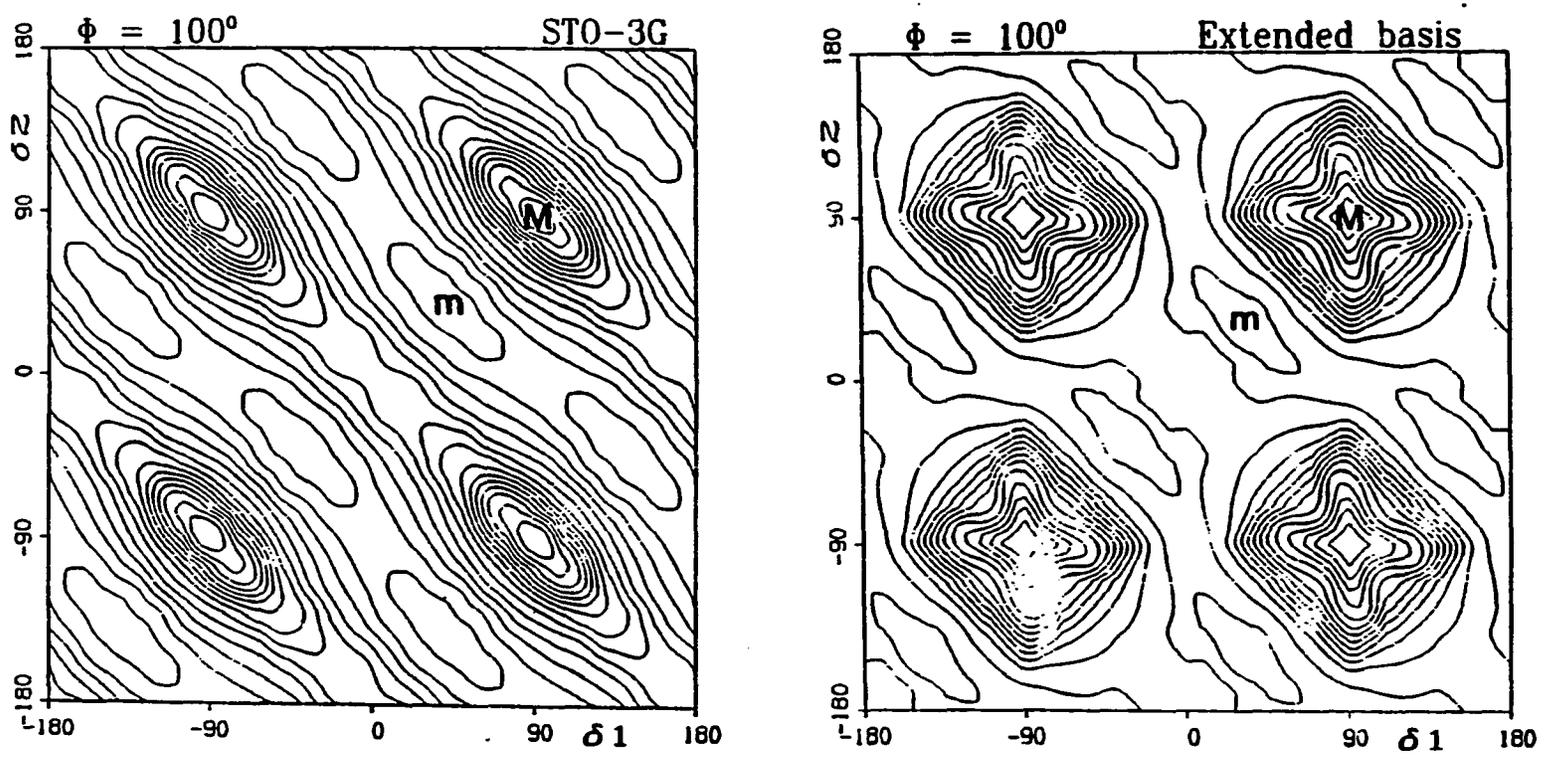

Figure 9. Cyclopropylidene at ψ = 100 from the minimal basis (left) and extended basis (right) calculations of Ruedenberg et al.

steric effects. A contour plot for the cis-2,3-dimethyl and trans-2,3-dimethyl species is shown in Figure 10.

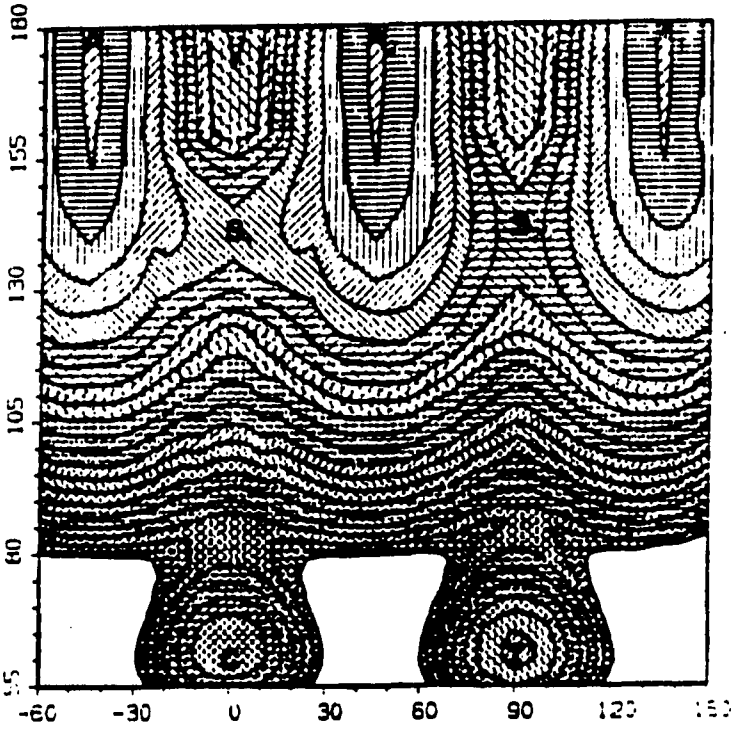

Figure 10. Contour plot for cis and trans-2,3-dimethyl-cyclopropylidene: ϕ vs δ, where $\delta = (\delta_1+\delta_2)/2$, from calculations by Ruedenberg et al.

The work of Jones and Krause (16) and of Ruedenberg et al. (36) was the source of our interest in the cyclopropylidene to allene ring opening. The nature of the transition state for this ring opening has not been determined experimentally and is quite complex for a detailed theoretical determination, at a high level of theory. The theoretical and experimental evidence to date point towards a transition state which should exhibit cationic character. Such a system should be influenced electronically by

electron donors and acceptors. In order to minimize steric interactions we chose trans diaryl cyclopropylidenes for our study; by substituting these aryl groups in the para position we can also effect the donor/acceptor influence on the transition state of 3'. Finally, since absolute rates

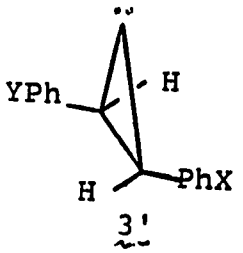

3'

of ring opening are not possible (cyclopropylidene has yet to be isolated) a partitioning trap for cyclopropylidene must be introduced, so that relative rate may be obtained.

Methanol has been chosen as the trapping agent, it provides diffusion control trapping (40) and forms kinetically simple products with cyclopropylidene. It is reasonable that 3' may be formed at various methanol concentrations and the relative rates of ring opening and trapping may be correlated with electronic influences from the para substituents.

RESULTS AND DISCUSSION

The preparation of compounds 18a-j was effected by the method of Walbrick et al. (41) with several modifications. The trans-stilbenes 13a-j were prepared via a standard Wittig reaction. The crude product mixture was then isomerized to give only the trans olefins (Scheme 9). The isocyanates 16a-j were prepared from the acids 15a-j in a single step (Scheme 10), using diphenylphosphoryl azide (DPPA) (42) in refluxing benzene. This is a superior method to that of Walbrick et al. in terms of yield, convenience and functionality tolerance. Further, the isocyanates may be converted to the carbamates 17a-j in the same reaction pot, in an overall yield of 50-85 percent. The method of nitrosation of the carbamates was also altered. The amount of acetic acid in the solvent was reduced from 30 percent to a trace, as several of the N-nitroso carbamates (18a-j) proved to be very acid sensitive.

The reaction of 18a ($\sim 10^{-3}$ M) with sodium methoxide, in toluene/methanol solution (5-25 M methanol), is illustrative of the reactions of 18a-j (Scheme 11). The principal products are 1,3-diphenylallene, 19a, and trans-2,3-diphenylcyclopropyl methyl ether, 20a. The ring opening of trans-2,3-diphenylcyclopropylidene, 22a, gives the allene and methanol trapping of 22a provides the ether.

Scheme 9

11 a-e

12 a-e

11 a, Y=H b, Y=Me c, Y=OMe
d, Y=Cl e, Y=CF_3

12 a, X=H b, X=Me c, X=OMe
d, X=Cl e, X=CF_3

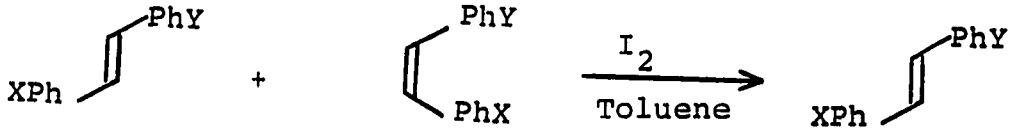

13 a-j

13'a-j

13 a-j

13 a, X/Y=H/H b, X/Y=Me/Me c, X/Y=OMe/OMe
d, X/Y=Cl/Cl e, X/Y=CF_3/CF_3 f, X/Y=H/Me
g, X/Y=H/Cl h, X/Y=H/CF_3 i, X/Y=Me/Cl
j, X/Y=Me/CF_3

Scheme 10

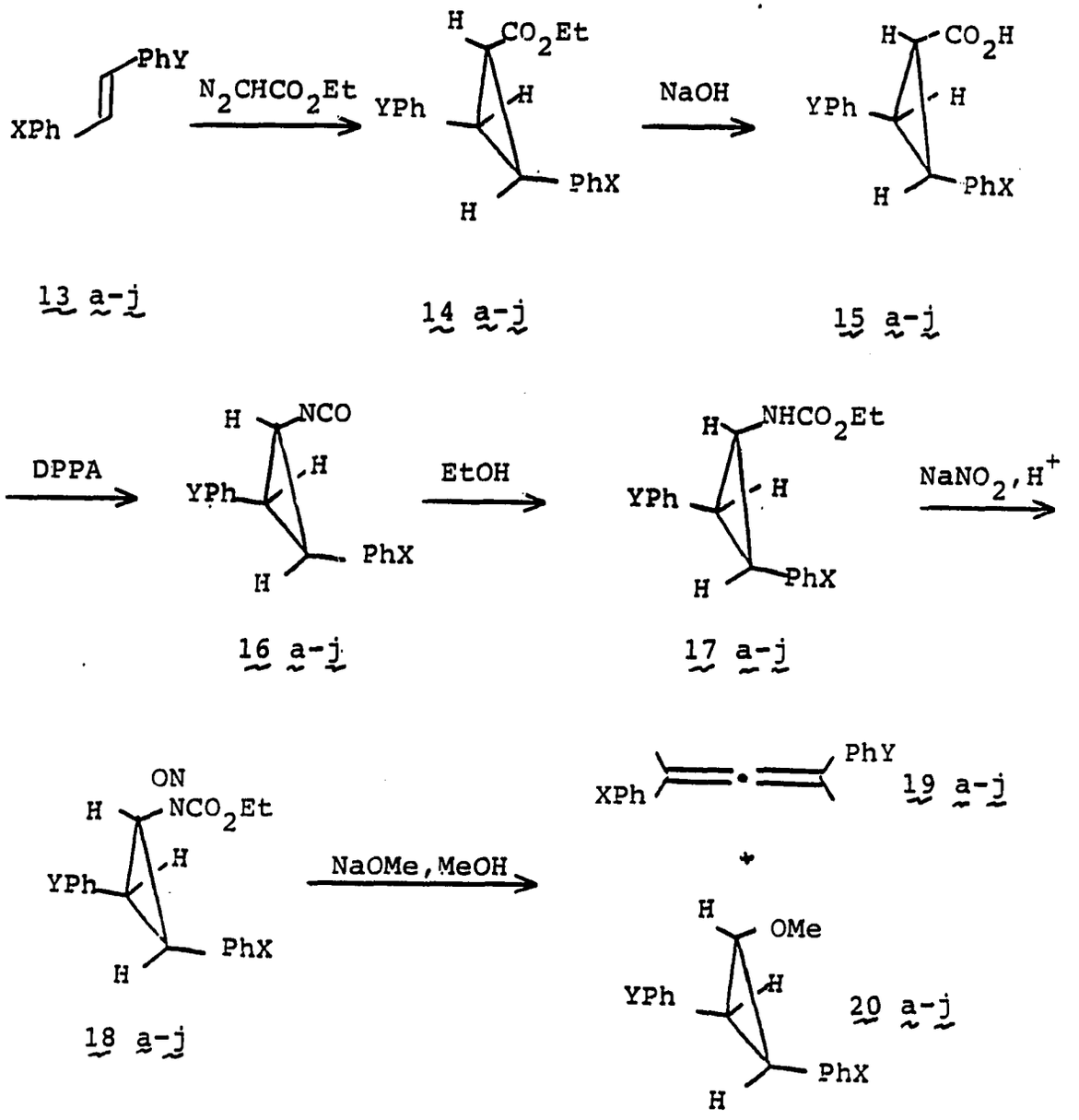

13 a-j 14 a-j 15 a-j

16 a-j 17 a-j

18 a-j 19 a-j 20 a-j

13-20 a,X/Y=H/H b,X/Y=Me/Me c,X/Y=OMe/OMe
d,X/Y=Cl/Cl e,X/Y=CF_3/CF_3 f,X/Y=H/Me
g,X/Y=H/Cl h,X/Y=H/CF_3 i,X/Y=Me/Cl
j,X/Y=Me/CF_3

Scheme 11

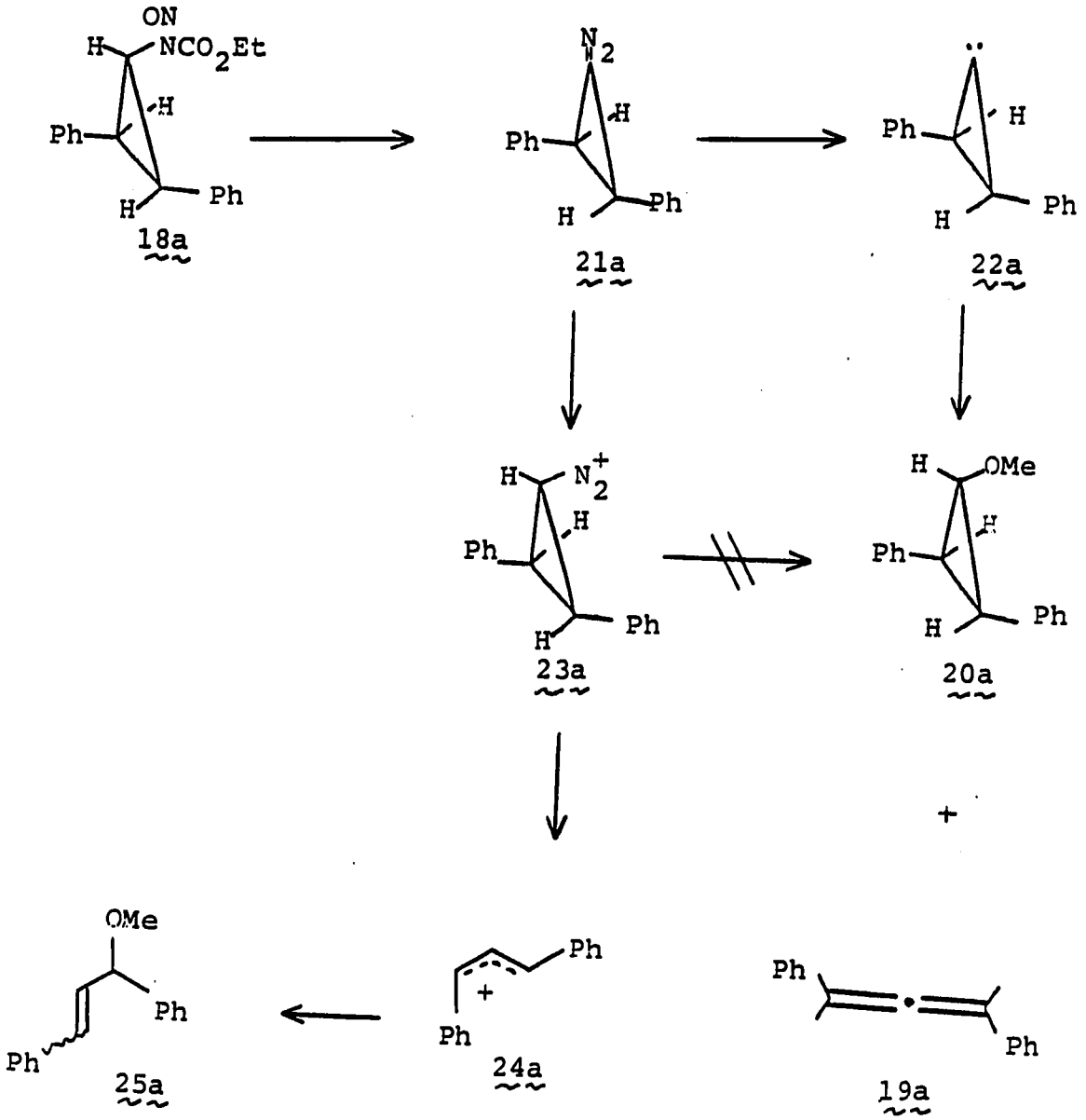
ON
H
NCO2Et
H
Ph
H
Ph
18a
N2
H
Ph
H
Ph
21a
H
Ph
H
Ph
22a
H
N2+
H
Ph
H
Ph
23a
H
OMe
H
Ph
H
Ph
20a
+
OMe
Ph
Ph
25a
Ph
+
Ph
24a
Ph
Ph
19a

Independent synthesis of 19a was effected by decomposing the corresponding dibromocyclopropane with methyllithium. The ether 20a was prepared from trans-stilbene and α,α-dichloromethyl methyl ether treated with methyllithium. Both products showed identical spectra and retention times when coinjected on a capillary GLPC column.

When the concentration of base is low, side products of the type 25a are generated via diazonium ion chemistry. The reaction path from 21a to 25a was shown not to cross over to give products 19a or 20a. This was demonstrated in two ways: first, 1,3-diphenylallyl cation was generated from the tosylate, the p-nitrobenzoate, and the action of hydrochloric acid on the alcohol in methanol solution, whereby 25a was the only detectable product. Secondly, when high concentrations (> 5 M) of soluble base were used, the diazonium ion pathway was averted (no 25a was detected), and the ratio of 20a/19a was the same as when 25a was observed.

A stirred solution of 18a was decomposed by addition of an excess (> 10 equivalents) of solid sodium methoxide. The solutions were stirred for 3-5 minutes although the reaction appeared to be over after about 30 seconds. The reactions were neutralized with ammonium chloride solution and extracted into ether before analysis. The product ratio 20a/19a was obtained via capillary GLPC analysis over a range of methanol concentrations (4.9 M to 24.7 M).

Response factor ratios were applied to all data to correct the product ratios to mole ratios. The response factor was that number which when multiplied by the GLPC ratio would give the mole ratio. To obtain these values, an NMR sample was prepared which contained a mixture of 20a and 19a. Mole ratios were determined by integration of a 200 scan 300 MHz NMR spectrum. The NMR sample was then analyzed by GLPC (average of 4 determinations) and Equation (1) was used to calculate the response factor ratio (RF = response factor, PN = proton number to correct to the mole ratio).

$$\frac{RF\ (20a)}{RF\ (19a)} = \left[NMR\ \frac{(20a)}{(19a)} \times PN\ \frac{(19a)}{(20a)}\right] \times GLPC\ \frac{(19a)}{(20a)} \qquad (1)$$

The results were interpreted in terms of the kinetic model shown in Scheme 12. Equation (2) was derived with presumption that 22a is a common intermediate for the generation of 19a and 20a. This predicts that a plot of 20a/19a versus the concentration of methanol should be linear with a zero intercept. All plots are indeed linear with intercepts which lie within experimental error of zero. The intercepts are consistently positive, which perhaps requires some attention. Several authors (43, 44) have noted that high concentrations (> 1 M) of methanol (as were used in this work) react somewhat faster with carbenes than do submolar concentrations. These small but consistently

Scheme 12

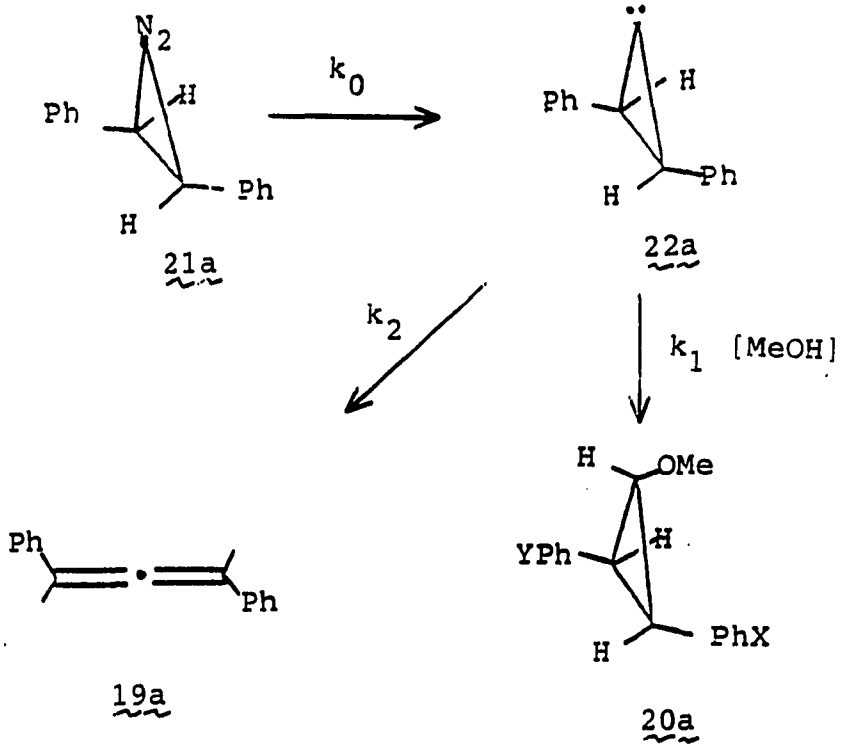

$$\frac{\underset{\sim\sim}{20a}}{\underset{\sim\sim}{19a}} = \frac{k_1}{k_2} \cdot [MeOH] \qquad (2)$$

positive intercepts, therefore, may be the result of an unfair extrapolation of the data. Further, due to the uncertain nature of condensed phase reactions (45), no attempt has been made to correct the data for monomer, dimer and oligomer concentrations of methanol, or for the dielectric constant of the medium. The data for $\underset{\sim\sim}{18a}$ are collected in Tables 1 and 2; Figures 11-16 display the data graphically.

Table 1. Product ratios[a] 20a/19a for the reaction of 18a in toluene/methanol solution at 271 K, 297 K and 313 K

T(K)	[MeOH], M 4.94	9.88	14.81	19.75	24.69
271	0.11±0.01	0.18±0.01	0.24±0.01	0.35±0.03	0.46±0.02
297	0.11±0.02	0.17±0.01	0.23±0.01	0.30±0.01	0.41±0.02
313	0.11±0.01	0.17±0.01	0.21±0.02	0.29±0.01	0.40±0.03

[a]Product ratios represent the corrected average of at least 4 but not more than 15 kinetic experiments with a tolerance of ± one sample standard deviation.

Table 2. Eyring data for 18a at 271 K, 297 K and 313 K

T(K)	k_2/k_1	ΔΔS* (e.u.)	ΔΔH* (kcal/mol)
271	55.56		
297	66.67	11.7 ± 0.3	1.0 ± 0.1
313	71.43		

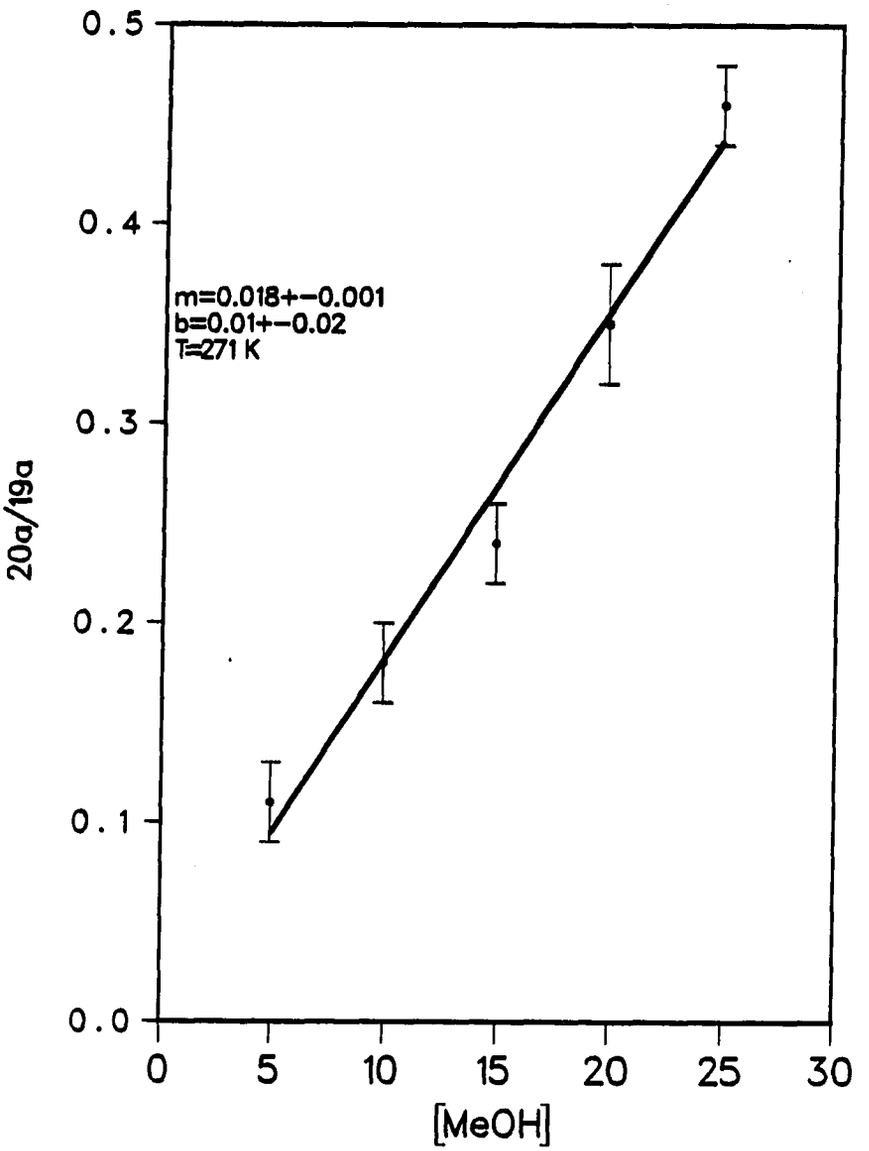

Figure 11. Plot of 20a/19a versus [MeOH] at 271 K

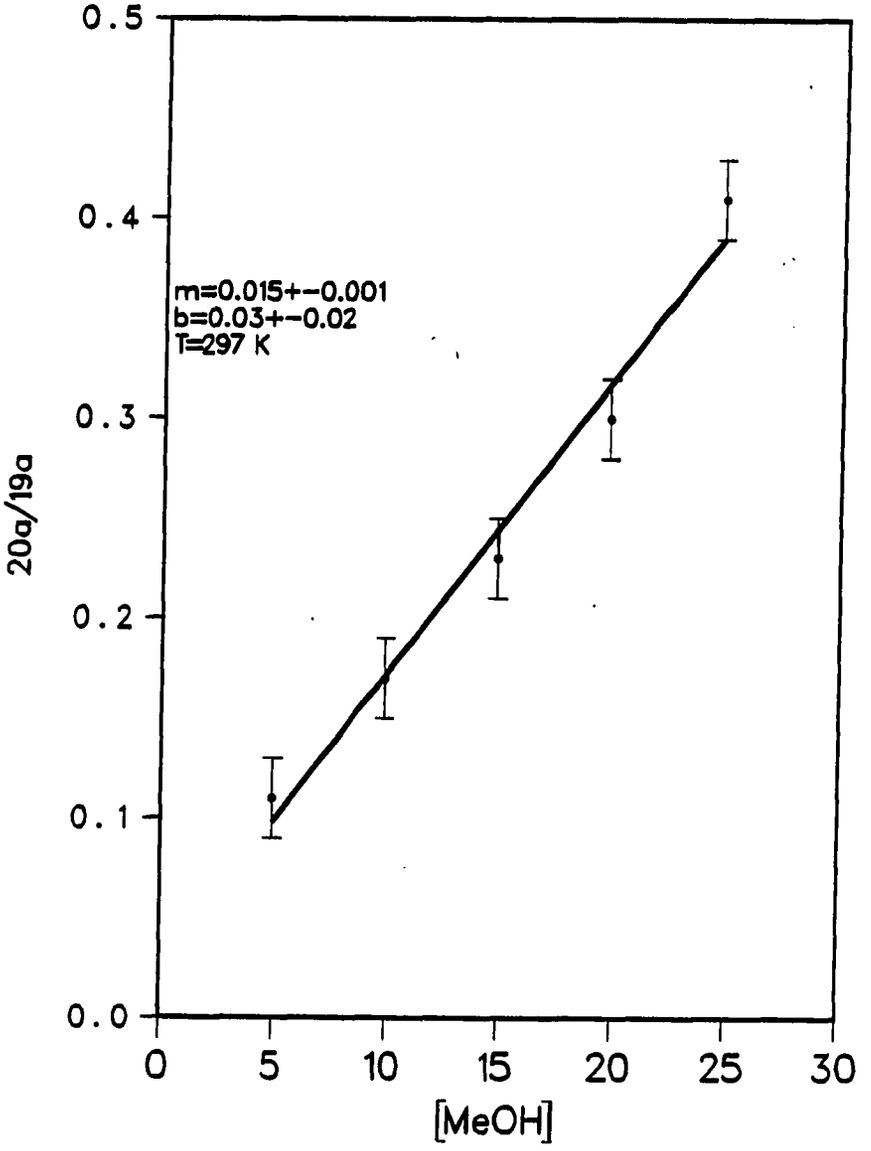

Figure 12. Plot of 20a/19a versus [MeOH] at 297 K

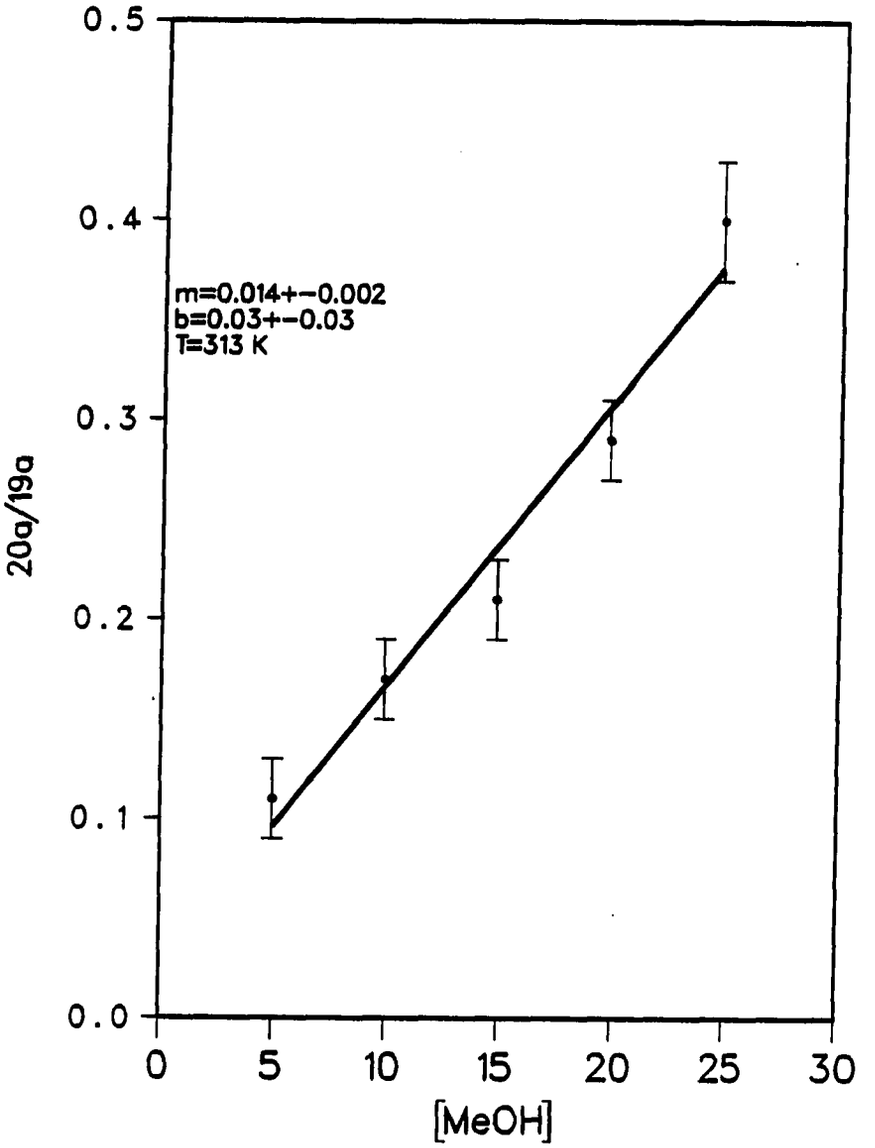

Figure 13. Plot of 20a/19a versus [MeOH] at 313 K

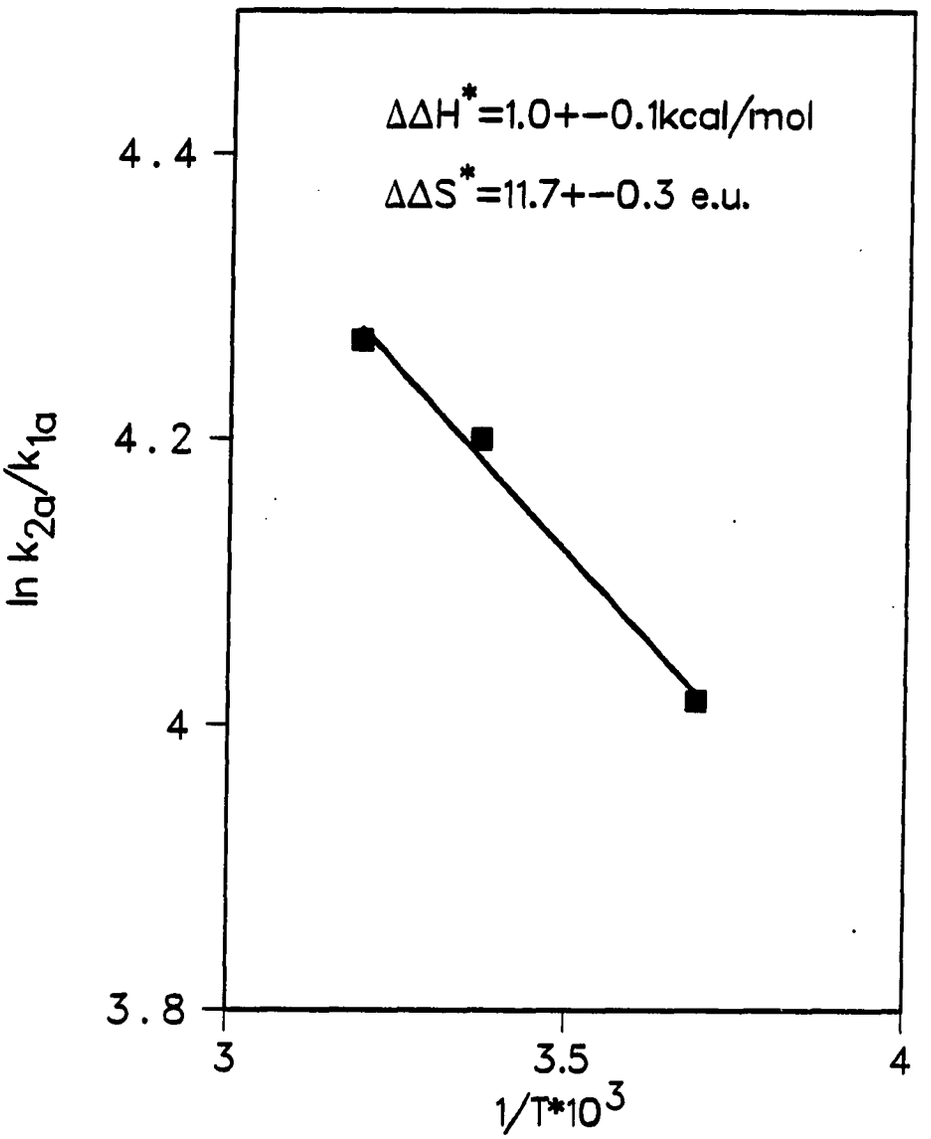

Figure 14. Eyring plot of ln k_{2a}/k_{1a} versus 1/T (K^{-1})

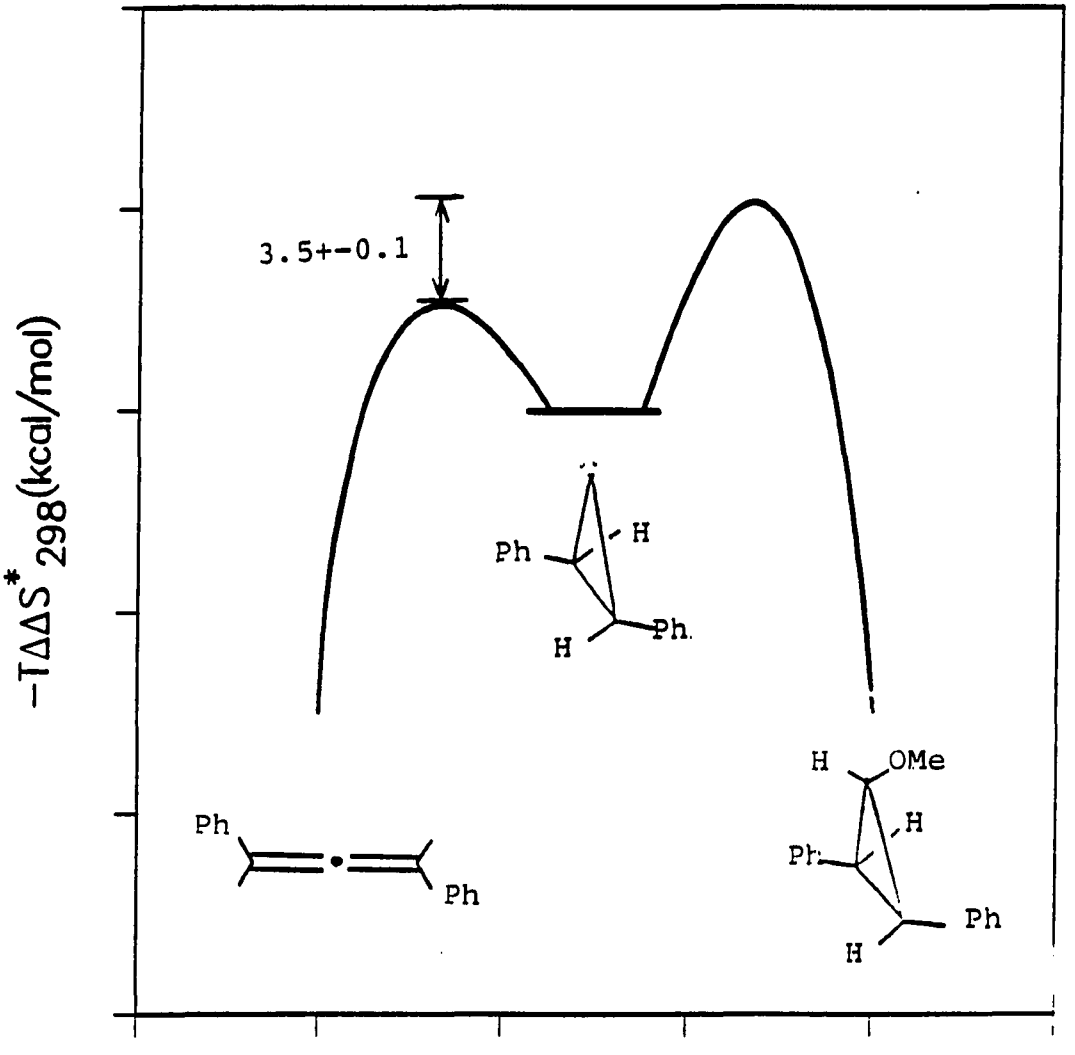

Figure 15. Entropy diagram -T(ΔS*(allene)-ΔS*(ether))

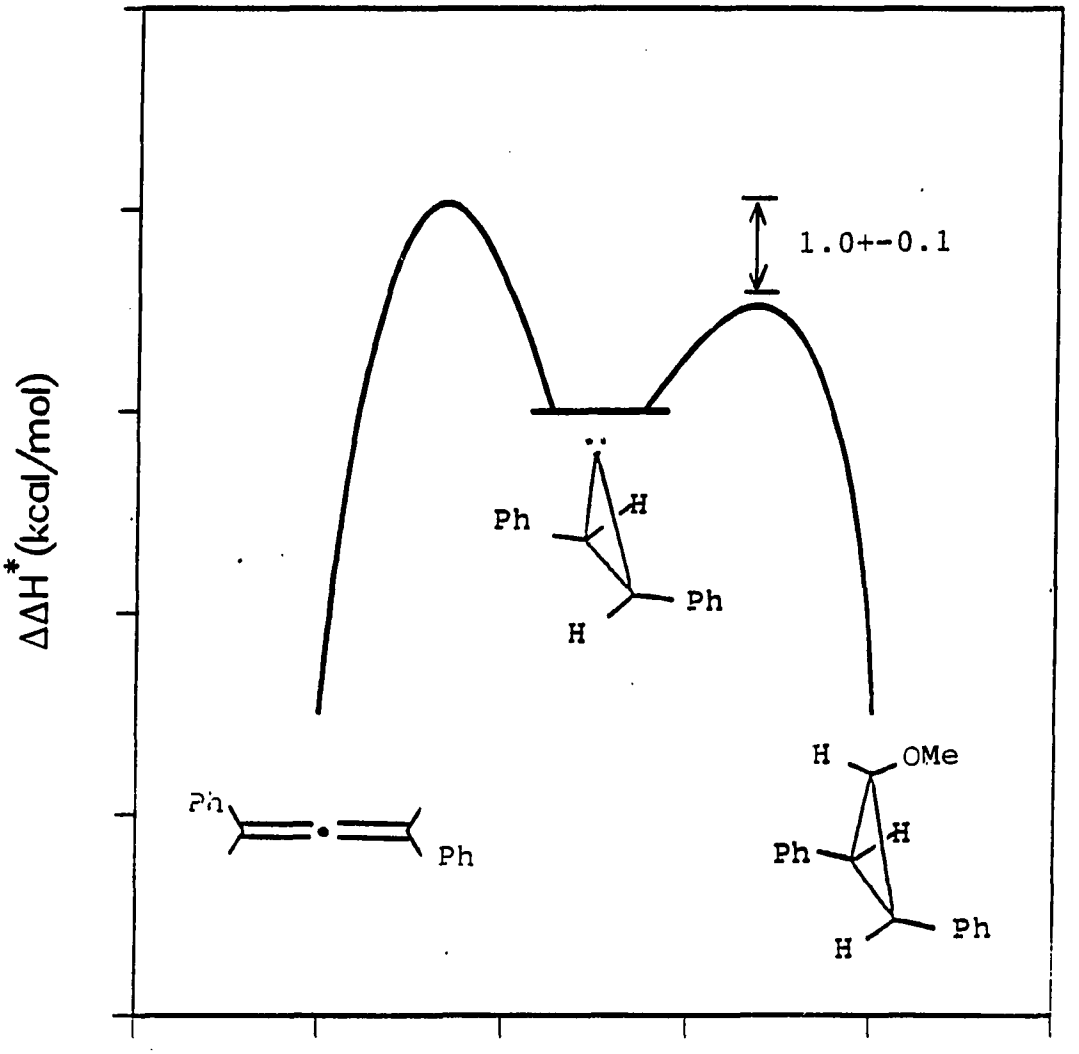

Figure 16. Enthalpy diagram -(ΔH* (allene)-ΔH* (ether))

The data were analyzed with the aid of a statistical non-linear least squares (NLLSQ) program (46). The NLLSQ program provides the slope and intercept along with the standard deviation of each. Approximate values for the slope and intercept were obtained by a least squares analysis on a TI-55 111 programable hand calculator. From these values, the NLLSQ program provided the final results in an average of only four iterative cycles.

The temperature dependence of the rates of ring opening and trapping of 22a was analyzed with the Eyring equation (Equation (3)). Equation (3) may be written as Equation (4) for use with relative rate constants. Thus

$$k = \kappa \frac{RT}{Nh} \exp(\Delta S^*/R) \exp(-\Delta H^*/RT) \qquad (3)$$

$$k_2/k_1 = \exp\left(\frac{\Delta S_2^* - \Delta S_1^*}{R}\right) \exp\left(\frac{\Delta H_1^* - \Delta H_2^*}{RT}\right) \qquad (4)$$

a plot of k_2/k_1 versus 1/T will provide the relative entropies and enthalpies of activation for allene formation versus ether formation (Table 2).

The remaining systems, 18b-j, were analyzed in the same fashion (note that 18c was not prepared and is, therefore, omitted). Tables 3-6 show the kinetic data for 18b-j, and Figures 17-44 display the results graphically. For systems 18b, d, f, h for which multi temperature data have

Table 3. The product ratios[a] of 20/19 for the reaction of 18 (b-d) in toluene/methanol solution

T(K)	20/19	[MeOH], M 4.94	9.88	14.81	19.75	24.69
271	b	0.06±0.01	0.10±0.01	0.12±0.01	0.17±0.01	0.25±0.02
297	b	0.06±0.01	0.08±0.01	0.12±0.01	0.16±0.01	-
313	b	0.05±0.01	0.08±0.01	0.11±0.01	0.13±0.01	0.18±0.01
297	c	0.05±0.01	0.07±0.02	0.10±0.03	0.12±0.02	0.16±0.05
271	d	0.15±0.02	0.27±0.05	0.36+0.02	0.51+0.01	-
297	d	0.16±0.03	0.25±0.05	0.31±0.06	0.45±0.06	0.57±0.08
313	d	0.17±0.01	0.26±0.02	0.36±0.01	0.38±0.01	0.52±0.01

[a]Product ratios represent the corrected average of at least 4 but not more than 15 kinetic experiments with a tolerance of ± one sample standard deviation.

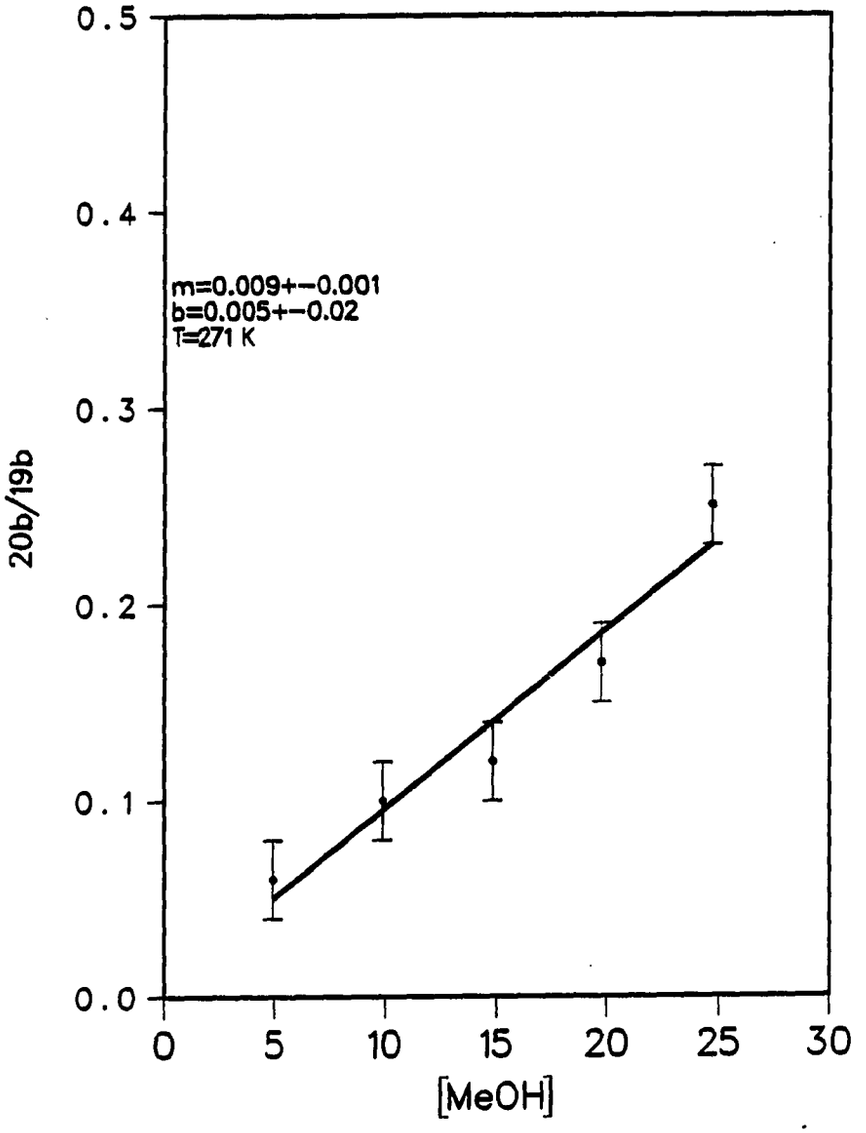

Figure 17. Plot of 20b/19b versus [MeOH] at 271 K

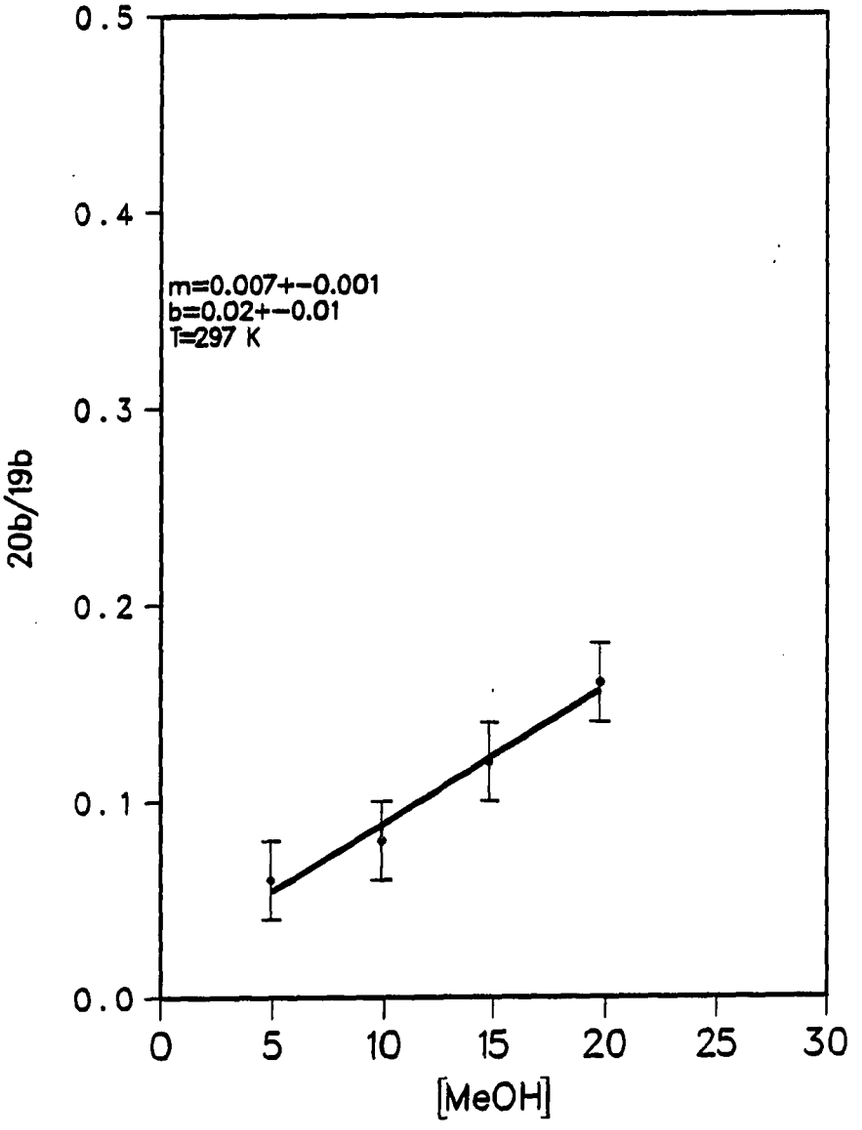

Figure 18. Plot of 20b/19b versus [MeOH] at 297 K

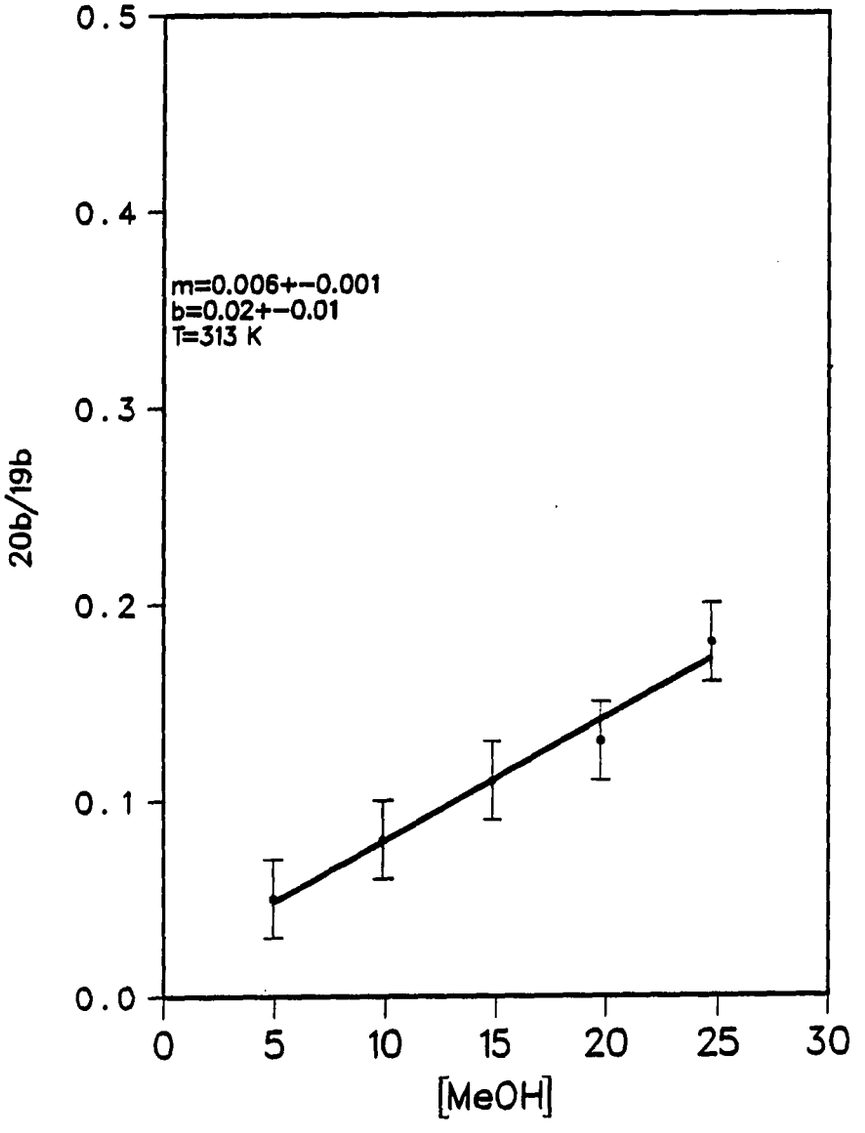

Figure 19. Plot of 20b/19b versus [MeOH] at 313 K

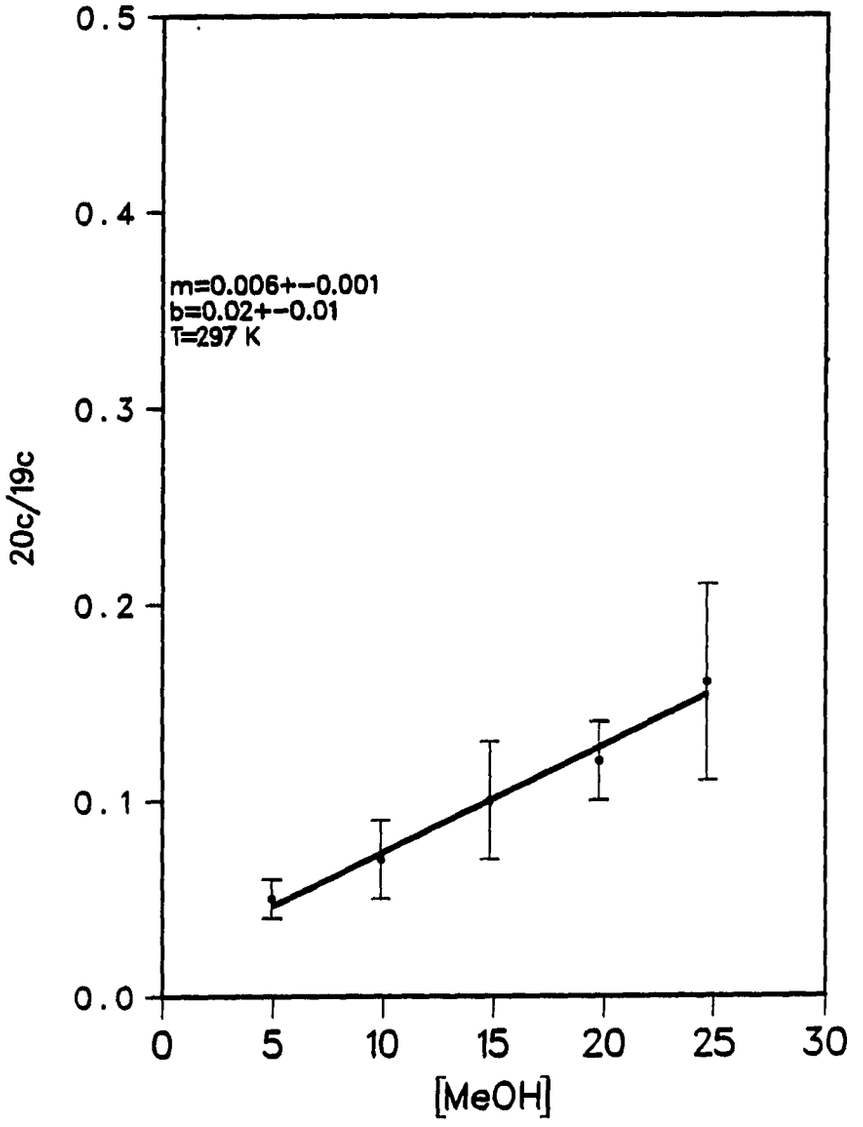

Figure 20. Plot of 20c/19c versus [MeOH] at 297 K

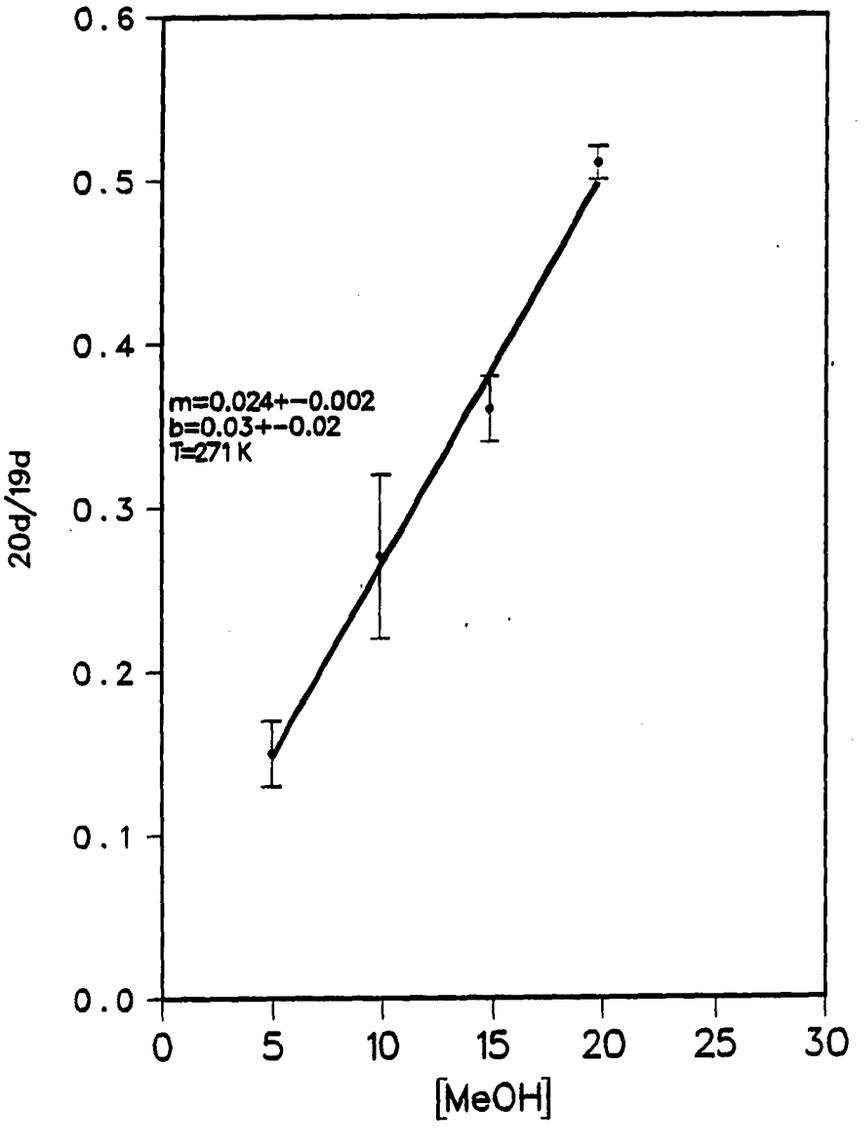

Figure 21. Plot of $\underset{\sim\sim}{20d}/\underset{\sim\sim}{19d}$ versus [MeOH] at 271 K

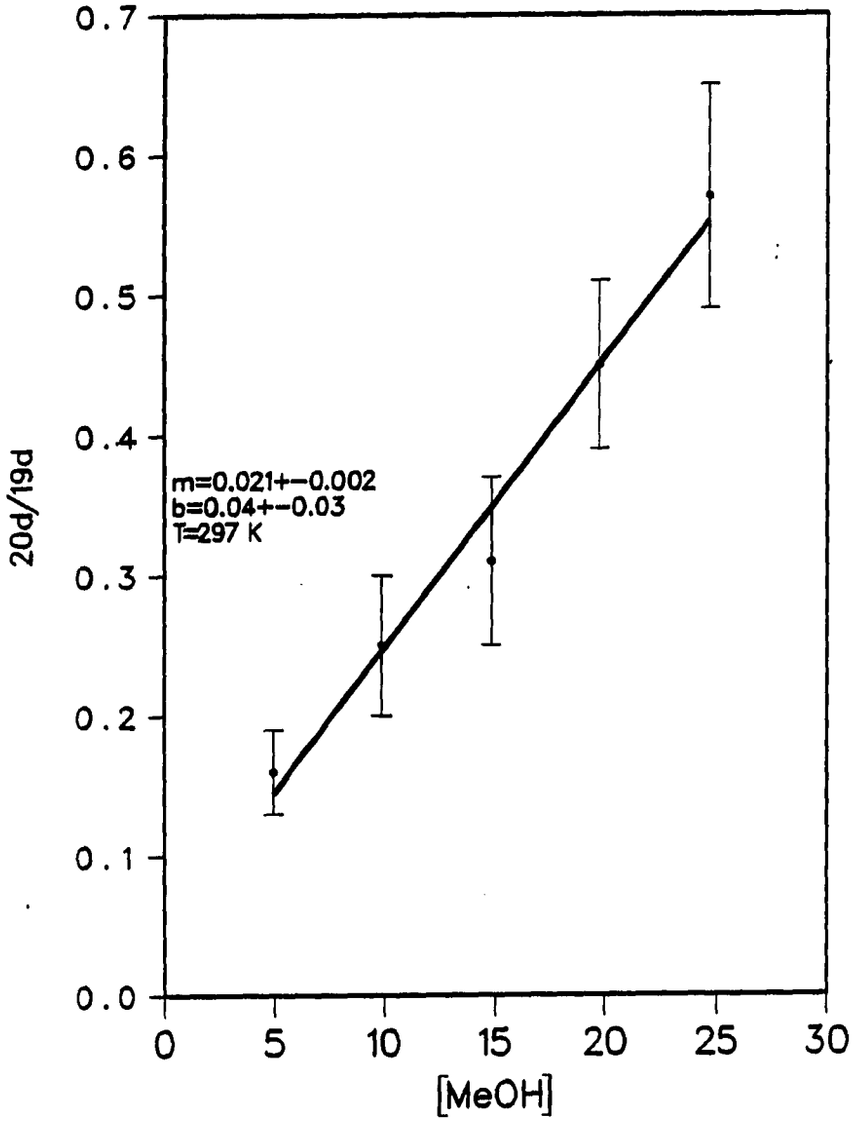

Figure 22. Plot of 20d/19d versus [MeOH] at 297 K

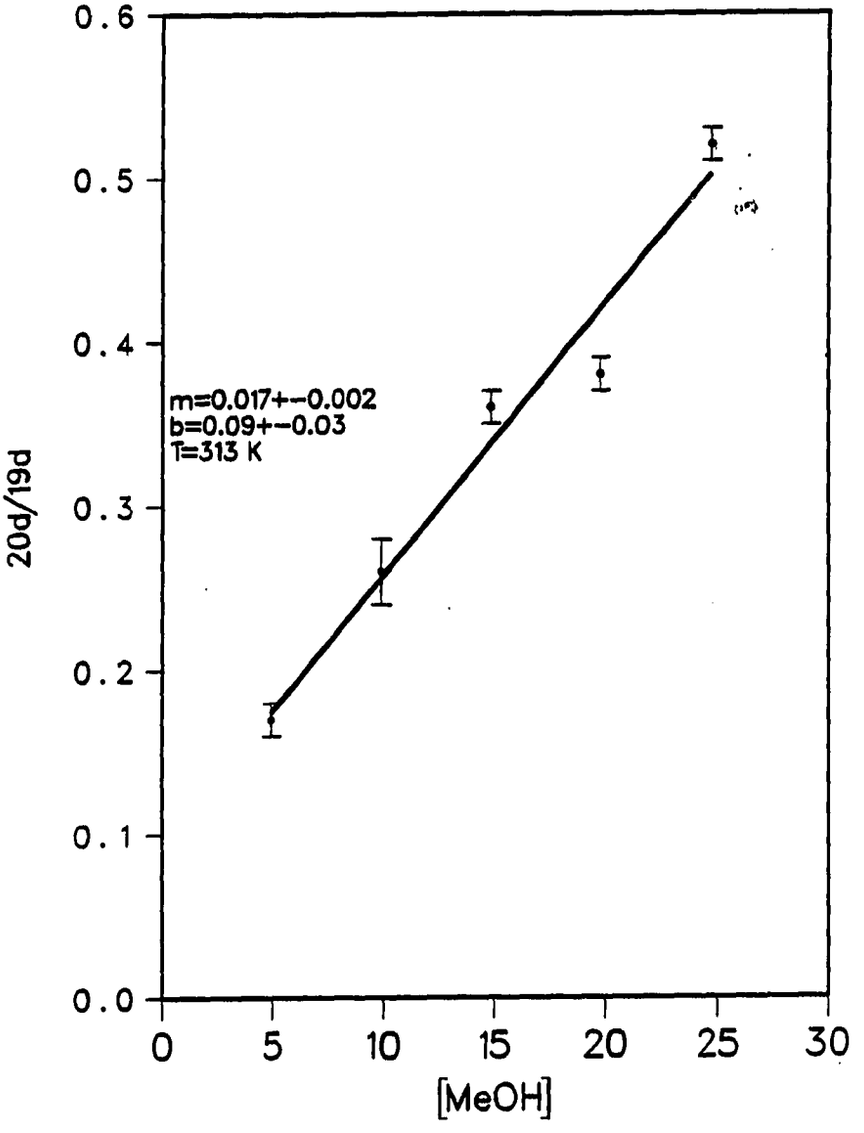

Figure 23. Plot of 20d/19d versus [MeOH] at 313 K

Table 4. Eyring data for 18b and 18d at 271 K, 297 K and 313 K

T(K)	k_2/k_1	ΔΔS* (e.u.)	ΔΔH* (kcal/mol)
271	111.11[a]		
297	142.86[a]	14.6 ± 0.3[a]	1.4 ± 0.1[a]
313	166.67[a]		
271	41.67[b]		
297	47.62[b]	12 ± 2[b]	1.4 ± 0.4[b]
313	58.82[b]		

[a]Data for 18b.

[b]Data for 18d.

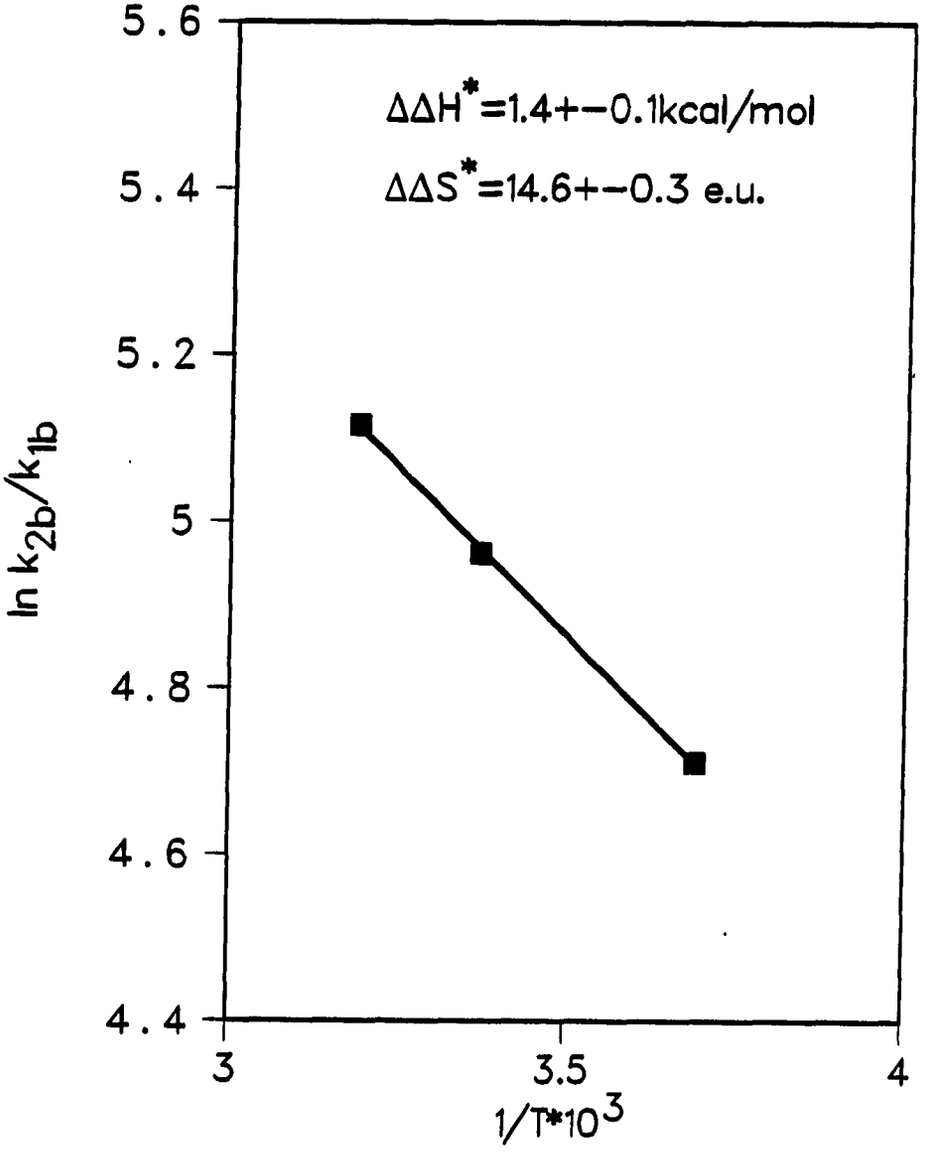

Figure 24. Eyring plot of ln k_{2b}/k_{1b} versus 1/T (K^{-1})

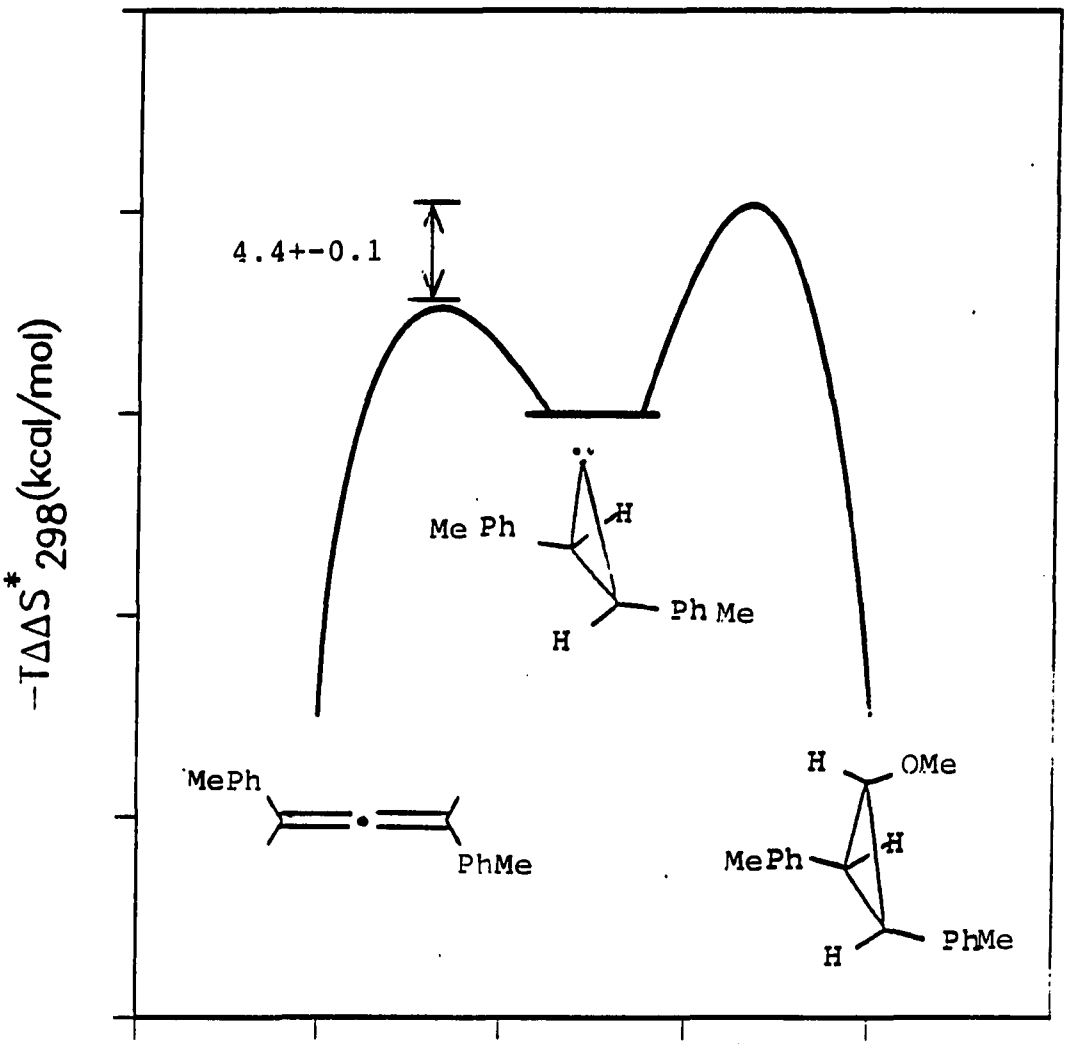

Figure 25. Entropy diagram for system b - T (ΔS^* (allene)-ΔS^*(ether))

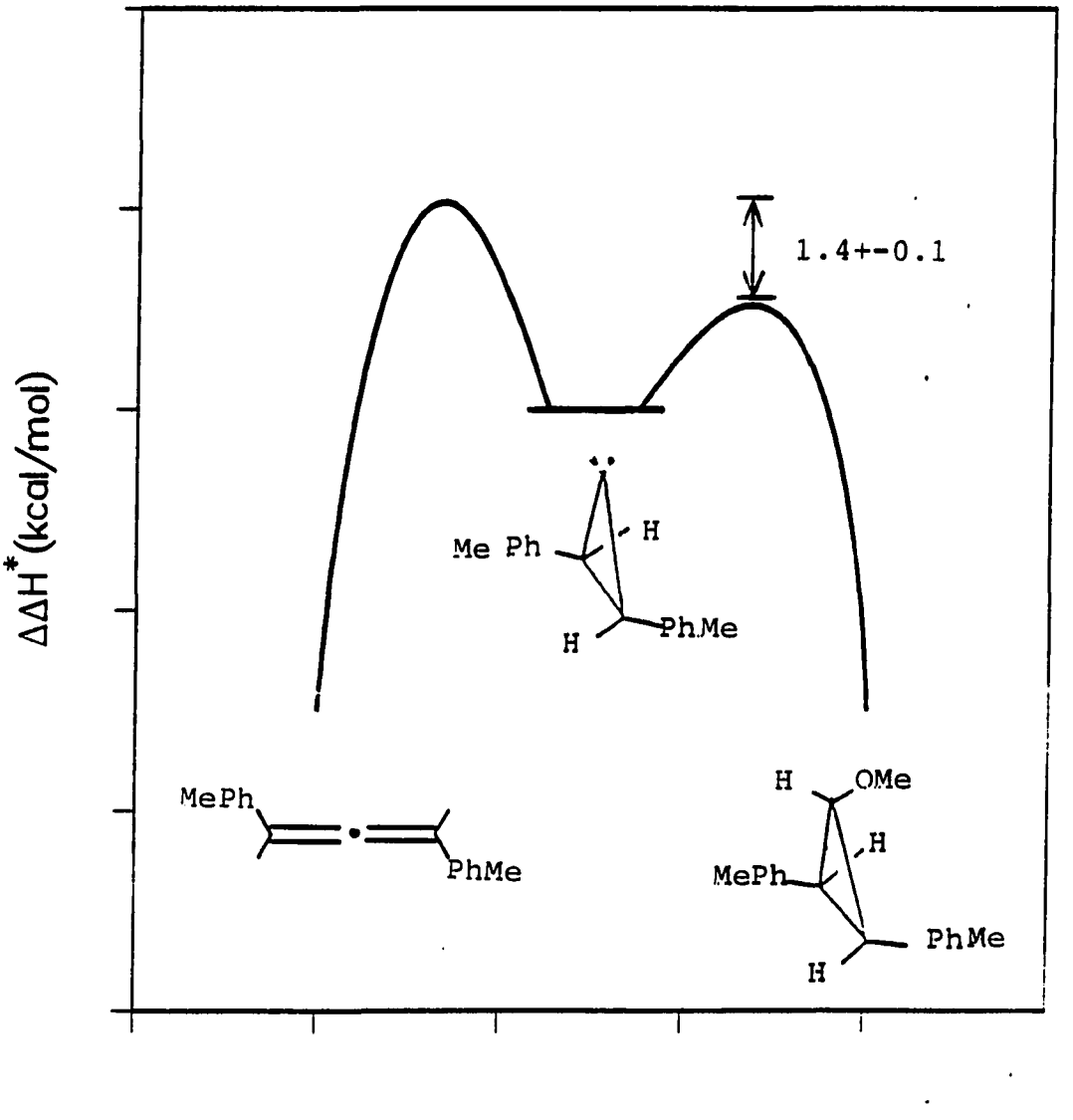

Figure 26. Enthalpy diagram for system b - (ΔH* (allene)-ΔH* (ether))

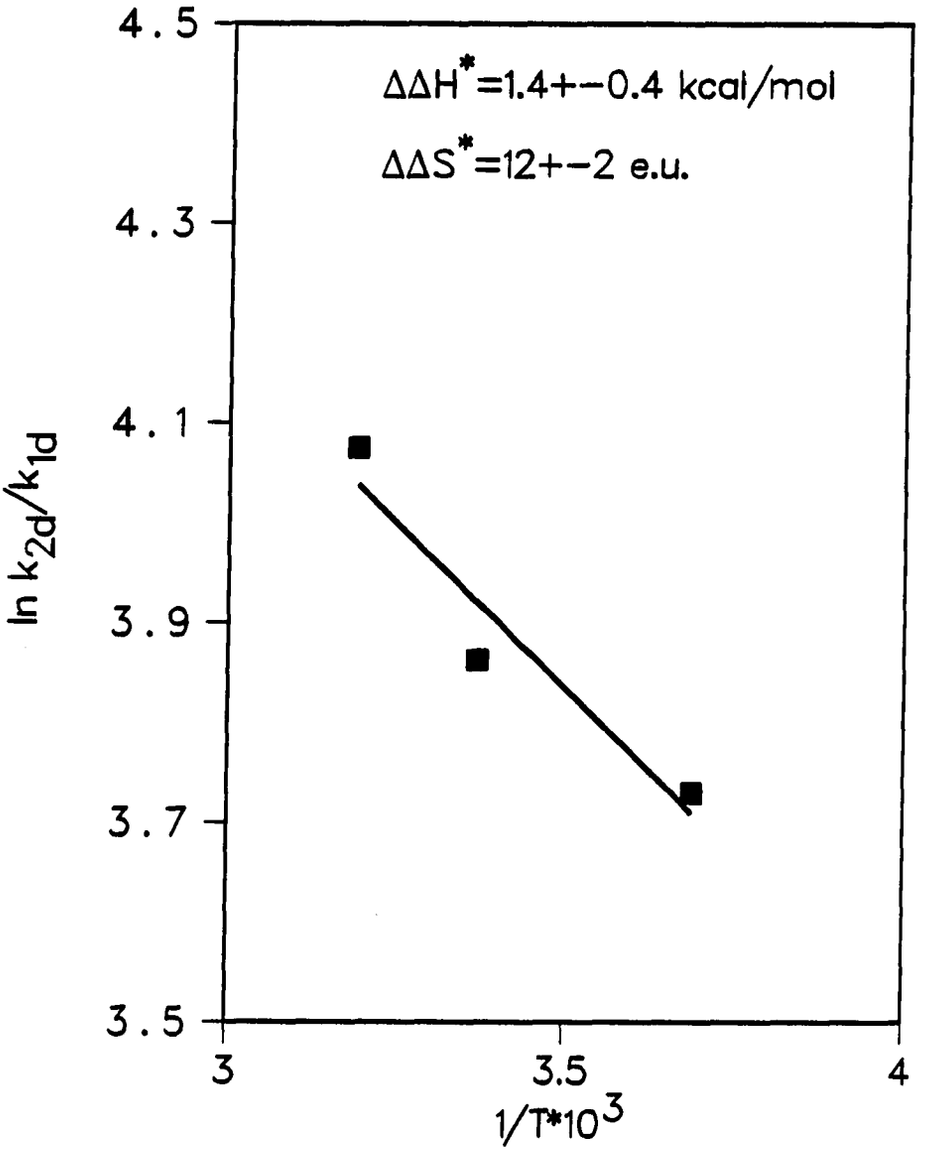

Figure 27. Eyring plot of ln k_{2d}/k_{1d} versus 1/T (K^{-1})

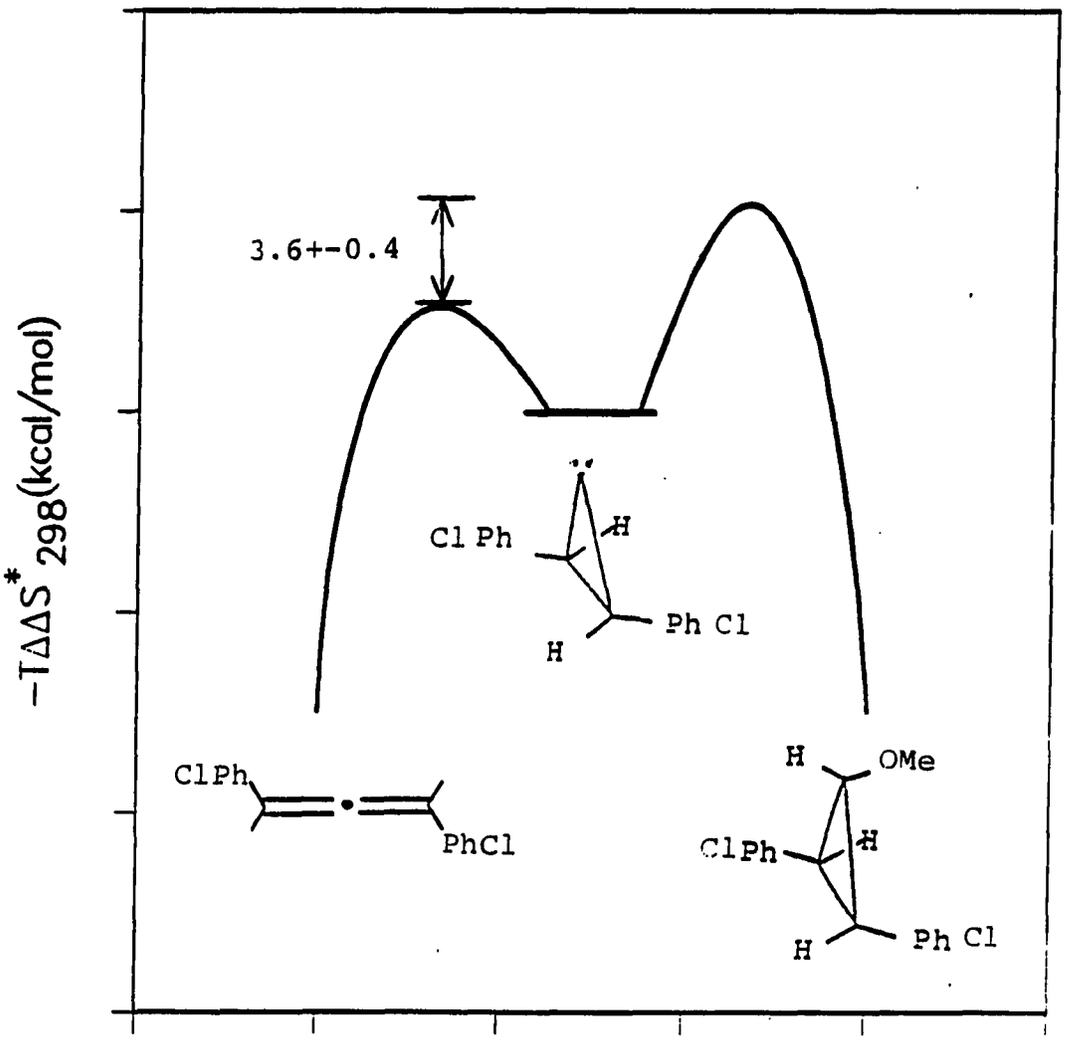

Figure 28. Entropy diagram for system d - T (ΔS* (allene)-ΔS* (ether))

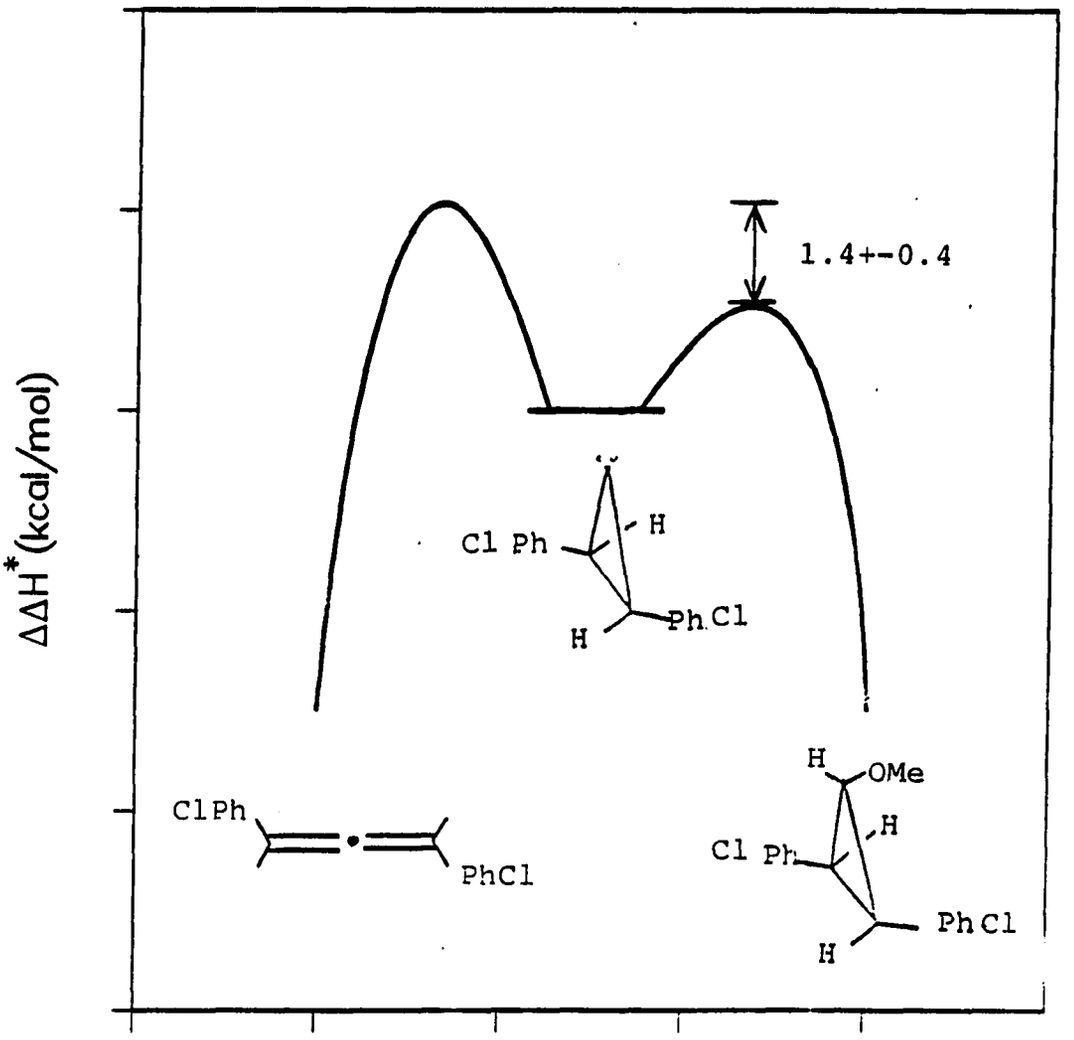

Figure 29. Enthalpy diagram for system d - (ΔH^* (allene)- ΔH^* (ether))

Table 5. Product ratios[a] 20/19 for the reaction of 18 (f-j) in toluene/methanol solution

T(K)	20/19	[MeOH], M 4.94	9.88	14.81	19.75	24.69
271	f	0.08±0.01	0.13±0.01	0.17±0.01	0.22±0.01	0.32±0.01
297	f	0.08±0.01	0.12±0.01	0.17±0.01	0.21±0.01	0.30±0.02
313	f	0.07±0.01	0.11±0.01	0.14±0.01	0.19±0.01	0.28±0.01
297	g	0.17±0.01	0.26±0.01	0.34±0.01	0.48±0.03	0.72±0.03
271	h	0.19±0.01	0.43±0.04	0.57±0.02	0.86±0.02	1.20±0.09
297	h	0.27±0.01	0.41±0.04	0.56±0.05	0.71±0.03	0.93±0.01
313	h	0.27±0.01	0.36±0.01	0.51±0.02	0.68±0.01	0.87±0.04
297	i	0.04±0.01	0.06±0.01	0.09±0.02	0.13±0.03	0.19±0.01
297	j	0.15±0.01	0.24±0.02	0.33±0.02	0.44±0.07	0.59±0.09

[a]Product ratios represent the corrected average of at least 4 but not more than 15 kinetic experiments with a tolerance of ± one sample standard deviation.

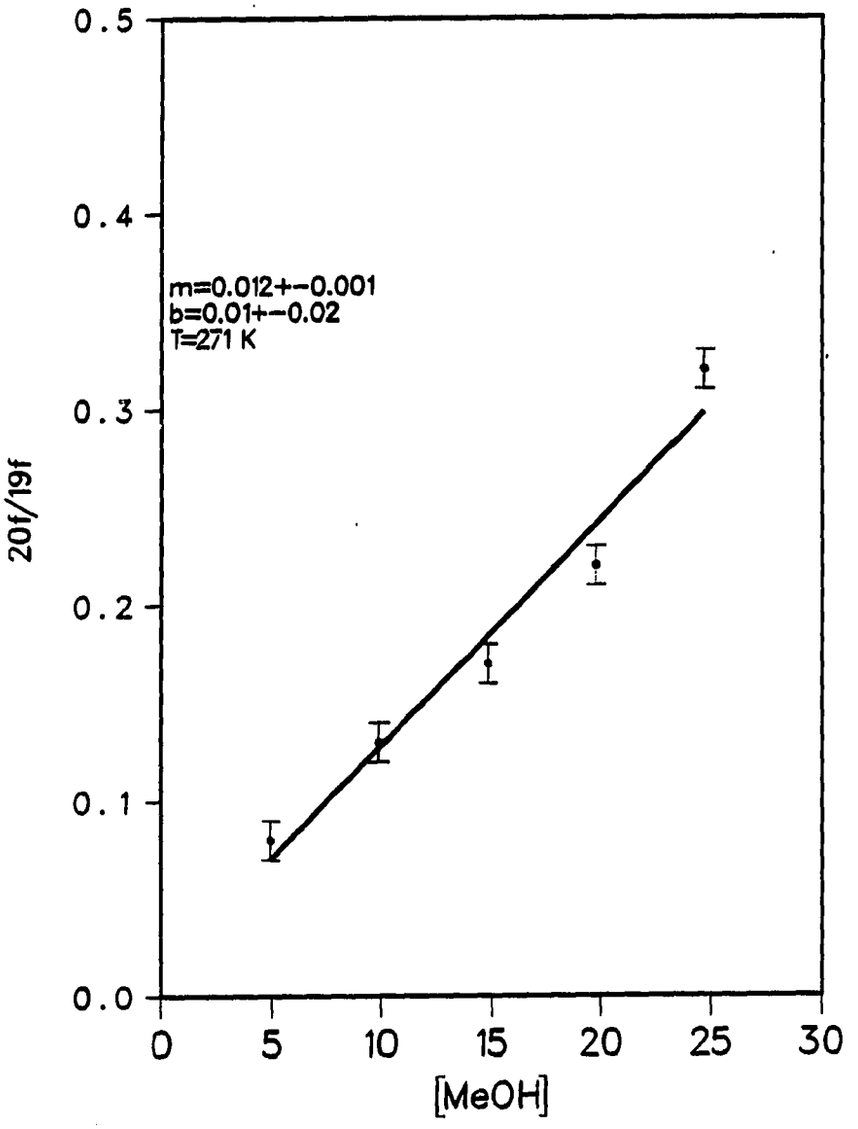

Figure 30. Plot of 20f/19f versus [MeOH] at 271 K

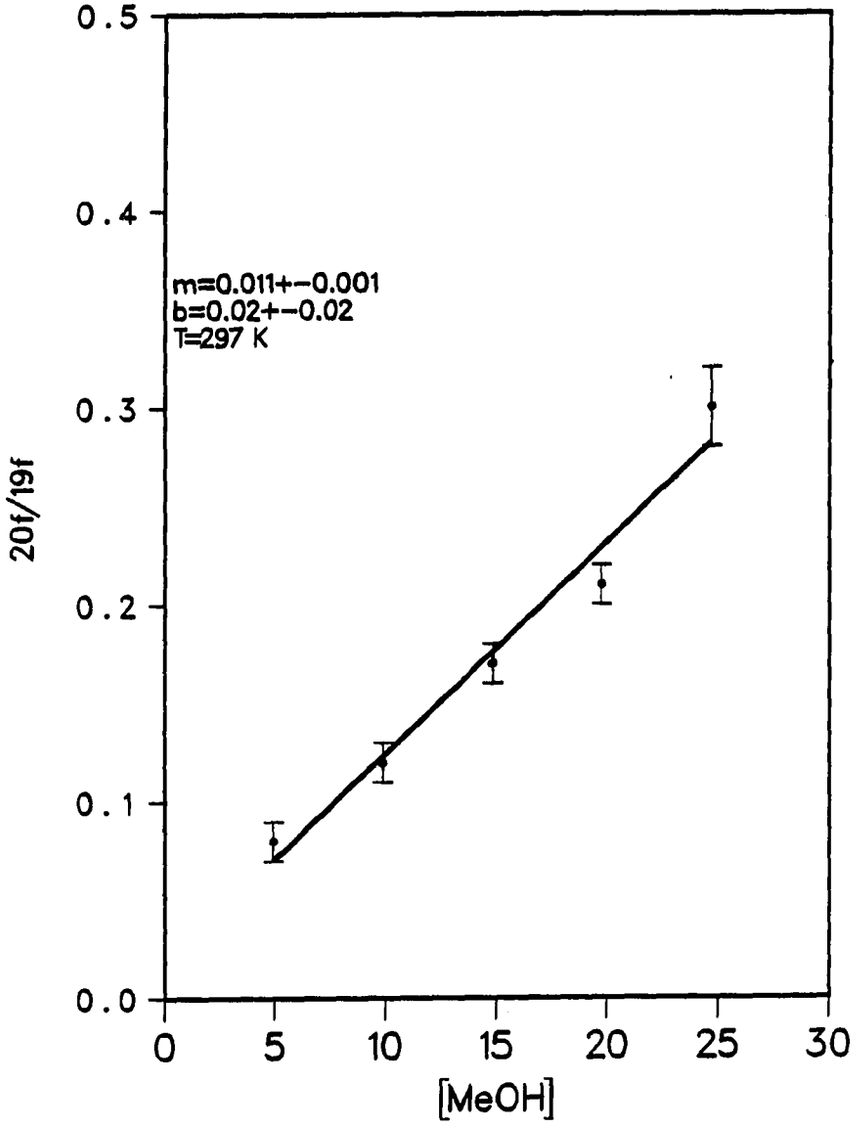

Figure 31. Plot of 20f/19f versus [MeOH] at 297 K

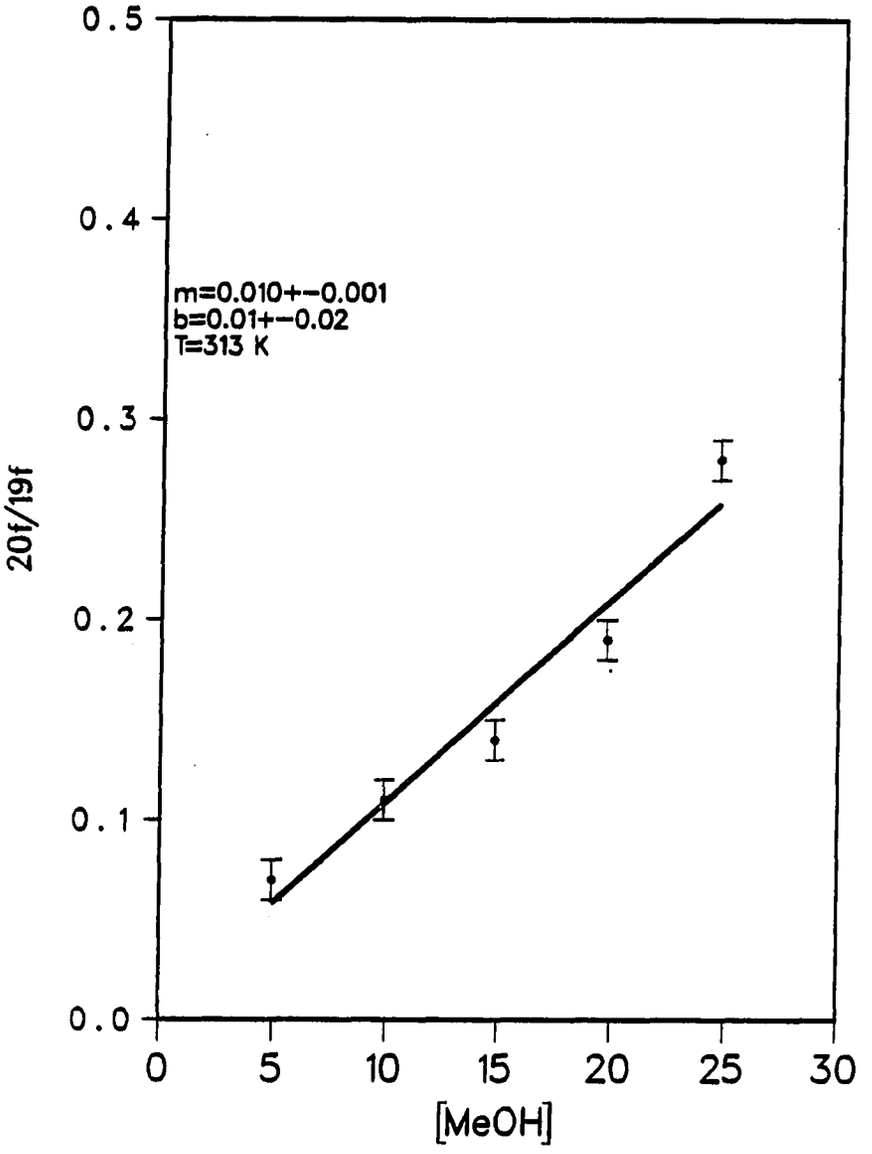

Figure 32. Plot of 20f/19f versus [MeOH] at 313 K

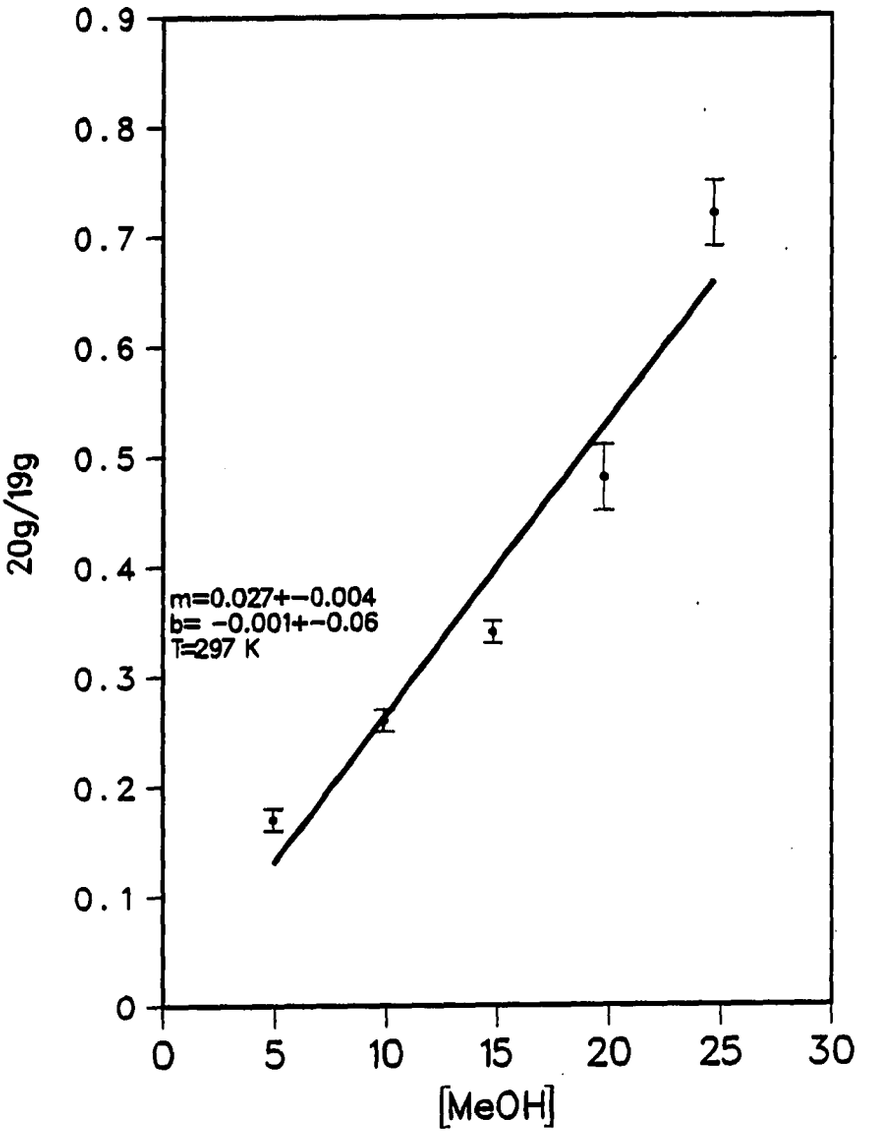

Figure 33. Plot of $\underset{\sim\sim}{20g}/\underset{\sim\sim}{19g}$ versus [MeOH] at 297 K

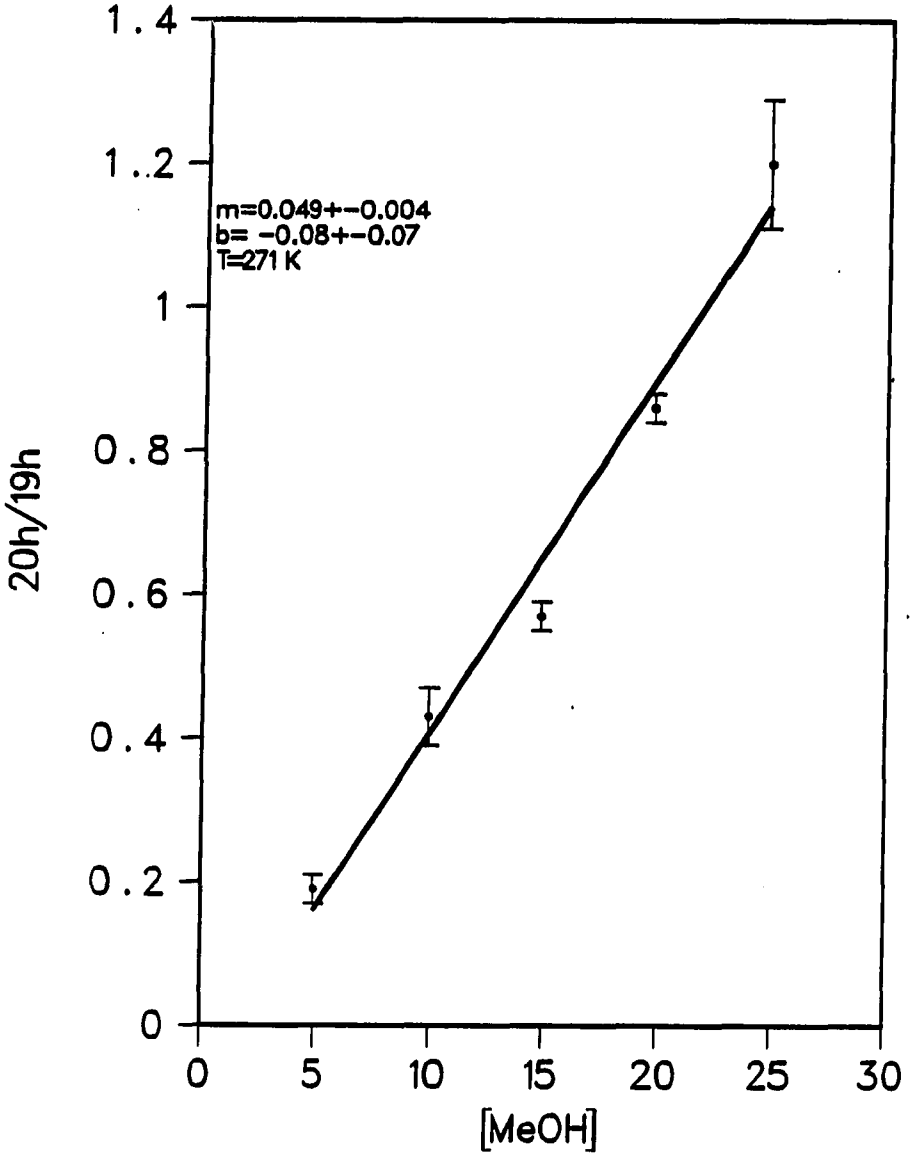

Figure 34. Plot of 20h/19h versus [MeOH] at 271 K

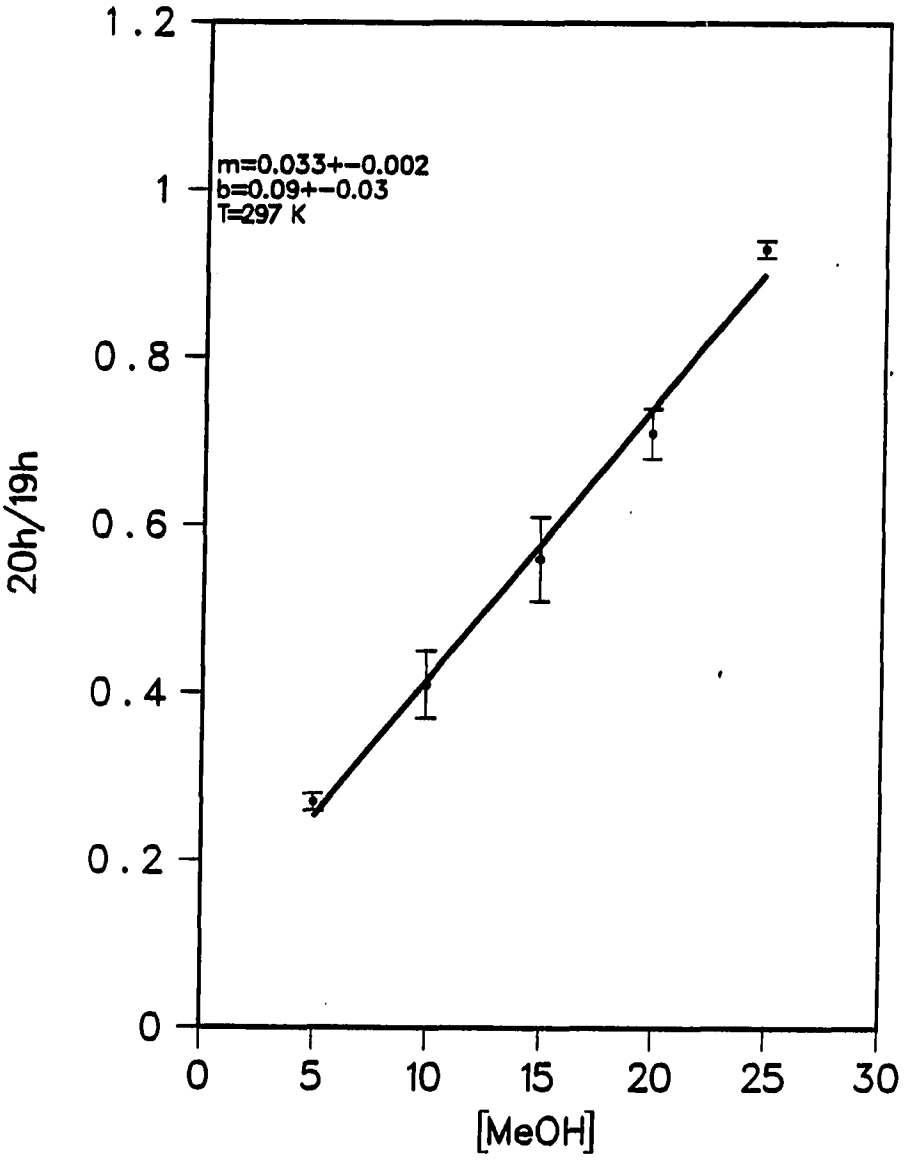

Figure 35. Plot of 20h/19h versus [MeOH] at 297 K

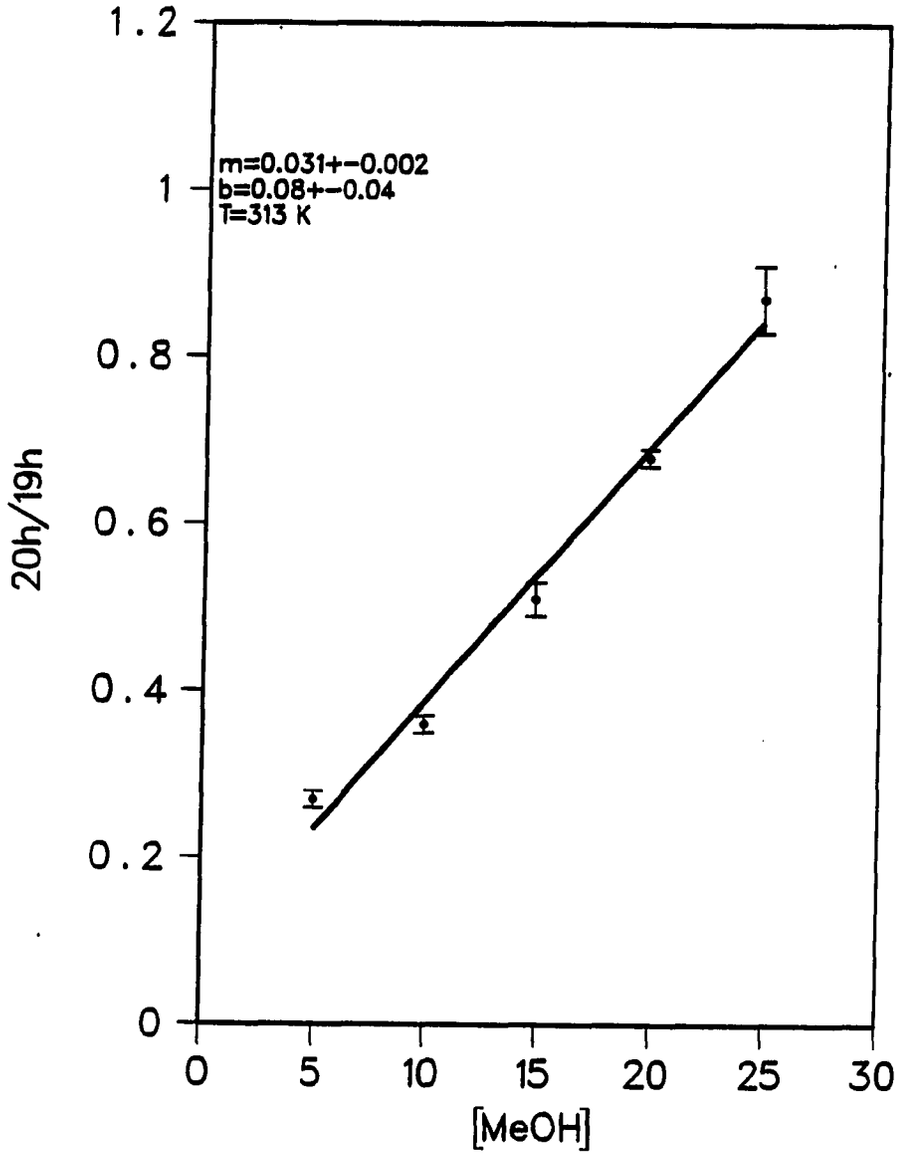

Figure 36. Plot of 20h/19h versus [MeOH] at 313 K

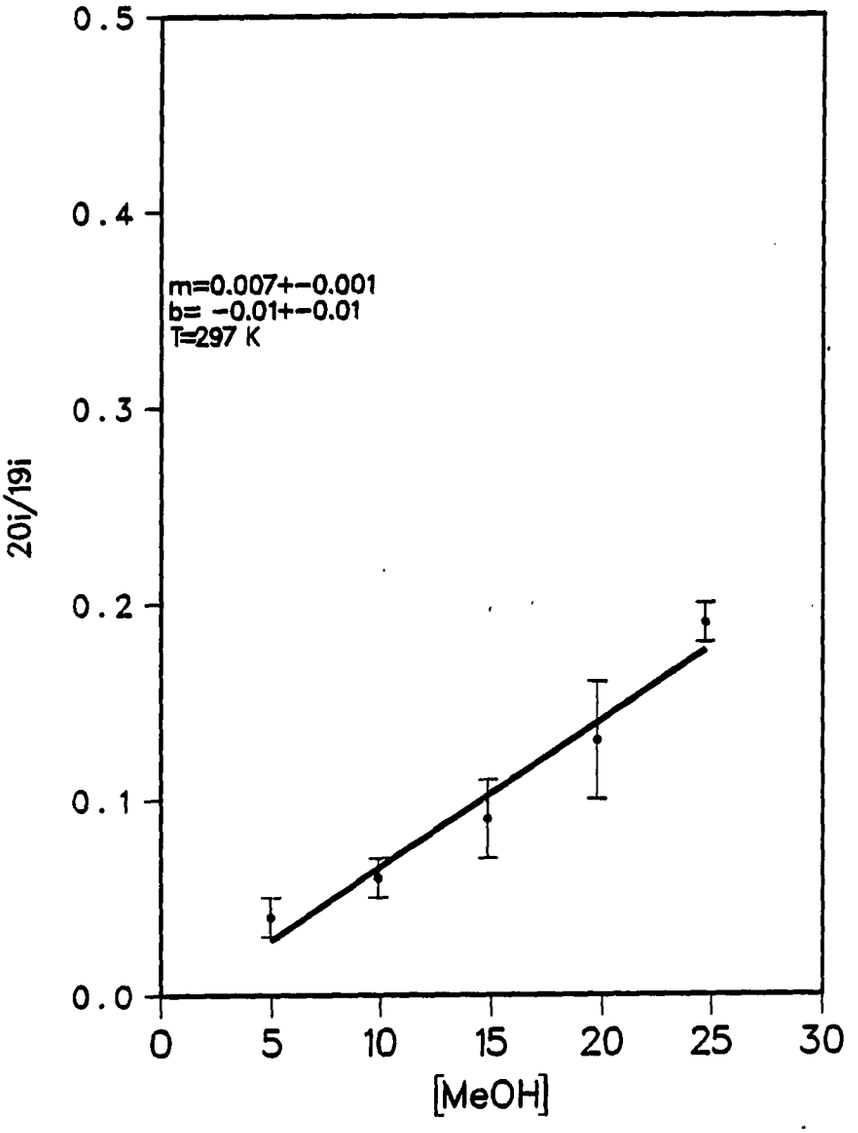

Figure 37. Plot of 20i/19i versus [MeOH] at 297 K

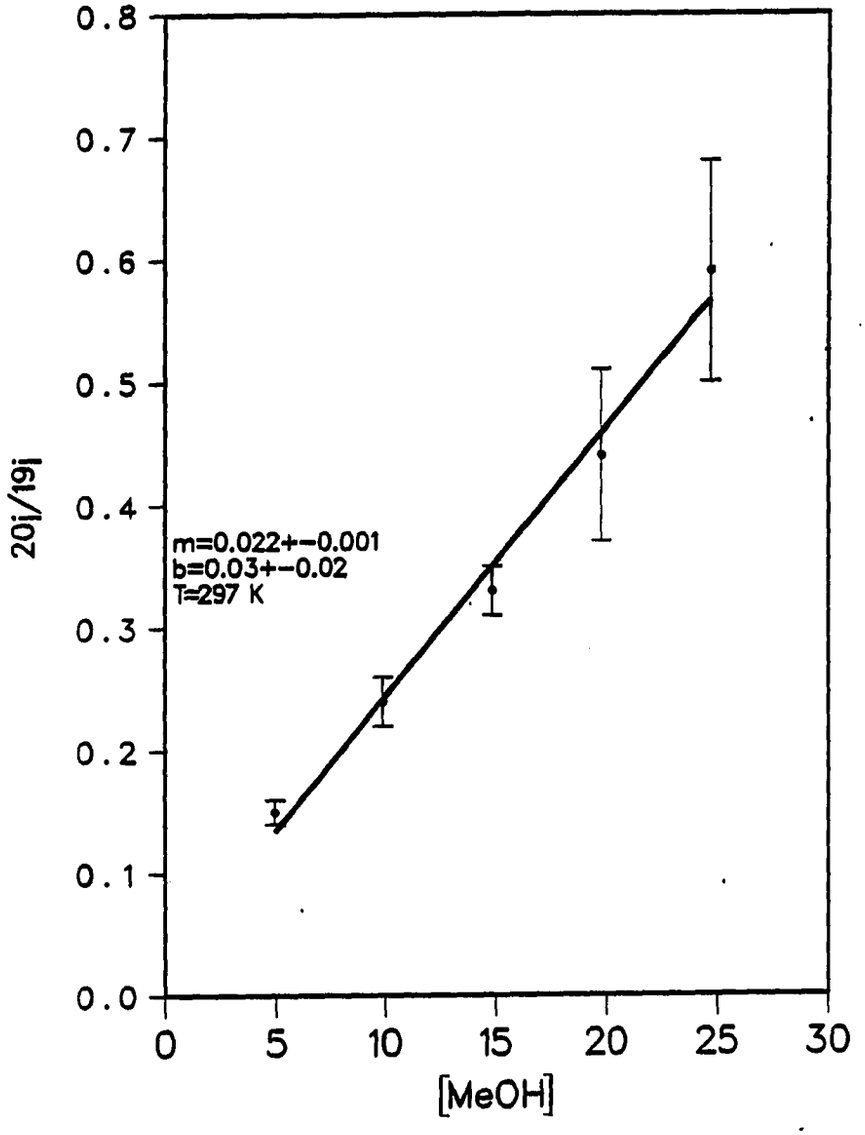

Figure 38. Plot of 20j/19j versus [MeOH] at 297 K

Table 6. Eyring data for 18f and 18h at 271 K, 297 K and 313 K

T(K)	k_2/k_1	ΔΔS* (e.u.)	ΔΔH* (kcal/mol)
271	83.33[a]		
297	90.91[a]	11.4 ± 0.5[a]	0.7 ± 0.1[a]
313	100.00[a]		
271	20.41[b]		
297	30.30[b]	13 ± 2[b]	1.8 ± 0.5[b]
313	32.26[b]		

[a]Data for 18f.

[b]Data for 18h.

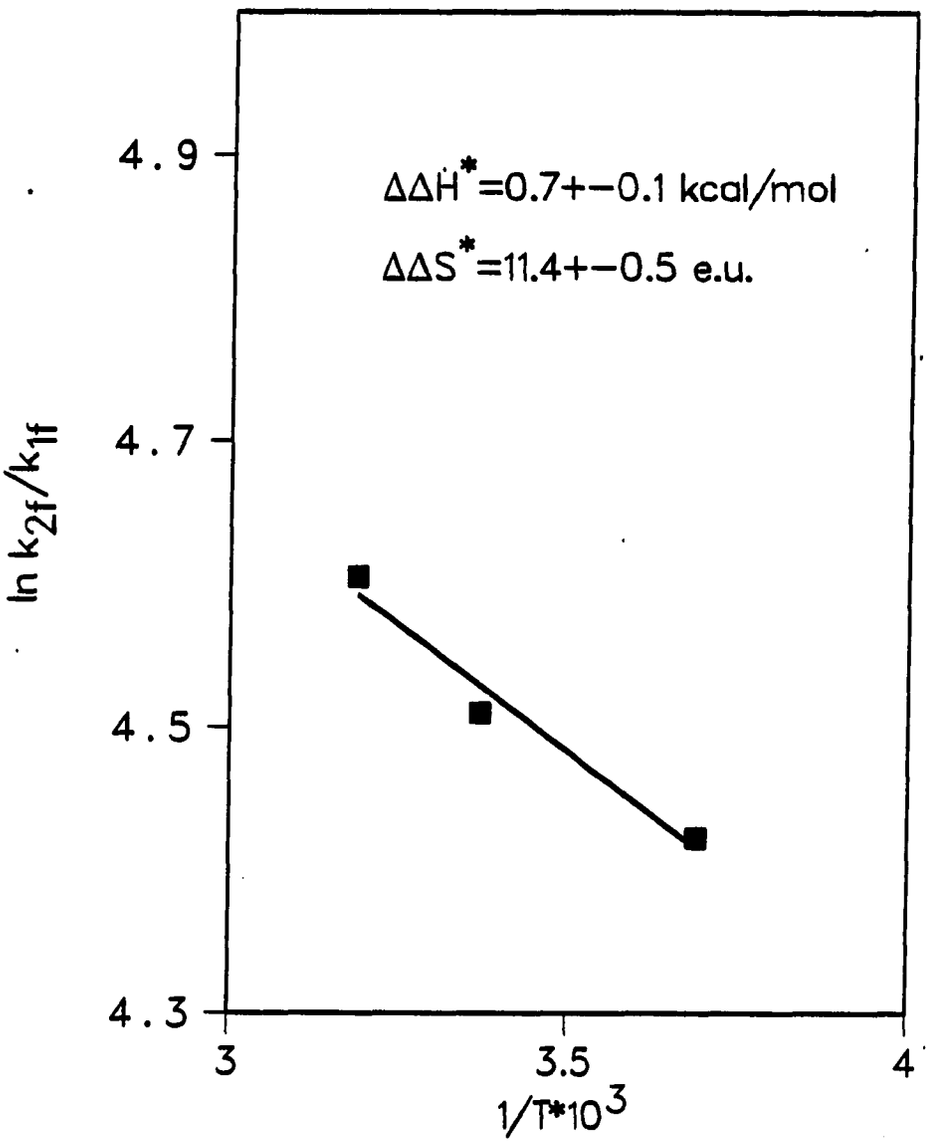

Figure 39. Eyring plot of ln k_{2f}/k_{1f} versus 1/T (K^{-1})

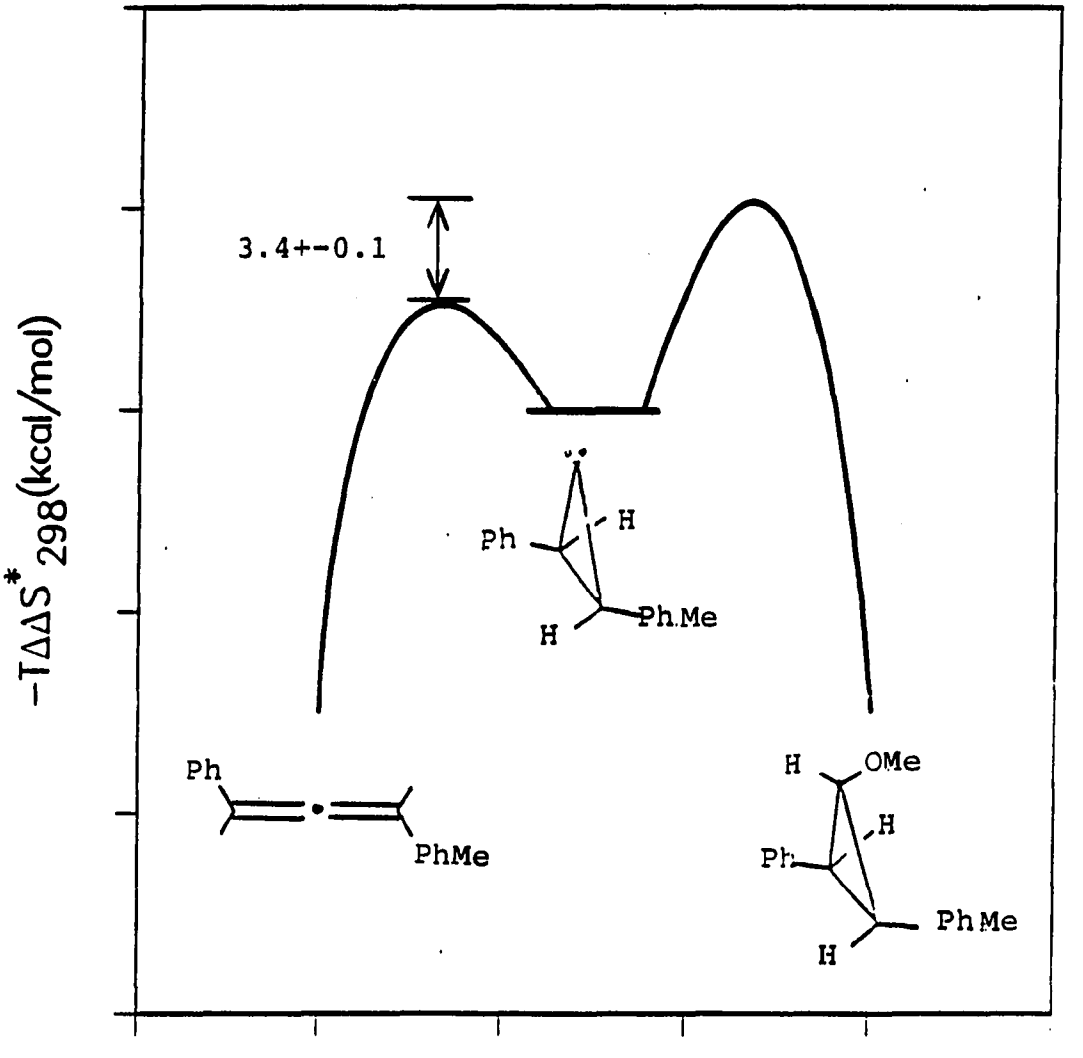

Figure 40. Entropy diagram for system $\underset{\sim}{f}$ - T (ΔS* (allene)-ΔS* (ether))

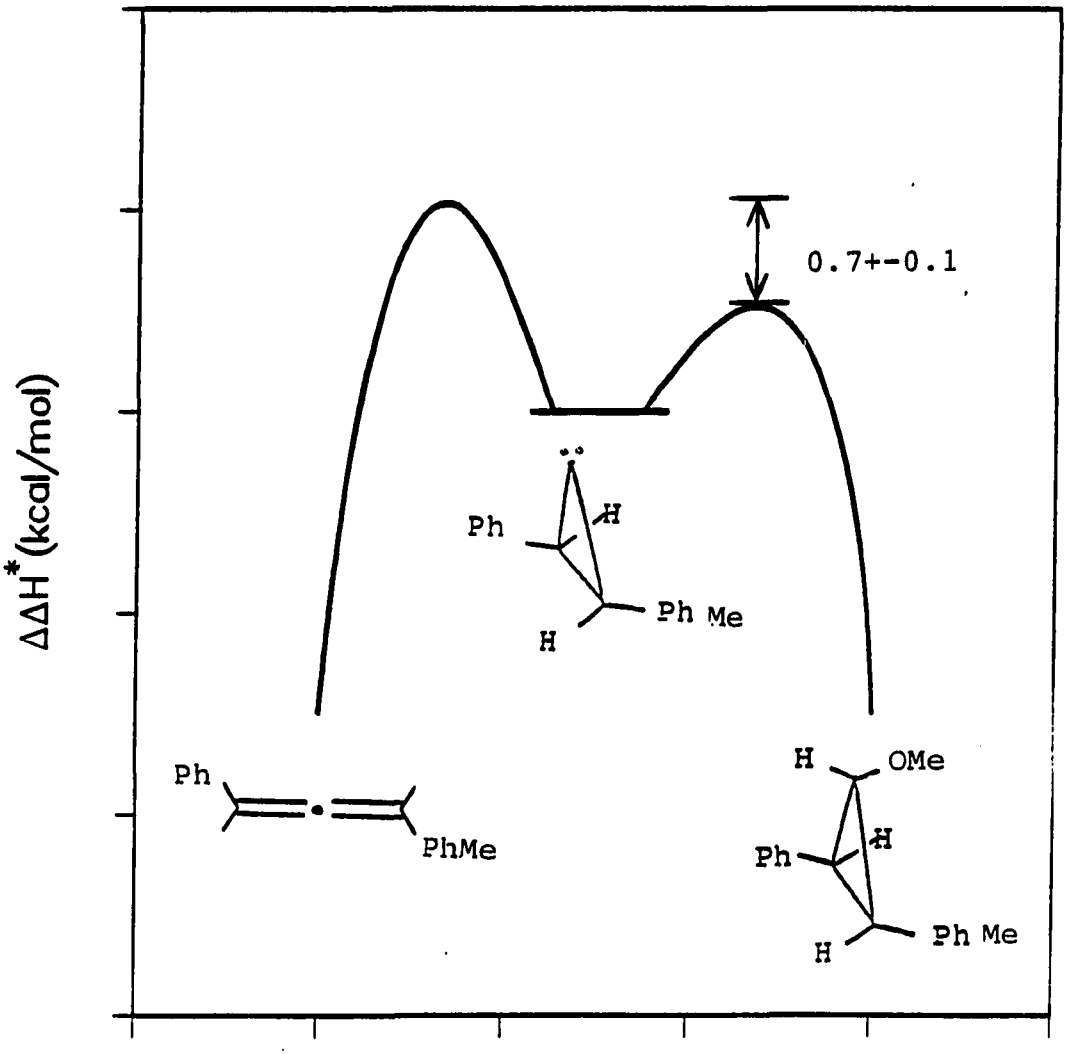

Figure 41. Enthalpy diagram for system f - (ΔH^* (allene)- ΔH^* (ether))

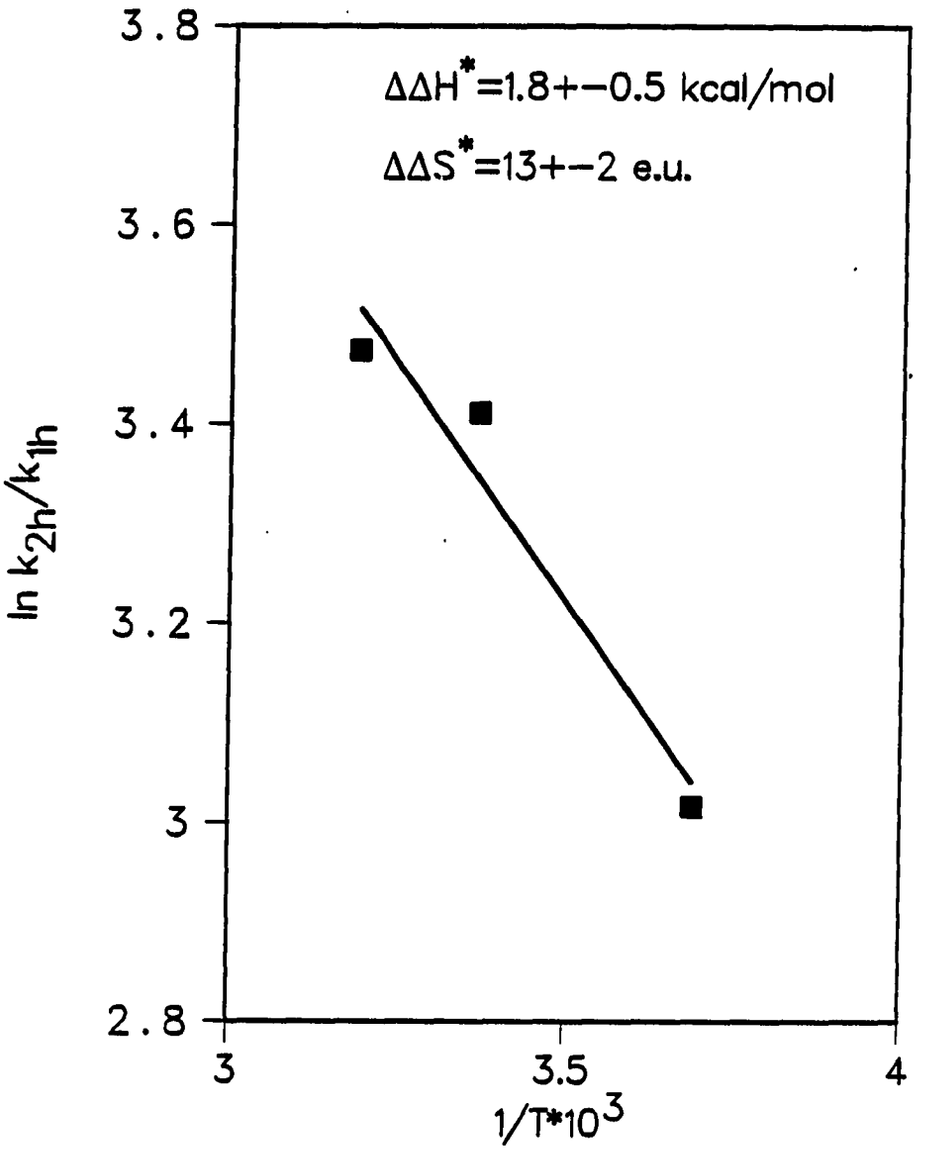

Figure 42. Eyring plot of ln k_{2h}/k_{1h} versus $1/T$ (K^{-1})

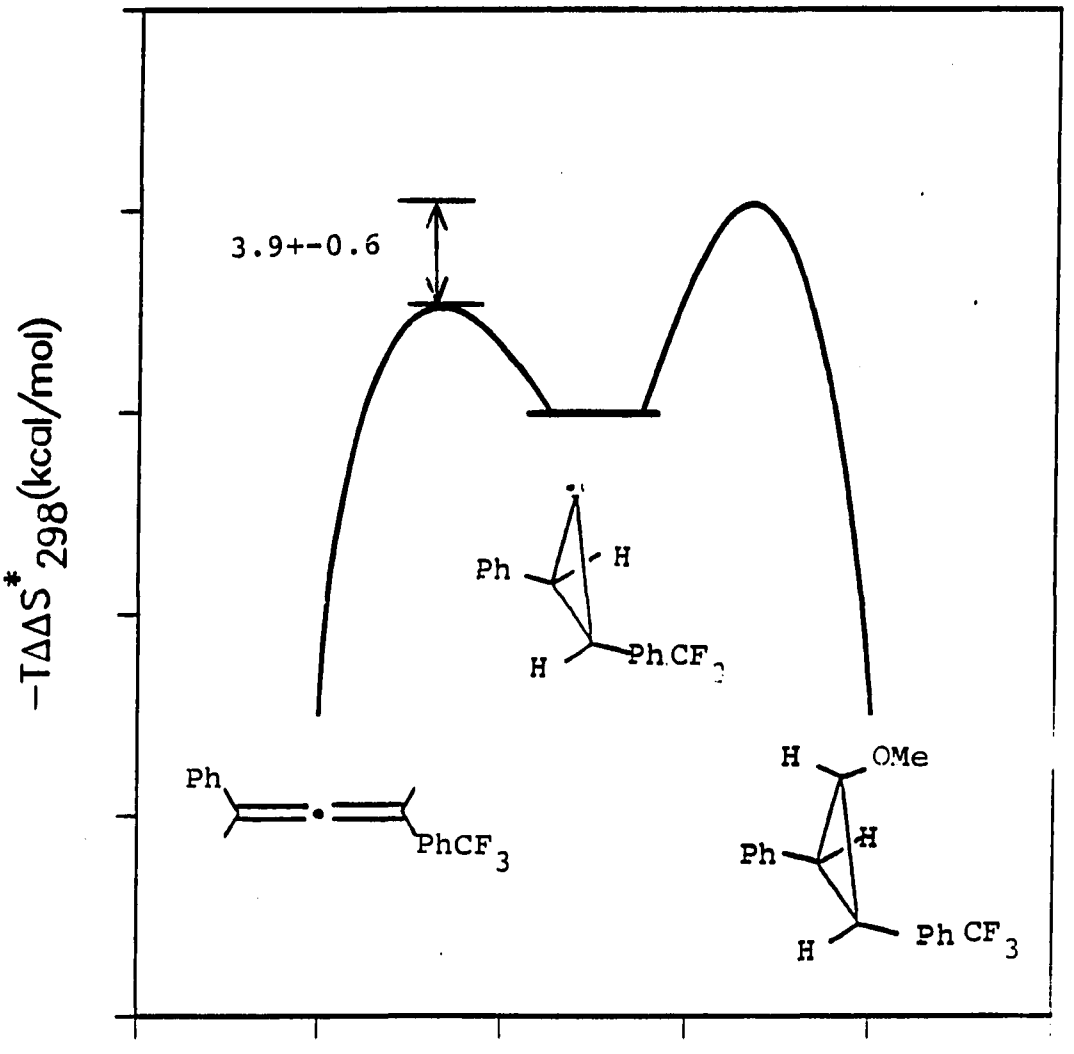

Figure 43. Entropy diagram for system h - T (ΔS* (allene)-ΔS* (ether))

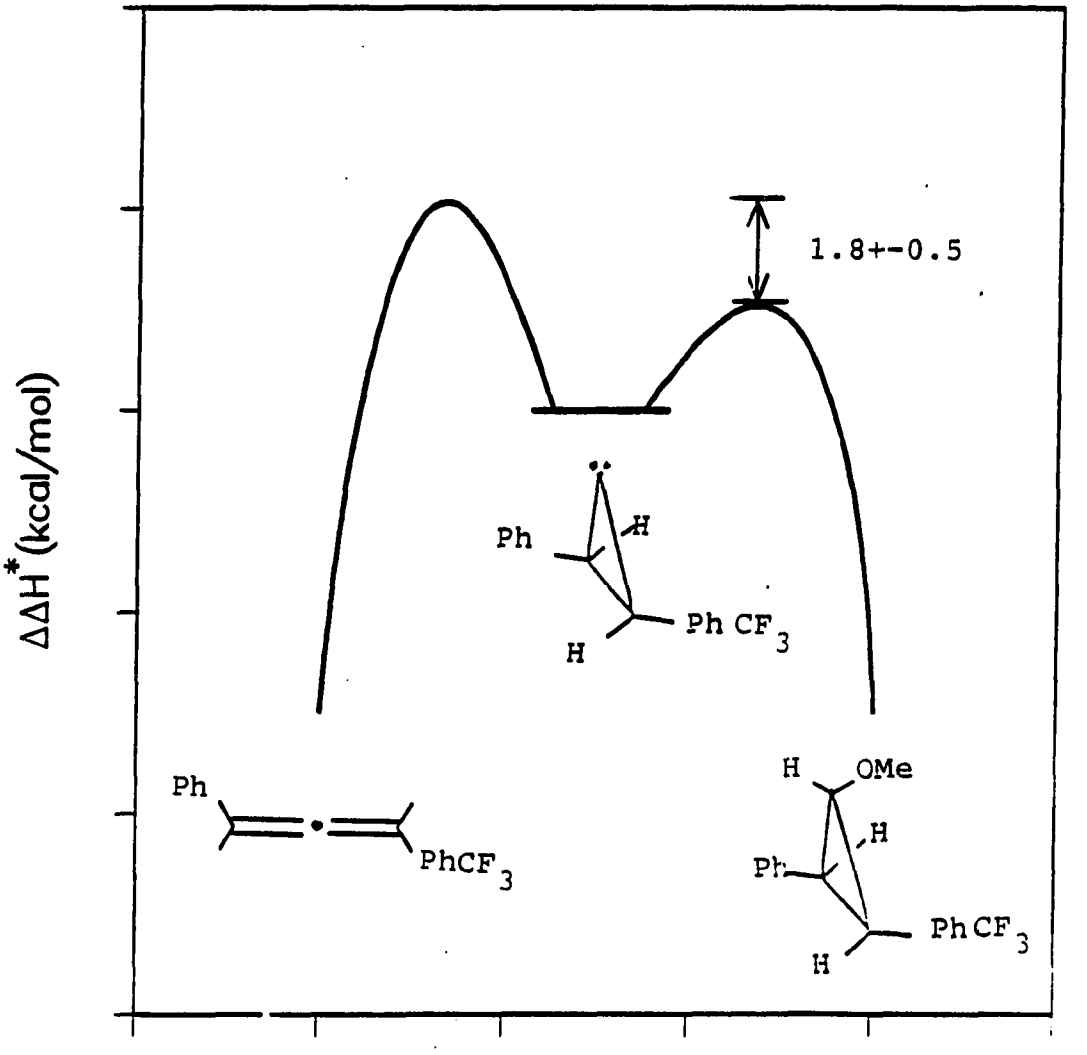

Figure 44. Enthalpy diagram for system h - (ΔH* (allene)-ΔH* (ether))

been collected, Eyring plots were made in order to obtain the relative activation parameters. The thermodynamic data were evaluated with the NLLSQ program in order to obtain the relative entropy and enthalpy of activation along with the sample standard deviations. Although the data were generally well behaved, it is not reasonable to suppose that such limited data would have such small errors. It is, therefore, proposed (although not supported) that errors may be $\pm$ 1 kcal/mol for enthalpies and $\pm$ 3-5 e.u. for entropies.

The rate constant ratios k_2/k_1, for systems a-j, and the Hammett sigma constants (45) are collected in Table 7. When these values are correlated via the Hammett equation (Equation (5)), Equation (6) results, where k_H is the rate constant for the unsubstituted case. Equation (7) may be

$$\log k_x = \log k_H + \rho\sigma \qquad (5)$$

$$\log \frac{k_{2x}}{k_{1x}} = \log \frac{k_{2H}}{k_{1H}} + \rho\sigma \qquad (6)$$

$$\log \left(\frac{k_{2x}}{k_{1x}} \cdot \frac{k_{1H}}{k_{2H}}\right) = \rho\sigma \qquad (7)$$

simplified if one assumes that k_{1x} and k_{1H} are equal. Methanol has been shown to react at a diffusion controlled rate with other carbenes (40). Since theoretical results suggest that carbene orbitals in ground state cyclopropylidene do not interact with other molecular

orbitals, one would expect at least equal reactivity for cyclopropylidene, relative to other carbenes. Equation (7), therefore, may reasonably be written as Equation (8).

$$\log \frac{k_{2x}}{k_{2H}} = \rho\sigma \qquad (8)$$

Figure 45 shows the correlation plot for the data in Table 7; rho was found to be -0.72 ± 0.07 for the seven points indicated. The two points which do not fit the rest of the data may require separate treatment.

The rho value of -0.72 may be rationalized in terms of the transition state structure. The negative sign indicates that the transition state is stabilized by electron donation and destabilized by electron withdrawal. This is consistent with the idea that allyl cation character exists in the transition state. The magnitude of 0.72 gives an indication of the extent of electron demand at the transition state. This demand is tempered in two ways: first the distance between the aryl ring and the reaction center; and secondly, the degree of ring opening and consequent conjugation (orbital rotation affects the ability of the cyclopropyl orbitals to overlap with those of the carbene center).

When discussing correlation analyses, it is useful to compare similar systems. In this way relative rho values may be compared. The solvolysis of aryl substituted

Table 7. Ratio of rate constants k_{2x}/k_{2H} and the corresponding Hammett sigma values

X_1/X_2	k_{2x}/k_{2H}[a]	$\sigma_1 + \sigma_2$
H/H	1.000	0.00
Me/Me	2.143	-0.34
OMe/OMe	2.500	-0.54
Cl/Cl[b]	0.714	+0.46
H/Me	1.364	-0.17
H/Cl	0.556	+0.23
H/CF_3	0.455	+0.54
Me/Cl[b]	2.143	+0.06
Me/CF_3	0.682	+0.37

[a]Actually $k_{2x}k_{1H}/k_{1x}k_{2H}$; see text for why this has been simplified.

[b]Values were not used to determine the slope of the line.

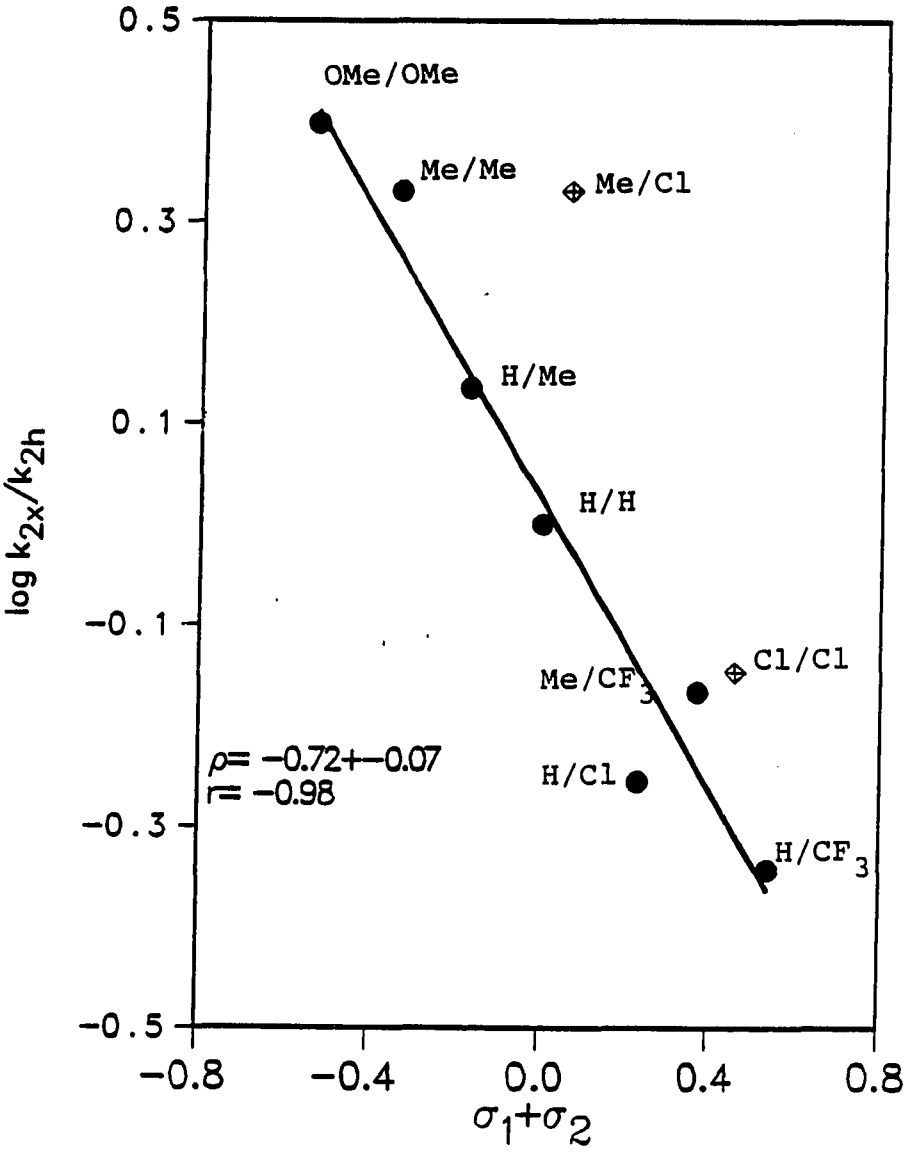

Figure 45. Correlation plot of log k_{2x}/k_{2H} versus the sum of substituent sigmas

cyclopropyl tosylates does show similarities to the cyclopropylidene ring opening. The cyclopropylidene ring opening and the cyclopropyl tosylate solvolysis are both 2π concerted ring openings and develop positive charge in the transition state. One should keep in mind, however, that the solvolysis of cyclopropyl tosylates are assisted by the ring opening; the situation is different for cyclopropylidene (free cyclopropylidene is the sole source of products (15)). The rho value of -0.72 for cyclopropylidene is, therefore, reasonably large when compared to rho = -2.3 for the cyclopropyl tosylate solvolysis. Theoretical calculations had suggested that electronic influences on ring opening of cyclopropylidenes were negligible (36).

In cases where the cyclopropylidene was symmetrically disubstituted, the transition structure could resemble 26. However, the systems that are unsymmetrically substituted

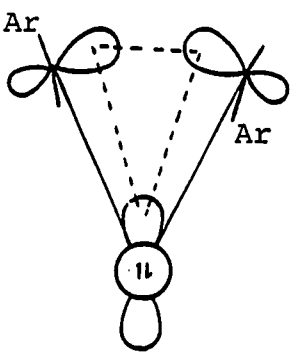

26

have three possible transition structures 26, 27 and 28. It is clear that 28 does not represent a reasonable geometry,

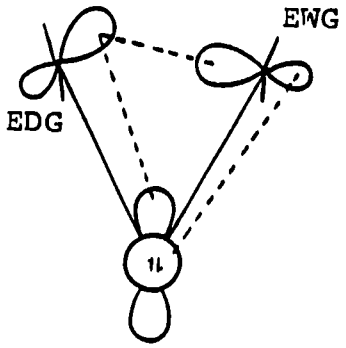

27

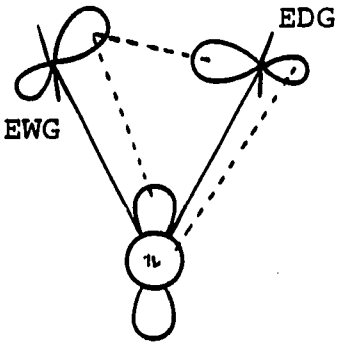

28

and is higher in energy than 27. Structure 27 may be achieved by a concerted disrotatory ring opening in which C_2 C_3 rotation is not synchronus. This would allow electron withdrawing groups to remain better aligned with the filled carbene orbital, and electron donating groups to be better aligned with the empty carbene orbital.

In seven of the nine systems studied, the sigma values of the substituents appear to be additive and generate a linear correlation. However, 18d and 18i show a marked acceleration in ring opening rates over what was expected based on the results for the other seven cases. Both of these disubstituted systems contain a para chloro-substituent which may be the source of the discrepancy. Since chlorine is relatively soft and polarizable, it is tempting to speculate that this polarizability leads to a

net increase in the rate of ring opening. There is, however, no direct evidence to support such a suggestion.

Finally, it is evident from the thermodynamic data that the ring opening of cyclopropylidenes is an entropically favored reaction, relative to methanol trapping. Internal rotational degrees of freedom apparently overcome the C_2-C_3 bond energy in driving the reaction toward allene.

In summary, the following conclusions may be offered:

(i) The cyclopropylidene to allene ring opening rate increases when electron donors are attached to C_2 and/or C_3, and decrease when electron acceptors are similarly attached.

(ii) The transition state is cationic in nature insofar as C_2 and C_3 are concerned, with a fairly large interaction existing between the carbene center and the developing p-orbitals at C_2 and C_3.

(iii) Relative to insertion into methanol, the ring opening of cyclopropylidene is favored entropically, while being disfavored enthalpically.

(iv) It is predicted that at least some unsymmetrically disubstituted cyclopropylidenes pass through ring-opening transition states which are unsymmetrical with respect to the developing p-orbitals. It is further predicted that if these compounds were optically active, they would yield allenes of higher optical purity than symmetrically

disubstituted cyclopropylidenes (this would be reasonable evidence for structure 27 and of electronic control of the stereochemical outcome).

EXPERIMENTAL

General

Infrared spectra were recorded on an IBM FT-IR98 spectraphotometer. The proton and carbon magnetic resonance spectra were obtained on a Nicolet 300 FT-NMR spectrometer, using deuterochloroform, perdeutero-benzene and perdeutero-acetone as solvents. Exact mass and GLPC exact mass spectra were recorded on the High Resolution MS-50 mass spectrometer. GLPC analysis was performed on a Hewlett-Packard HP5890 gas chromatograph, which was fitted with a 30 meter DB-1 capillary column and a flame ionization detector. Melting points were taken on a Thomas-Hoover melting point apparatus and were not corrected.

Synthesis and reactions

Preparation of diphenylphosphoryl azide (21) (Figure 46)

A 250 ml round bottom flask was charged with 94 g of phenol and 76 g of phosphorous oxychloride. The stirred mixture was heated to 180°C for 2 hours, the product was then vacuum distilled. The product diphenylphosphoryl chloride was collected at 130-140°C at 0.15 Torr. The product fraction gave 13.9 g, 40% yield based on 50% conversion. The 13.9 g of diphenylphosphoryl chloride was dissolved in 20 ml of acetone and treated with 6.6 g of sodium azide in 20 ml of water, for 3 hours at room temperature. The product 21 was

extracted into ether and dried over magnesium sulfate. Yield of 21 was 12.8 g, 90% from diphenylphosphoryl chloride.

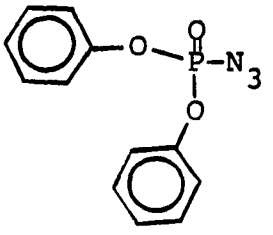

21

FT-IR (neat): 3406 (w), 3078 (w), 2172 (s), 1602 (s), 1485 (s) cm^{-1}.

Preparation of ethyl diazoacetate A 500 ml 3 neck round bottom flask was charged with 70 g of ethyl glycinate hydrochloride in 100 ml of water, 250 ml of methylene chloride and 42 g of sodium nitrite in 80 ml of water. The mechanically stirred solution was then cooled to -20°C and 45 g of 5% sulfuric acid was added over 5 minutes. The reaction was over in 15 minutes and the cold solution was poured into a 1 l separatory funnel. The organic phase was washed with several portions of cold 5% sodium bicarbinate solution. The organic phase was dried over magnesium sulfate and the solvent was removed under reduced pressure. The golden-yellow product was used without further purification.

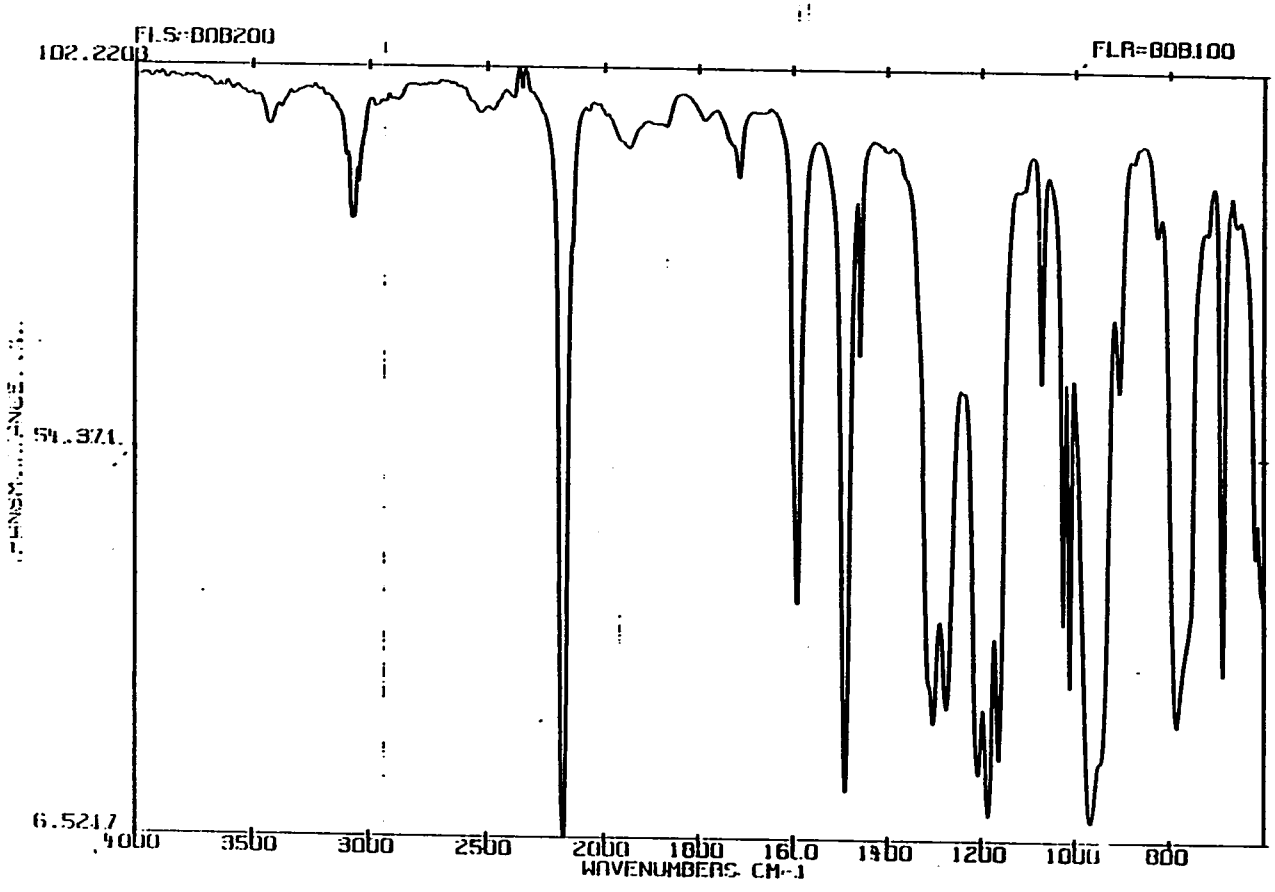

Figure 46. FT-IR of 21 neat

General synthesis of para substituted benzyltriphenylphosphonium halides (11 a-e)

Preparation of benzyltriphenylphosphonium chloride (11a)

A 250 ml round bottom flask was charged with 10 g of benzyl chloride, 100 ml of xylene and 21.6 g of triphenylphosphine. The stirred mixture was refluxed for 18 hours to give 20.1 g of white crystalline precipitate 11a in 70% yield, m.p. > 300°C.

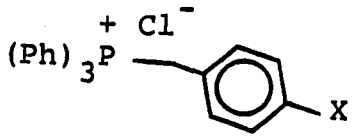

11a-e

X = H (a), CH_3 (b), OCH_3 (c), Cl (d), CF_3 (e)

p-Methylbenzyltriphenylphosphonium chloride (11b)

Prepared from α-chloro-p-xylene in 86% yield, m.p. > 300°C.

p-Methoxybenzyltriphenylphosphonium chloride (11c)

Prepared from p-methoxybenzyl chloride in 83% yield, m.p. > 300°C.

p-Chlorobenzyltriphenylphosphonium chloride (11d)

Prepared from p-chlorobenzyl chloride in 86% yield m.p. > 300°C.

p-Trifluoromethylbenzyltriphenylphosphonium bromide (11e) Prepared from p-trifluoromethylbenzyl bromide in 96% yield m.p. 245-246°C.

General synthesis of trans-4,4'-disubstituted stilbenes (13a-j)

Preparation of trans-4,4'-dimethylstilbene (13b) (Figures 47, 48) A 250 ml round bottom flask was charged with 34 g of 11b, 100 ml of absolute ethanol and 10 g of p-tolualdehyde. To this was added 10 g of potassium t-butoxide and the reaction stirred for 1 hour. Then 40 ml of water was added and the product was filtered off to give 9.2 g of 13b as a crystalline white solid in 53% yield, m.p. 179-180°C (lit. m.p. 180°C (47)). In cases where the cis isomer is significant it may be isomerized to trans by refluxing the crude reaction mixture in toluene with iodine present.

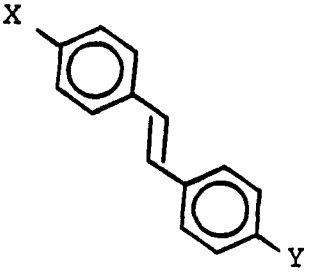

13a-j

X/Y = H/H (a), CH_3/CH_3 (b), OCH_3/OCH_3 (c), Cl/Cl (d), CF_3/CF_3 (e), H/CH_3 (f), H/Cl (g), H/CF_3 (h), CH_3/Cl (i), CH_3/CF_3 (j)

HRMS: Calculated $C_{16}H_{16}$ m/e 208.12520
measured m/e 208.12520 error 0.0 ppm.

^{1}H NMR ($CDCl_3$): δ 7.38 (d), δ 7.14 (d), δ 7.00 (s), δ 2.35 (s).

FT-IR ($CDCl_3$): 3031 (w), 3000 (w), 2922 (w), 1520 (w), 980 (s), 820 (s) cm^{-1}.

^{13}C NMR ($CDCl_3$): δ 137.2 (rel. intens. 30), δ 134.7 (29), δ 129.3 (60), δ 127.6 (40), δ 126.3 (100), δ 21.3 (20).

Trans-stilbene (13a) The commercial product was used without further purification.

Trans-4,4'-dimethoxystilbene (13c) (Figures 49, 50)

Prepared from 11c and p-methoxybenzaldehyde in 87% yield, m.p. 207-210°C (lit. m.p. 214-215°C (48)).

HRMS: Calculated $C_{16}H_{16}O_2$ m/e 240.11503
measured 240.11519 error 0.7 ppm.

^{1}H NMR ($CDCl_3$): δ 7.40 (d), δ 6.91 (s), δ 6.87 (d), δ 3.81 (s).

FT-IR ($CDCl_3$): 2969 (w), 2953 (w), 2938 (w), 1544 (w), 1508 (m), 1410 (m), 1009 (s) cm^{-1}.

^{13}C NMR ($CDCl_3$): δ 159.0 (rel. intens. 40), δ 130.5 (38), δ 127.4 (100), δ 126.2 (60), δ 114.1 (100), δ 55.3 (80).

Trans-4,4'-dichlorostilbene (13d) (Figures 51, 52)

Prepared from 11d and p-chlorobenzyaldehyde in 78% yield, isomerized with iodine in refluxing toluene, m.p. 173-174°C (lit. m.p. 177-178°C (49)).

HRMS: Calculated $C_{14}H_{10}Cl_2$ m/e 248.01596
measured m/e 248.01629 error 1.3 ppm.

^1H NMR ($CDCl_3$): δ 7.41 (d), δ 7.31 (d), δ 6.99 (s).

FT-IR ($CDCl_3$): 3000 (w), 1610 (w), 1500 (m), 1408 (m), 980 (s), 810 (s) cm^{-1}.

^{13}C NMR ($CDCl_3$): δ 135.5 (rel. intens. 30), δ 133.4 (30), δ 128.9 (100), δ 128.0 (60), δ 127.7 (80).

Trans-4,4'-bis(trifluoromethyl)stilbene (13e) (Figures 53, 54) Prepared from 11e and p-trifluoromethylbenzaldehyde, isomerized with iodine in refluxing toluene in 76% yield, m.p. 133-133.5°C (lit. m.p. 124-127°C (50)).

HRMS: Calculated $C_{16}H_{10}F_6$ m/e 316.06868
measured m/e 316.06820 error -1.5 ppm.

^1H NMR ($CDCl_3$): δ 7.61 (s), δ 7.18 (s).

FT-IR ($CDCl_3$): 1612 (m), 1333 (s), 1178 (m), 1111 (s), 1067 (s) cm^{-1}.

^{13}C NMR ($CDCl_3$): δ 140.1 (rel. intens. 50), δ 129.6 (80), δ 126.8 (100), δ 125.7 (80).

Trans-4-methylstilbene (13f) (Figures 55, 56)

Prepared from 11a and p-tolualdehyde, isomerized with iodine in refluxing toluene in 75% yield, m.p. 116-118°C (lit. m.p. 120°C (51)).

HRMS: Calculated $C_{15}H_{14}$ m/e 194.10955
measured m/e 194.10975 error 1.0 ppm.

^1H NMR ($CDCl_3$): δ 7.60-7.00 (m), δ 2.37 (s).

FT-IR ($CDCl_3$): 3000 (w), 1590 (w), 1000 (m), 920 (s), 805 (s), 750 (s), cm^{-1}.

^{13}C NMR ($CDCl_3$): δ 137.5 (rel. intens. 30), δ 137.4 (30), δ 134.5 (15), δ 129.3 (95), δ 128.6 (90), δ 127.6 (40), δ 127.3 (40), δ 126.4 (100), δ 21.2 (25).

Trans-4-chlorostilbene (13g) (Figures 57, 58)

Prepared from 11d and benzaldehyde, isomerized with iodine in refluxing toluene in 66% yield, m.p. 126-128°C (lit. m.p. 130°C (52)).

HRMS: Calculated $C_{14}H_{11}Cl$ m/e 214.05493
measured m/e 214.05513 error 0.9 ppm.

^1H NMR (Acetone-d6):
δ 7.6-7.5 (m), δ 7.4-7.3 (m), δ 7.3-7.2 (m).

FT-IR ($CDCl_3$): 3000 (w), 1420 (m), 1400 (m), 982 (s), 809 (s) cm^{-1}.

^{13}C NMR ($CDCl_3$): δ 136.9 (rel. intens. 40), δ 135.8 (39), δ 133.1 (20), δ 129.3 (60), δ 128.8 (100), δ 128.6 (90), δ 127.8 (60), δ 127.3 (50), δ 126.5 (65).

Trans-4-trifluoromethylstilbene (13h) (Figures 59, 60)

Prepared from 11a and p-trifluoromethylbenzaldehyde, isomerized with iodine in refluxing toluene in 65% yield, m.p. 127-130°C (lit. m.p. 132-133°C (53)).

HRMS: Calculated $C_{15}H_{11}F_3$ m/e 248.08129
measured m/e 248.08146 error 0.7 ppm.

^1H NMR ($CDCl_3$): δ 7.2-6.6 (m).

FT-IR ($CDCl_3$): 3000 (w), 1600 (w), 1380 (m), 1115 (s), 806 (m) cm^{-1}.

^{13}C NMR ($CDCl_3$): δ 140.8 (rel. intens. 20), δ 136.5 (30), δ 132.1 (10), δ 132.0 (10), δ 131.2 (60), δ 128.7 (90), δ 128.2 (70), δ 127.1 (50), δ 126.7 (95), δ 126.5 (100), δ 125.6 (50), δ 125.5 (40).

Trans-4-chloro-4'-methylstilbene (13i) (Figures 61, 62)

Prepared from 11d and p-tolualdehyde in 70% yield, m.p. 200-204°C (lit. m.p. 203-204°C (54)).

HRMS: Calculated $C_{15}H_{13}Cl$ m/e 228.07058
measured m/e 228.07082 error 1.0 ppm.

^1H NMR ($CDCl_3$): δ 7.5-7.1 (m), δ 7.01 (q), δ 2.35 (s).

FT-IR ($CDCl_3$): 3000 (w), 908 (m), 810 (s) cm^{-1}.

^{13}C NMR ($CDCl_3$): δ 136.0 (rel. intens. 30), δ 134.2 (40), δ 129.4 (100), δ 129.2 (30), δ 128.8 (90), δ 127.5 (90), δ 126.4 (95), δ 126.3 (50), δ 21.3 (5).

Trans-4-methyl-4'-trifluoromethylstilbene (13j) (Figures 63, 64) Prepared from 11b and p-trifluoromethylbenzaldehyde, isomerized with iodine in refluxing toluene in 83% yield, m.p. 187-189°C.

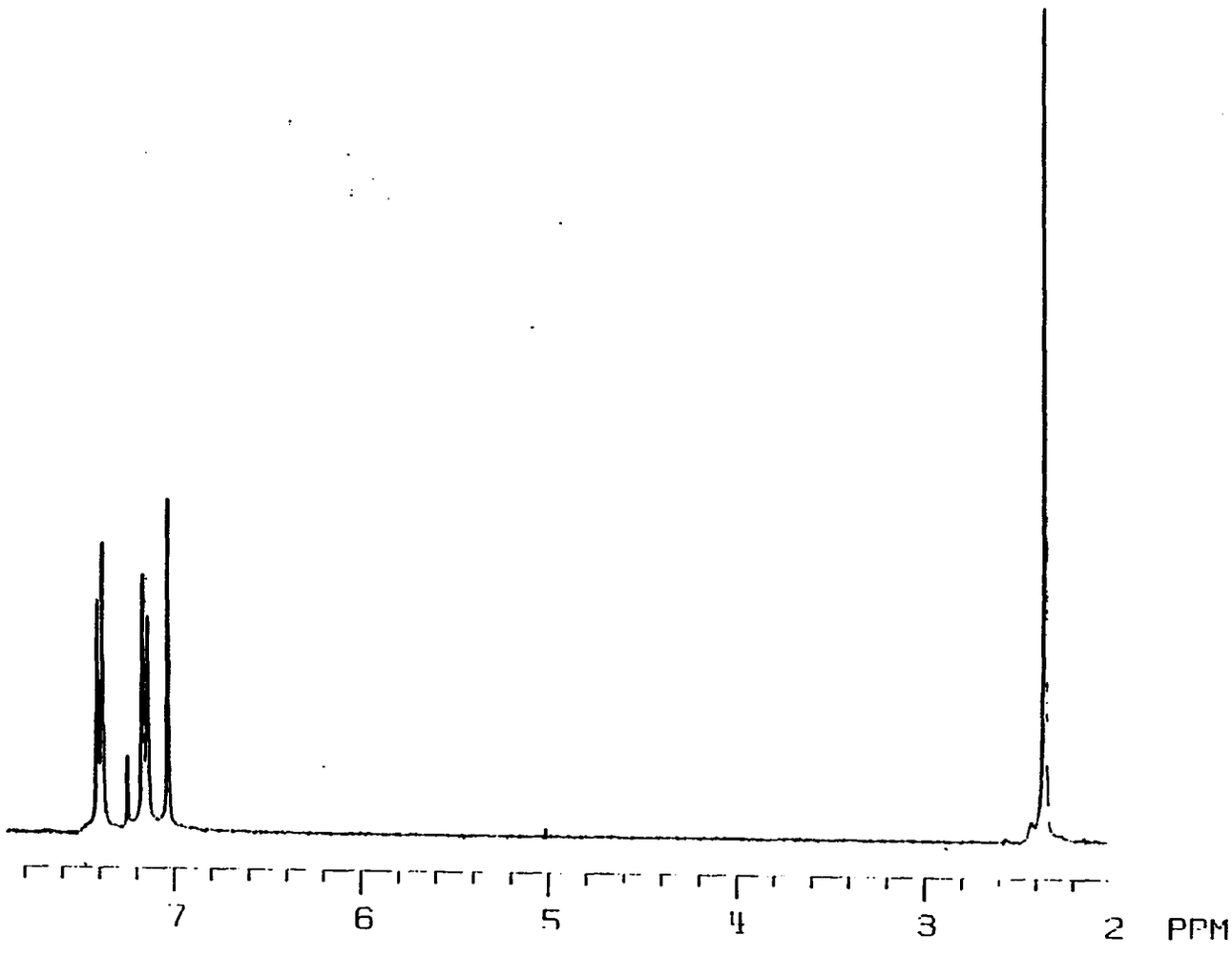

Figure 47. ^{1}H NMR of 13b in $CDCl_3$

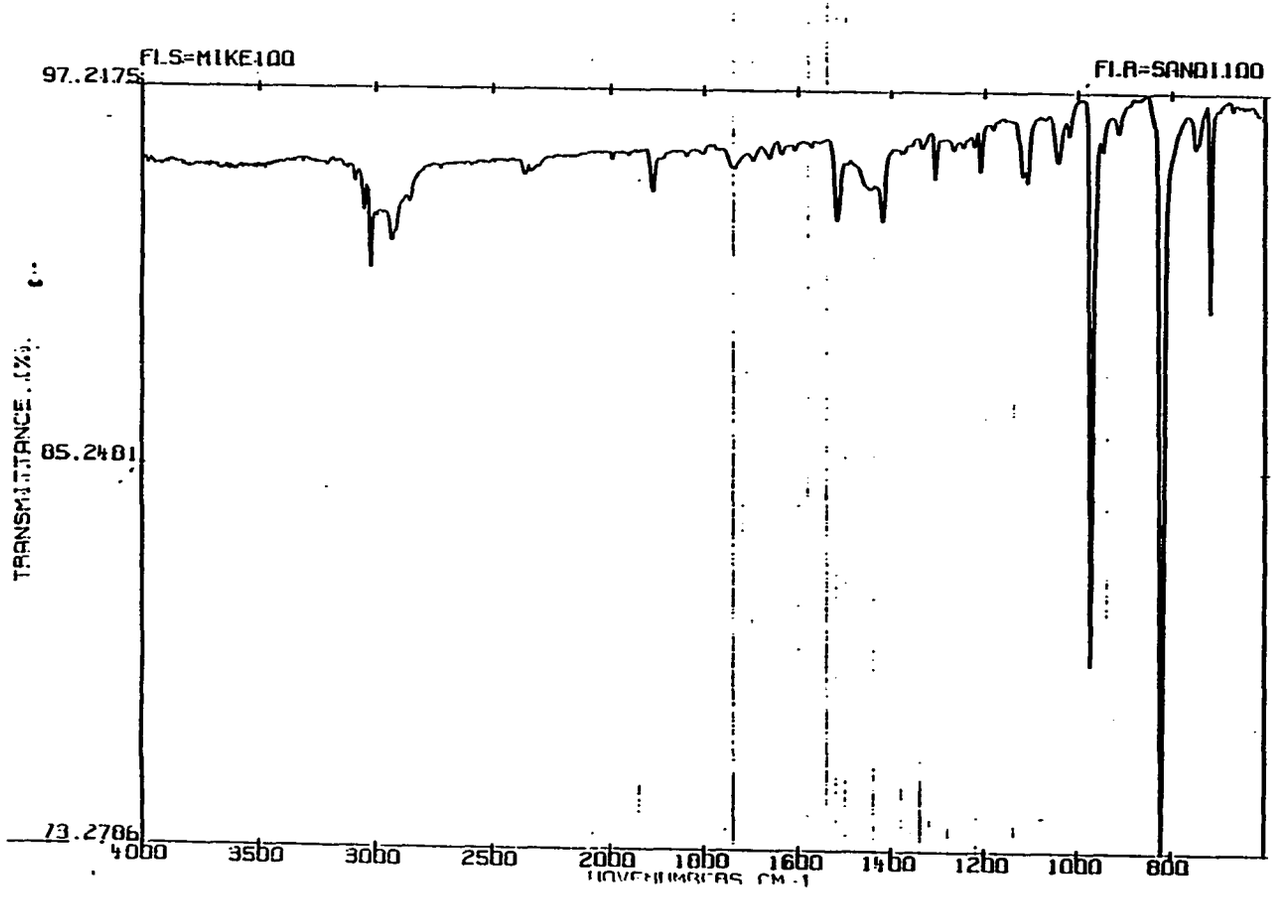

Figure 48. FT-IR of 13b in $CDCl_3$

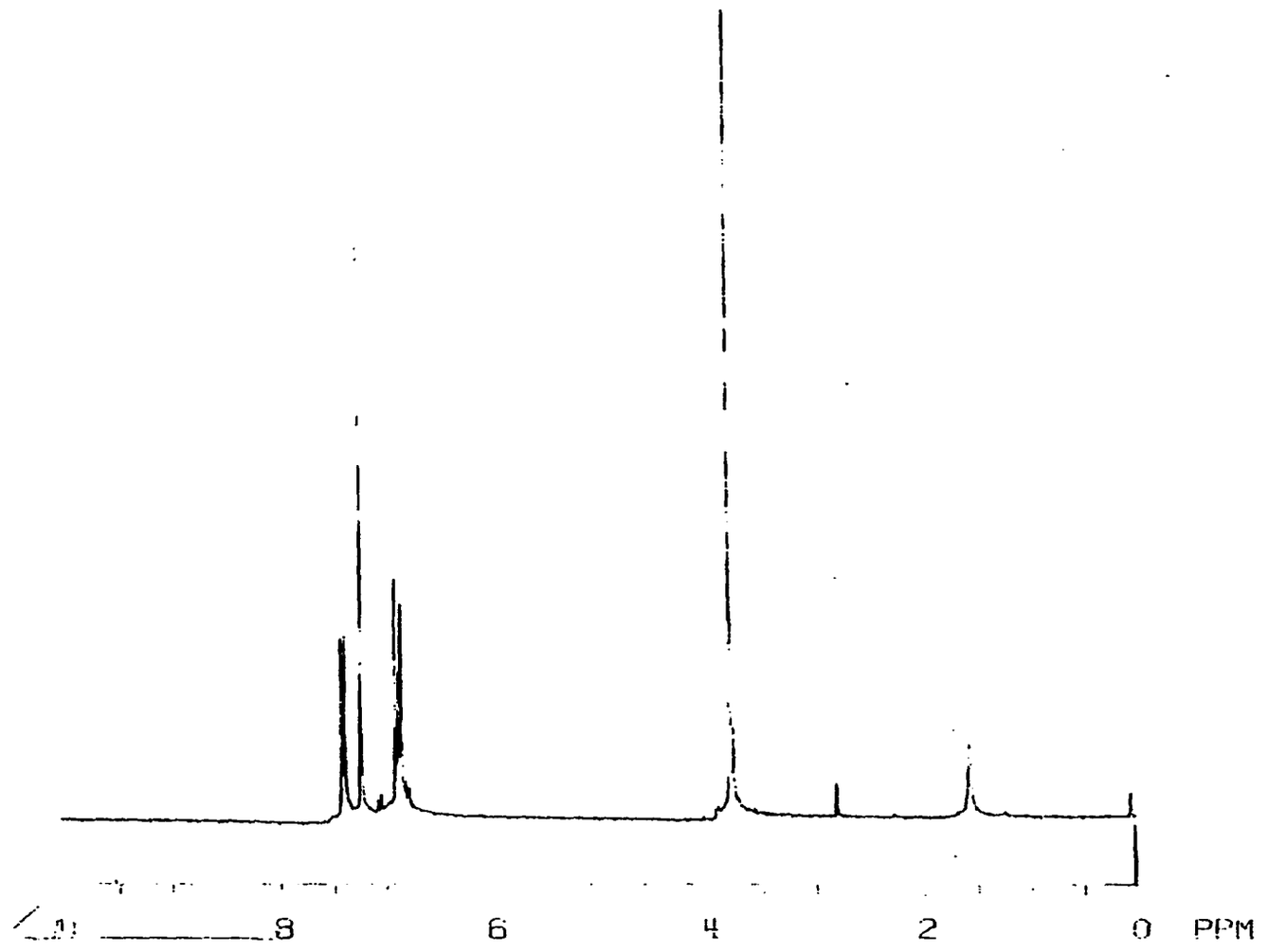

Figure 49. ^1H NMR of 13c in $CDCl_3$

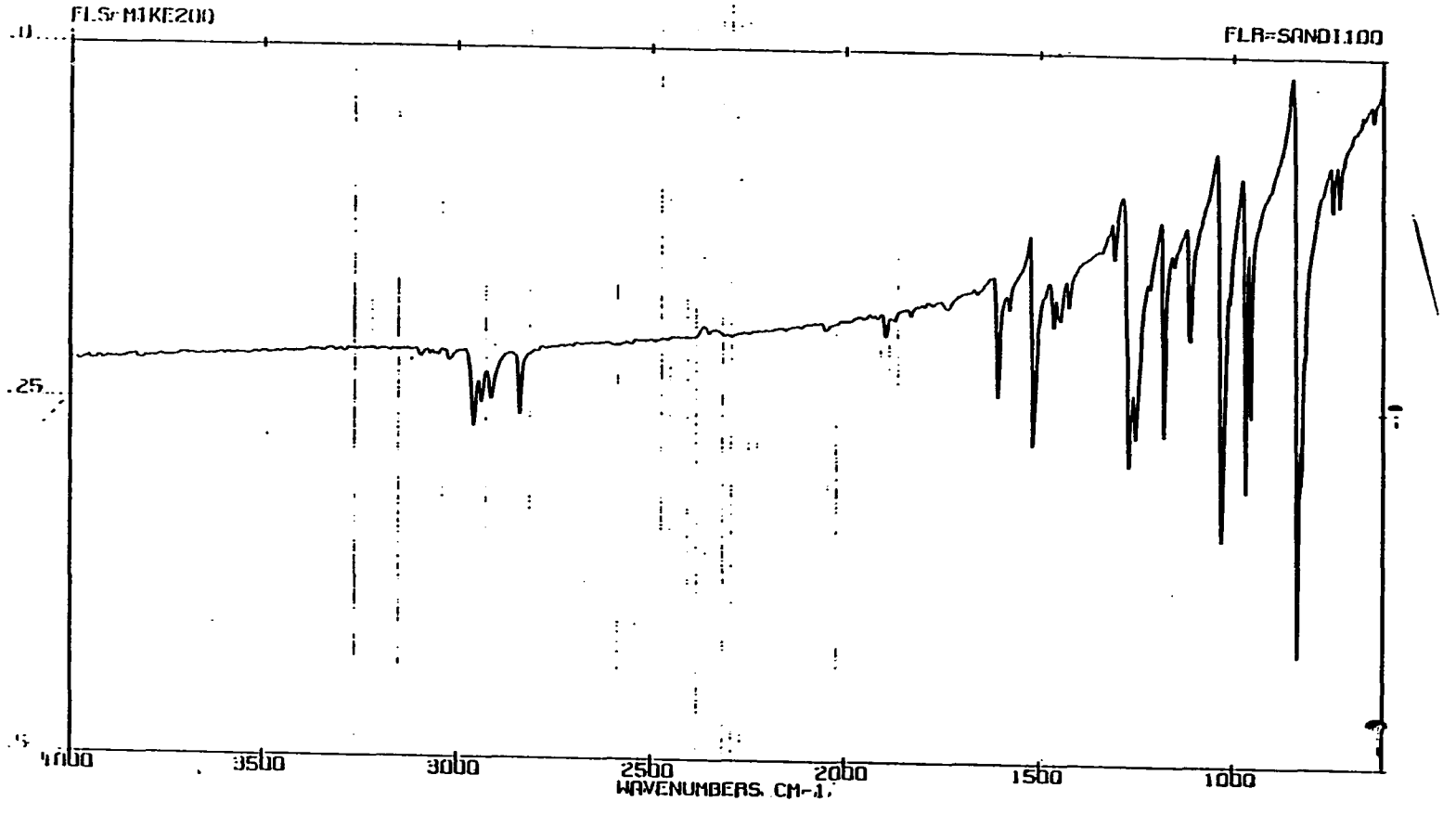

Figure 50. FT-IR of 13c in $CDCl_3$

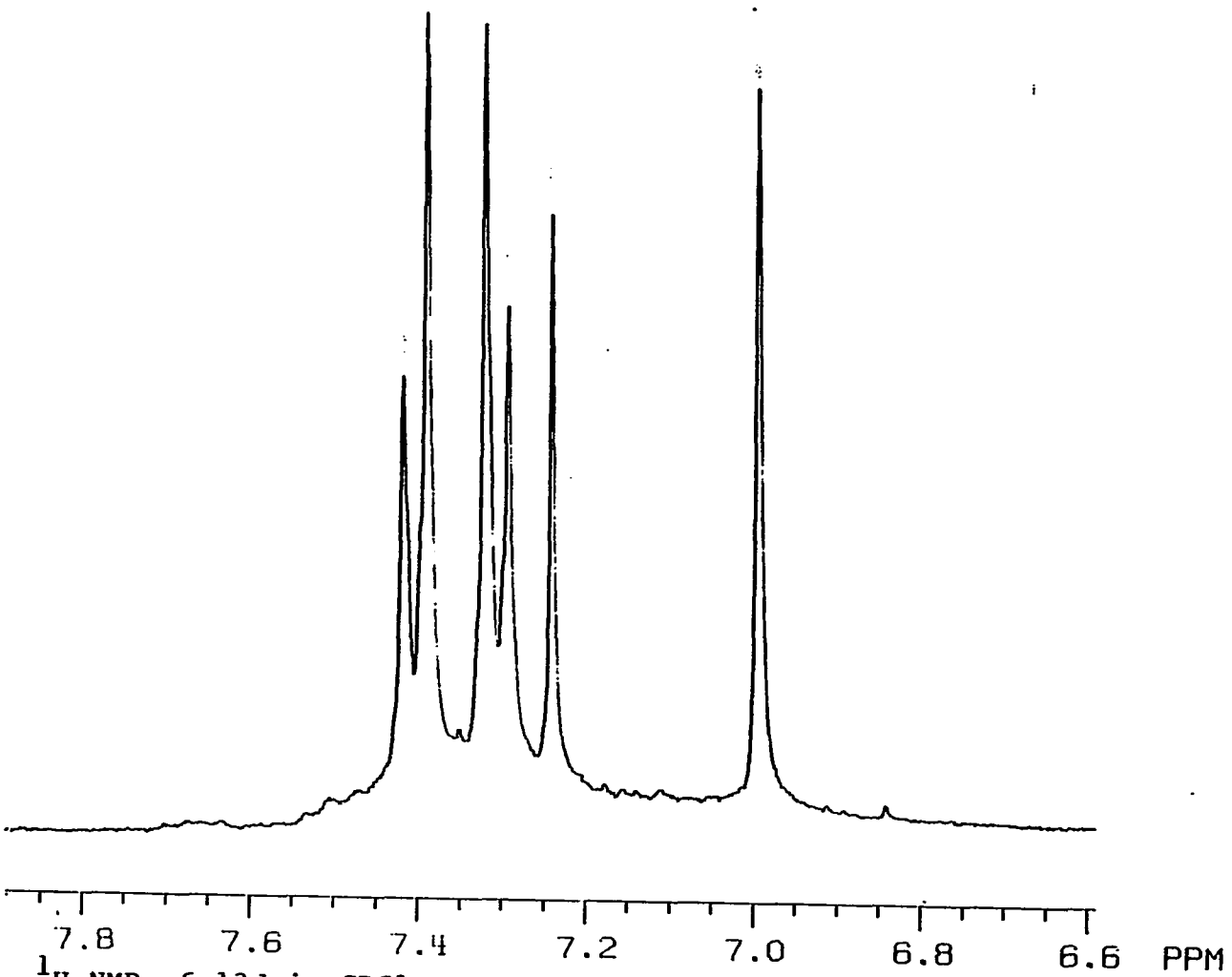

Figure 51. ^{1}H NMR of 13d in $CDCl_3$

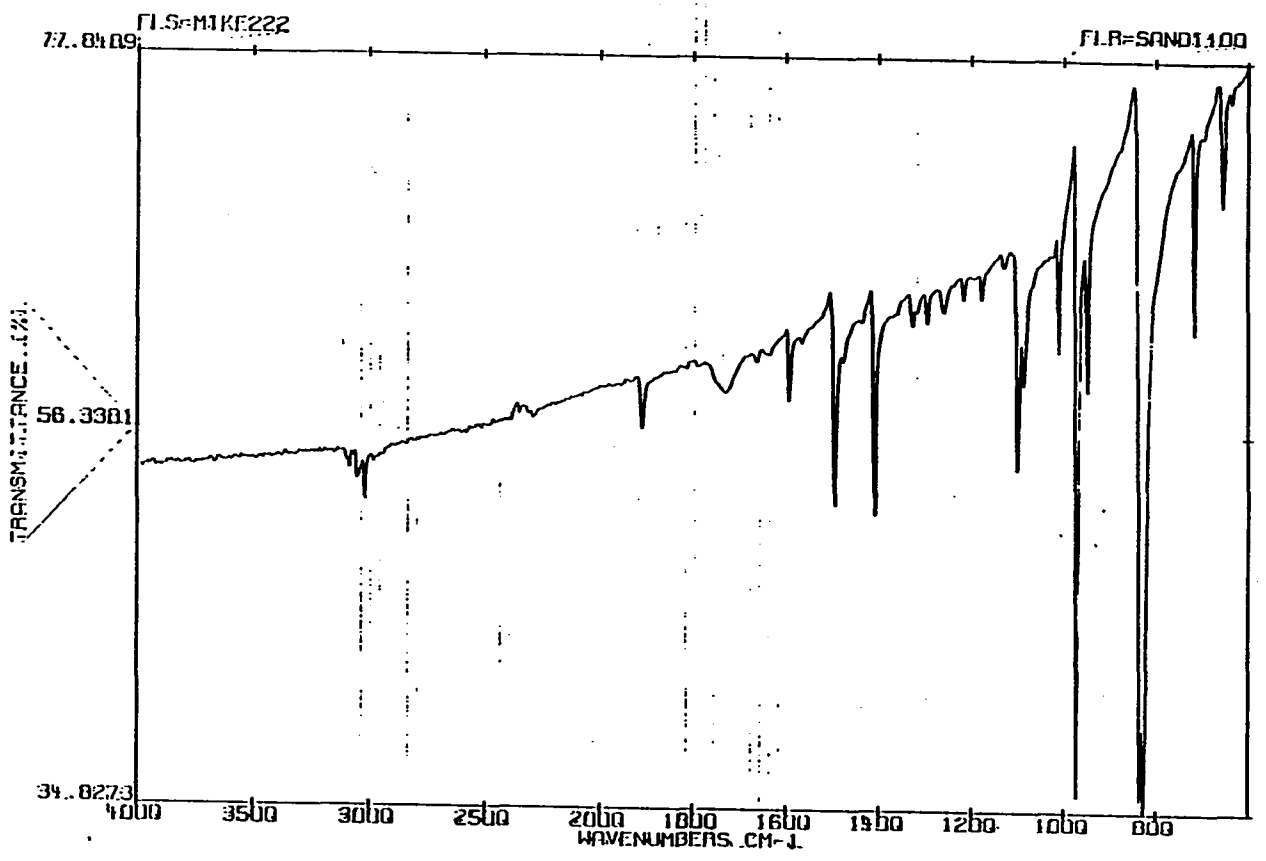

Figure 52. FT-IR of 13d in $CDCl_3$

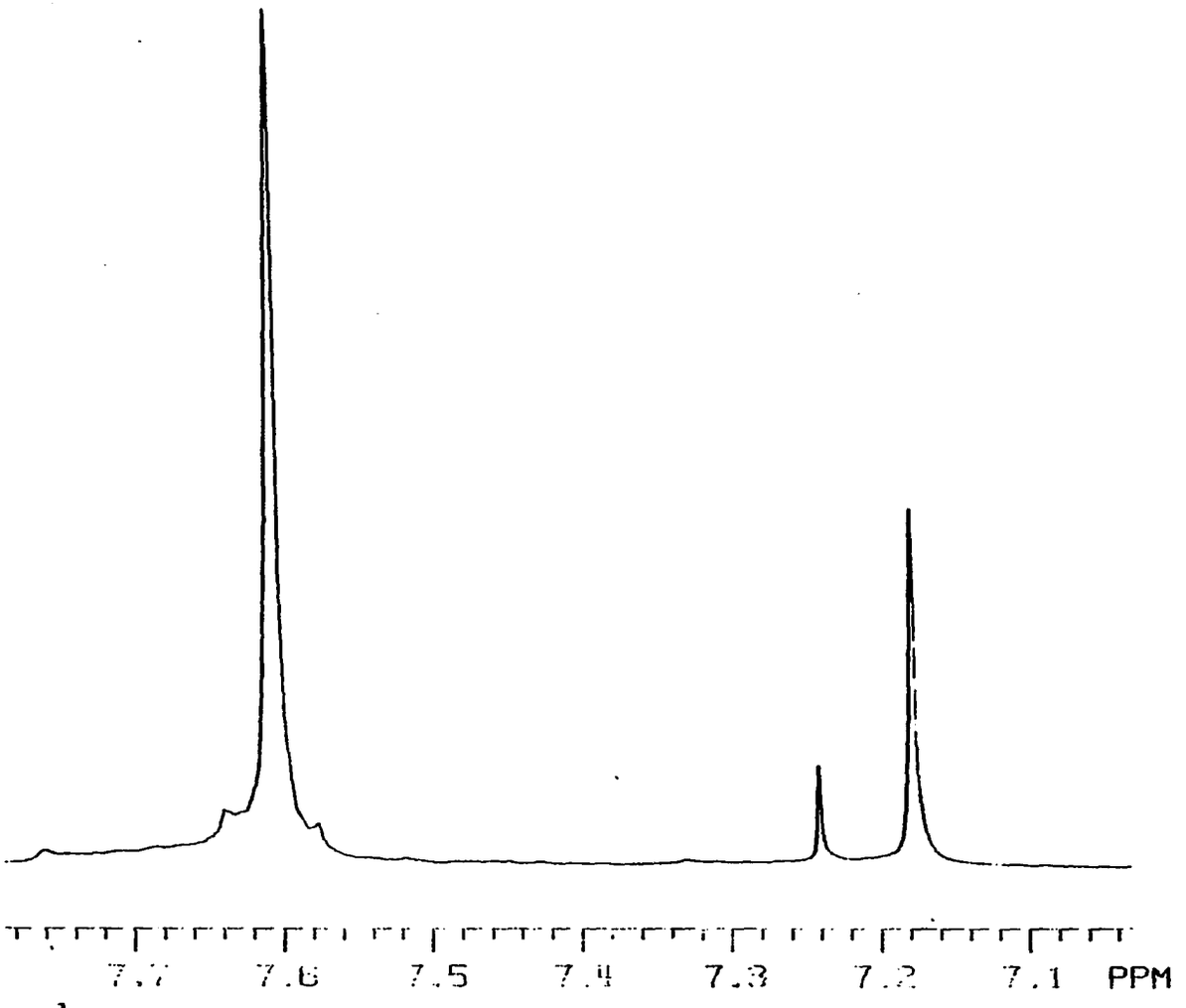

Figure 53. ^{1}H NMR of 13e in $CDCl_3$

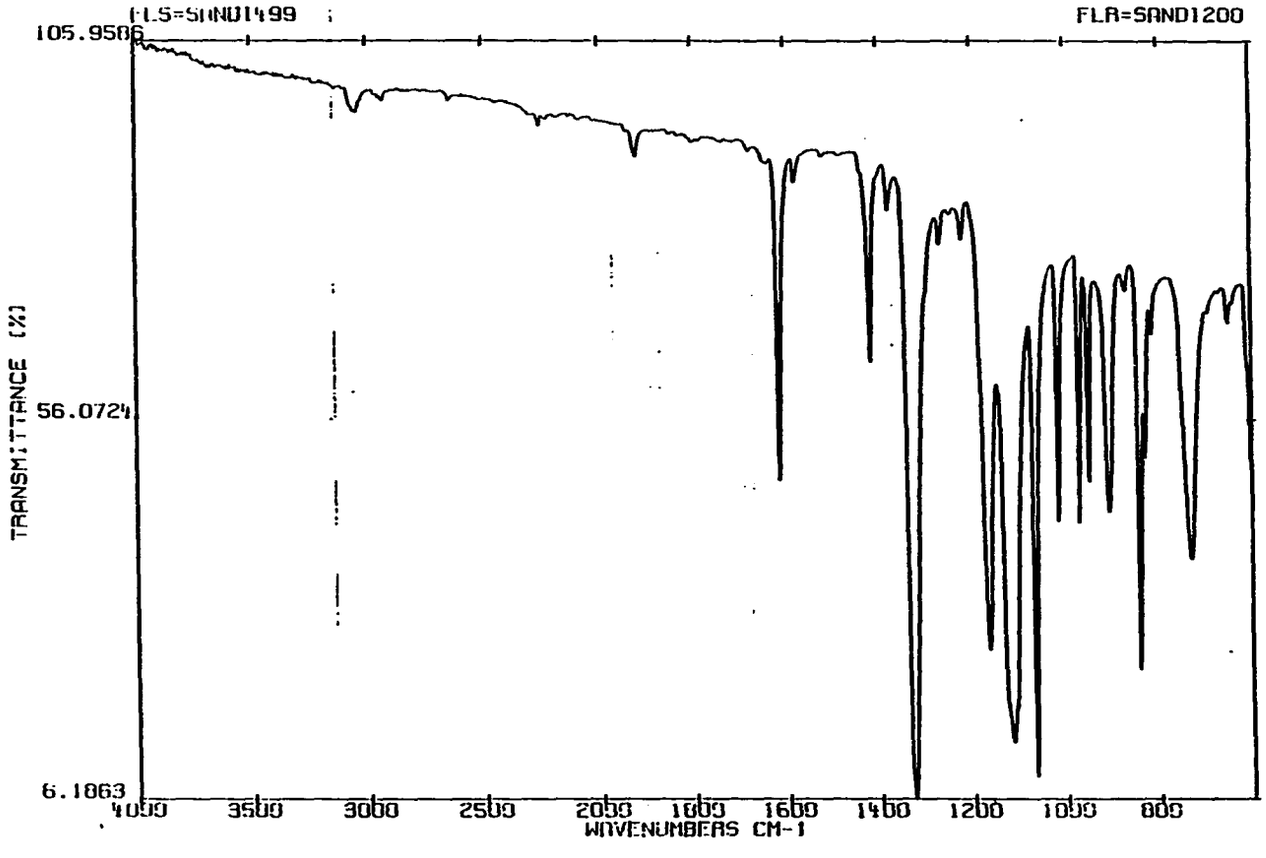

Figure 54. FT-IR of 13e in $CDCl_3$

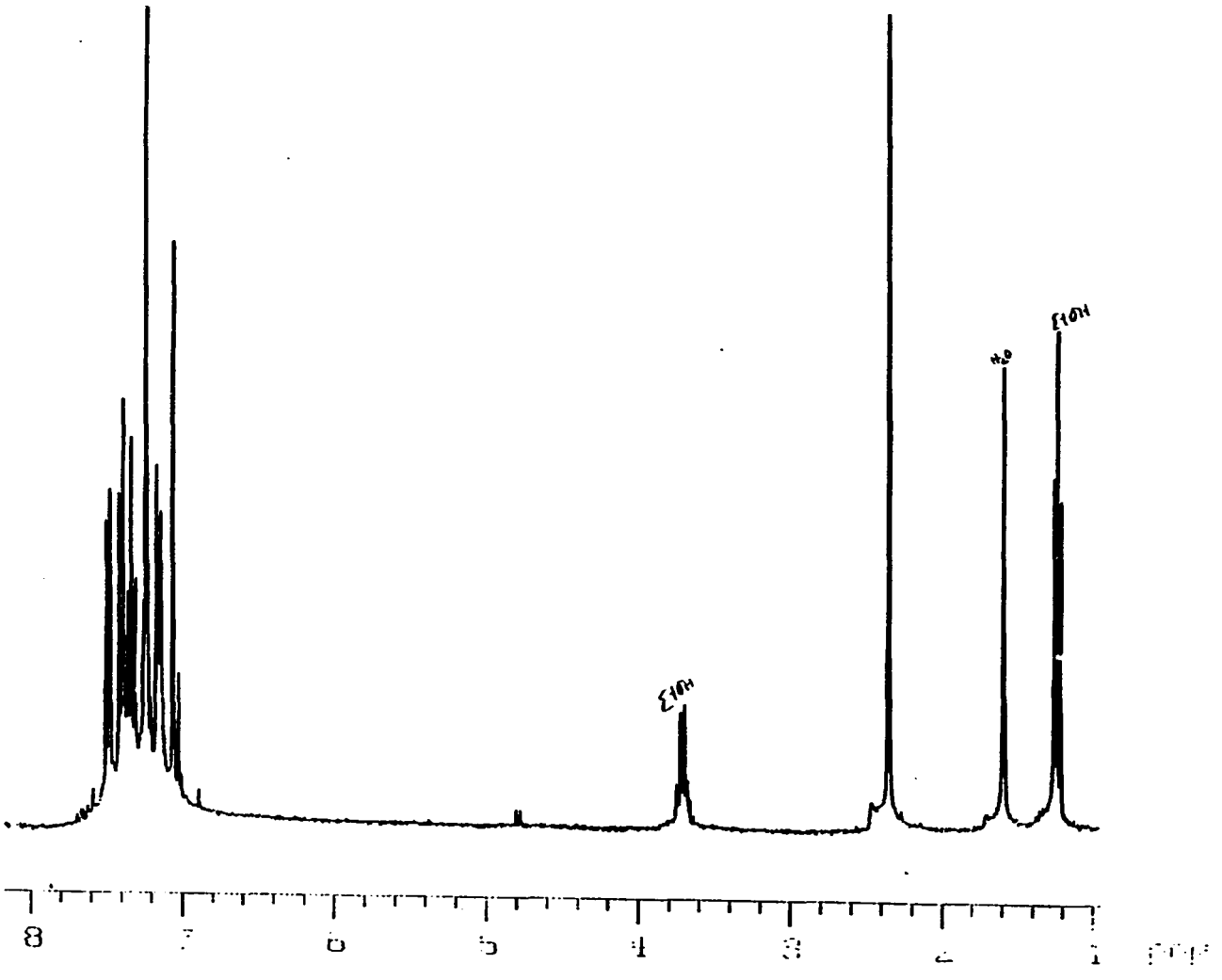

Figure 55. ^{1}H NMR of 13f in $CDCl_3$

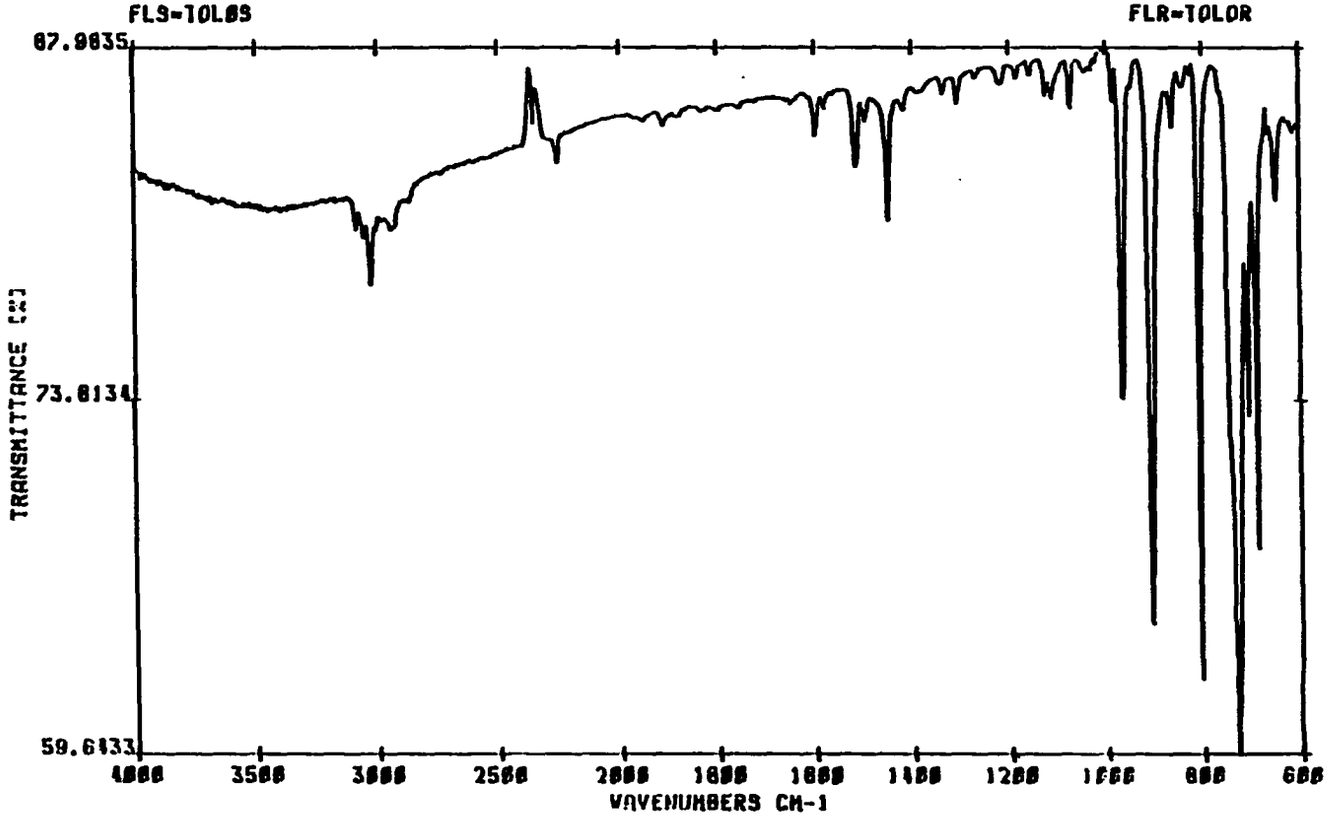

Figure 56. FT-IR of 13f in $CDCl_3$

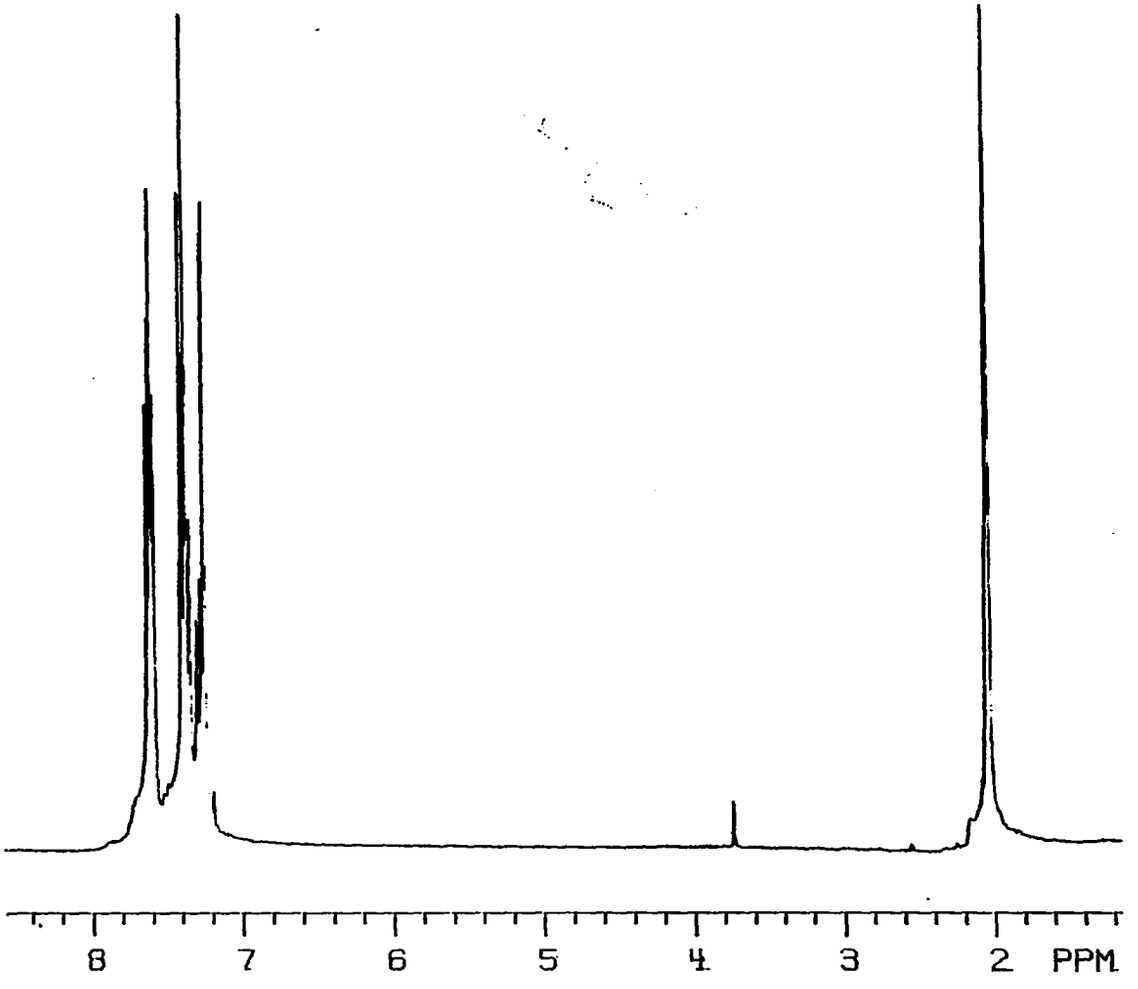

Figure 57. ^{1}H NMR of 13g in d-6 acetone

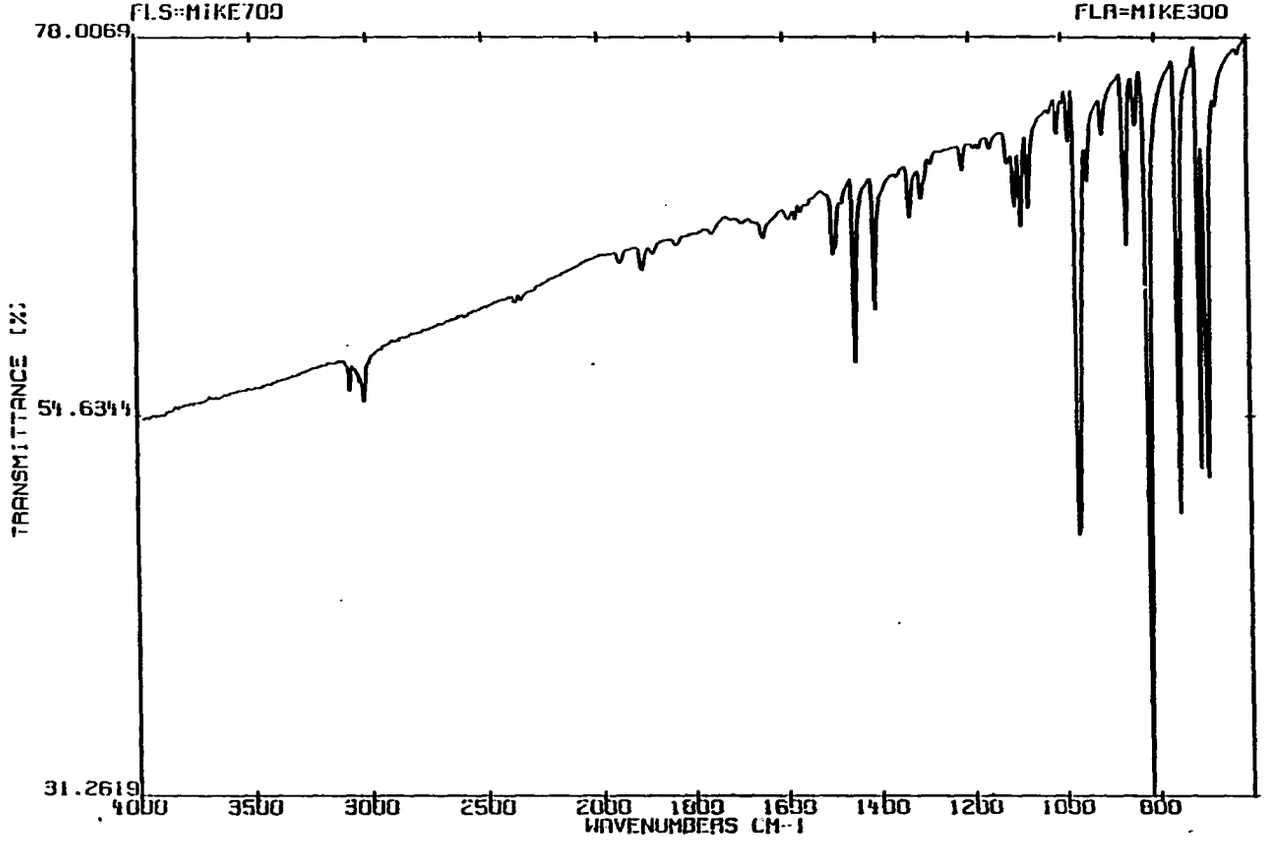

Figure 58. FT-IR of 13g in $CDCl_3$

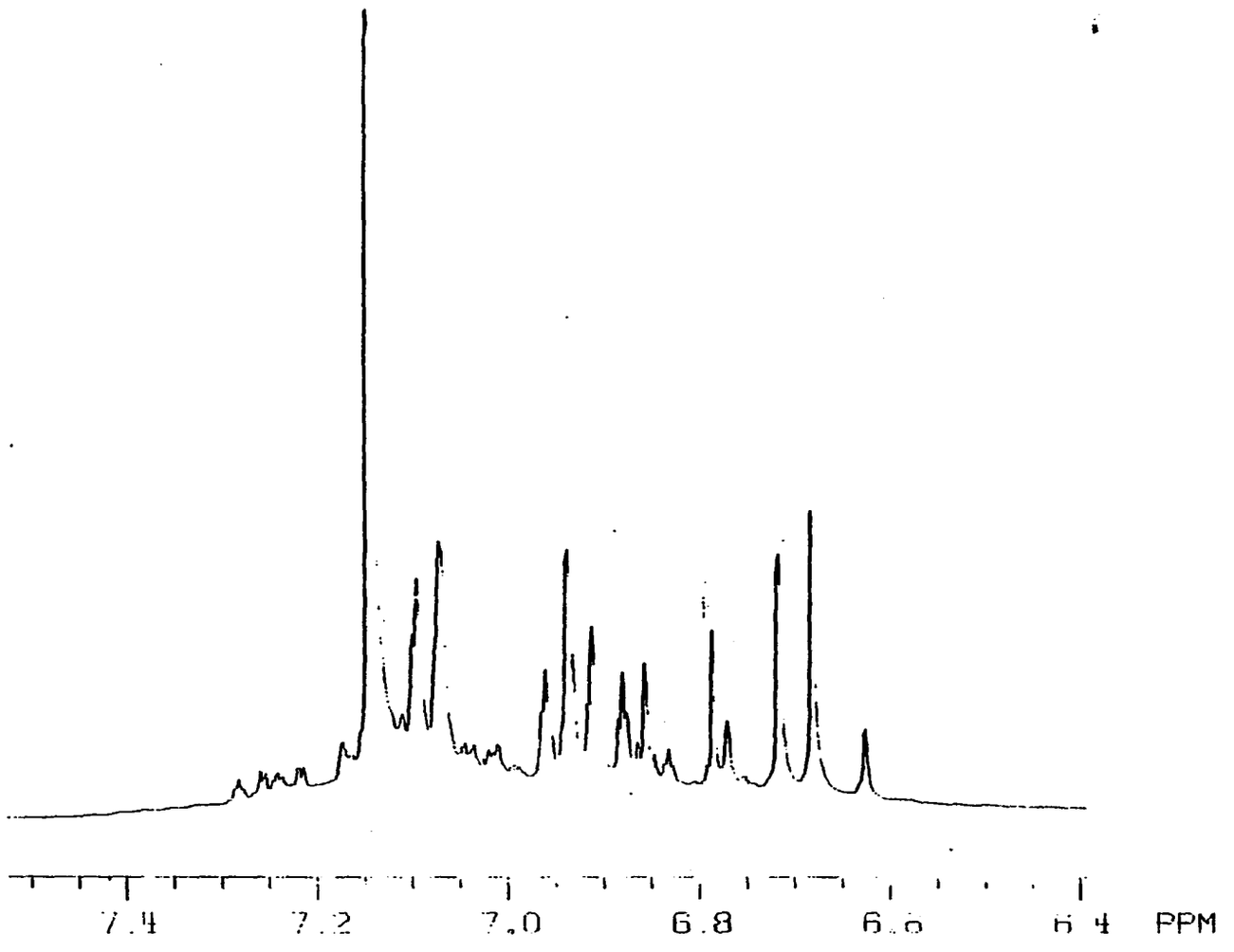

Figure 59. ^{1}H NMR of 13h in $CDCl_3$

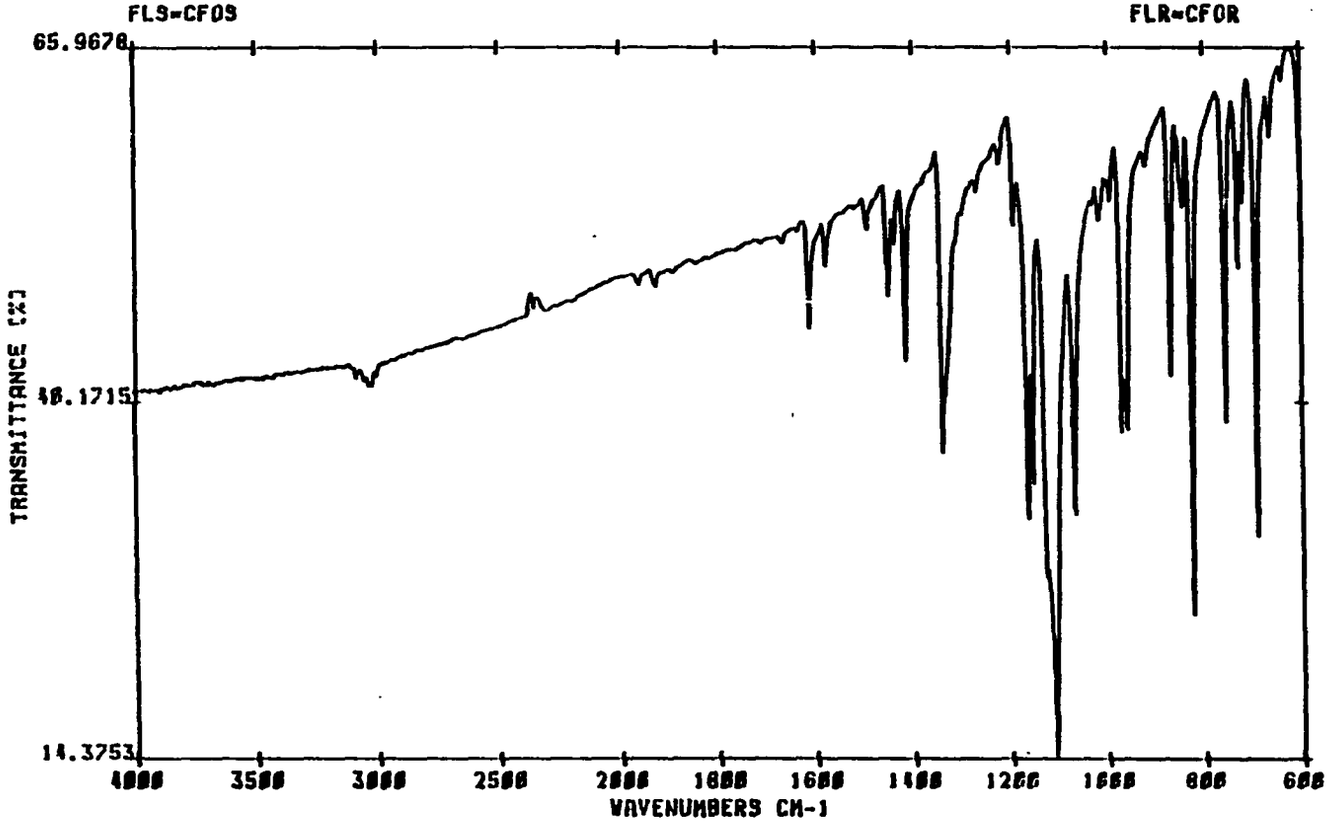

Figure 60. FT-IR of 13h in $CDCl_3$

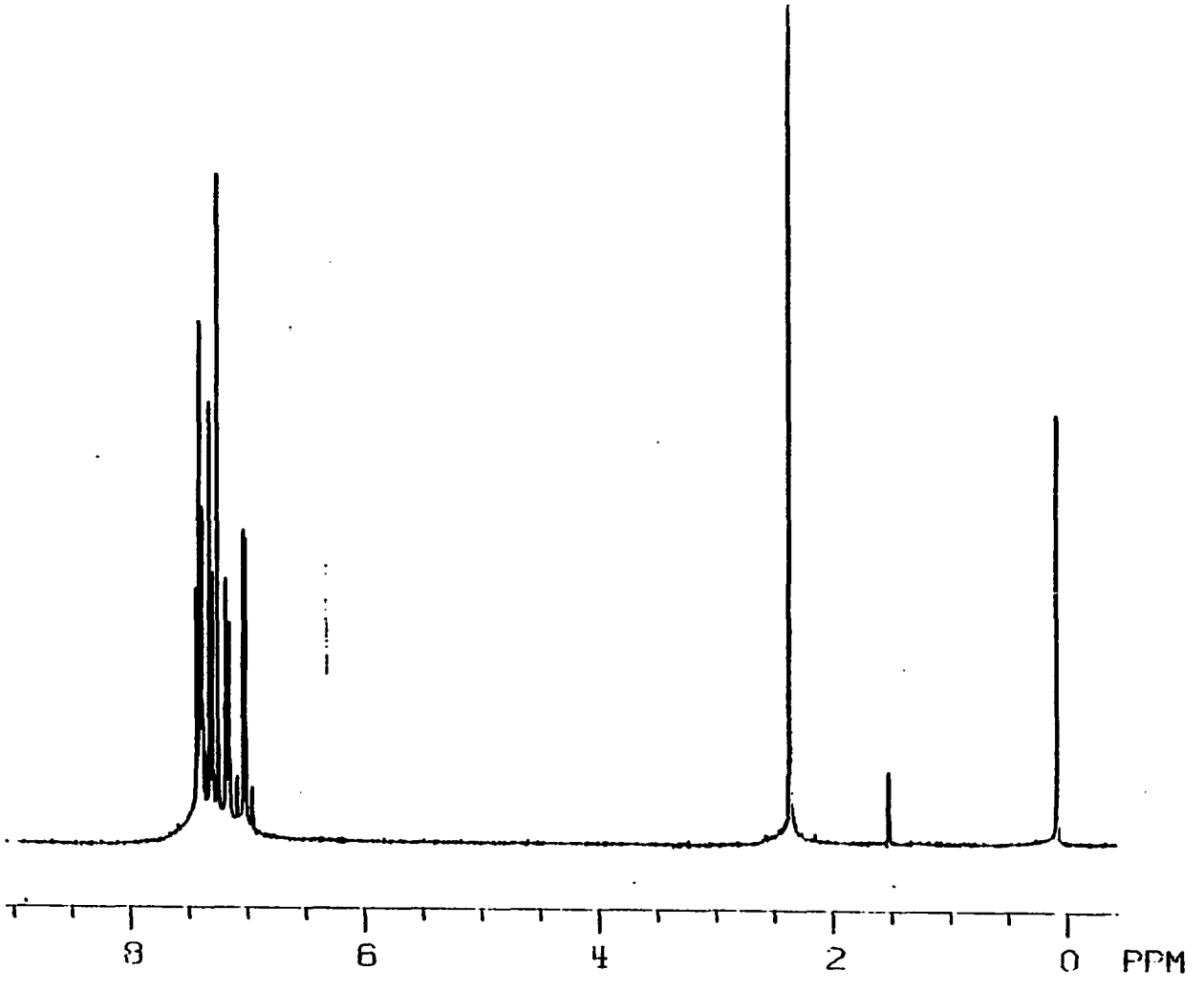

Figure 61. ^{1}H NMR of 13i in $CDCl_3$

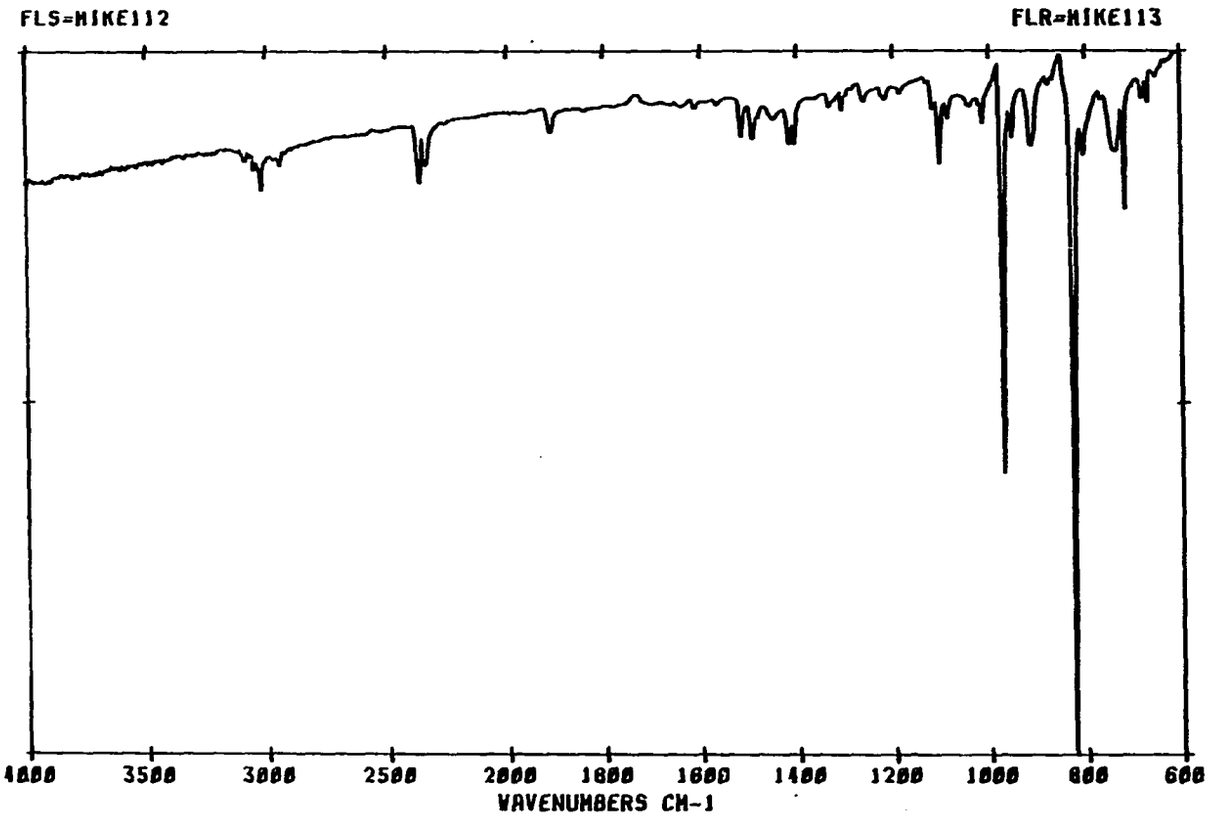

Figure 62. FT-IR of 13i in $CDCl_3$

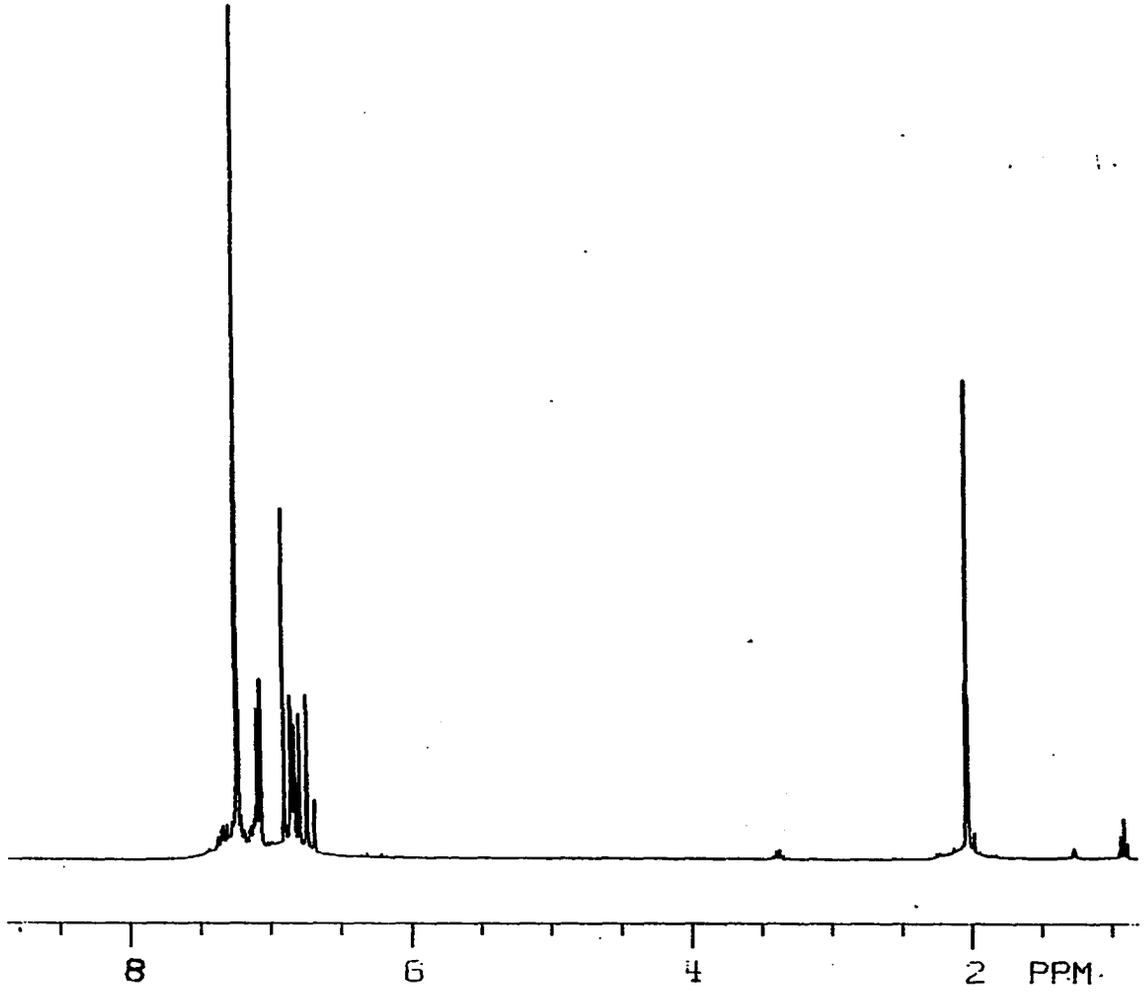

Figure 63. ^{1}H NMR of 13j in $CDCl_3$

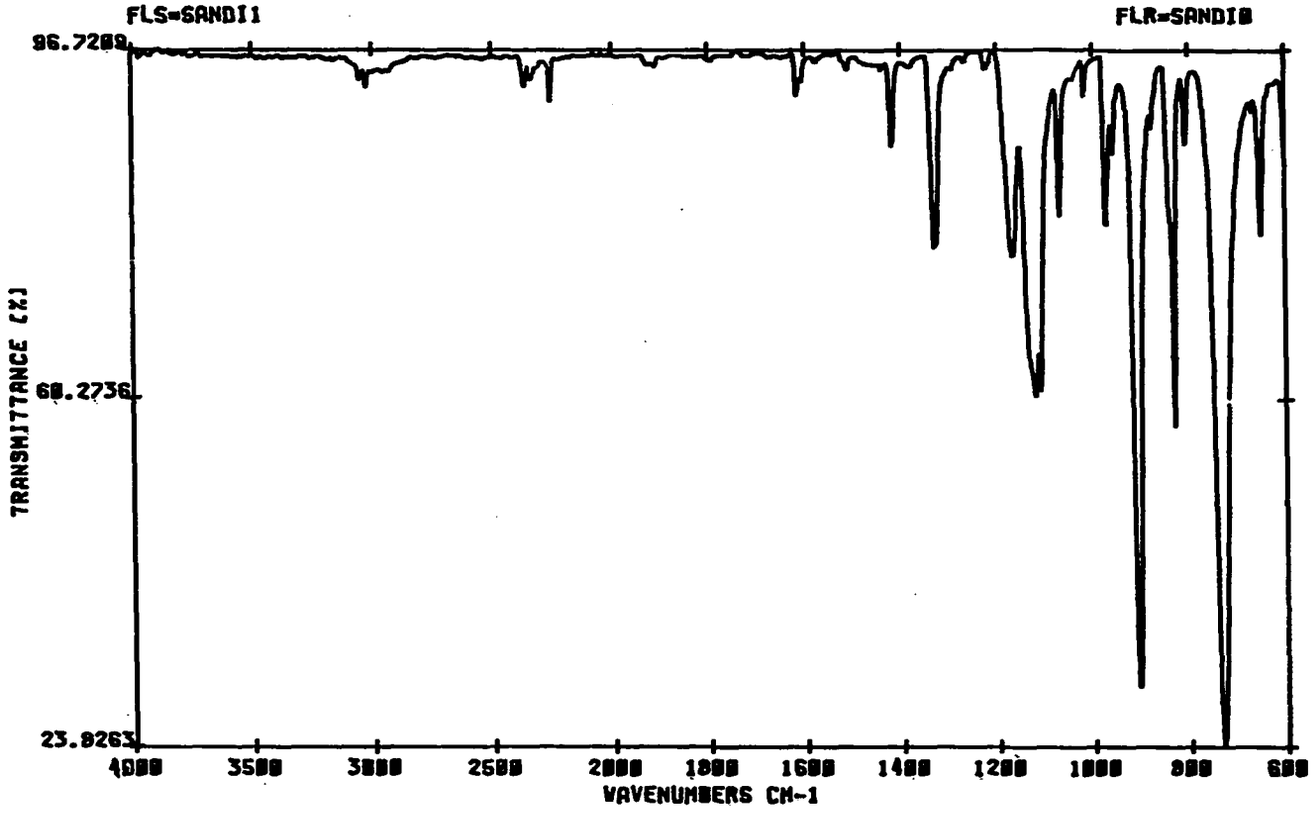

Figure 64. FT-IR of 13j in $CDCl_3$

HRMS: Calculated $C_{16}H_{13}F_3$ m/e 262.09694
measured m/e 262.09713 error 0.7 ppm.

^1H NMR ($CDCl_3$): δ 7.085 (d), δ 6.91 (s), δ 6.9-6.7 (m), δ 2.03 (s).

FT-IR ($CDCl_3$): 3030 (w), 2400 (w), 1610 (w), 1545 (m), 906 (s), 765 (s) cm^{-1}.

^{13}C NMR ($CDCl_3$): δ 140.9 (rel. intens. 15), δ 138.3 (25), δ 133.8 (20), δ 132.0 (10), δ 131.1 (45), δ 129.5 (100), δ 126.7 (95), δ 126.4 (70), δ 126.1 (50), δ 125.5 (40), δ 21.3 (30).

General synthesis of trans-2,3-diarylcyclopropanecarboxylic acids (15a-j)

Preparation of trans-2,3-diphenylcyclopropanecarboxyclic acid (15a) (Figures 65, 66) A 250 ml round bottom flask was charged with 15 g of 13a, 0.75 g of anhydrous copper sulfate, and 100 ml of dry benzene. The mechanically stirred mixture was heated to 75°C and treated with 23.7 g (2.5 eq.) of ethyl diazoacetate over 4 hours. The cooled reaction mixture was filtered to remove the catalyst and the benzene was removed under reduced pressure. The crude product mixture was dissolved in 100 ml of 70% ethanol. A second filtration removed the unreacted 13a. The crude ester was then saponified with sodium hydroxide to give the acid 15a. The basic solution was extracted twice with 50 ml portions of ether and acidified to precipitate the acid.

The crude 15a was then recrystallized from ethanol and water to give 3.3 g of 15a as a white crystalline solid in 21% yield based on starting olefin. m.p. 153-154°C (lit. m.p. 153-154°C (9)).

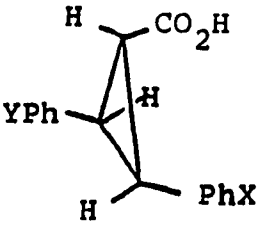

15a-j X/Y = H/H (a), CH_3/CH_3 (b), OCH_3/OCH_3 (c), Cl/Cl (d), CF_3/CF_3 (e), H/CH_3 (f), H/Cl (g), H/CF_3 (h), CH_3/Cl (i), CH_3/CF_3 (j)

HRMS: Calculated $C_{16}H_{14}O_2$ m/e 238.09938
measured m/e 238.09956 error 0.8 ppm.

^{1}H NMR ($CDCl_3$): δ 7.4-7.19 (m), δ 3.16 (d,d), δ 2.97 (dd), δ 2.36 (dd).

FT-IR ($CDCl_3$): 3000 (m), 1688 (s), 1480 (m), 1190 (m) cm^{-1}.

^{13}C NMR ($CDCl_3$): δ 176.0 (rel. intens. 40), δ 139.3 (25), δ 135.3 (30), δ 129.3 (75), δ 129.1 (90),

δ 128.7 (85), δ 126.9 (100), δ 35.3 (40), δ 29.3 (35), δ 28.7 (50).

Trans-2,3-bis(p-methylphenyl)cyclopropanecarboxylic acid (15b) (Figures 67, 68) Prepared from 13b in 71% yield m.p. 137-139°C.

HRMS: Calculated $C_{18}H_{18}O_2$ m/e 266.13055
measured m/e 266.13068 error -0.5 ppm.

^1H NMR ($CDCl_3$): δ 7.3-7.1 (m), δ 3.23 (dd), δ 3.03 (dd), δ 2.44 (dd), δ 2.45 (s), δ 2.44 (s).

FT-IR ($CDCl_3$): 3024 (s), 1697 (s), 1518 (m), 1456 (m), 1227 (m), 908 (s), 735 (s) cm^{-1}.

^{13}C NMR ($CDCl_3$): δ 175.6 (rel. intens. 20), δ 136.4 (30), δ 136.2 (45), δ 132.5 (40), δ 129.2 (80), δ 128.9 (82), δ 128.8 (100), δ 126.6 (81), δ 58.4 (15), δ 34.8 (50), δ 30.7 (40), δ 30.0 (45), δ 21.1 (35), δ 21.0 (40).

Trans-2,3-bis(p-methoxyphenyl)cyclopropanecarboxylic acid (15c) (Figures 69, 70) Prepared from 13c in 50% yield, m.p. 159-160°C.

HRMS: Calculated $C_{18}H_{18}O_4$ m/e 298.12051
measured m/e 298.12029 error -0.7 ppm.

^1H NMR ($CDCl_3$): δ 7.23 (d), δ 7.13 (d), δ 6.82 (t), δ 3.78 (s), δ 3.72 (s), δ 3.08 (dd), δ 2.86 (dd), δ 2.25 (dd).

FT-IR ($CDCl_3$): 3000 (w), 1693 (s), 1612 (w), 1514 (s), 1248 (s), 1178 (m), 1034 (m) cm^{-1}.

^{13}C NMR ($CDCl_3$): δ 176.0 (rel. intens. 40), δ 158.5 (50), δ 131.2 (20), δ 130.1 (80), δ 127.8 (100), δ 127.5 (42), δ 114.0 (75), δ 113.5 (85), δ 55.3 (45), δ 55.2 (50), δ 34.4 (45), δ 30.6 (30), δ 29.8 (35).

Trans-2,3-bis(p-chlorophenyl)cyclopropanecarboxylic acid (15d) (Figures 71, 72) Prepared from 13d in 50% yield, m.p. 189-192°C.

HRMS: Calculated $C_{16}H_{12}Cl_2O_2$ m/e 306.02144 measured m/e 306.02121 error -0.8 ppm.

^1H NMR ($CDCl_3$): δ 7.3-7.1 (m), δ 3.10 (dd), δ 2.88 (dd), δ 2.33 (dd).

FT-IR ($CDCl_3$): 3000 (w), 1700 (m), 1500 (m), 902 (s), 750 (s) cm^{-1}.

^{13}C NMR ($CDCl_3$): δ 175.0 (rel. intens. 50), δ 137.1 (45), δ 133.5 (55), δ 130.3 (70), δ 128.9 (100), δ 128.3 (98), δ 128.0 (70), δ 34.3 (50), δ 30.7 (40), δ 29.6 (39).

Trans-2,3-bis(trifluoromethylphenyl)cyclopropanecarboxylic acid (15e) The reaction of 13e with 5 eq. of ethyl diazoacetate gave less than 1% of the product, which was not isolated.

Trans-2-(p-methylphenyl)-3-phenylcyclopropanecarboxylic acid (15f) (Figures 73, 74) Prepared from 13f in 30% yield, m.p. 125-135°C.

HRMS: Calculated $C_{17}H_{16}O_2$ m/e 252.11503
measured m/e 252.11519 error 0.6 ppm.

^1H NMR ($CDCl_3$): δ 7.5-7.0 (m), δ 3.13 (dd), δ 2.94 (dd), δ 2.35 (dd), δ 2.32 (s), δ 2.31 (s).

FT-IR ($CDCl_3$): 3020 (m), 1696 (s), 1480 (m), 1250 (m), 900 (m) cm^{-1}.

^{13}C NMR ($CDCl_3$): δ 176.44 (rel. intens. 39), δ 176.40 (40), δ 139.1 (50), δ 136.4 (49), δ 136.3 (50), δ 135.9 (20), δ 135.5 (50), δ 132.3 (55), δ 129.2 (90), δ 129.0 (95), δ 128.9 (85), δ 128.8 (100), δ 128.5 (85), δ 128.0 (70), δ 126.9 (60), δ 126.5 (100), δ 126.48 (110), δ 35.0 (50), δ 34.9 (55), δ 30.74 (48), δ 30.7 (50), δ 30.2 (60), δ 29.9 (60), δ 21.0 (50), δ 20.9 (50).

Trans-2-(p-chlorophenyl)-3-phenylcyclopropanecarboxylic acid (15g) (Figures 75, 76) Prepared from 13g in 14% yield, m.p. 135-137°C.

HRMS: Calculated $C_{16}H_{13}ClO_2$ m/e 272.06041
measured m/e 272.06004 error -1.4 ppm.

^1H NMR ($CDCl_3$): δ 7.4-7.1 (m), δ 3.12 (dd), δ 2.92 (dd), δ 2.35 (dd).

FT-IR ($CDCl_3$): 3000 (m), 1694 (s), 1500 (m), 1210 (m) cm^{-1}.

^{13}C NMR ($CDCl_3$): δ 175.7 (rel. intens. 50), δ 175.6 (25), δ 138.6 (30), δ 137.5 (35), δ 135.0 (10), δ 133.9 (30), δ 132.7 (20), δ 132.6 (15), δ 130.4 (60), δ 129.0 (84), δ 128.6 (90), δ 128.2 (100), δ 128.1 (86), δ 128.0 (80), δ 127.1 (20), δ 126.9 (40), δ 126.5 (60), δ 35.1 (50), δ 34.3 (55), δ 30.7 (60), δ 30.2 (55), δ 29.4 (45).

Trans-2-phenyl-3-(p-trifluoromethylphenyl)cyclopropane-carboxylic acid (15h) (Figures 77, 78) Prepared from 13h in 8% yield, obtained as a brown oil.

HRMS: Calculated $C_{17}H_{13}F_3O_2$ m/e 306.08677 measured m/e 306.08709 error 1.0 ppm.

^1H NMR ($CDCl_3$): δ 7.6-7.2 (m), δ 3.21 (dd), δ 3.00 (dd), δ 2.44 (dd).

FT-IR ($CDCl_3$): 3000 (m), 1698 (s), 1340 (s), 1120 (s) cm^{-1}.

^{13}C NMR ($CDCl_3$): δ 175.5 (rel. intens. 20), δ 175.4 (19), δ 143.2 (20), δ 139.6 (18), δ 138.4 (15), δ 134.8 (30), δ 132.0 (10), δ 129.4 (90), δ 128.9 (85), δ 128.7 (75), δ 128.2 (80), δ 127.2 (60), δ 126.9 (75), δ 126.5 (100), δ 125.5 (65), δ 125.0 (68), δ 35.3 (30),

δ 34.5 (40), δ 31.0 (28), δ 30.9 (33),
δ 30.3 (35), δ 29.6 (30).

Trans-2-(p-chlorophenyl)-3-(p-methylphenyl)cyclopropane-carboxylic acid (15i) (Figures 79, 80) Prepared from 13i in 50% yield, m.p. 131-138°C.

HRMS: Calculated $C_{17}H_{15}ClO_2$ m/e 286.07606
measured m/e 286.07615 error 0.3 ppm.

^1H NMR ($CDCl_3$): δ 7.3-7.0 (m), δ 3.11 (dd), δ 2.39 (dd), δ 2.33 (s), δ 2.32 (s), δ 2.30 (dd).

FT-IR ($CDCl_3$): 3000 (m), 1700 (s), 1510 (m), 1215 (m) cm^{-1}.

^{13}C NMR ($CDCl_3$): δ 136.7 (rel. intens. 30), δ 135.6 (30), δ 134.1 (30), δ 132.0 (28), δ 130.4 (90), δ 129.3 (70), δ 128.9 (100), δ 128.7 (50), δ 128.2 (90), δ 128.0 (50), δ 126.5 (80), δ 34.9 (30), δ 34.3 (33), δ 30.8 (20), δ 30.1 (30), δ 29.6 (28), δ 21.1 (20), δ 21.0 (25).

Trans-2-(p-methylphenyl)-3-(p-trifluoromethylphenyl)-cyclopropanecarboxylic acid (15j) (Figures 81, 82)
Prepared from 13j in 6% yield, m.p. 105-111°C.

HRMS: Calculated $C_{18}H_{15}F_3O_2$ m/e 320.10242
measured m/e 320.10193 error 1.5 ppm.

^1H NMR ($CDCl_3$): δ 11.61 (s), δ 7.7-7.2 (m), δ 3.30 (m), δ 3.08 (m), δ 2.52 (m), δ 2.45 (s),

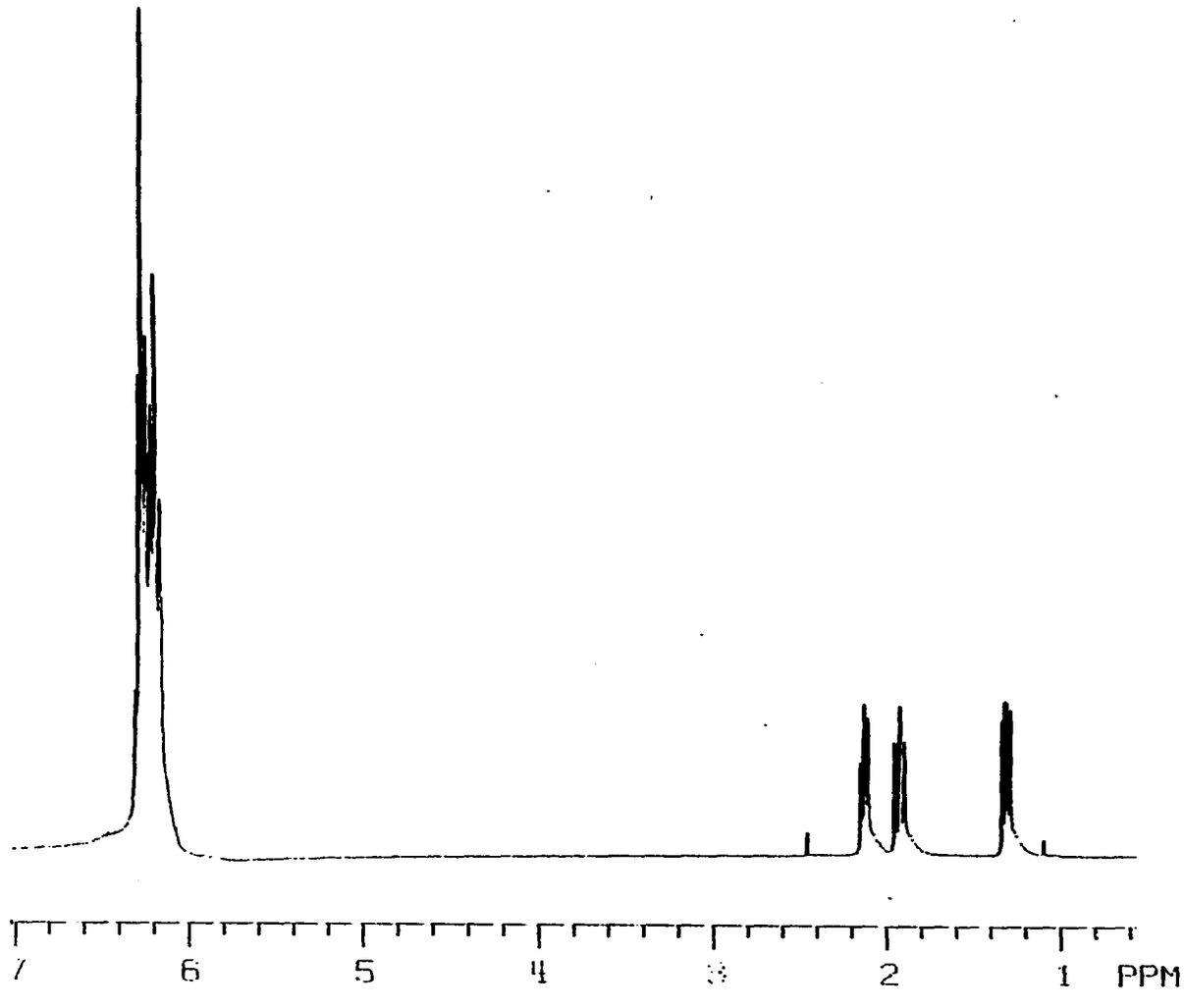

Figure 65. ^{1}H NMR of 15a in $CDCl_3$

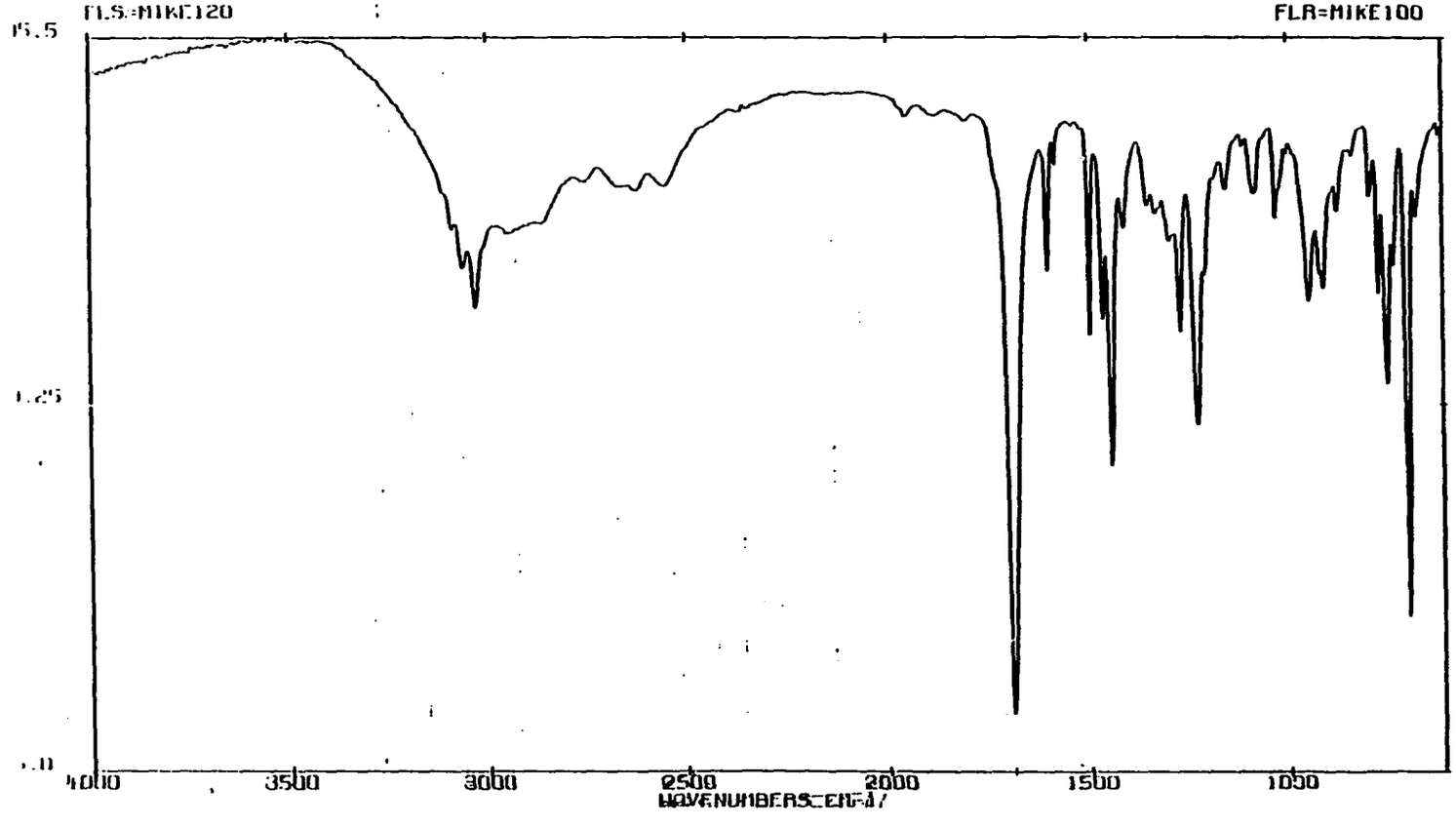

Figure 66. FT-IR of 15a in $CDCl_3$

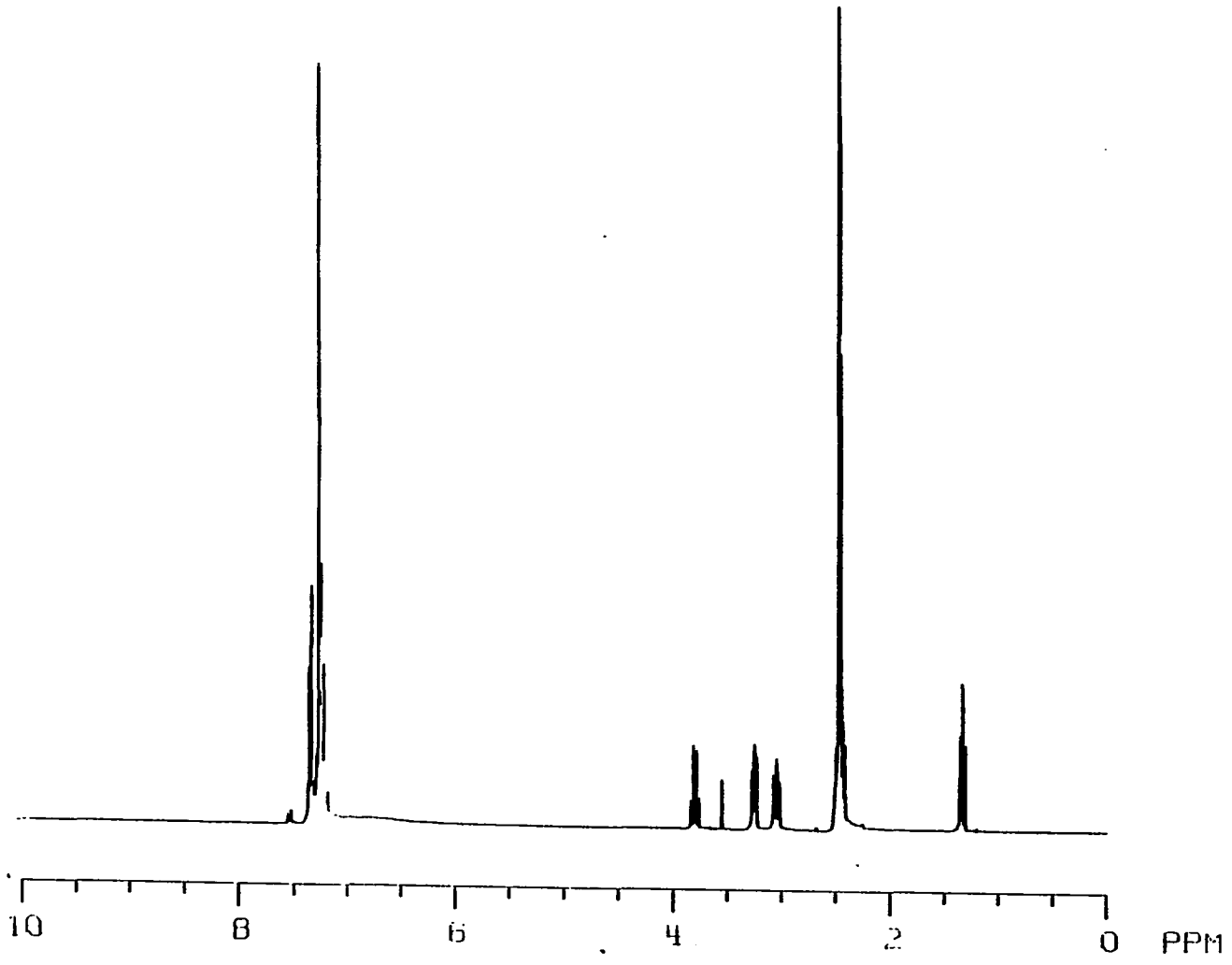

Figure 67. ^{1}H NMR of 15b in $CDCl_3$

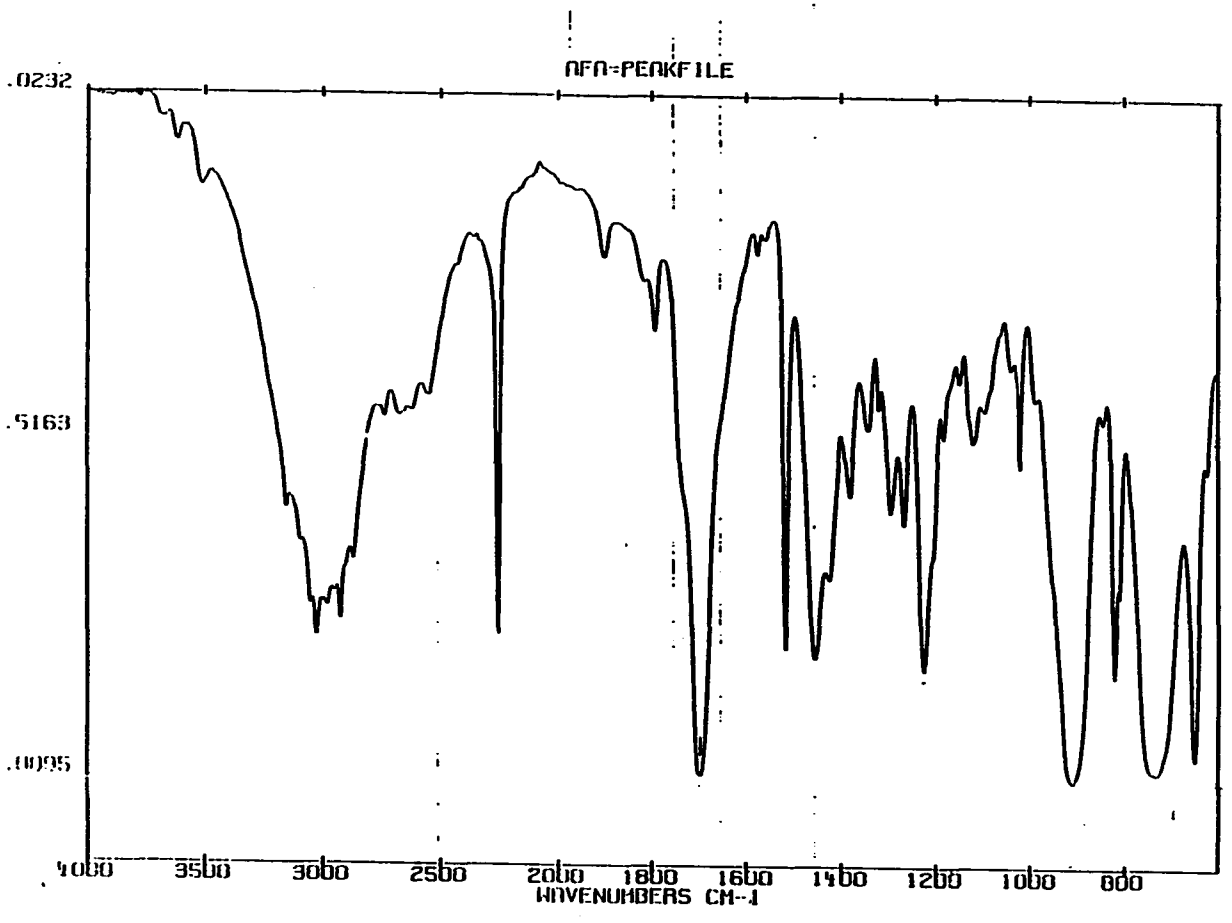

Figure 68. FT-IR of 15b in $CDCl_3$

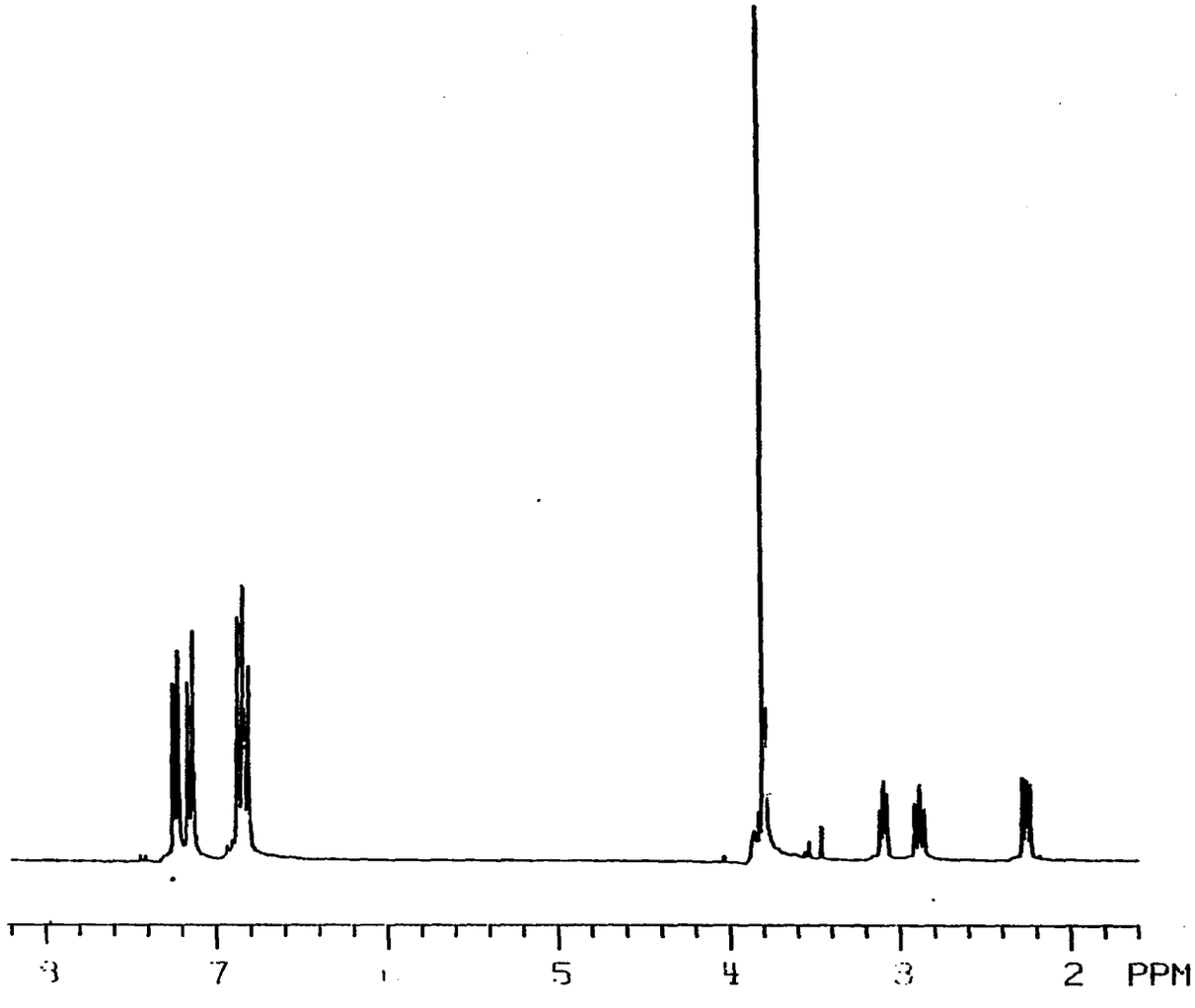

Figure 69. ^{1}H NMR of 15c in $CDCl_3$

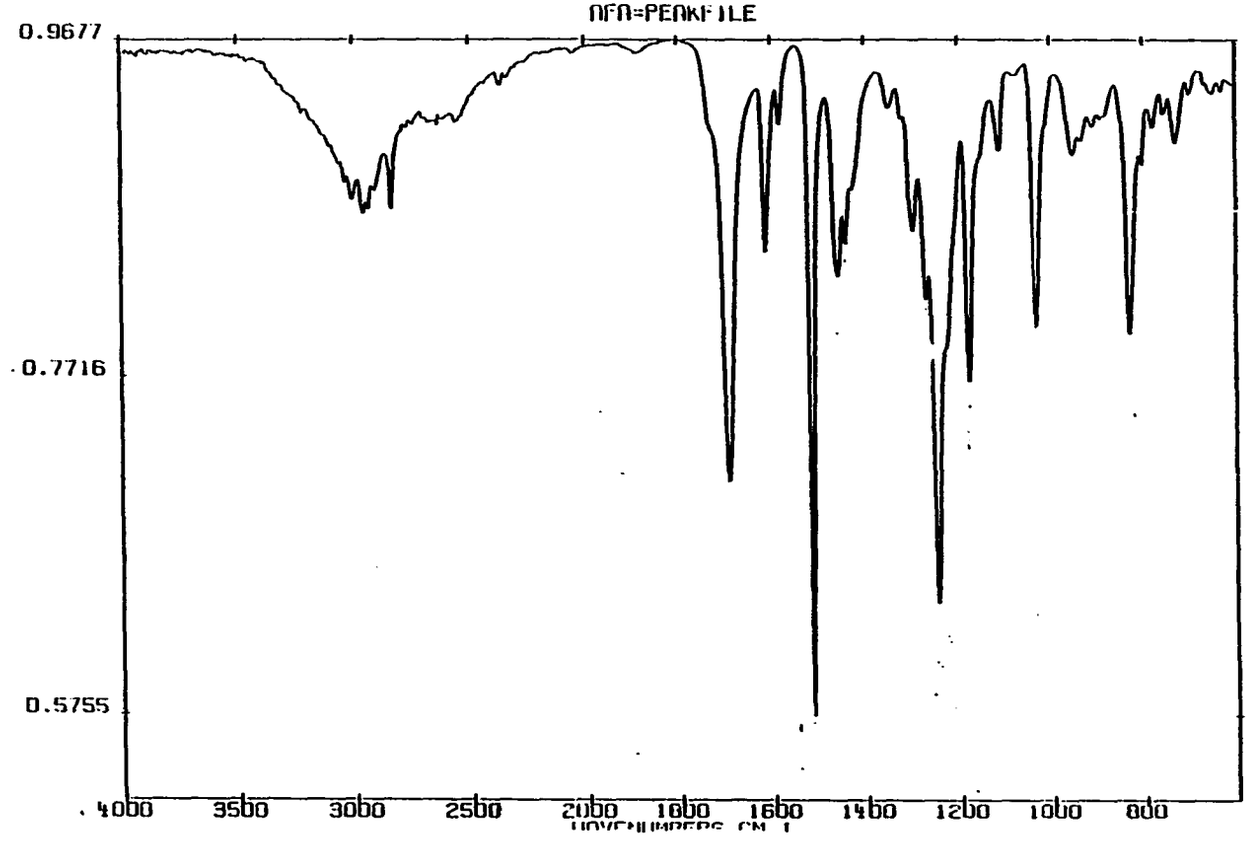

Figure 70. FT-IR of 15c in $CDCl_3$

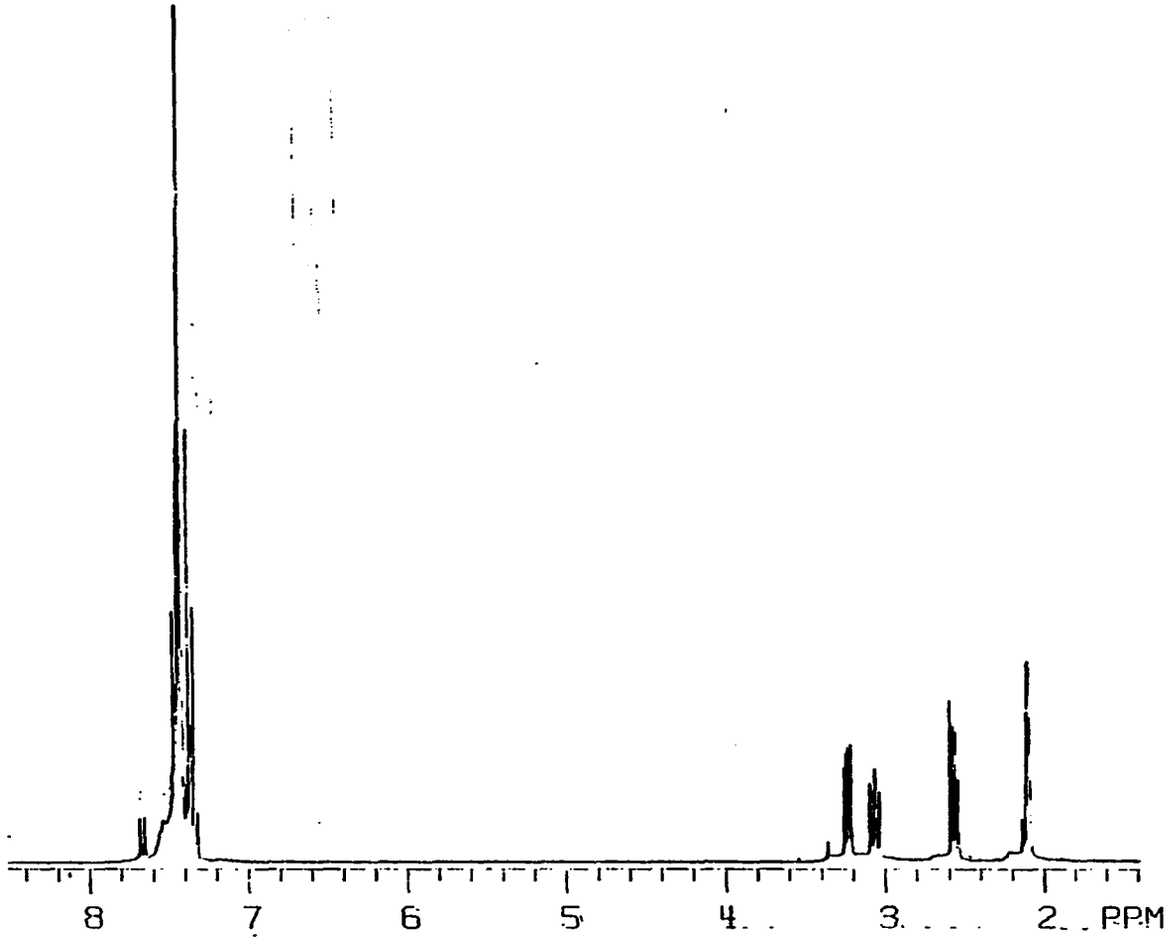

Figure 71. ^{1}H NMR of 15d in $CDCl_3$

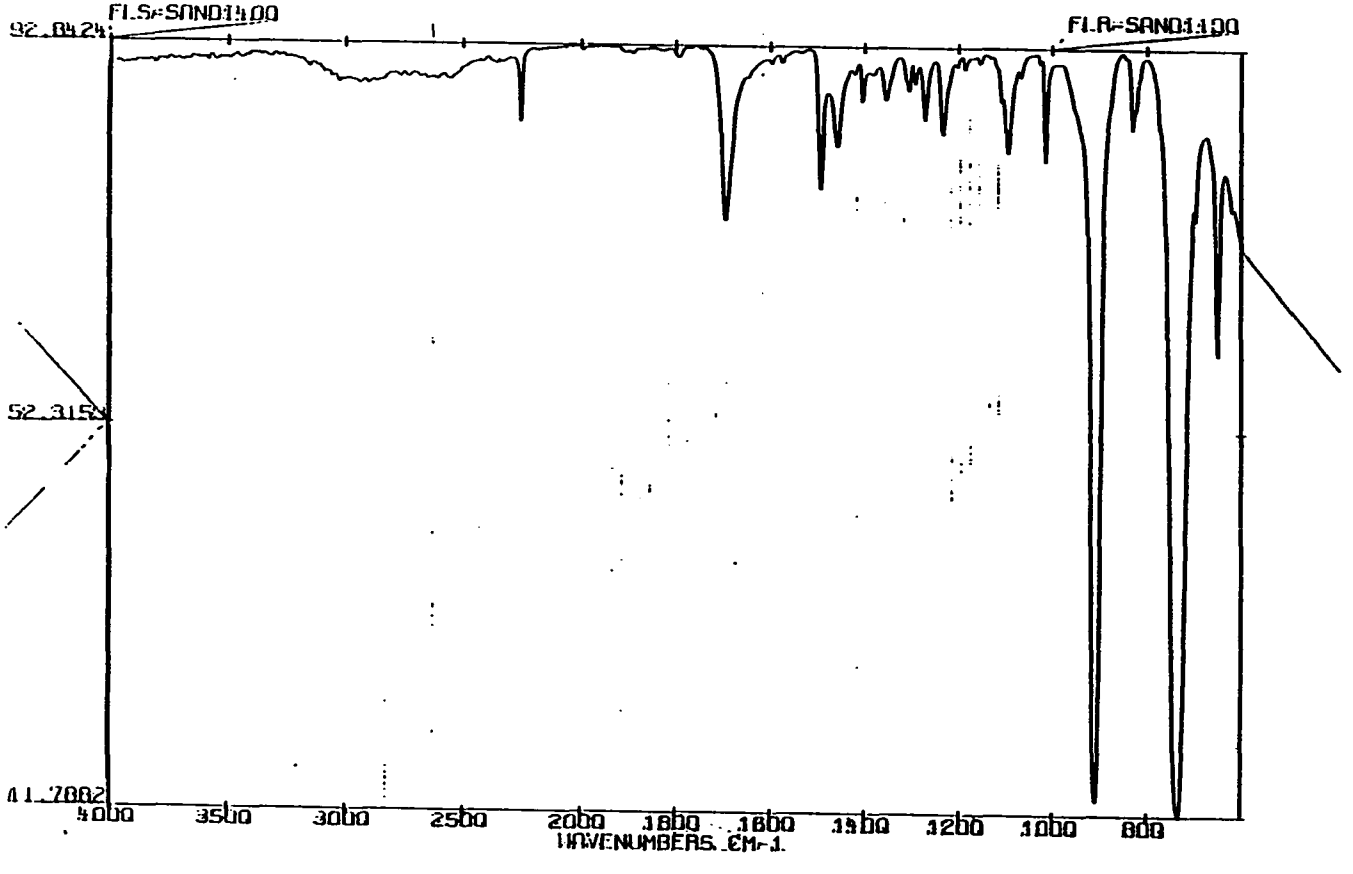

Figure 72. FT-IR of 15d in $CDCl_3$

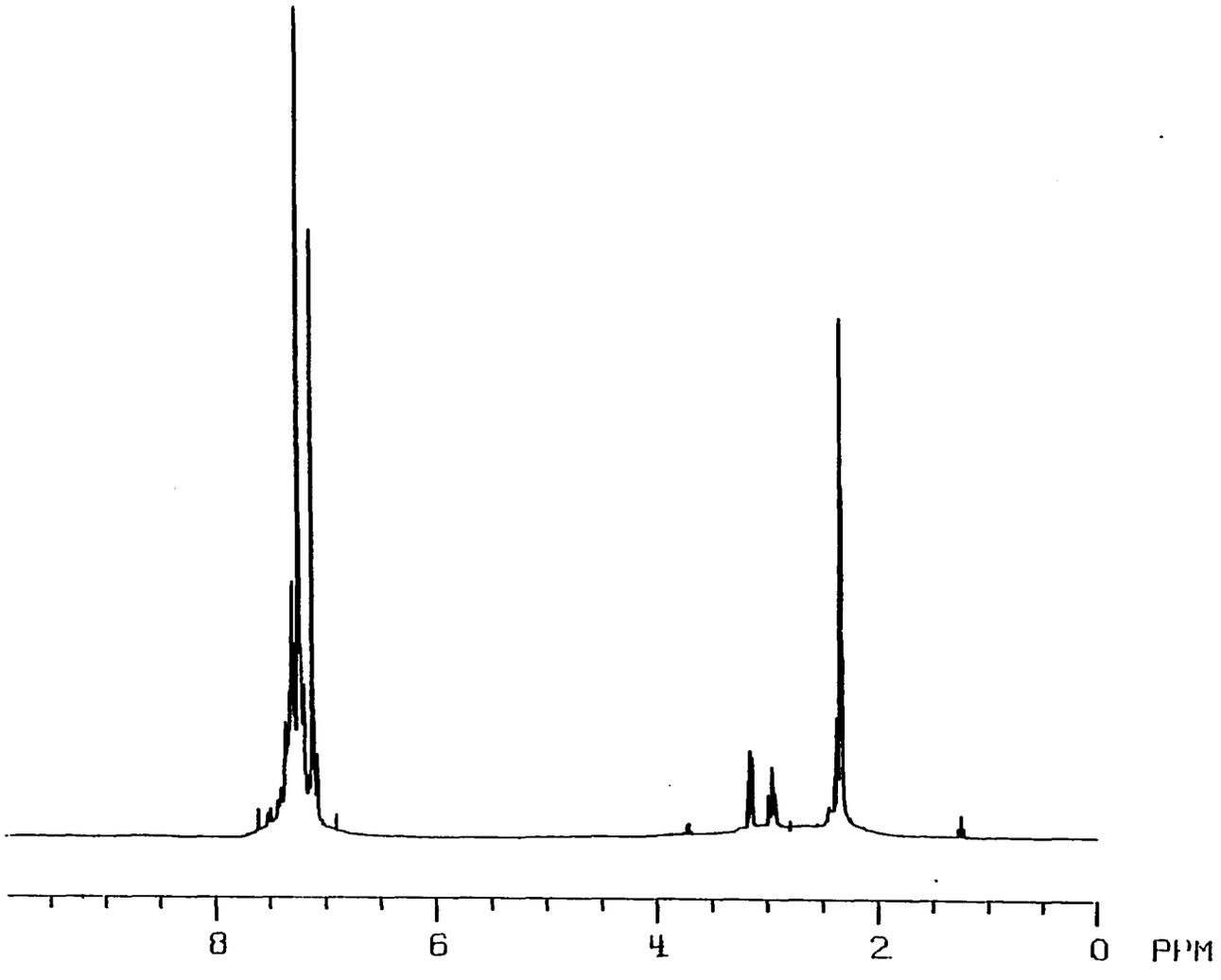

Figure 73. ^{1}H NMR of 15f in $CDCl_3$

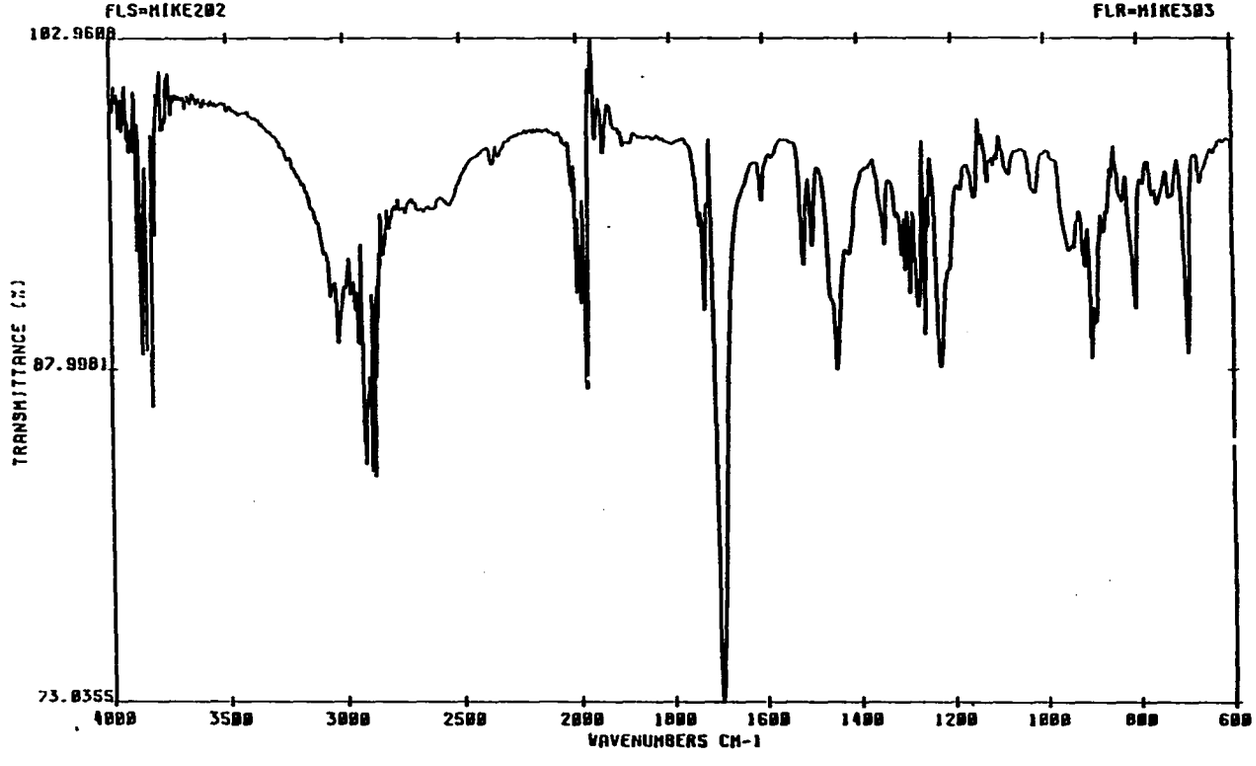

Figure 74. FT-IR of 15f in $CDCl_3$

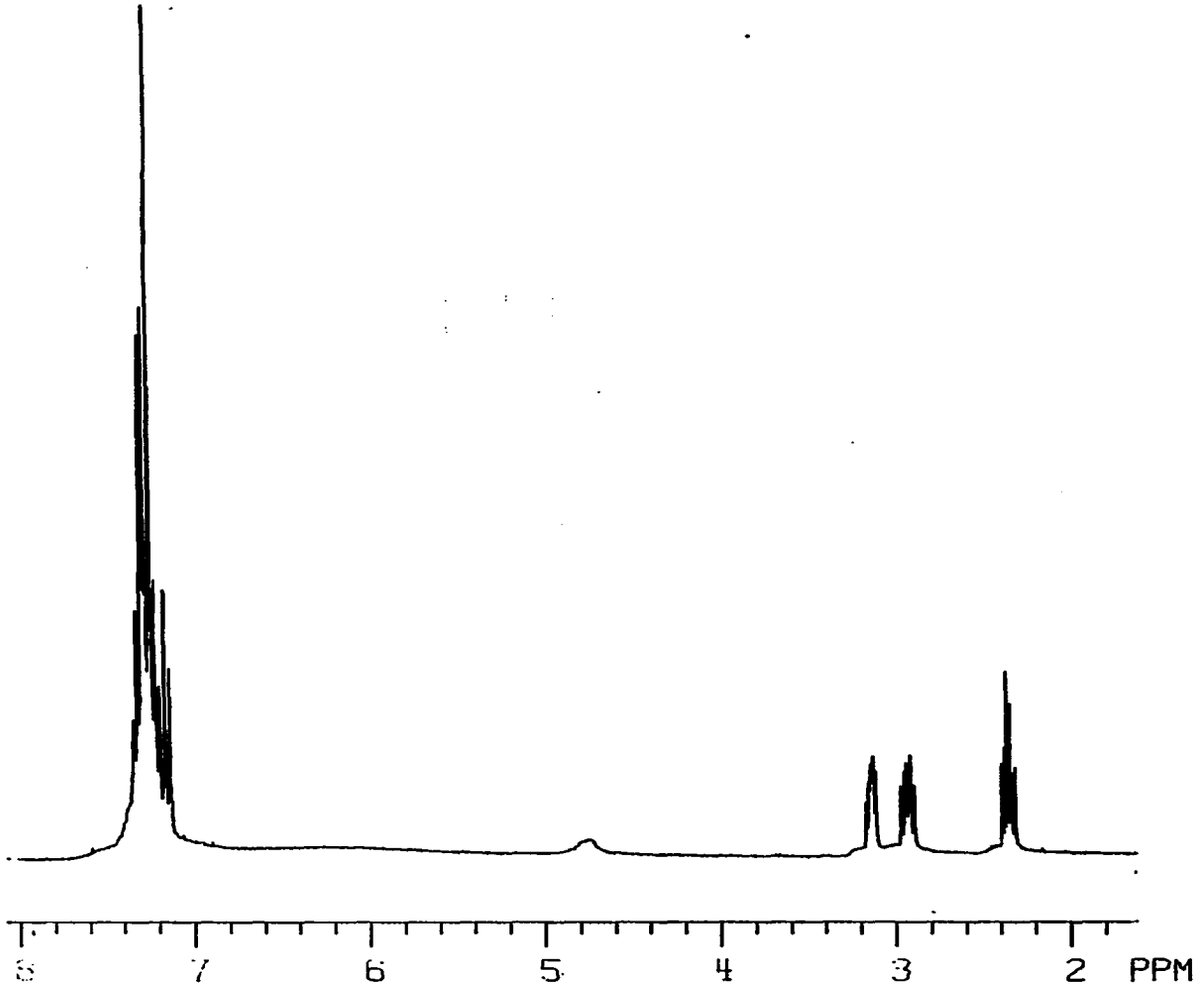

Figure 75. ^{1}H NMR of 15g in $CDCl_3$

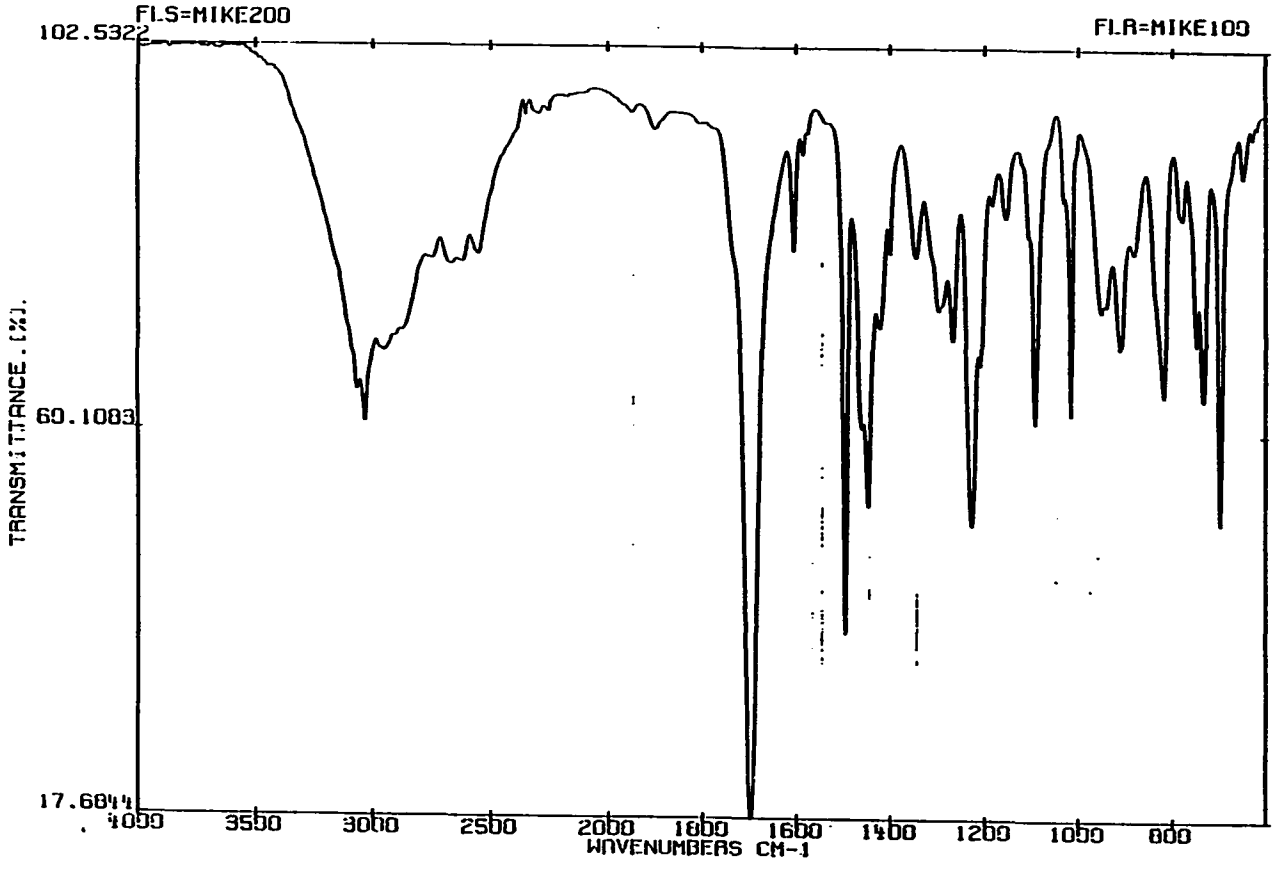

Figure 76. FT-IR of 15g in $CDCl_3$

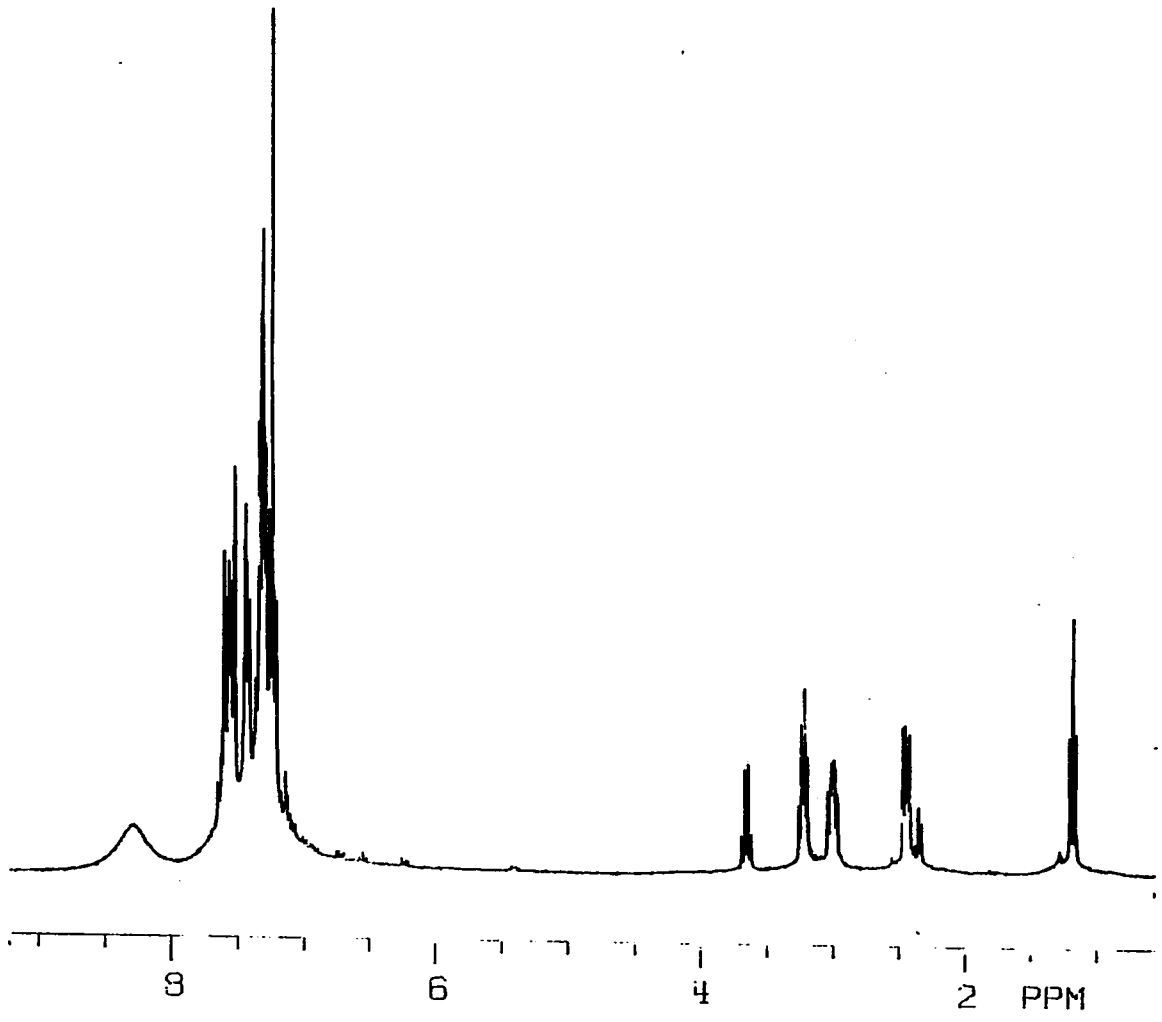

Figure 77. ^{1}H NMR of 15h in $CDCl_3$

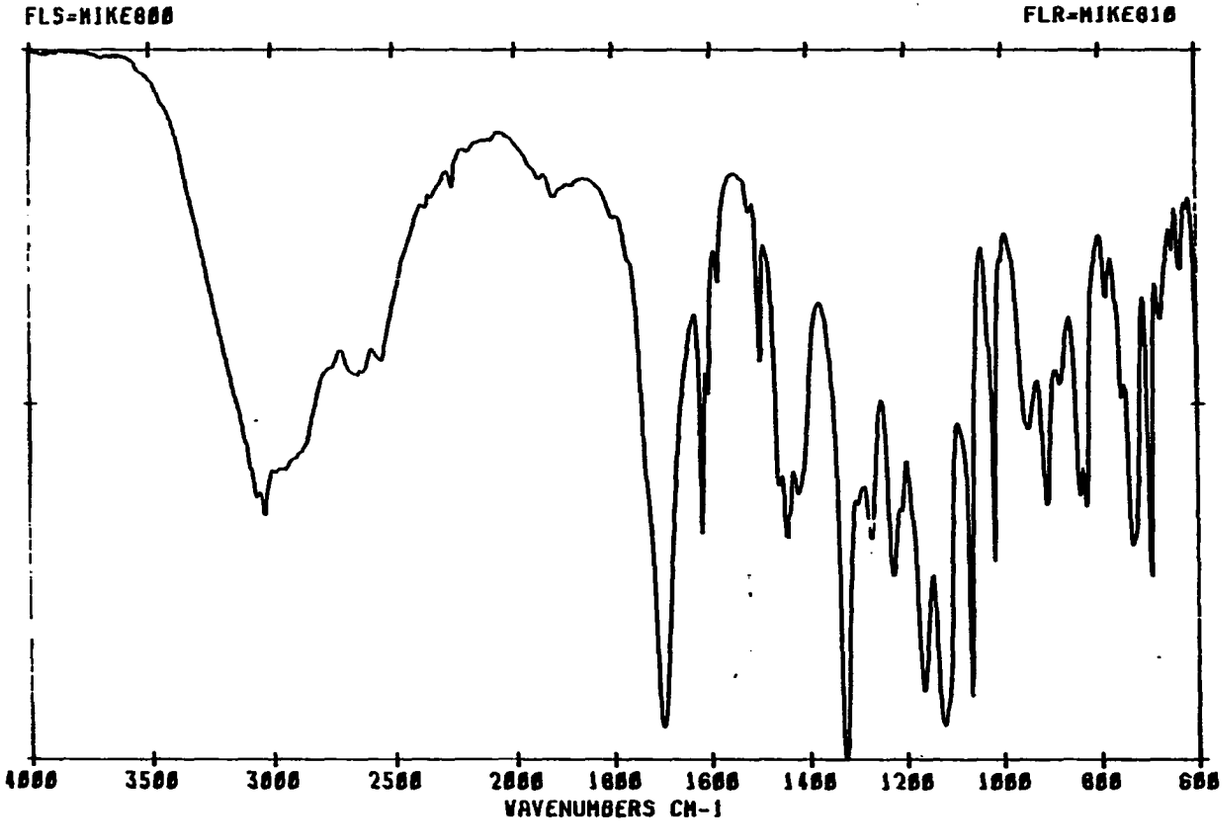

Figure 78. FT-IR of 15h in $CDCl_3$

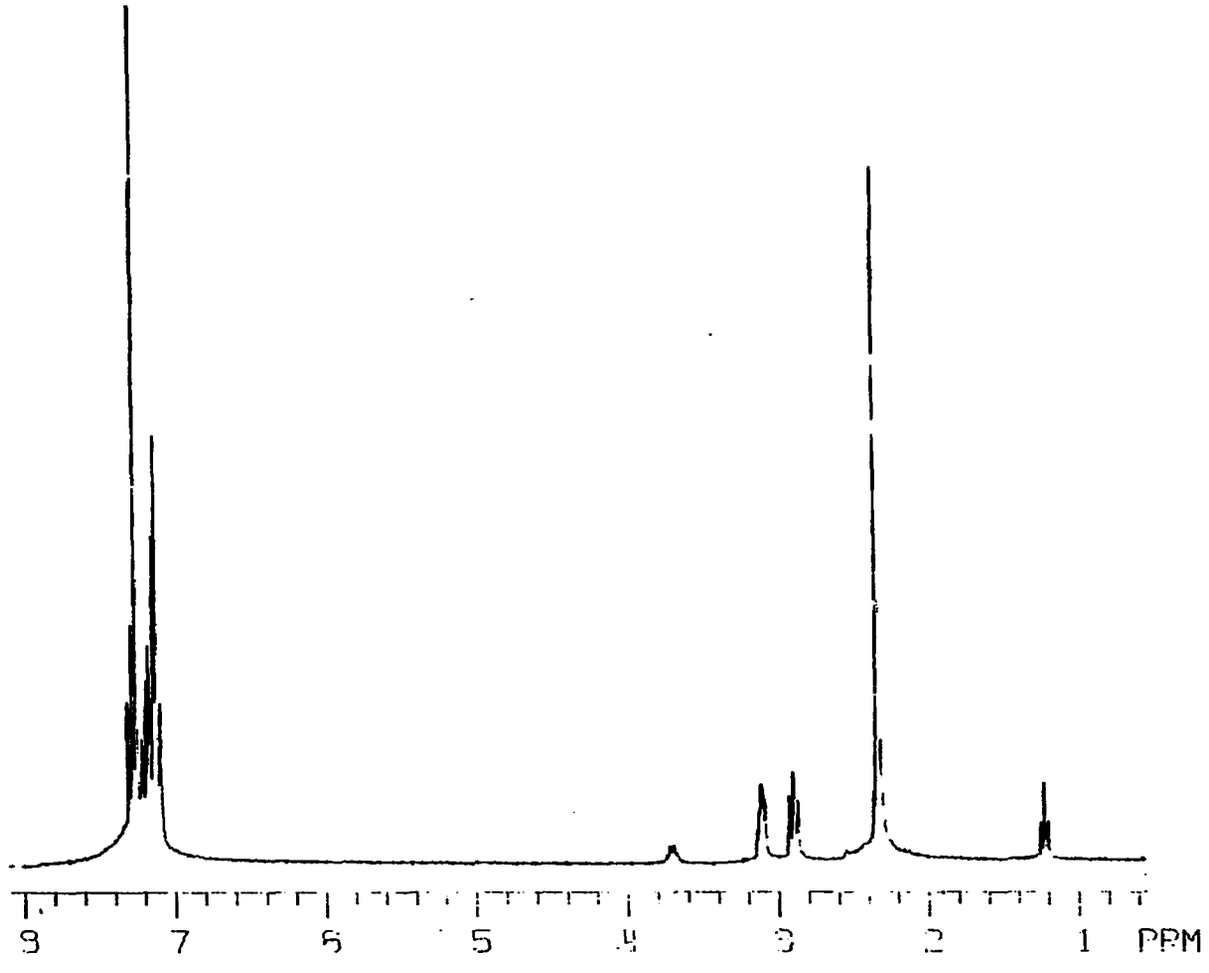

Figure 79. ^{1}H NMR of 15i in $CDCl_3$

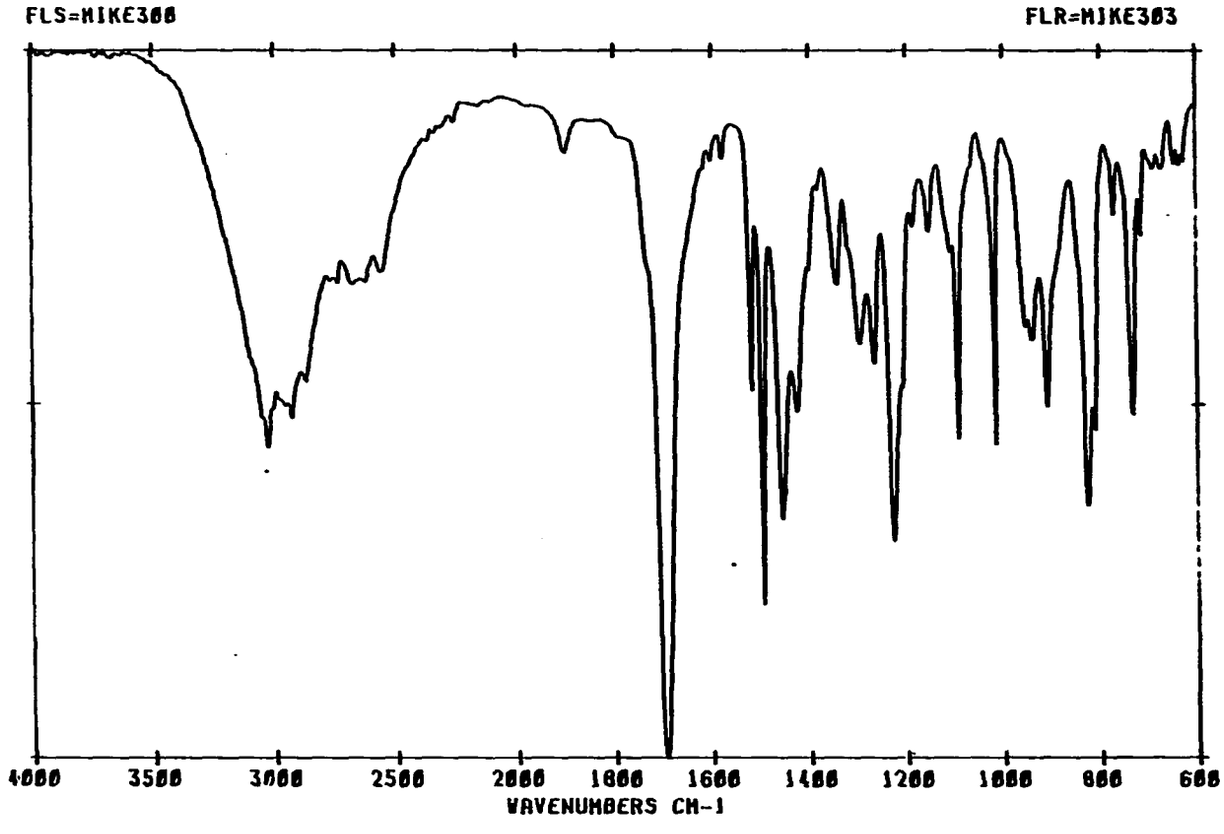

Figure 80. FT-IR of 15i in $CDCl_3$

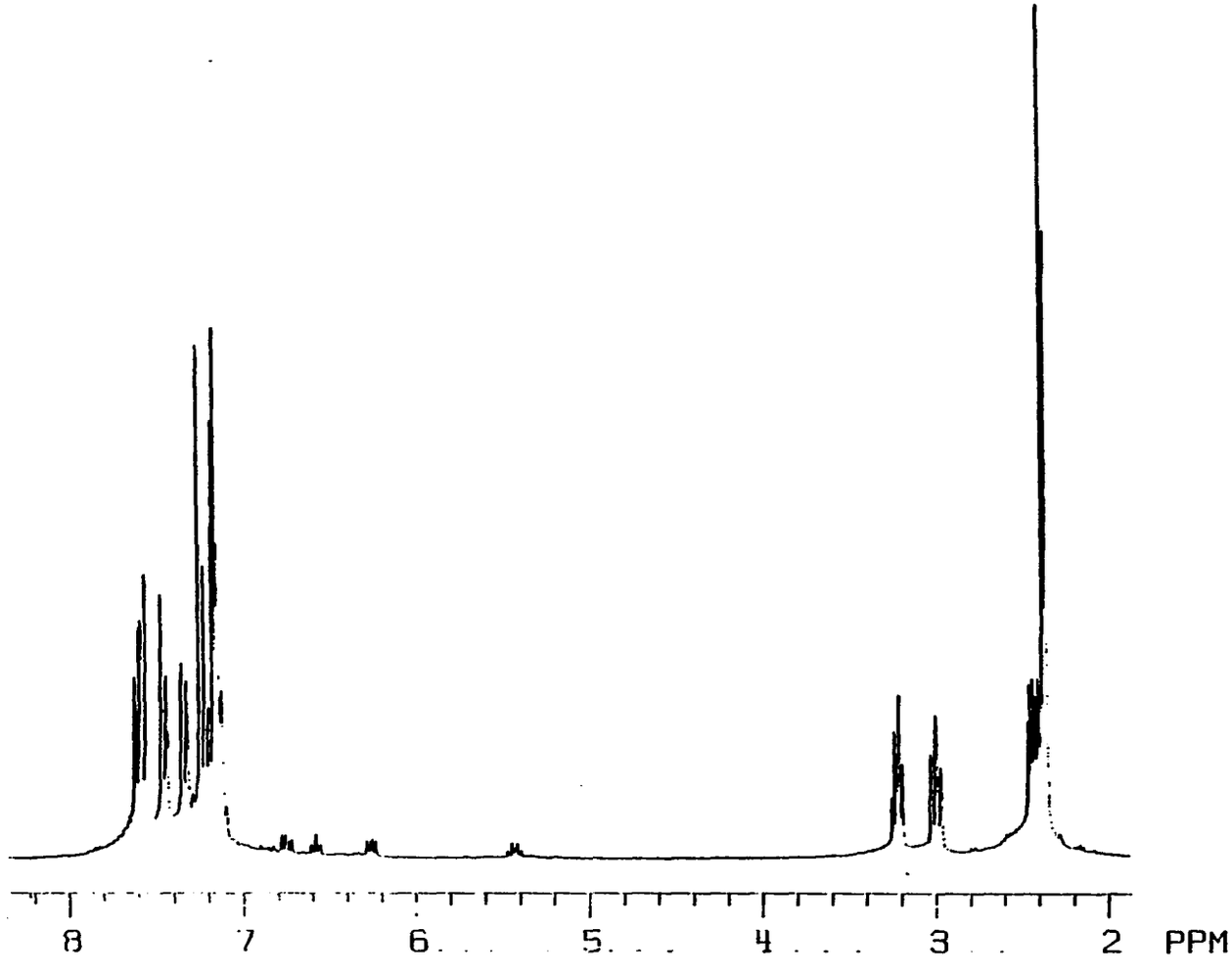

Figure 81. ^{1}H NMR of 15j in $CDCl_3$

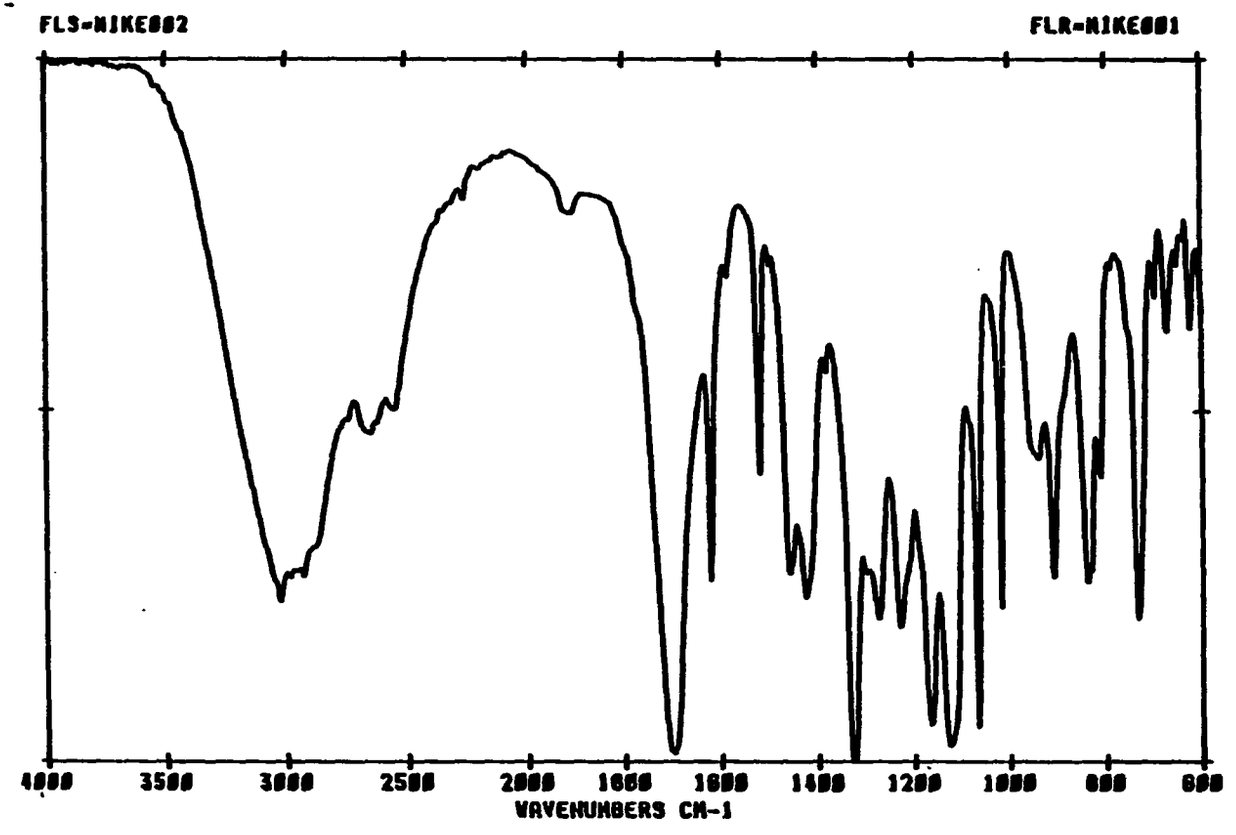

Figure 82. FT-IR of 15j in $CDCl_3$

δ 2.43 (s).

FT-IR ($CDCl_3$): 3000 (m), 1696 (s), 1603 (m), 1450 (m), 1367 (s), 1130 (s) cm^{-1}.

^{13}C NMR ($CDCl_3$): δ 176.1 (rel. intens. 25), δ 175.9 (27), δ 148.3 (25), δ 139.6 (28), δ 136.84 (15), δ 136.79 (35), δ 135.2 (40), δ 131.7 (30), δ 129.5 (60), δ 129.3 (100), δ 128.94 (62), δ 128.90 (62), δ 128.8 (70), δ 128.1 (50), δ 126.8 (65), δ 126.5 (65), δ 125.5 (40), δ 124.9 (40), δ 122.3 (10), δ 120.4 (10), δ 35.2 (40), δ 34.5 (50), δ 31.0 (40), δ 30.8 (50), δ 30.1 (60), δ 29.7 (50), δ 21.02 (50), δ 20.97 (65).

General synthesis of ethyl N-(trans-2,3-diarylcyclopropyl)-carbamates 17(a-j)

Preparation of ethyl N-(trans-2,3-diphenylcyclopropyl)-carbamate (17a) Figures (83, 84) A 250 ml round bottom flask was charged with 100 mg of 15a, 100 ml of dry benzene, 60 mg of triethylamine and 120 mg of diphenylphosphoryl azide (DPPA). The stirred mixture was heated to reflux and the reaction progress was monitored via GLPC. When isocyanate formation was complete (~ 5 hrs), a large excess of ethanol (50 ml) was added, and the mixture was refluxed an additional 3 hours. The product mixture was washed with 30 ml of 5% citric acid and 30 ml of saturated sodium

bicarbinate solution. The product was recrystallized from ethanol and water to give 71 mg of white crystalline solid 17a in 60% yield, m.p. 60-62°C.

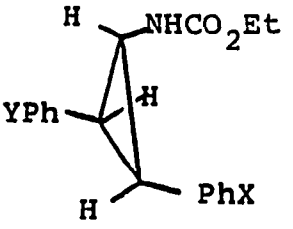

17(a-j)

X/Y = H/H (a), CH_3/CH_3 (b), OCH_3/OCH_3 (c), Cl/Cl (d), H/CH_3 (f), H/Cl (g), H/CF_3 (h), CH_3/Cl (i), CH_3/CF_3 (j)

HRMS: Calculated $C_{18}H_{19}NO_2$ m/e 281.14158
measured m/e 281.14117 error -1.5 ppm.

^{1}H NMR ($CDCl_3$): δ 7.5-7.0 (m), δ 4.5 (s), δ 4.1 (q), δ 3.3 (m), δ 2.7 (m), δ 2.6 (m), δ 1.2 (t)

FT-IR ($CDCl_3$): 3250 (m), 3000 (w), 1700 (s), 1520 (s), 700 (s) cm^{-1}.

^{13}C NMR ($CDCl_3$): δ 139.7 (rel. intens. 20), δ 128.7 (50), δ 128.5 (95), δ 128.4 (100), δ 127.1 (40), δ 128.8 (30), δ 126.4 (40), δ 37.6 (15), δ 31.1 (15).

Ethyl N-(trans-2,3-bis-(p-methylphenyl)cyclopropyl)-carbamate (17b) (Figures 85, 86) Prepared from 15b in 70% yield, m.p. 76-78°C.

HRMS: Calculated $C_{20}H_{23}NO_2$ m/e 309.17288
measured m/e 309.17271 error -0.6 ppm.

^1H NMR ($CDCl_3$): δ 7.5-7.0 (m), δ 4.5 (s), δ 4.1 (q), δ 3.1 (m), δ 2.6 (m), δ 2.4 (m), δ 2.34 (s), δ 2.32 (s), δ 1.2 (t).

FT-IR ($CDCl_3$): 3300 (w), 3000 (w), 1733 (s), 1535 (s) cm^{-1}.

^{13}C NMR ($CDCl_3$): δ 136.7 (rel. intens. 40), δ 136.4 (20), δ 135.9 (35), δ 129.2 (90), δ 129.1 (100), δ 128.6 (50), δ 127.1 (37), δ 60.8 (10), δ 59.0 (8), δ 37.3 (20), δ 30.5 (15), δ 21.0 (30), δ 14.6 (17).

Ethyl N-(trans-2,3-bis-(p-methoxyphenyl)cyclopropyl)-carbamate (17c) (Figures 87, 88) Prepared from 15c in 80% yield, m.p. 79-81°C.

HRMS: Calculated $C_{20}H_{23}NO_4$ m/e 341.16271
measured m/e 341.16339 error 2.0 ppm.

^1H NMR ($CDCl_3$): δ 7.2 (m), δ 6.8 (m), δ 4.6 (s), δ 4.1 (m), δ 3.8 (s), δ 3.7 (s), δ 3.1 (m), δ 2.5 (m), δ 2.4 (m), δ 1.2 (m).

FT-IR ($CDCl_3$): 3400 (w), 3000 (w), 1720 (m), 1518 (s), 1244 (s) cm^{-1}.

^{13}C NMR ($CDCl_3$): δ 158.4 (rel. intens. 50), δ 158.2 (30), δ 157.1 (10), δ 131.8 (40), δ 129.7 (60), δ 128.3 (50), δ 127.5 (8), δ 113.9 (100), δ 113.8 (98), δ 60.8 (10), δ 55.2 (80), δ 37.1 (30), δ 29.9 (25), δ 14.5 (25).

Ethyl N-(trans-2,3-bis-(p-chlorophenyl)cyclopropyl)-carbamate (17d) Figures 89, 90) Prepared from 15d in 60% yield, m.p. 88-91°C.

HRMS: Calculated $C_{18}H_{17}Cl_2NO_2$ m/e 349.06364
measured m/e 349.06376 error 0.3 ppm.

^1H NMR ($CDCl_3$): δ 7.3 (m), δ 4.5 (s), δ 4.1 (q), δ 3.1 (m), δ 2.5 (m), δ 2.48 (m), δ 1.2 (t).

FT-IR ($CDCl_3$): 3400 (w), 3000 (w), 1700 (m), 1500 (s), 1100 (m) cm^{-1}.

^{13}C NMR ($CDCl_3$): δ 156.9 (rel. intens. 25), δ 137.8 (30), δ 133.7 (10), δ 132.8 (30), δ 132.3 (15), δ 129.9 (40), δ 128.6 (99), δ 128.58 (100), δ 61.1 (10), δ 37.6 (15), δ 30.6 (14), δ 30.57 (12), δ 14.5 (8).

Ethyl N-(trans-2-(p-methylphenyl)-3-phenylcyclopropyl)-carbamate (17f) (Figures 91, 92) Prepared from 15f in 70% yield, m.p. 4-8°C.

HRMS: Calculated $C_{19}H_{21}NO_2$ m/e 295.15727
measured m/e 295.15692 error -1.1 ppm.

^{1}H NMR ($CDCl_3$): δ 7.2 (m), δ 4.6 (s), δ 4.1 (m), δ 3.2 (m), δ 2.6 (m), δ 2.5 (m), δ 2.36 (s), δ 2.35 (s), δ 1.2 (m).

FT-IR ($CDCl_3$): 3400 (m), 3000 (m), 1710 (s), 1500 (s), 1230 (s), 1070 (s) cm^{-1}.

^{13}C NMR ($CDCl_3$): δ 157.0 (rel. intens. 20), δ 156.9 (18), δ 139.8 (30), δ 136.6 (35), δ 136.3 (15), δ 135.9 (20), δ 129.2 (80), δ 129.0 (100), δ 128.6 (50), δ 128.4 (90), δ 126.9 (60), δ 126.6 (40), δ 126.2 (45), δ 60.9 (10), δ 60.8 (20), δ 37.4 (30), δ 31.0 (25), δ 30.7 (23), δ 30.5 (21), δ 20.9 (35), δ 14.5 (32).

Ethyl N-(trans-2-(p-chlorophenyl)-3-phenylcyclopropyl)-carbamate (17g) (Figures 93, 94) Prepared from 15g in 72% yield, m.p. 89-92°C.

HRMS: Calculated $C_{18}H_{18}ClNO_2$ m/e 315.10261 measured m/e 315.10218 error -1.4 ppm.

^{1}H NMR ($CDCl_3$): δ 7.2 (m), δ 4.6 (s), δ 4.1 (m), δ 3.3 (m), δ 2.5 (m), δ 2.4 (m), δ 1.2 (m).

FT-IR ($CDCl_3$): 3400 (w), 3000 (w), 1705 (s), 1490 (s), 1250 (m), 1090 (m), 1075 (m) cm^{-1}.

^{13}C NMR ($CDCl_3$): δ 156.95 (rel. intens. 20), δ 156.86 (20), δ 139.2 (50), δ 138.2 (18), δ 134.2 (15), δ 132.4 (30), δ 131.9 (25), δ 129.9 (35),

δ 128.4 (100), δ 126.8 (70), δ 126.4 (60), δ 60.9 (40), δ 37.6 (35), δ 30.9 (40), δ 30.4 (25), δ 29.9 (23), δ 14.4 (47).

Ethyl N-(trans-2-phenyl-3-(p-trifluoromethylphenyl)-cyclopropyl)carbamate (17h) (Figures 95, 96) Prepared from 15h in 60% yield, m.p. 92-99°C.

HRMS: Calculated $C_{19}H_{18}F_3NO_2$ m/e 349.12897
measured m/e 349.12896 error 0.03 ppm.

^{1}H NMR ($CDCl_3$): δ 7.2 (m), δ 4.6 (m), δ 4.1 (m), δ 3.3 (m), δ 2.7 (m), δ 1.2 (m).

FT-IR ($CDCl_3$): 3400 (w), 3000 (w), 1712 (s), 1530 (m), 1350 (s), 1190 (s), 1130 (s), 1090 (s) cm^{-1}.

^{13}C NMR ($CDCl_3$): δ 139.0 (rel. intens. 30), δ 128.7 (100), δ 126.7 (60), δ 125.3 (40), δ 38.1 (15), δ 30.9 (10), δ 14.5 (30).

Ethyl N-(trans-2-(p-chlorophenyl)-3-(p-methylphenyl)-cyclopropyl)carbamate (17i) (Figures 97, 98) Prepared from 15i in 55% yield, m.p. 85-88°C.

HRMS: Calculated $C_{19}H_{20}ClNO_2$ m/e 329.11826
measured m/e 329.11792 error -1.0 ppm.

^{1}H NMR ($CDCl_3$): δ 7.2 (m), δ 4.6 (s), δ 4.1 (m); δ 3.1 (m), δ 2.5 (m), δ 2.46 (m), δ 2.34 (s), δ 2.32 (s), δ 1.2 (m).

FT-IR ($CDCl_3$): 3400 (w), 3000 (w), 1702 (s), 1520 (m), 1500 (s), 1230 (m), 1120 (m) cm^{-1}.

^{13}C NMR ($CDCl_3$): δ 138.3 (rel. intens. 18), δ 136.2 (20), δ 136.1 (20), δ 132.5 (20), δ 132.1 (20), δ 130.0 (20), δ 129.3 (60), δ 129.2 (90), δ 128.5 (100), δ 126.9 (30), δ 37.5 (20), δ 30.3 (15), δ 21.0 (30), δ 14.5 (25).

Ethyl N-(trans-2-(p-methylphenyl)-3-(p-trifluoromethylphenyl)cyclopropyl)carbamate (17j) (Figures 99, 100)

Prepared from 15j in 50% yield, as a yellow oil.

GC-HRMS: Calculated $C_{20}H_{20}F_3NO_2$ m/e 363.14462 measured m/e 363.14529 error 1.8 ppm.

^1H NMR ($CDCl_3$): δ 7.6-7.2 (m), δ 4.91 (s), δ 4.75 (s), δ 4.11 (m), δ 3.55 (q), δ 3.26 (m), δ 2.65 (m), δ 2.42 (s), δ 2.40 (s), δ 1.28 (m).

FT-IR ($CDCl_3$): 3315 (m), 3000 (m), 1711 (s), 1519 (s), 1325 (s), 1068 (s) cm^{-1}.

^{13}C NMR ($CDCl_3$): δ 157.1 (rel. intens. 20), δ 150.3 (15), δ 144.1 (40), δ 140.3 (20), δ 136.7 (25), δ 136.2 (42), δ 135.9 (40), δ 129.7 (70), δ 129.3 (100), δ 129.2 (90), δ 128.7 (50), δ 128.4 (60), δ 127.2 (40), δ 126.8 (45), δ 125.5 (43), δ 125.3 (45), δ 125.1 (43), δ 120.1 (50), δ 65.7 (70), δ 60.9 (40), δ 37.9 (35), δ 37.7 (3), δ 31.5 (16),

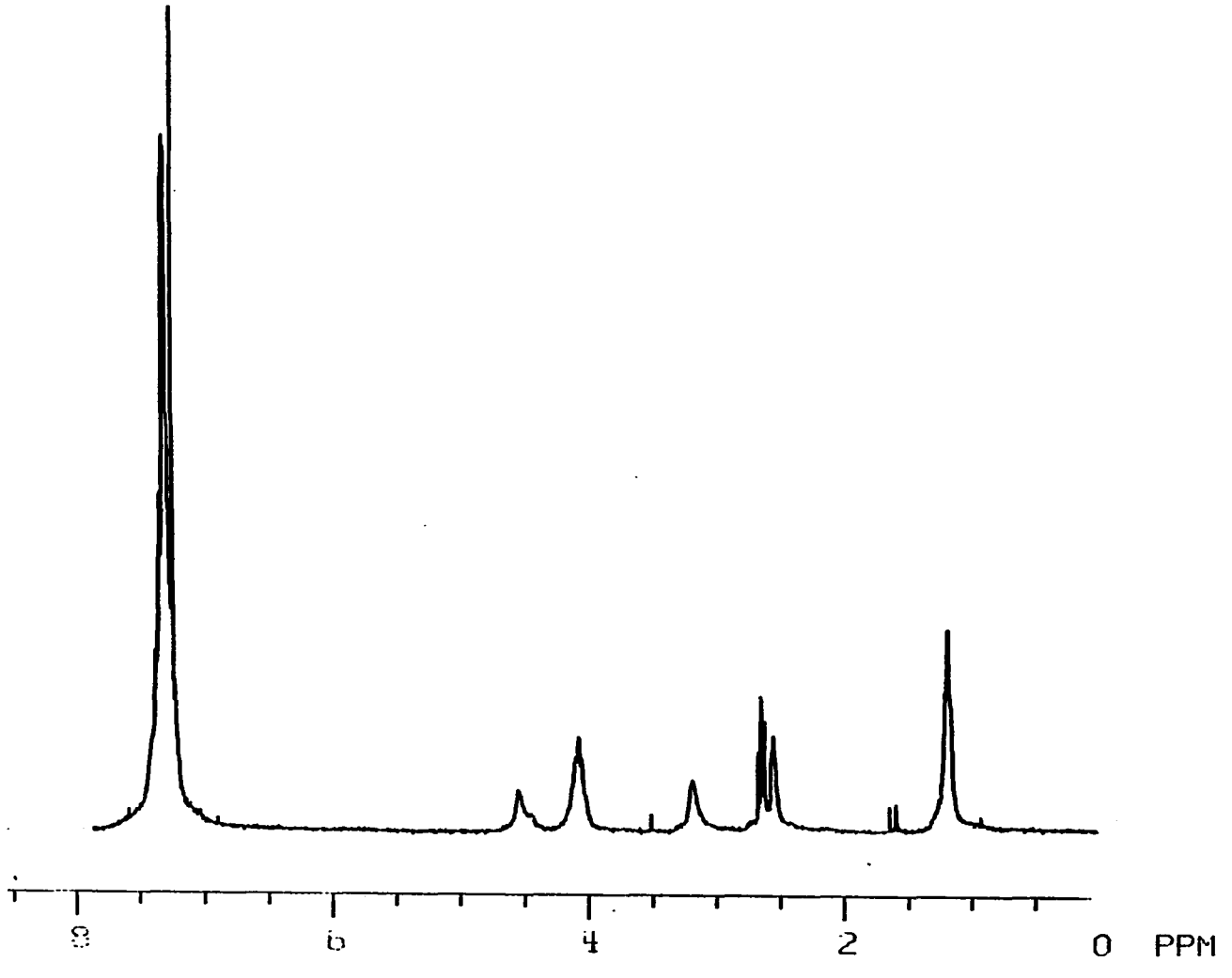

Figure 83. ^{1}H NMR of 17a in $CDCl_3$

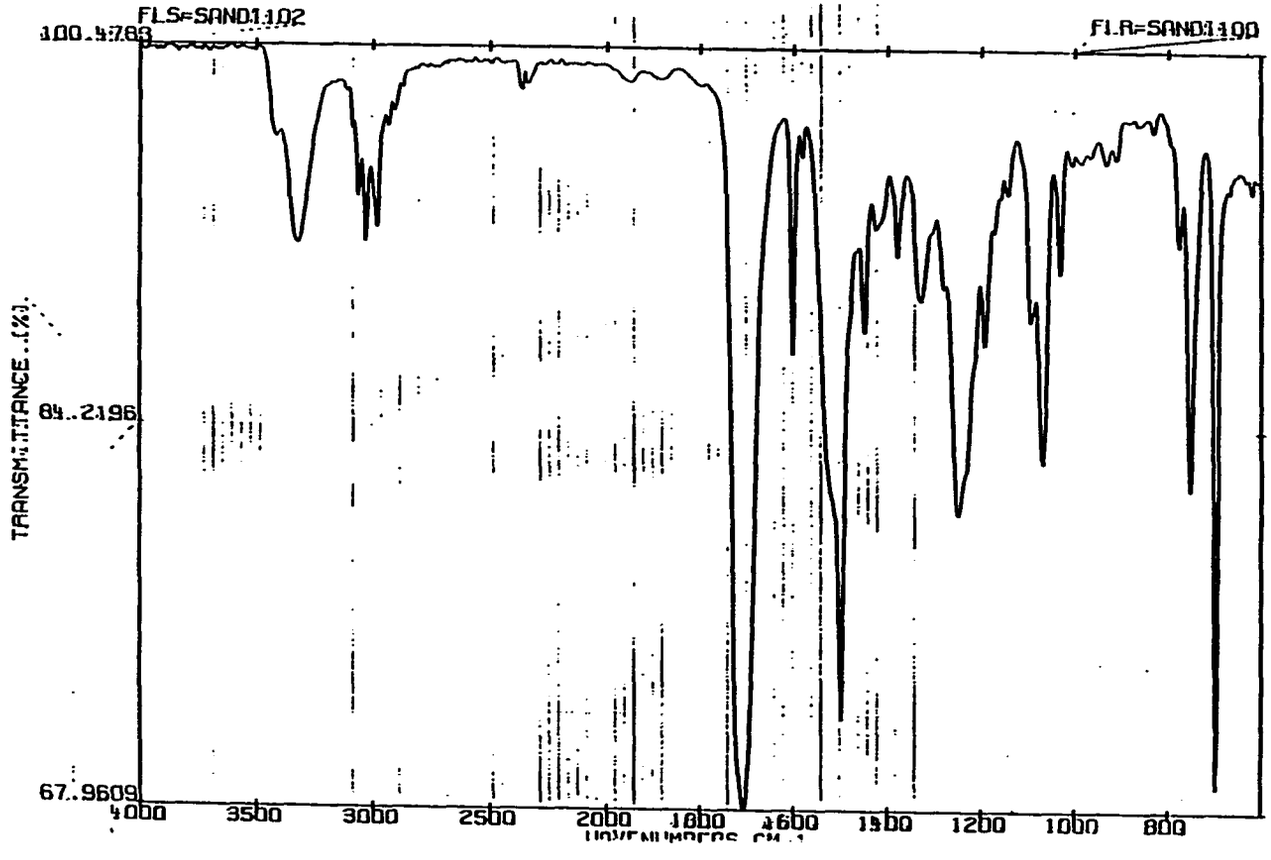

Figure 84. FT-IR of 17a in $CDCl_3$

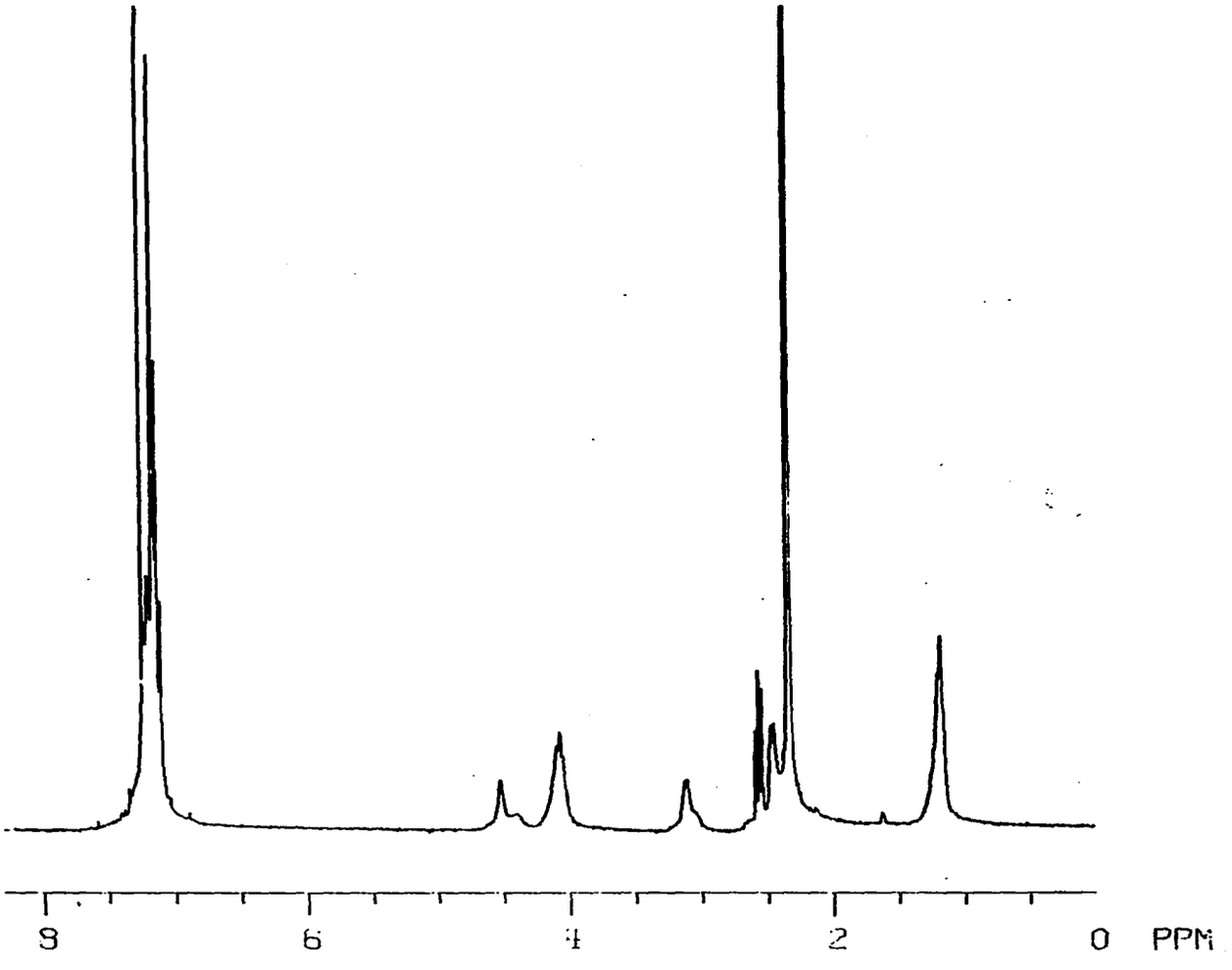

Figure 85. ^{1}H NMR of 17b in $CDCl_3$

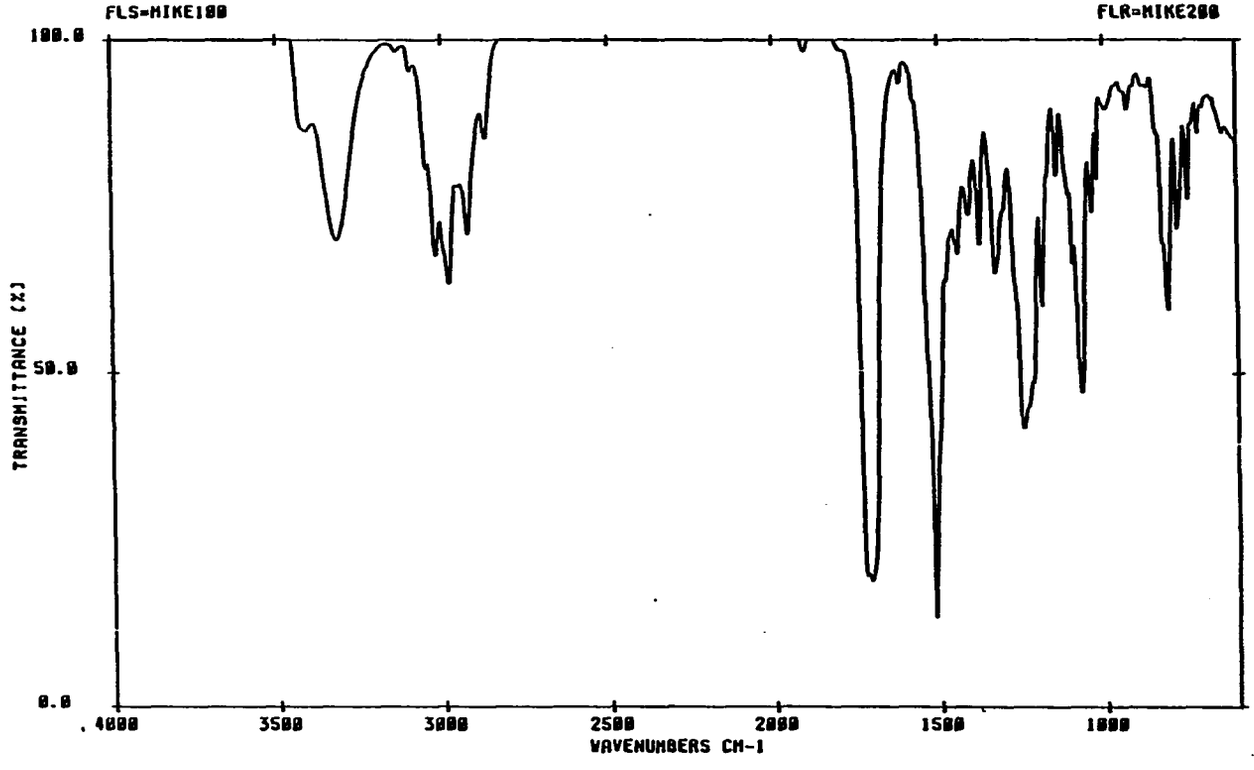

Figure 86. FT-IR of 17b in $CDCl_3$

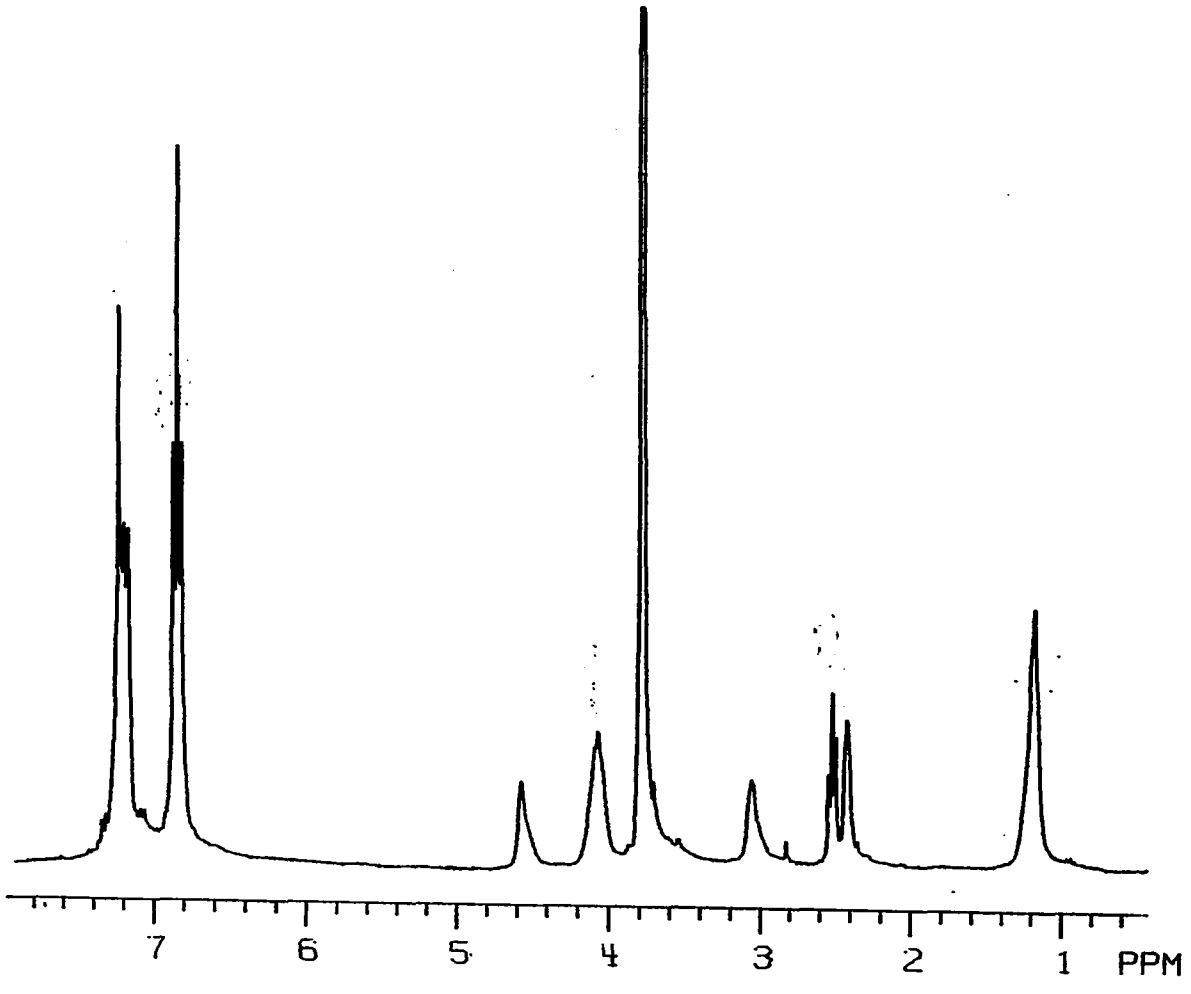

Figure 87. ^{1}H NMR of 17c in $CDCl_3$

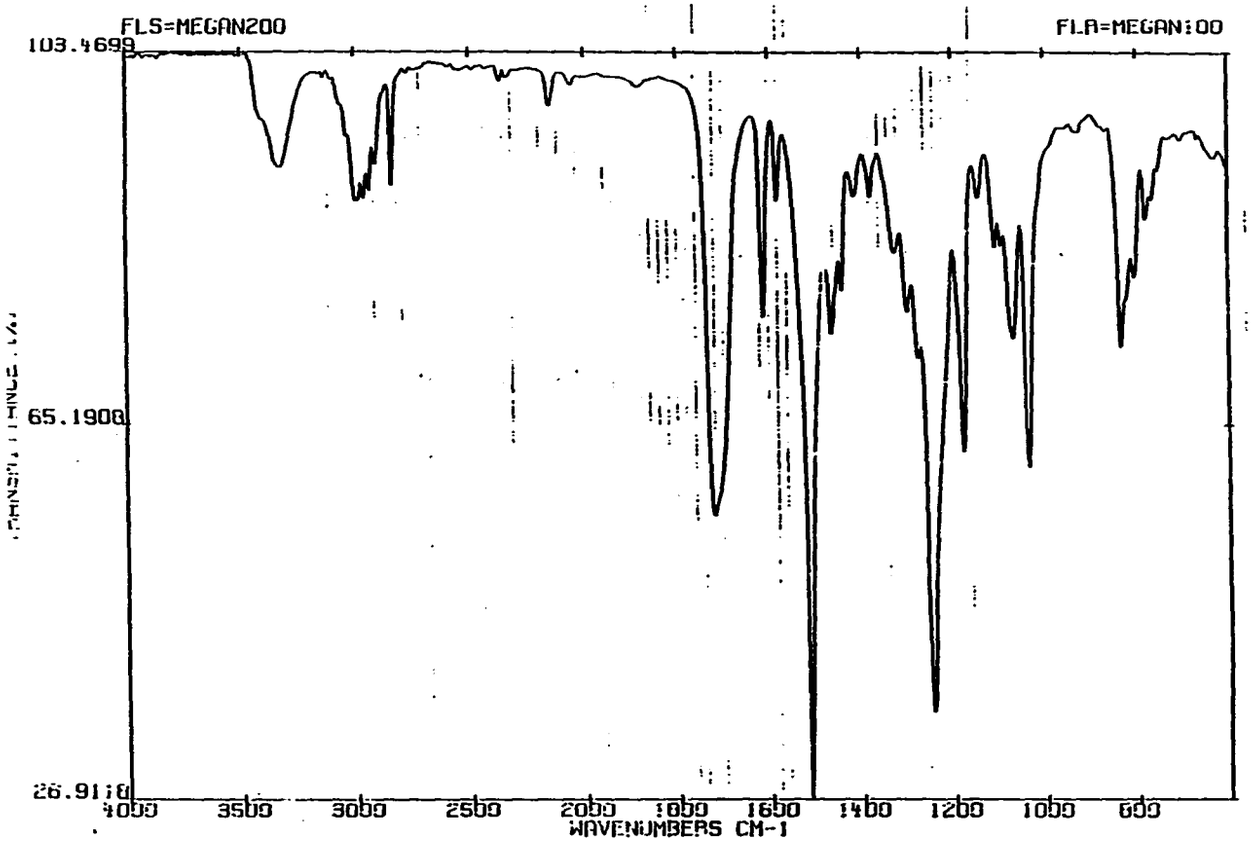

Figure 88. FT-IR of 17c in $CDCl_3$

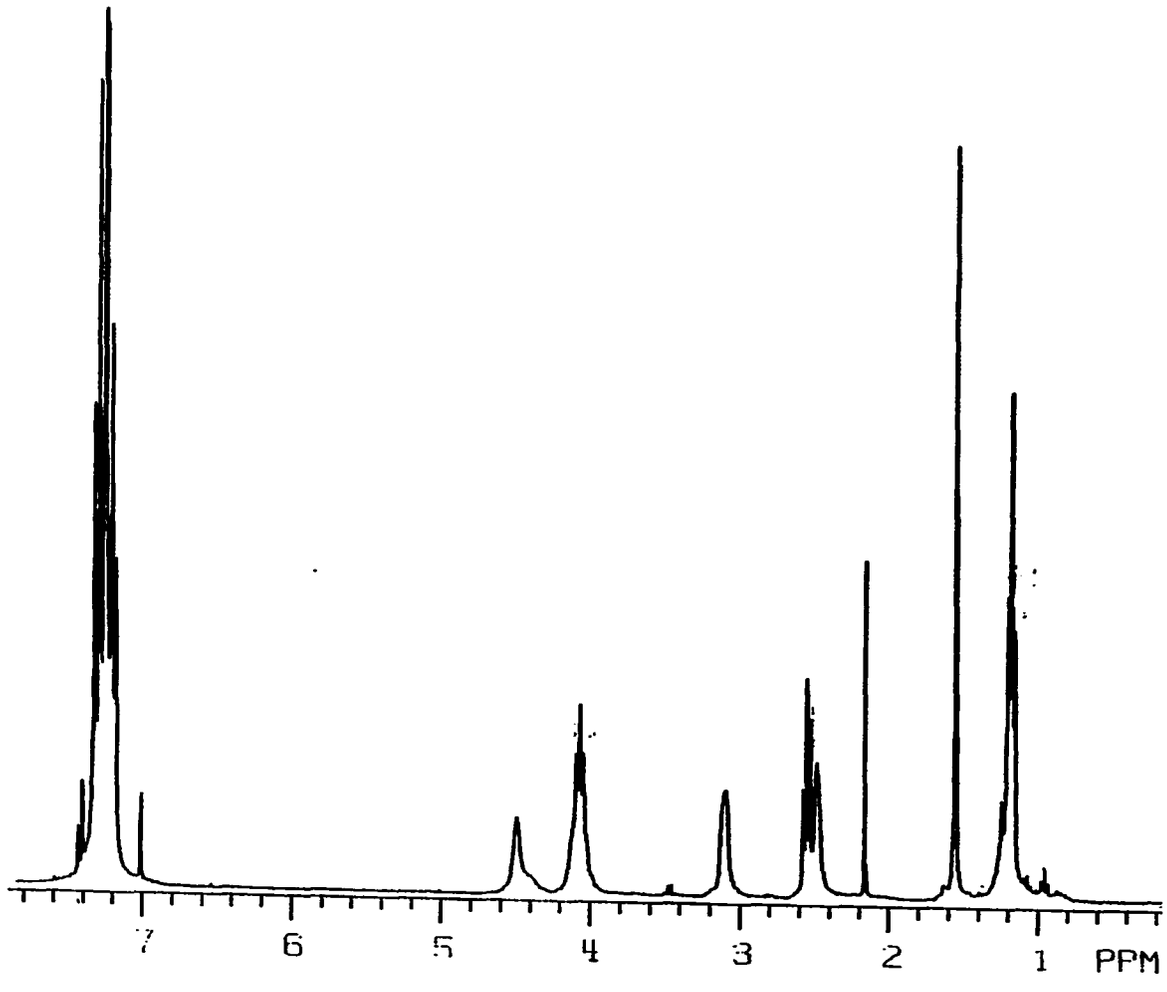

Figure 89. ^{1}H NMR of 17d in $CDCl_3$

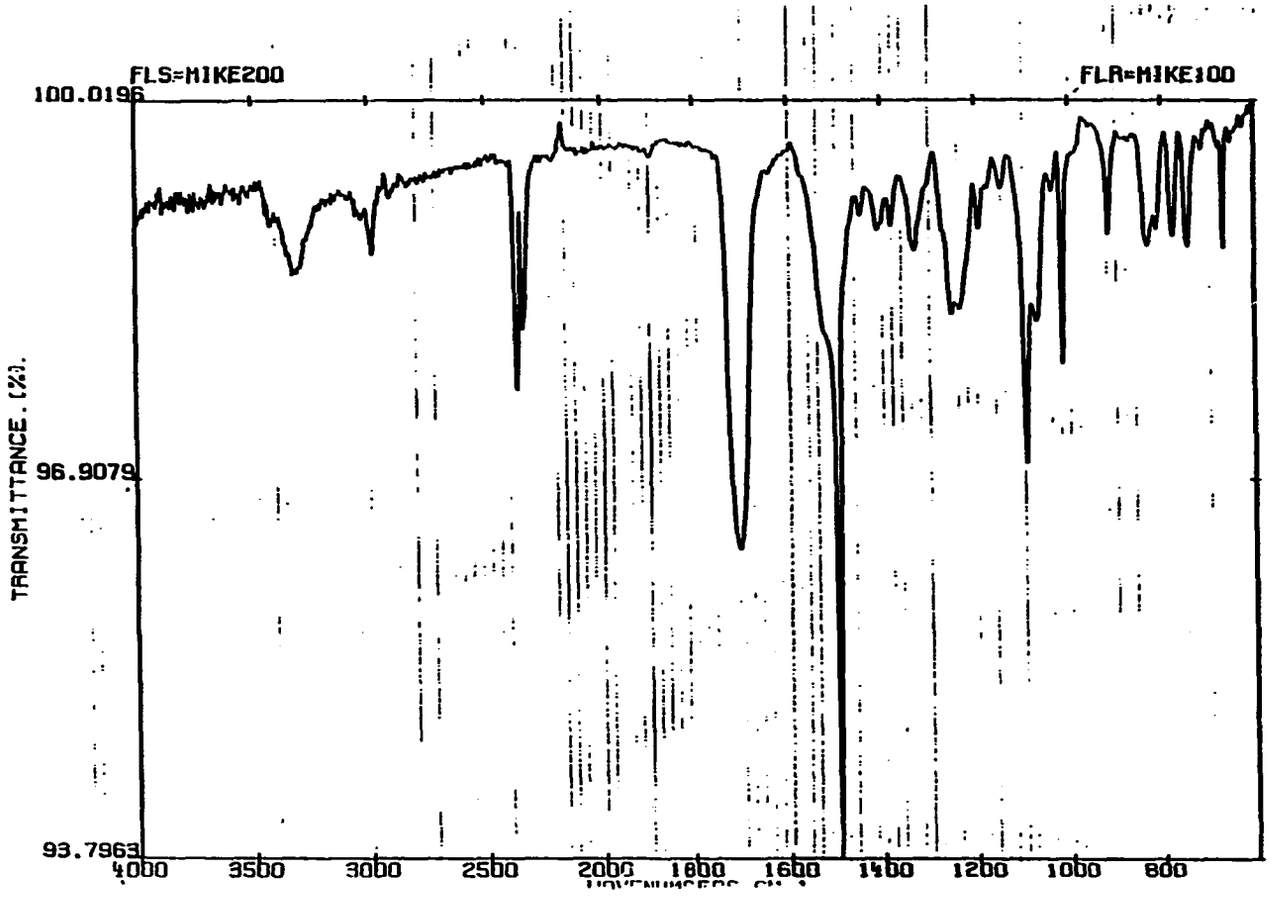

Figure 90. FT-IR of 17d in $CDCl_3$

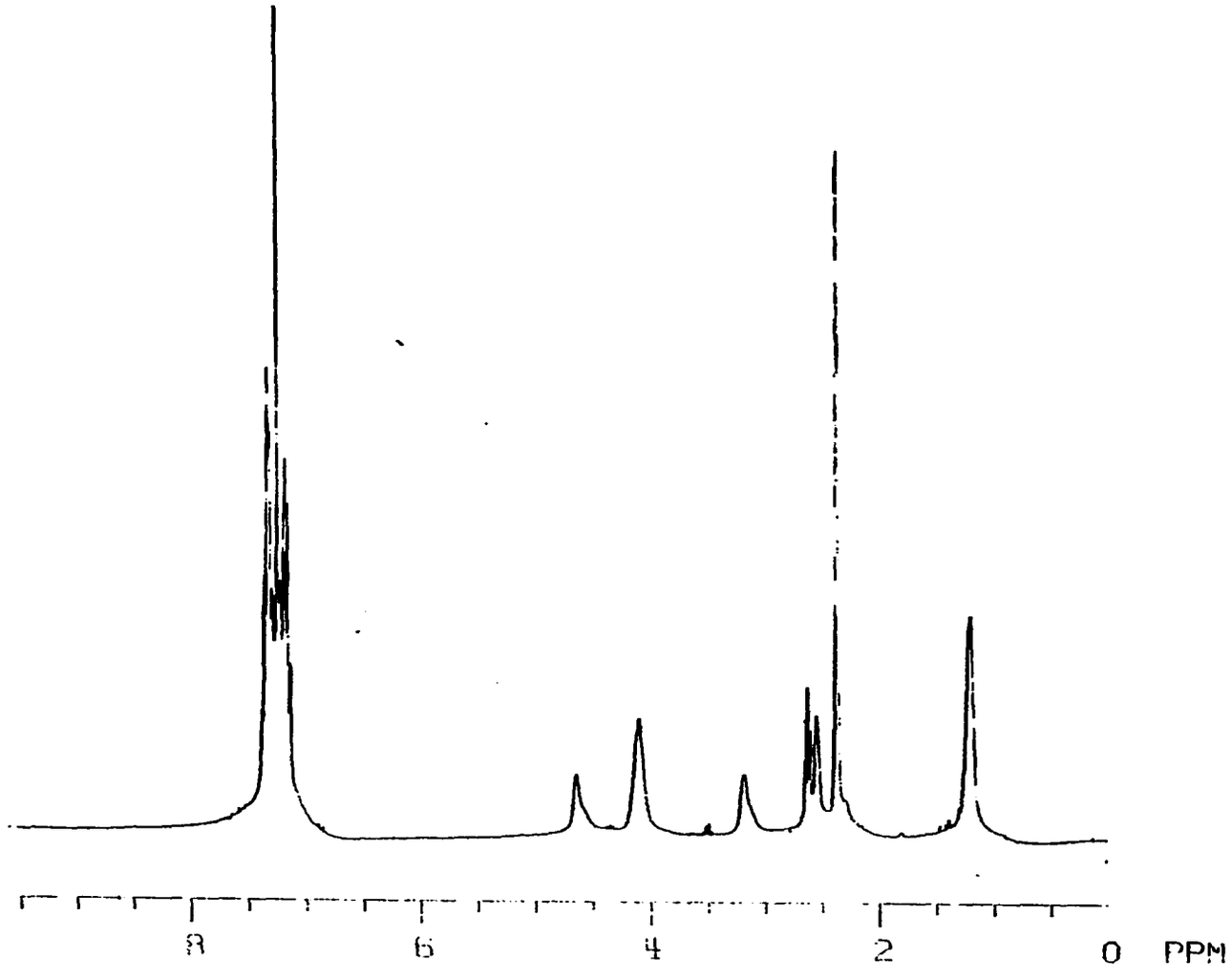

Figure 91. ^{1}H NMR of 17f in $CDCl_3$

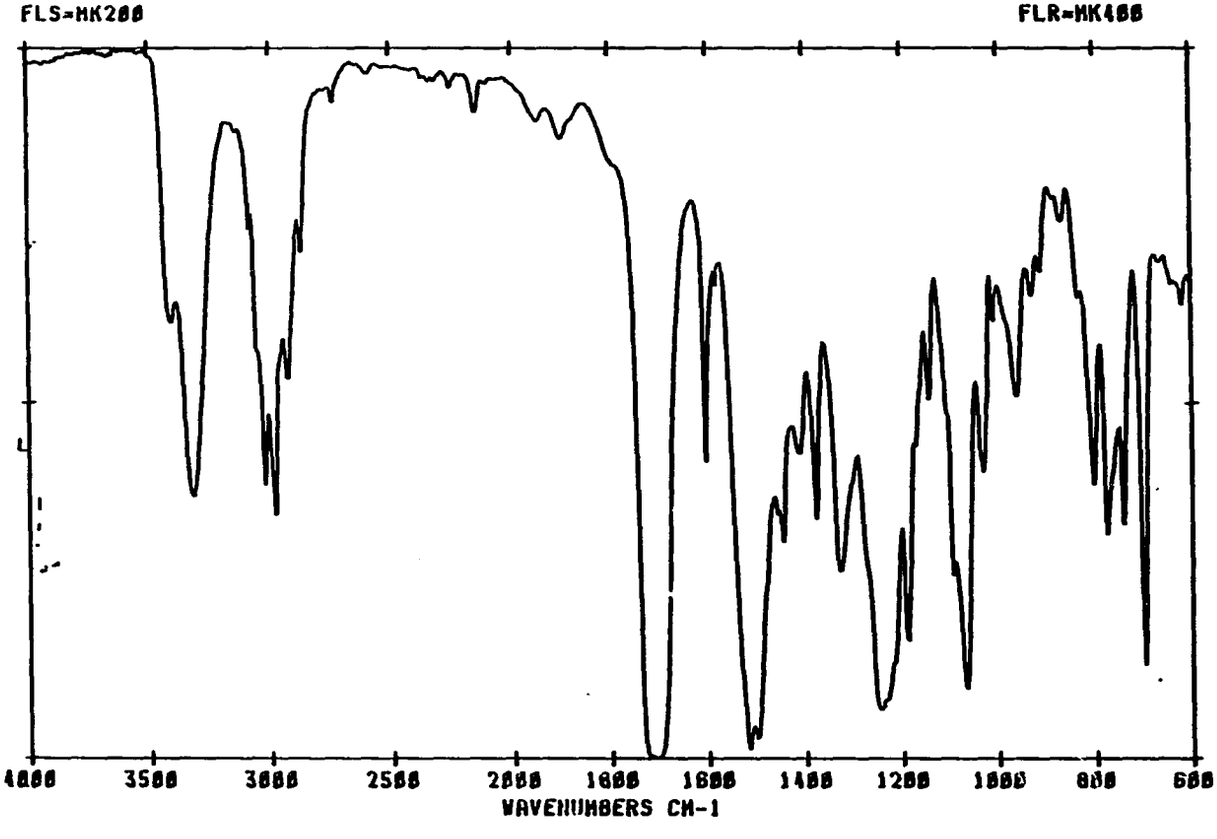

Figure 92. FT-IR of 17f in $CDCl_3$

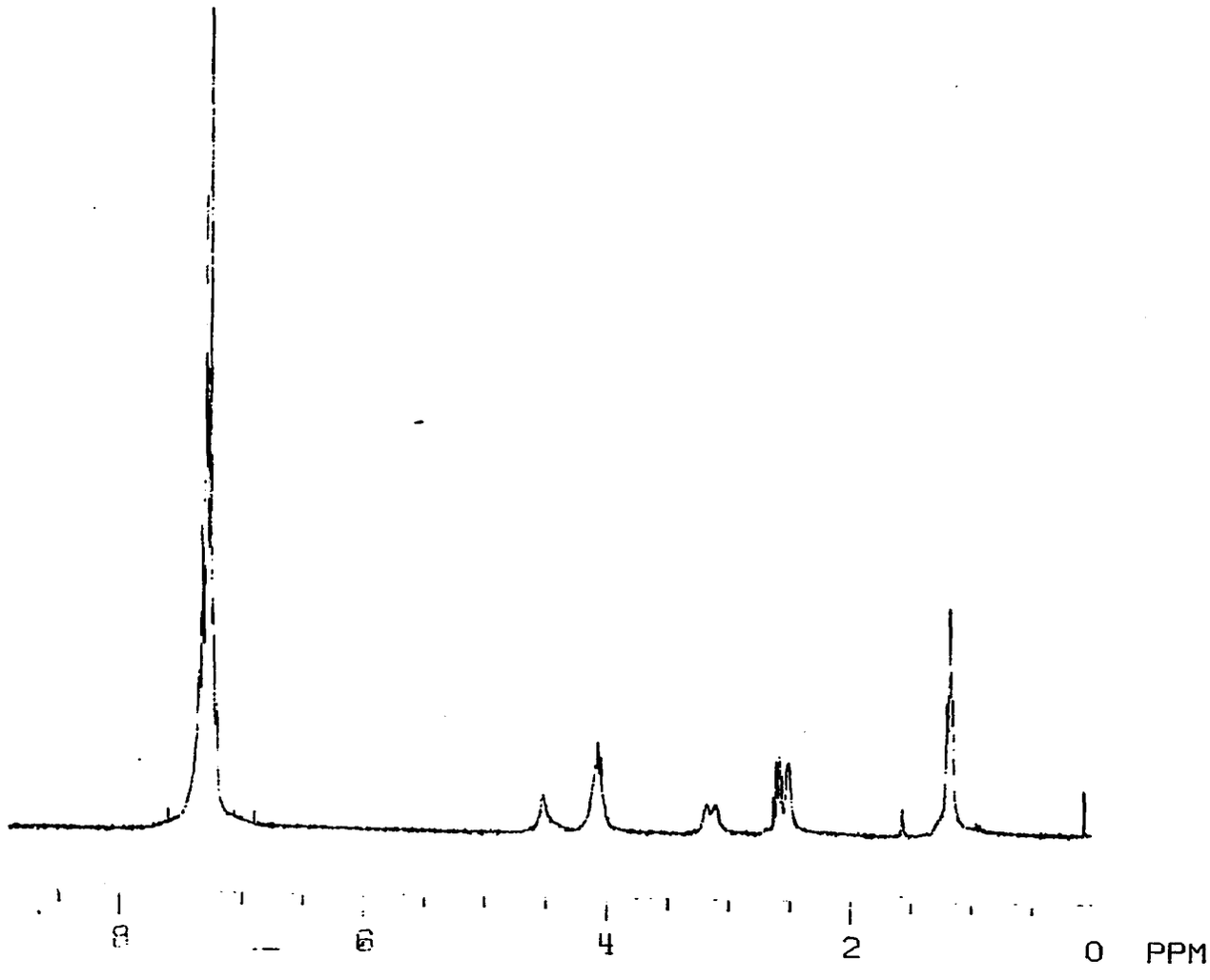

Figure 93. ^{1}H NMR of 17g in $CDCl_3$

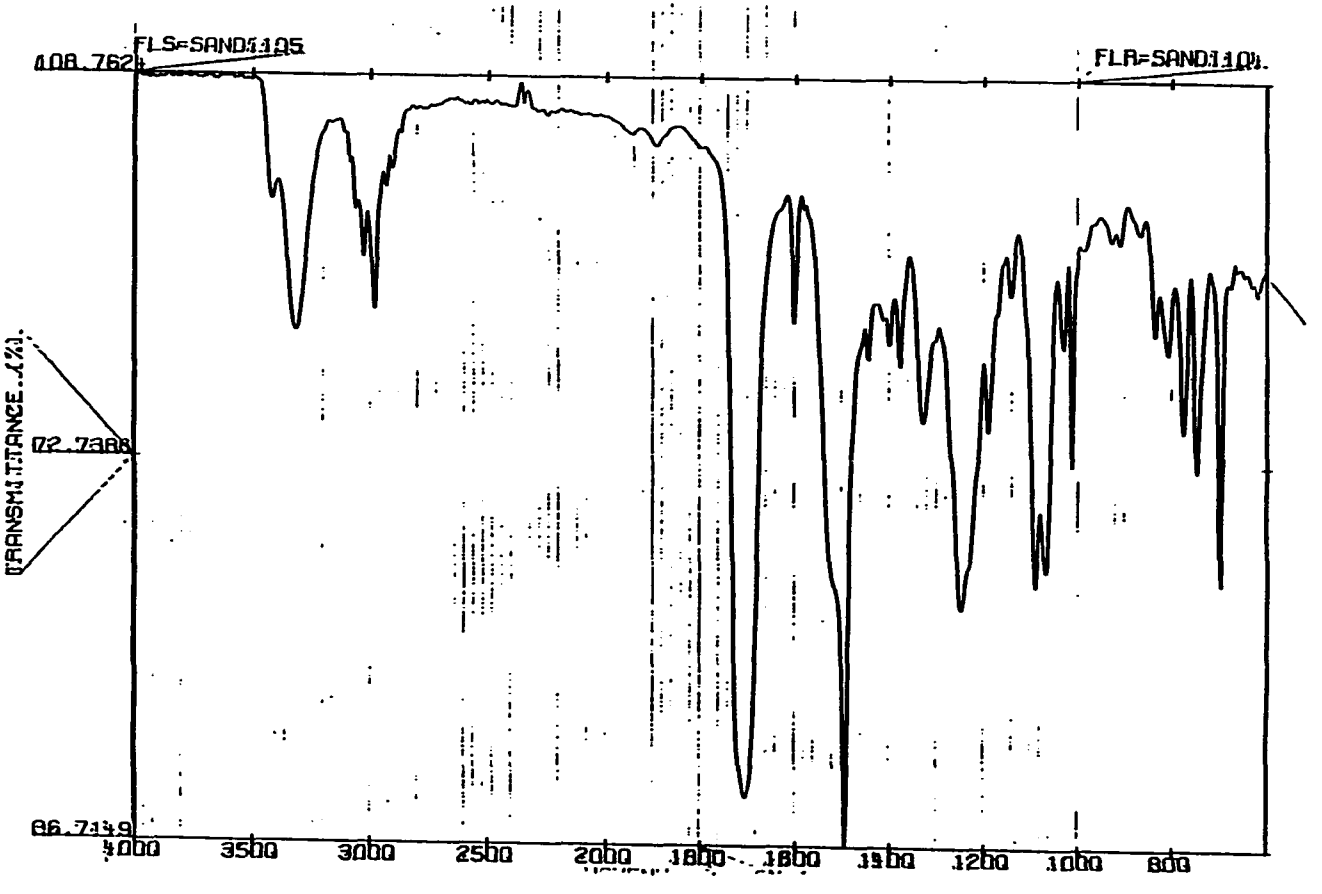

Figure 94. FT-IR of 17g in $CDCl_3$

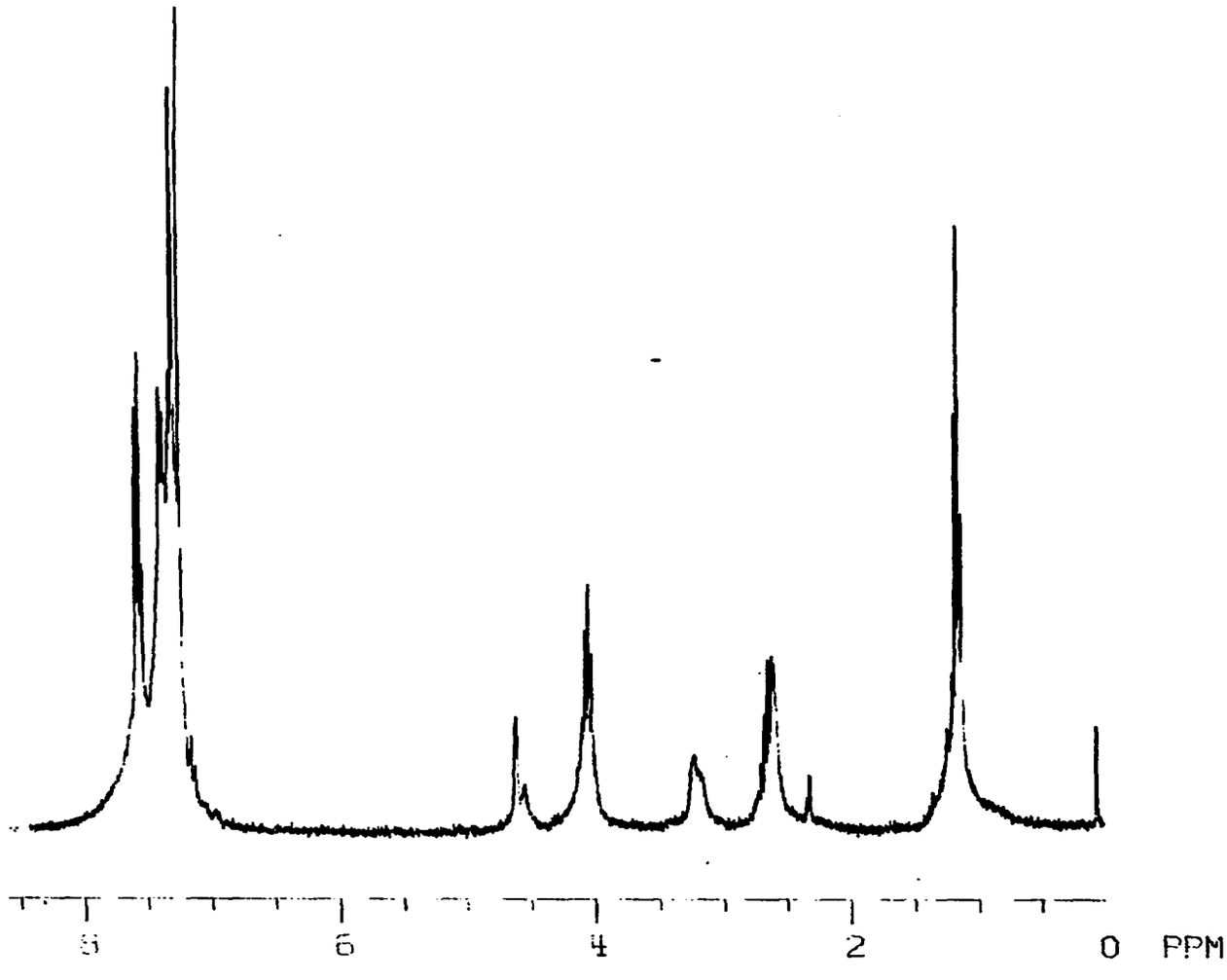

Figure 95. ^{1}H NMR of 17h in $CDCl_3$

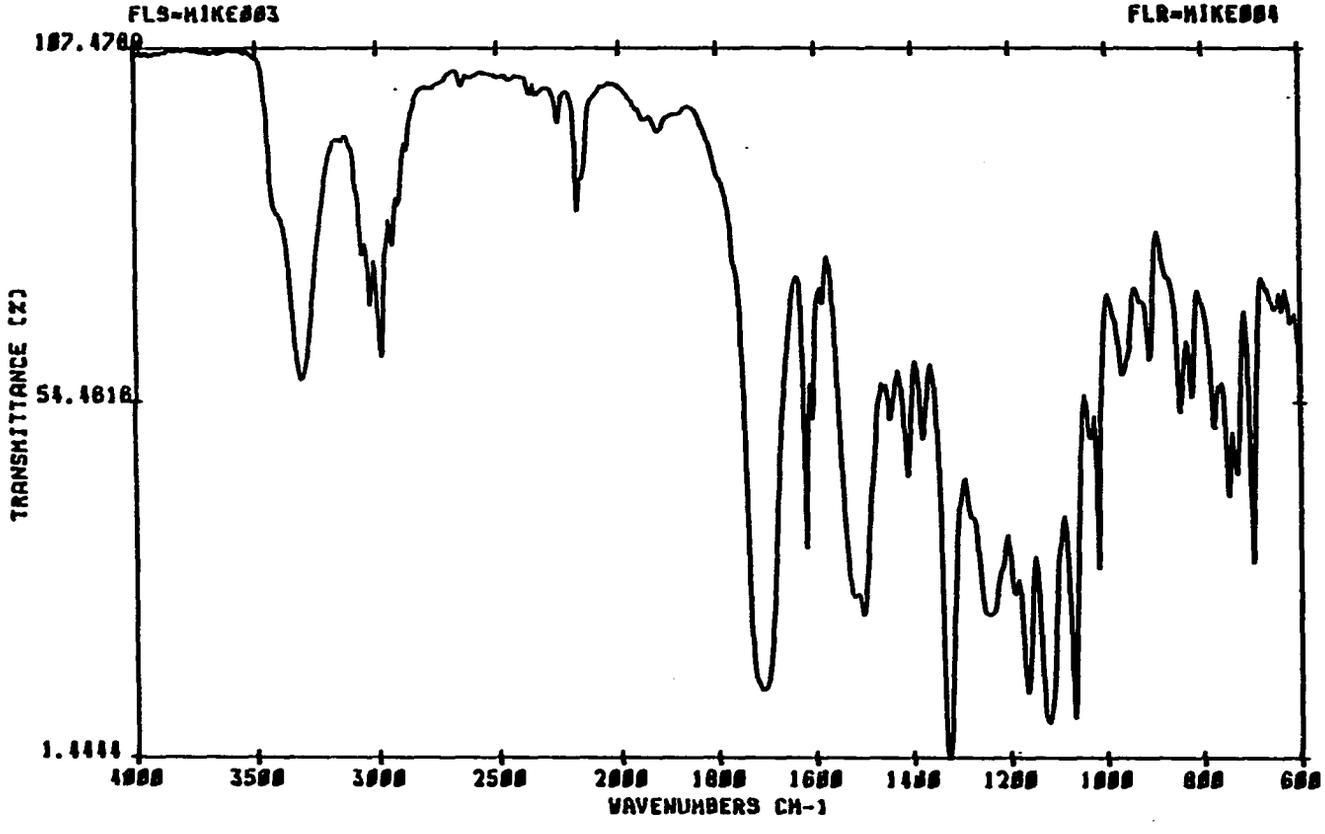

Figure 96. FT-IR of 17h in $CDCl_3$

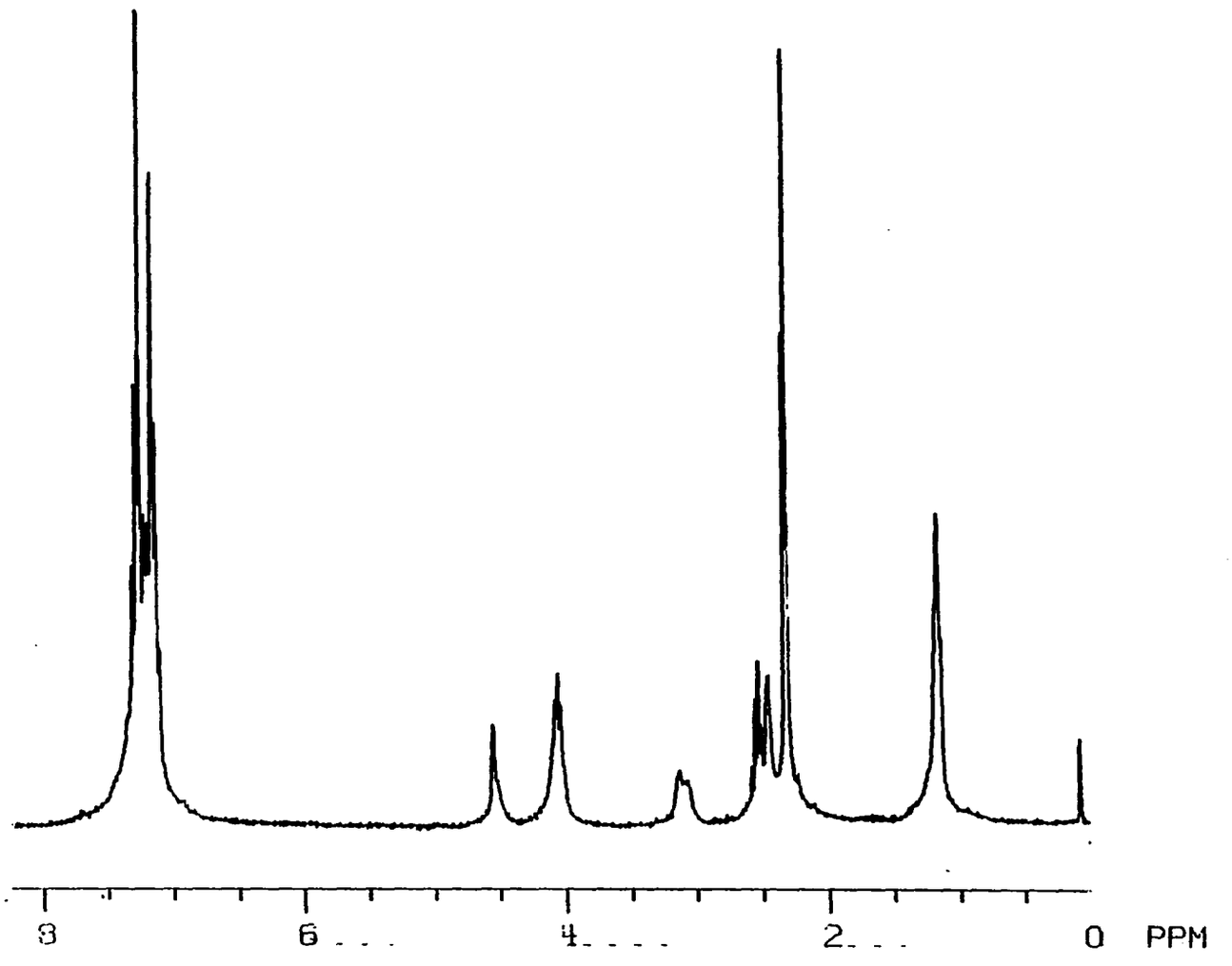

Figure 97. ^{1}H NMR of 17i in $CDCl_3$

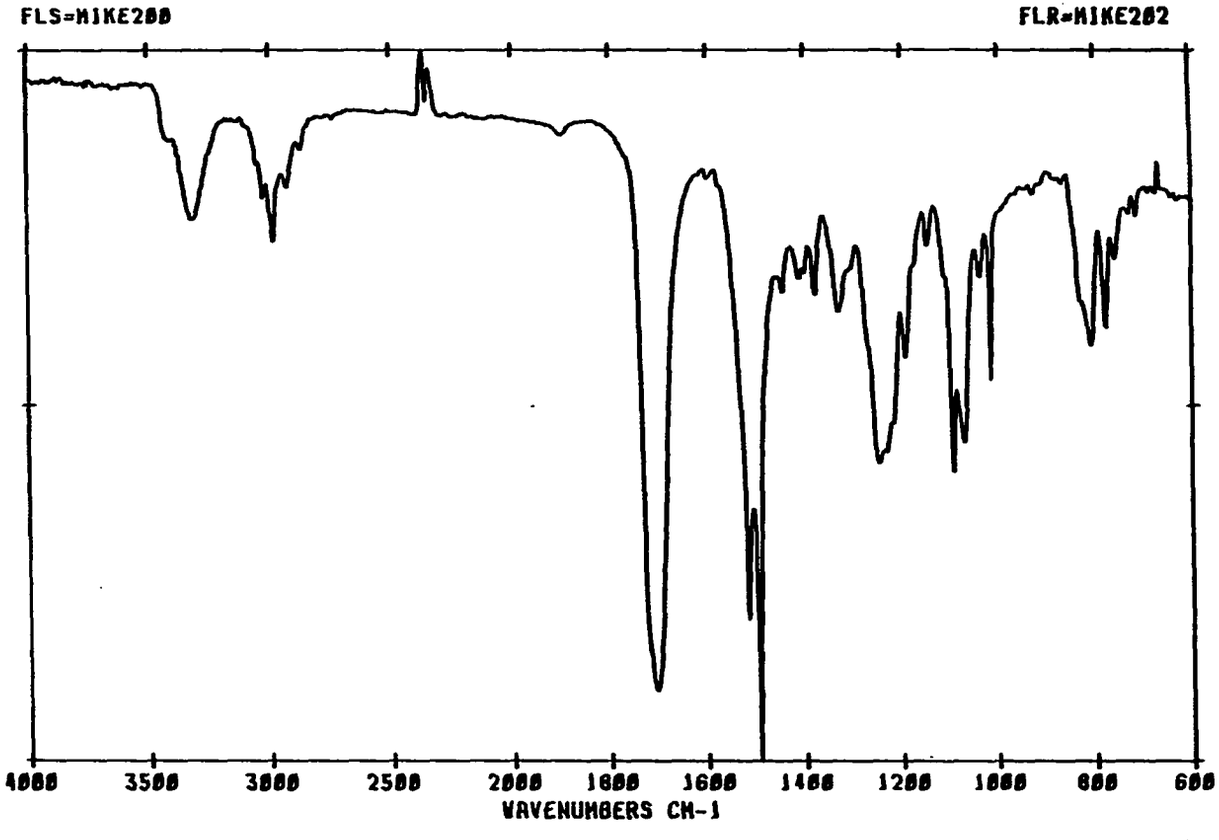

Figure 98. FT-IR of 17i in $CDCl_3$

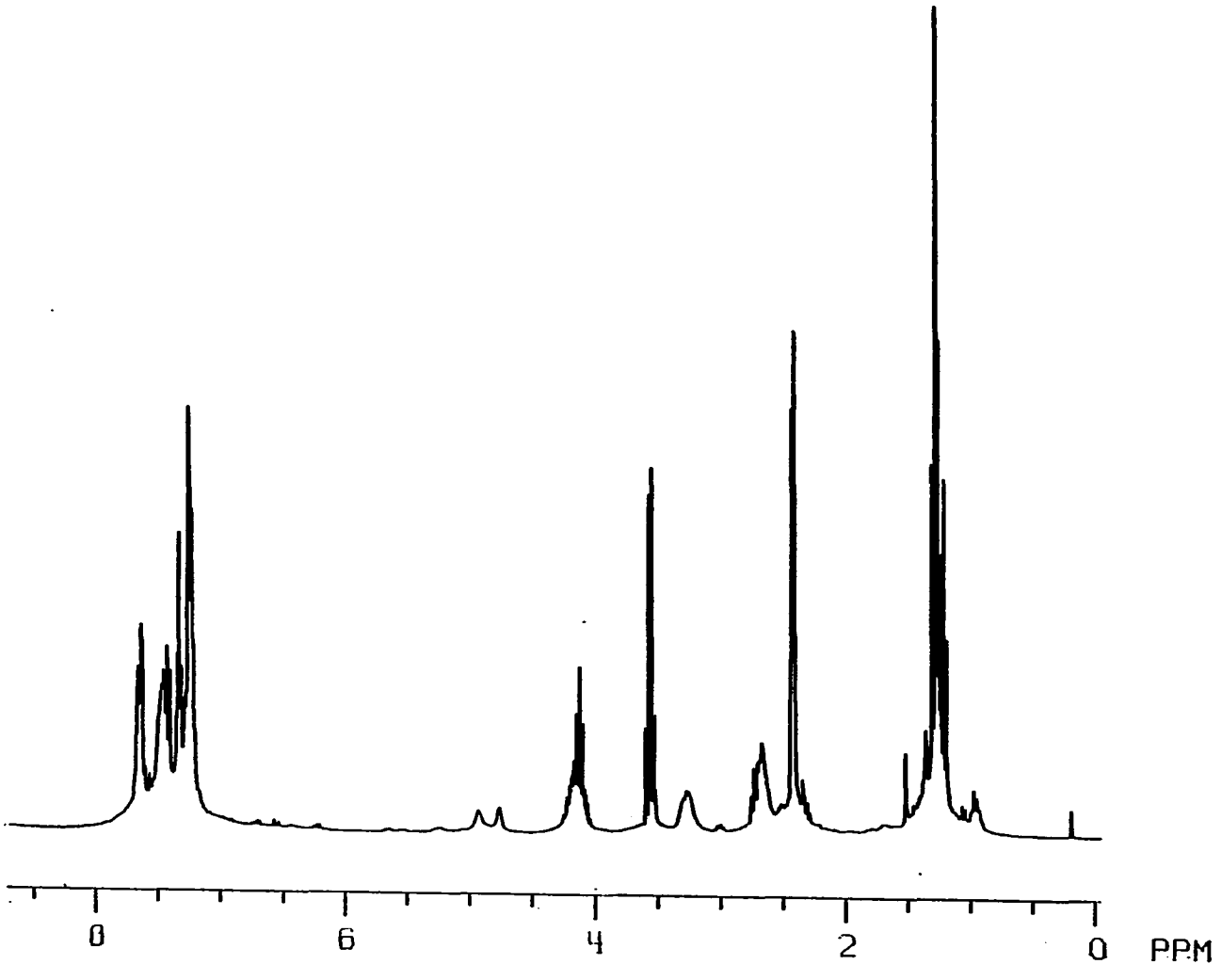

Figure 99. ^{1}H NMR of 17j in $CDCl_3$

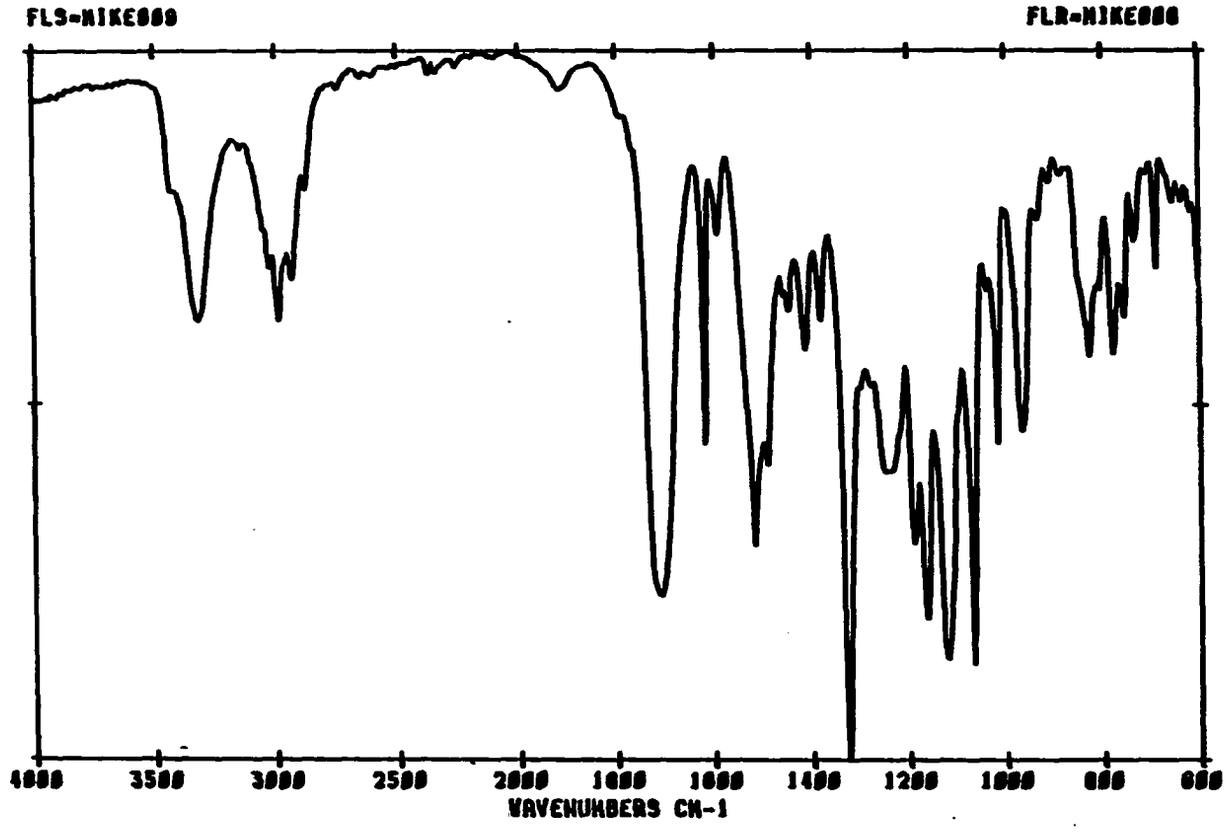

Figure 100. FT-IR of 17j in $CDCl_3$

δ 30.4 (28), δ 20.9 (70), δ 15.2 (50),
δ 14.5 (45).

General synthesis of ethyl N-nitroso N-(trans-2,3-diaryl-cyclopropyl)carbamates (18a-j)

Preparation of ethyl N-nitroso N-(trans-2,3-diphenyl-cyclopropyl)carbamate (18a) Figures 101, 102 A 25 ml round bottom flask was charged with 100 mg of 17a, 5 ml of acetic anhydride, 10 equivalents of sodium nitrite and 50 µl of glacial acetic acid. The reaction was cooled in an ice/water bath and allowed to stir for 2 hours. The product mixture was then poured into 250 ml of ice water and 200 ml of water was then decanted off. The organic phase was then dissolved in 150 ml of hexanes, this layer was washed with cold 5% sodium bicarbinate solution until it was slightly basic. The organic layer was then washed with water and the solvent was removed under reduced pressure. The product was dried on a high vacuum line as it reacts with magnesium sulfate. The product 18a was obtained as a yellow oil which was acid, base and heat sensitive.

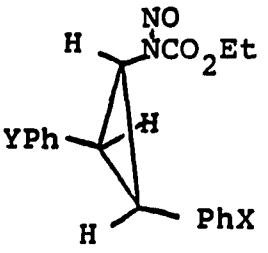

18(a-j)

X/Y = H/H (a), CH_3/CH_3 (b), OCH_3/OCH_3 (c), Cl/Cl (d), H/CH_3 (f), H/Cl (g), H/CF_3 (h), CH_3/Cl (i), CH_3/CF_3 (j)

^{1}H NMR ($CDCl_3$): δ 7.2 (m), δ 4.3 (m), δ 4.2 (m), δ 2.9 (m), δ 1.2 (t).

FT-IR ($CDCl_3$): 3000 (w), 1784 (s), 1500 (m), 1200 (m), 700 (s) cm^{-1}.

Ethyl N-nitroso N-(trans-2,3-bis(p-methylphenyl)-cyclopropyl)carbamate (18b) (Figures 103, 104) Prepared from 17b as a yellow oil.

^{1}H NMR ($CDCl_3$): δ 7.4-6.8 (m), δ 4.3 (m), δ 4.2 (m), δ 2.8 (m), δ 2.32 (s), δ 2.27 (s), δ 1.2 (t).

FT-IR ($CDCl_3$): 3000 (w), 1764 (s), 1520 (s), 1190 (m), 740 (s) cm^{-1}.

Ethyl N-nitroso N-(trans-2,3-bis(p-methoxyphenyl)-cyclopropyl)carbamate (18c) (Figures 105, 106) Prepared from 17c as a yellow oil.

^{1}H NMR ($CDCl_3$): δ 7.26 (m), δ 6.95 (d), δ 6.86 (d), δ 6.77 (d), δ 4.3 (m), δ 4.2 (m), δ 3.8 (s), δ 3.75 (s), δ 2.76 (t), δ 1.2 (t).

FT-IR ($CDCl_3$): 3000 (w), 1768 (s), 1512 (s), 1240 (s) cm^{-1}.

Ethyl N-nitroso N-(trans-2,3-bis(p-chlorophenyl)-cyclopropyl)carbamate (18d) (Figures 107, 108) Prepared from 17d as a yellow oil.

^{1}H NMR ($CDCl_3$): δ 7.5-7.0 (m), δ 4.3 (m), δ 4.2 (m), δ 2.7 (m), δ 1.2 (m).

FT-IR ($CDCl_3$): 3000 (w), 1730 (s), 1500 (s), 1084 (s) cm^{-1}.

Ethyl N-nitroso N-(trans-2-(p-methylphenyl)-3-phenyl-cyclopropyl)carbamate (18f) (Figures 109, 110) Prepared from 17f as a yellow oil.

^{1}H NMR ($CDCl_3$): δ 7.5-7.0 (m), δ 4.2 (m), δ 4.1 (m), δ 2.8 (m), δ 2.33 (s), δ 2.3 (m), δ 2.28 (s), δ 1.2 (m).

FT-IR ($CDCl_3$): 3000 (w), 2904 (s), 1770 (s), 1540 (s), 1240 (s) cm^{-1}.

Ethyl N-nitroso N-(trans-2-(p-chlorophenyl)-3-phenylcyclopropyl)carbamate (18g) (Figures 111, 112) Prepared from 17g as a yellow oil.

^{1}H NMR ($CDCl_3$): δ 7.4-7.2 (m), δ 7.1-6.9 (m), δ 4.3 (m), δ 2.8 (m), δ 1.2 (m).

FT-IR ($CDCl_3$): 3006 (w), 1757 (s), 1494 (m), 1381 (s), 1338 (m), 1186 (s), 1012 (m) cm^{-1}.

Ethyl N-nitroso N-(trans-2-phenyl-3-(p-trifluoromethylphenyl)cyclopropyl)carbamate (18h) (Figures 113, 114)

Prepared from 17h as a yellow oil.

^{1}H NMR ($CDCl_3$): δ 7.6-7.0 (m), δ 4.3 (m), δ 2.9 (m), δ 1.2 (m).

FT-IR ($CDCl_3$): 3000 (w), 1765 (s), 1341 (s), 1120 (s) cm^{-1}.

Ethyl N-nitroso N-(trans-2-(p-chlorophenyl)-3-(p-methylphenyl)cyclopropyl)carbamate (18i) (Figures 115, 116)

Prepared from 17i as a yellow oil.

^{1}H NMR ($CDCl_3$): δ 7.3-6.9 (m), δ 4.3 (m), δ 2.8 (m), δ 2.33 (s), δ 2.28 (s), δ 1.3 (m).

FT-IR ($CDCl_3$): 3000 (w), 1753 (s), 1518 (s), 1494 (s), 1182 (s) cm^{-1}.

Ethyl N-nitroso N-(trans-2-(p-methylphenyl)-3-(p-trifluoromethylphenyl)cyclopropyl)carbamate (18j) (Figures 117, 118) Prepared from 17j as a yellow oil.

^{1}H NMR ($CDCl_3$): δ 7.2 (m), δ 3.90 (m), δ 2.79 (t), δ 2.54

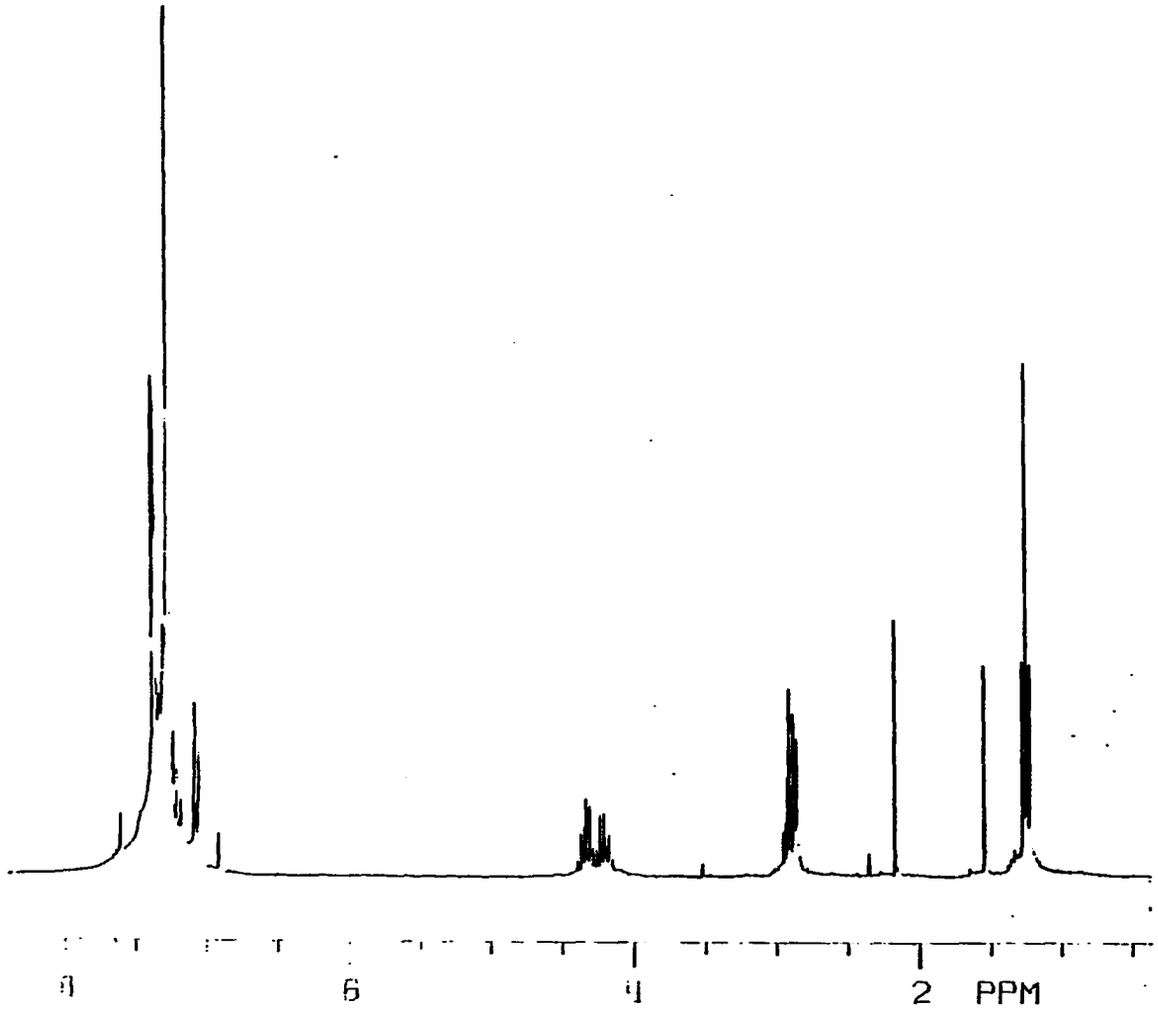

Figure 101. ^{1}H NMR of 18a in $CDCl_3$

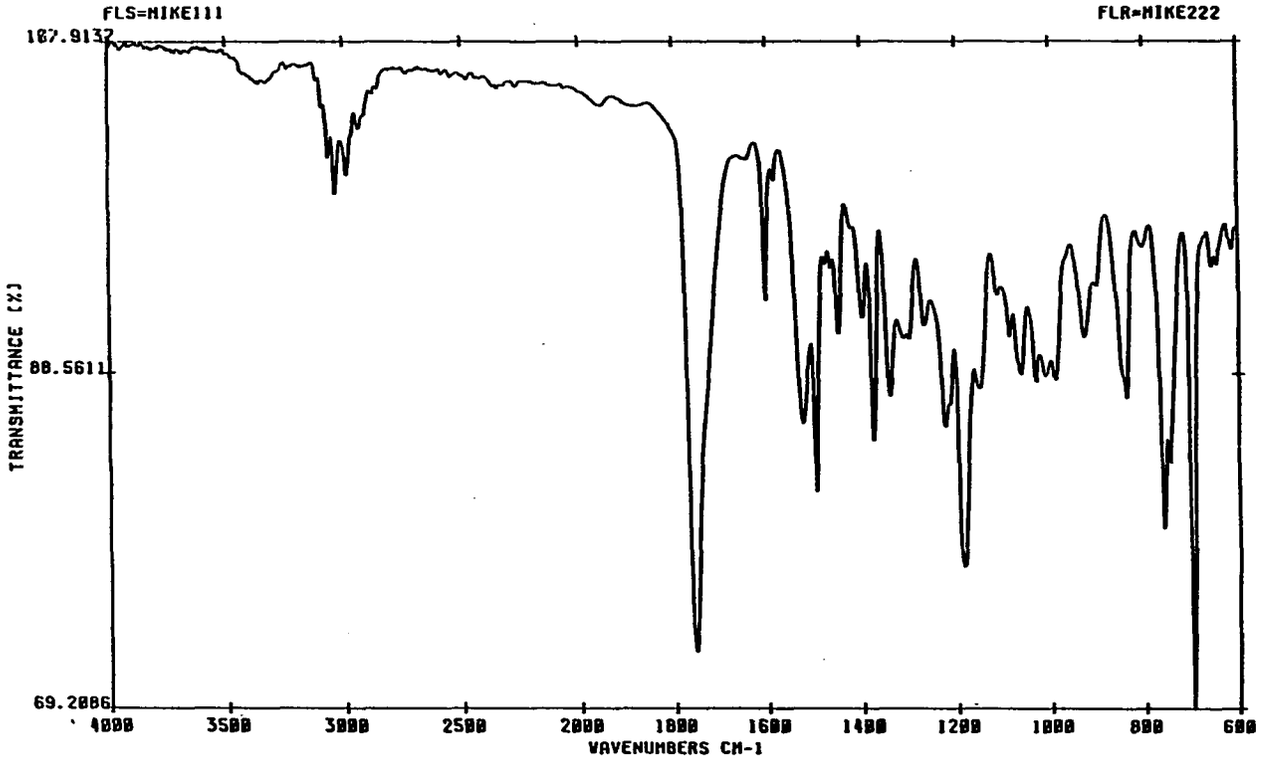

Figure 102. FT-IR of 18a in $CDCl_3$

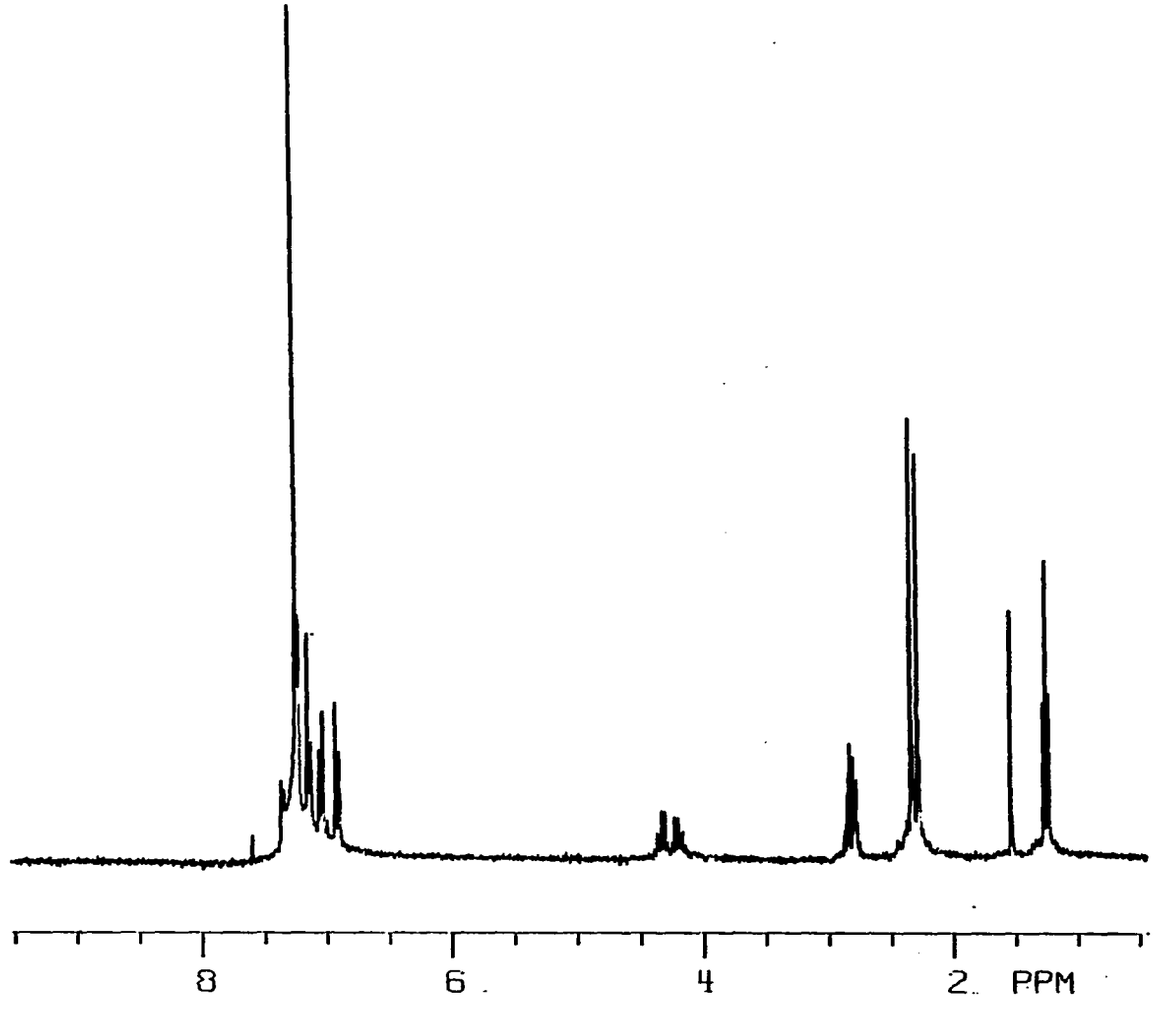

Figure 103. ^{1}H NMR of 18b in $CDCl_3$

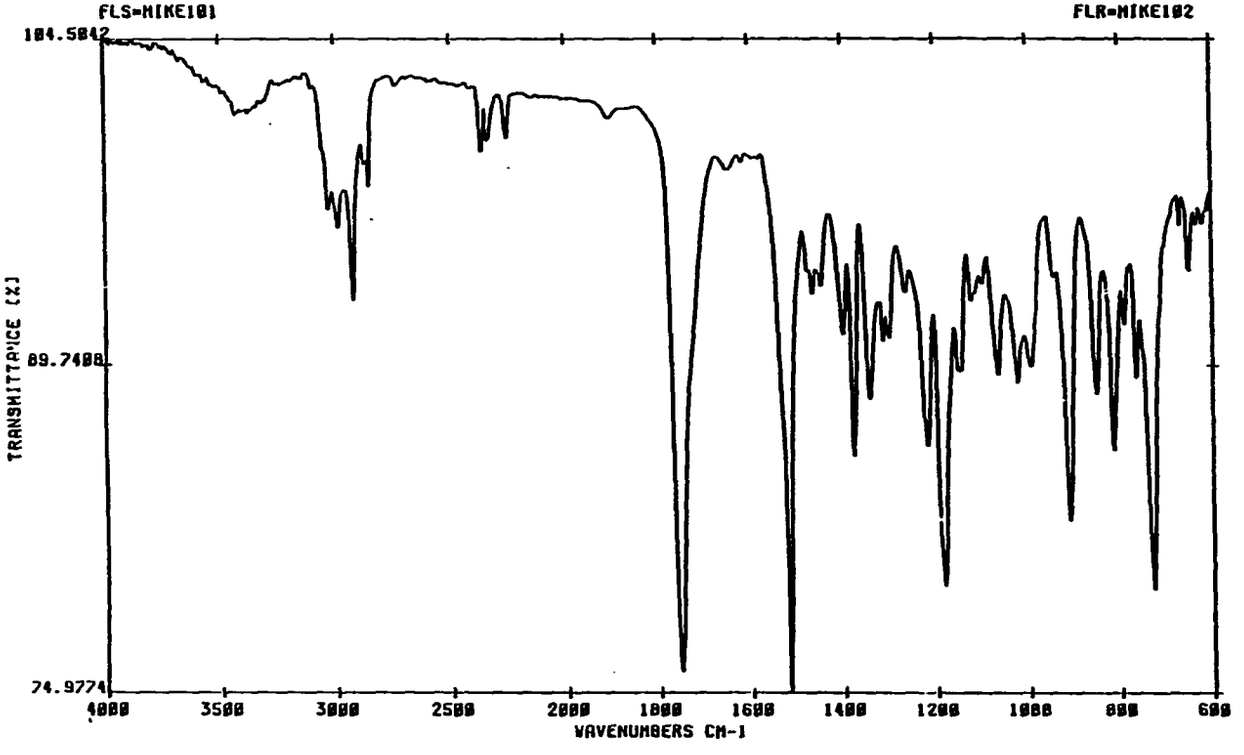

Figure 104. FT-IR of 18b in $CDCl_3$

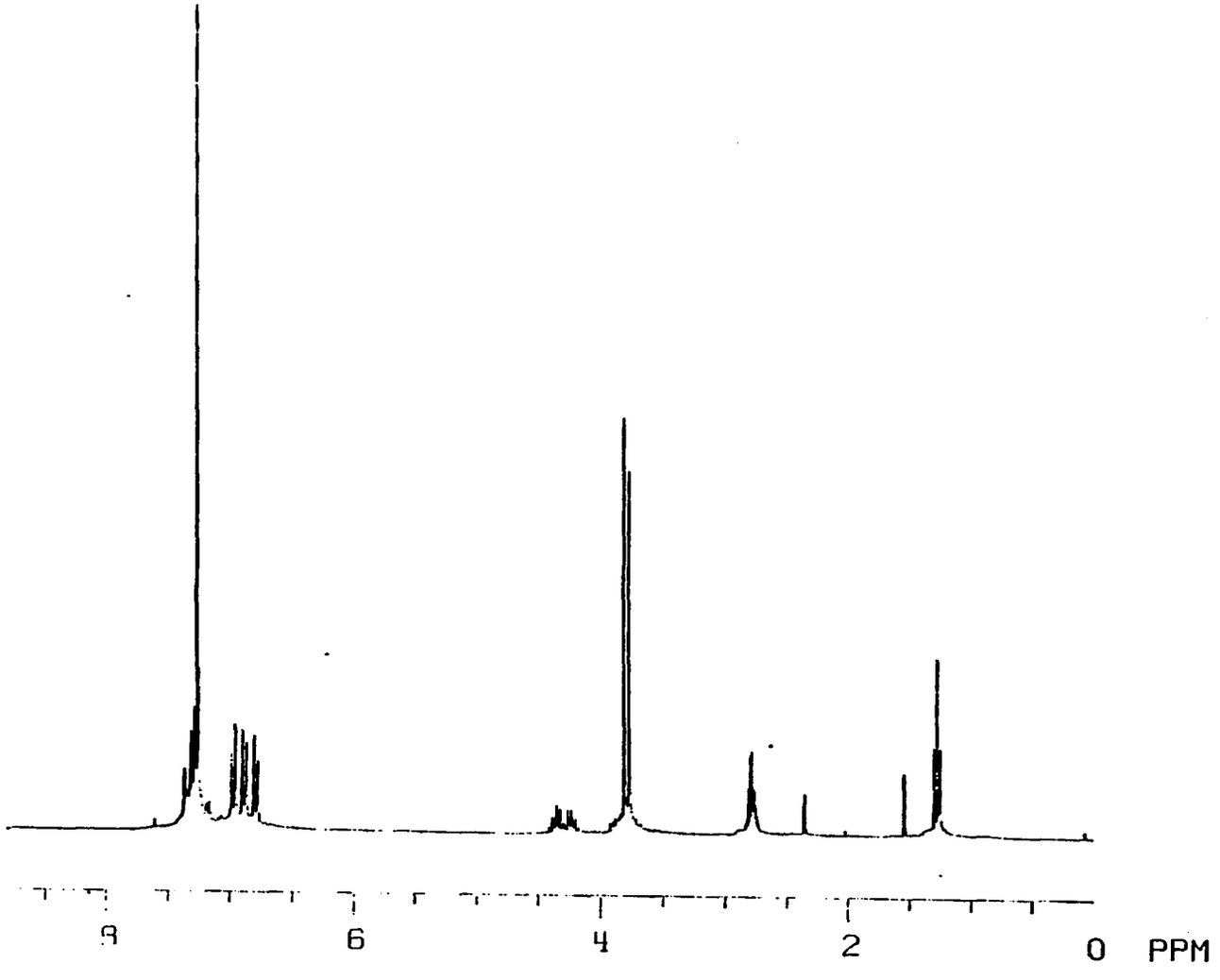

Figure 105. ^{1}H NMR of 18c in $CDCl_3$

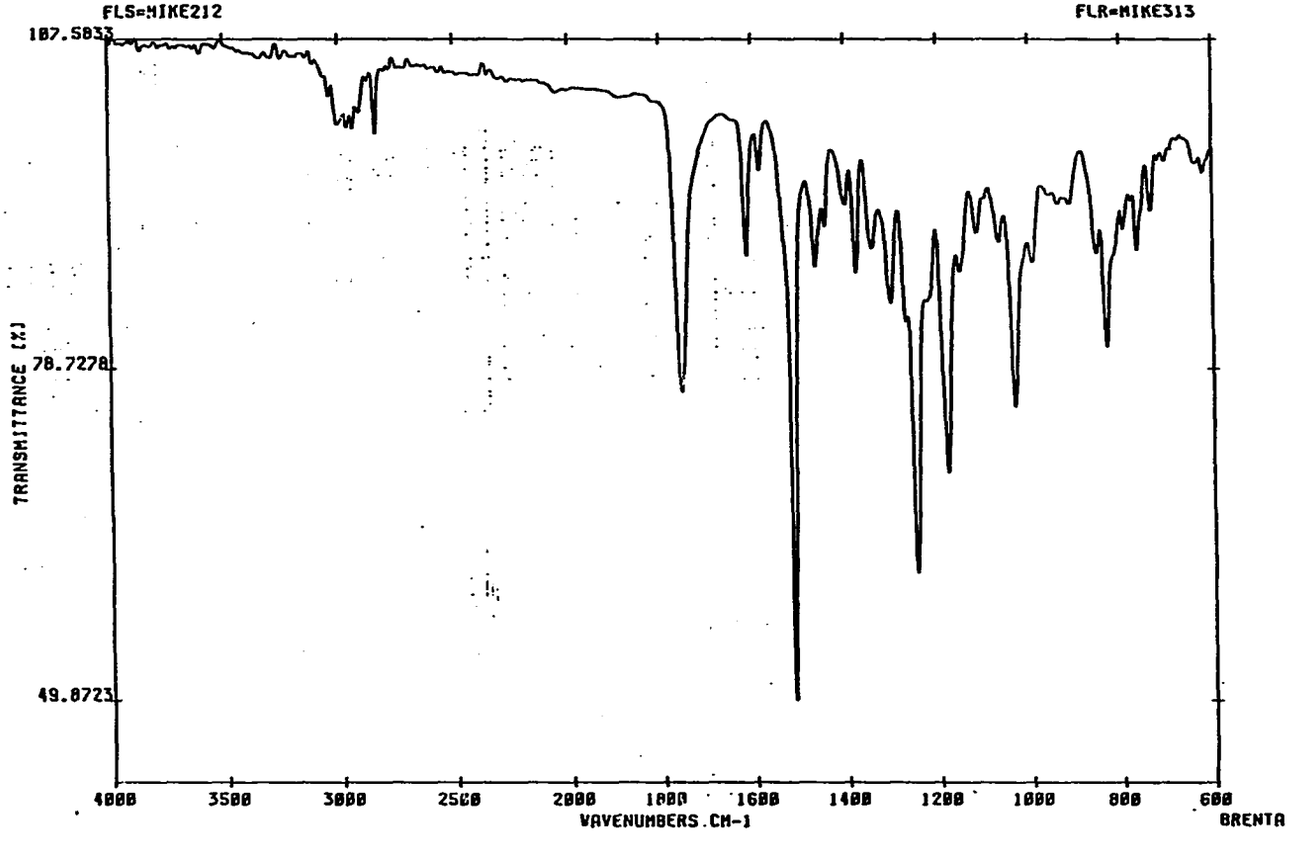

Figure 106. FT-IR of 18c in $CDCl_3$

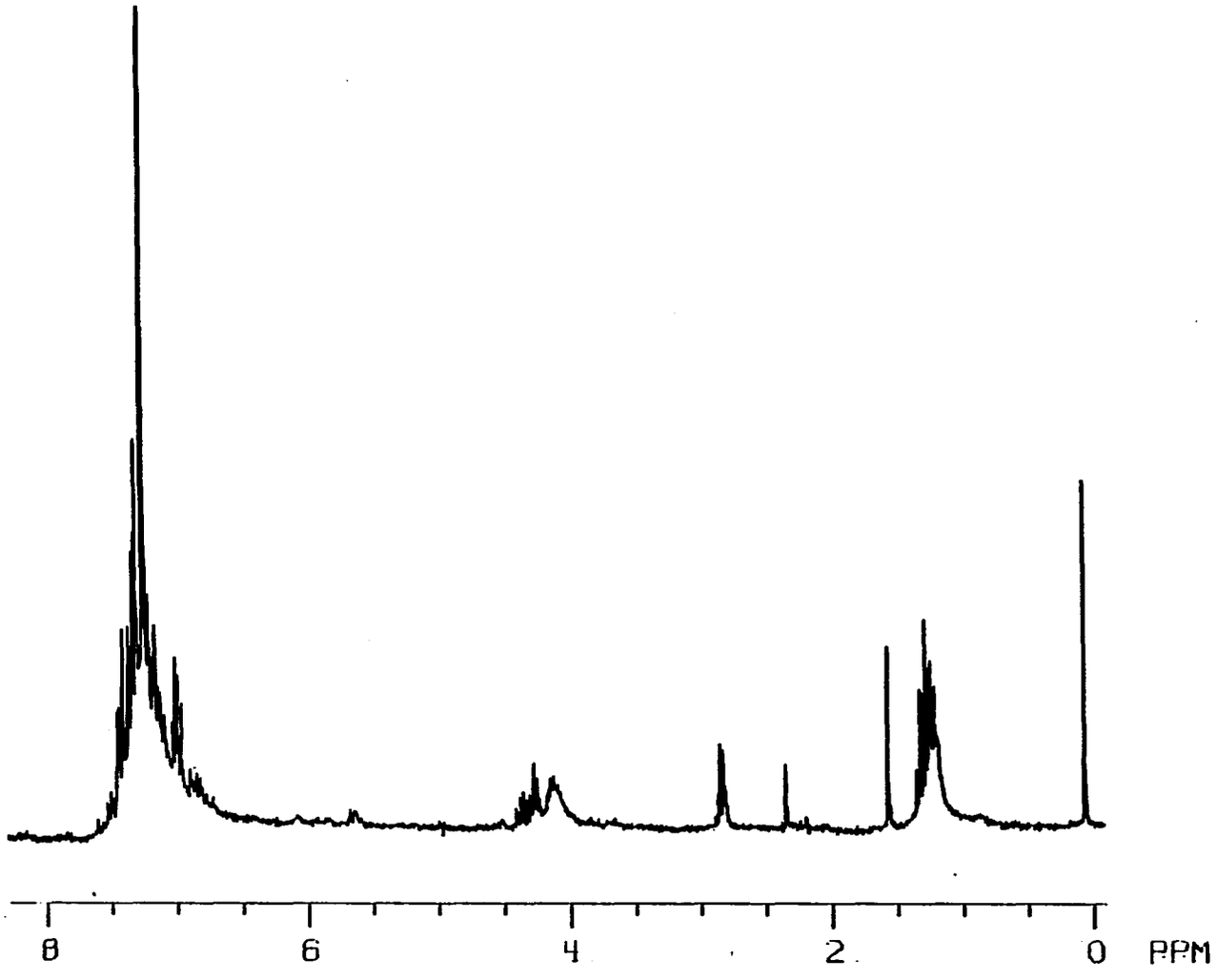

Figure 107. ^{1}H NMR of 18d in $CDCl_3$

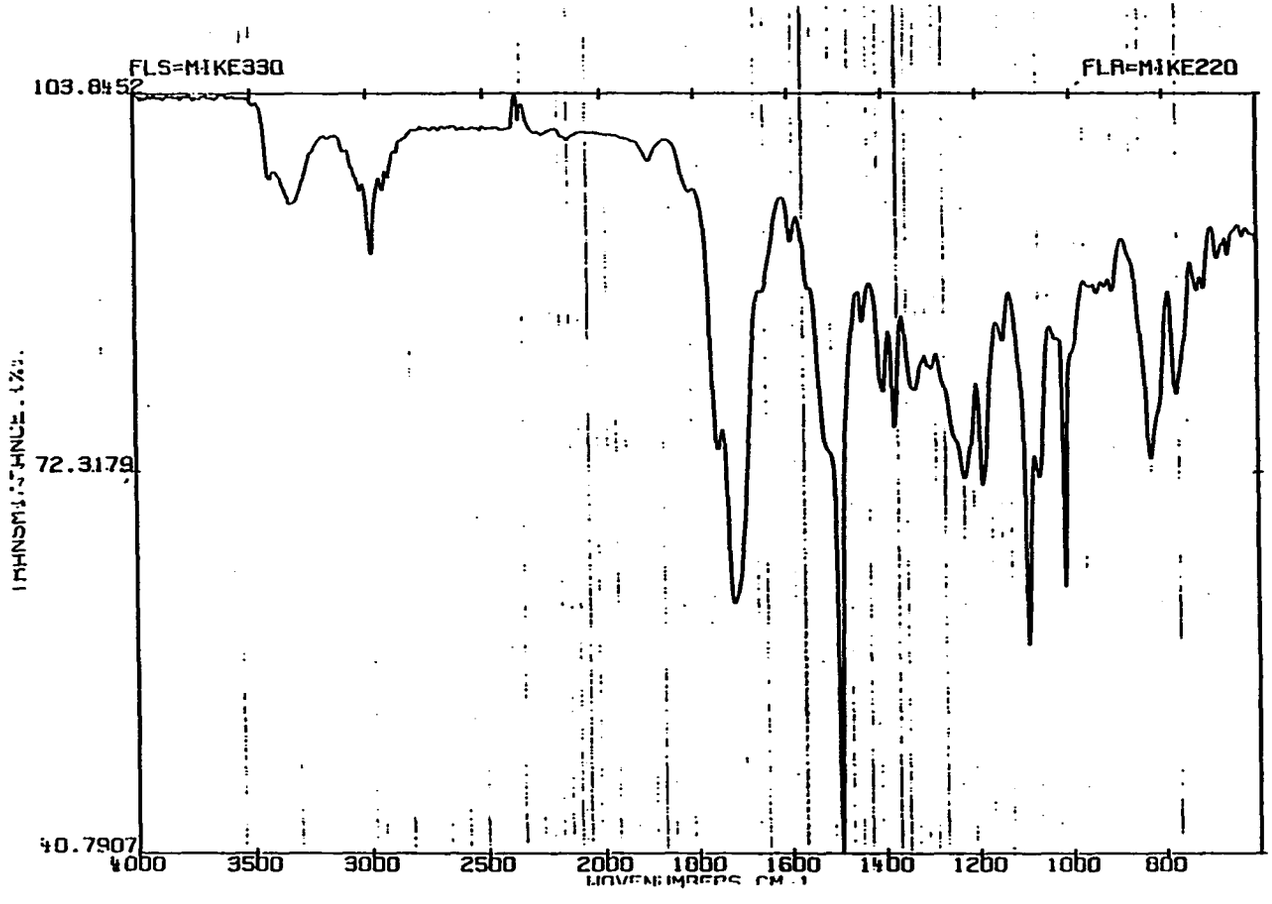

Figure 108. FT-IR of 18d in $CDCl_3$

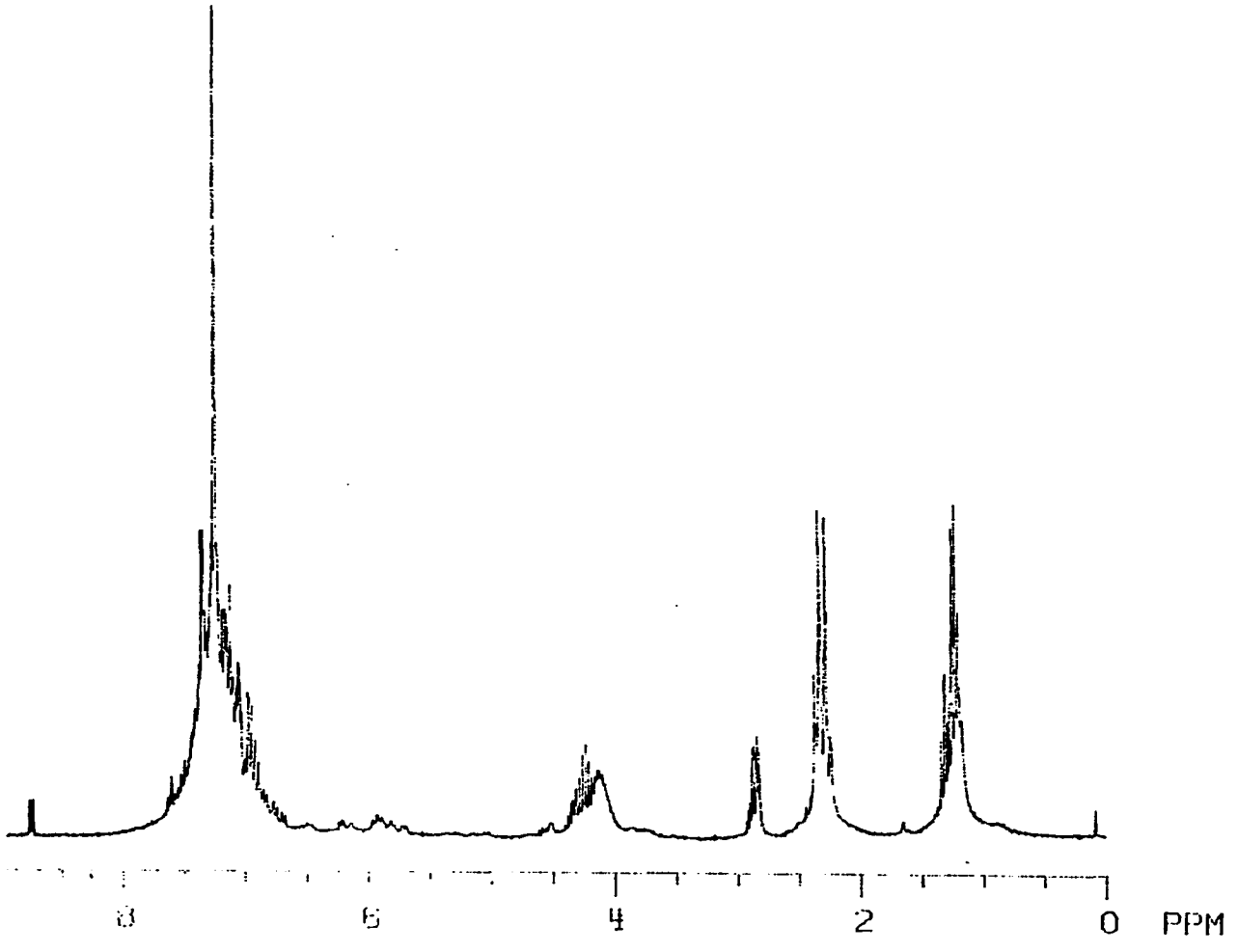

Figure 109. ^{1}H NMR of 18f in $CDCl_3$

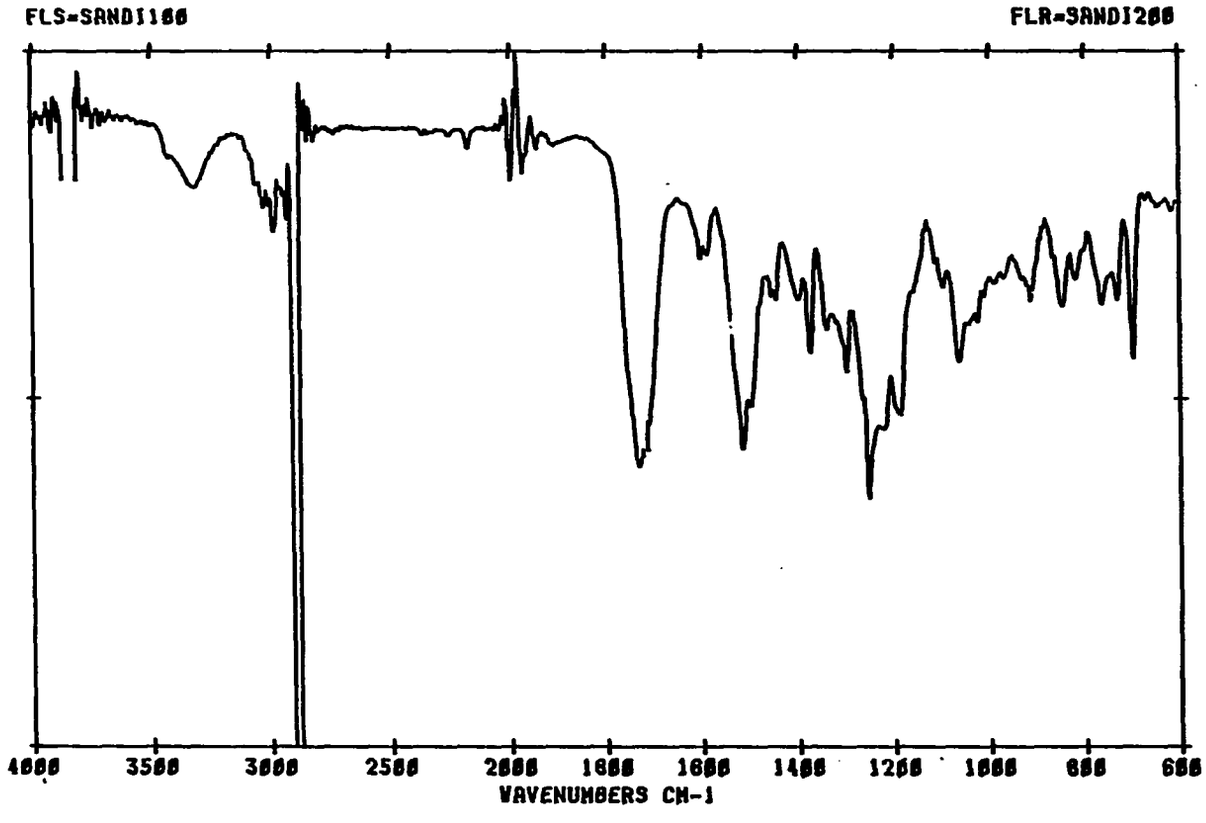

Figure 110. FT-IR of 18f in $CDCl_3$

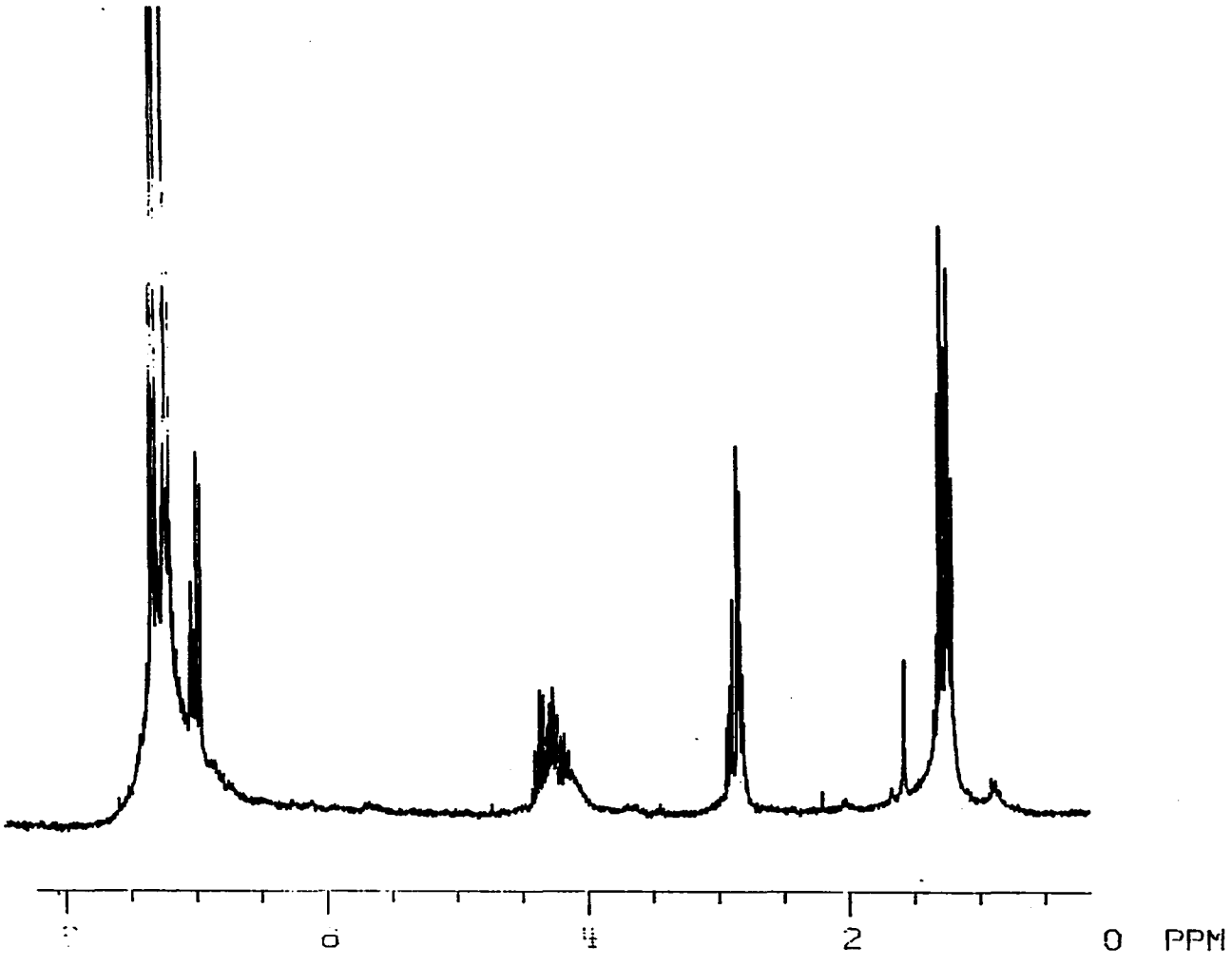

Figure 111. ^{1}H NMR of 18g in $CDCl_3$

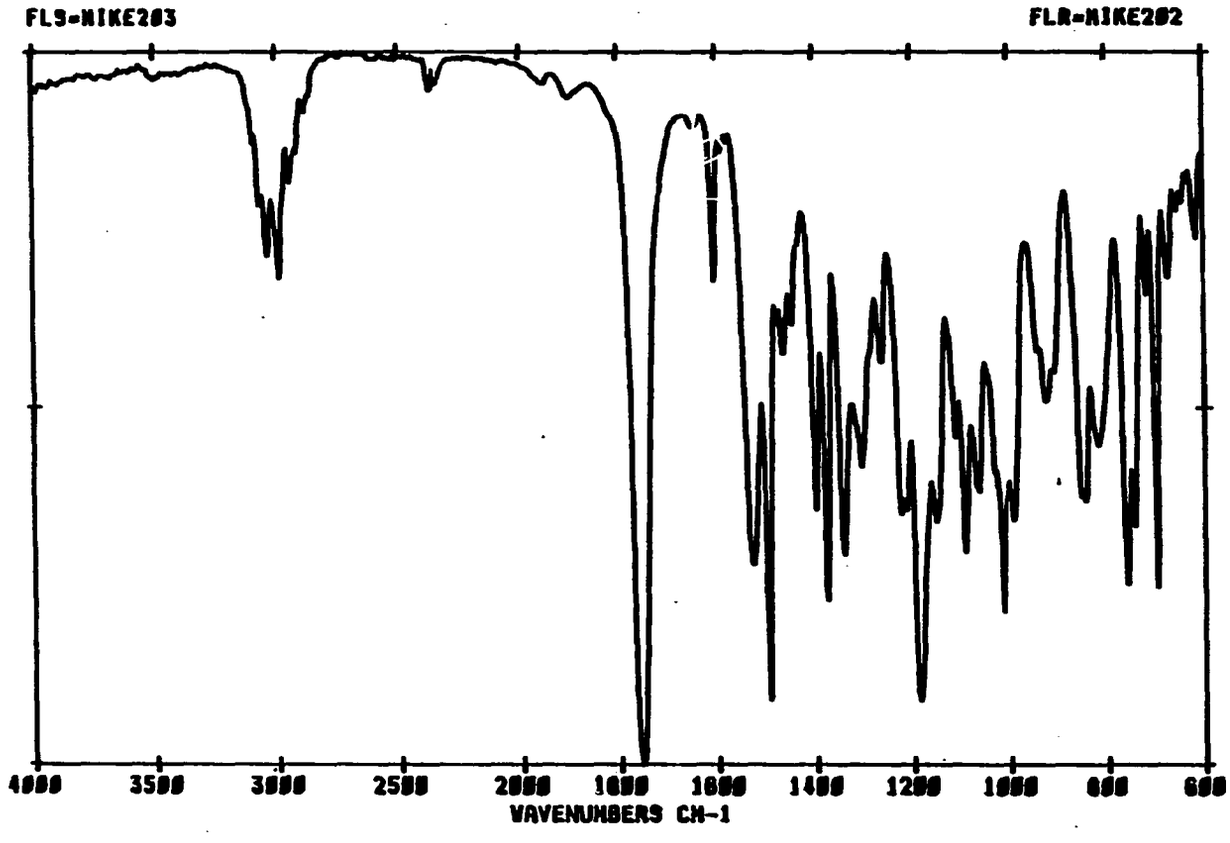

Figure 112. FT-IR of 18g in $CDCl_3$

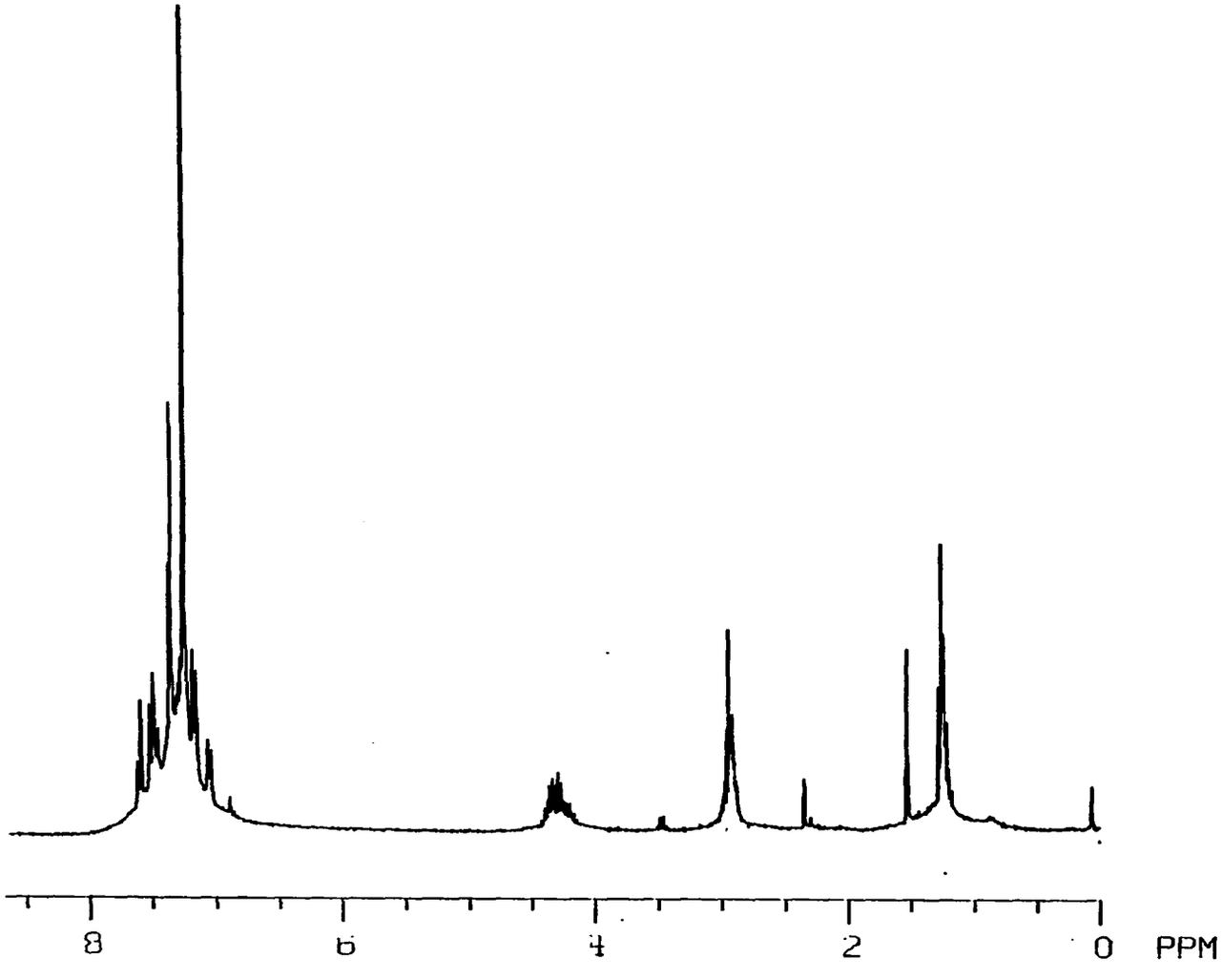

Figure 113. ^{1}H NMR of 18h in $CDCl_3$

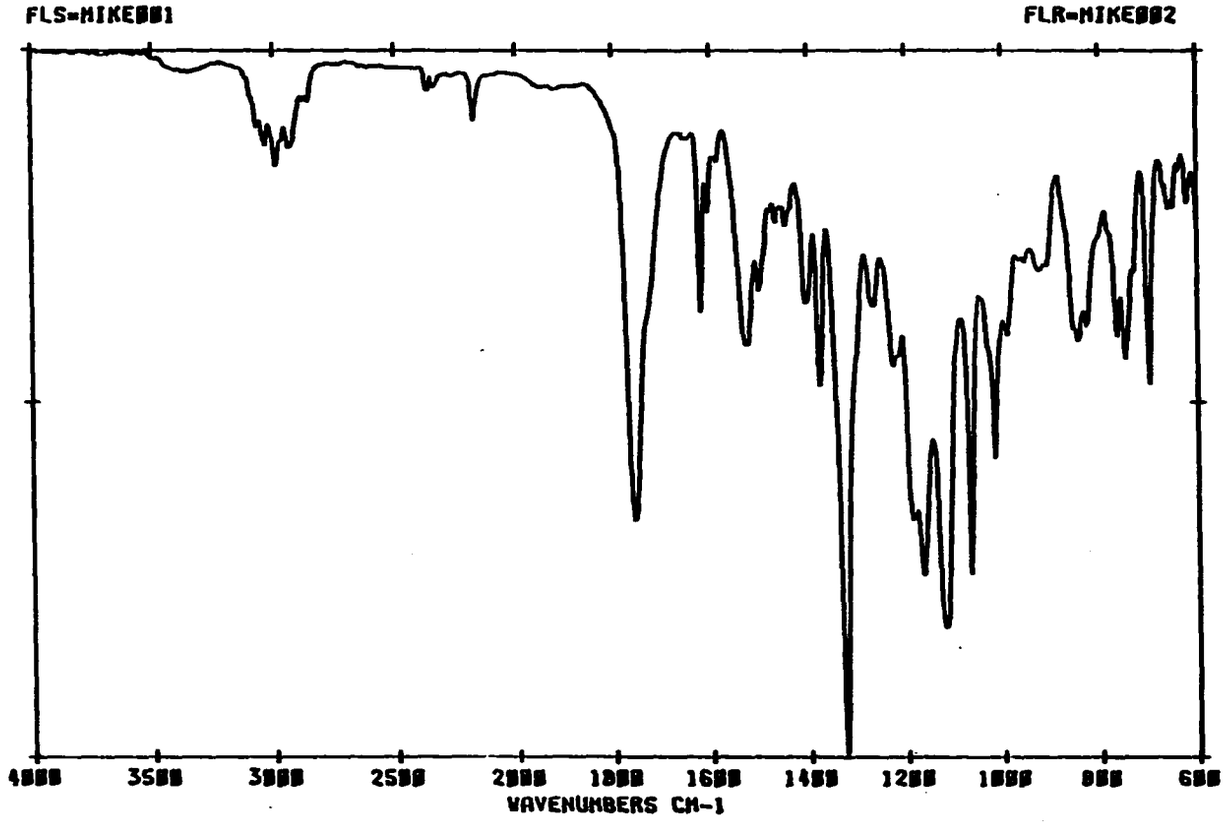

Figure 114. FT-IR of 18h in $CDCl_3$

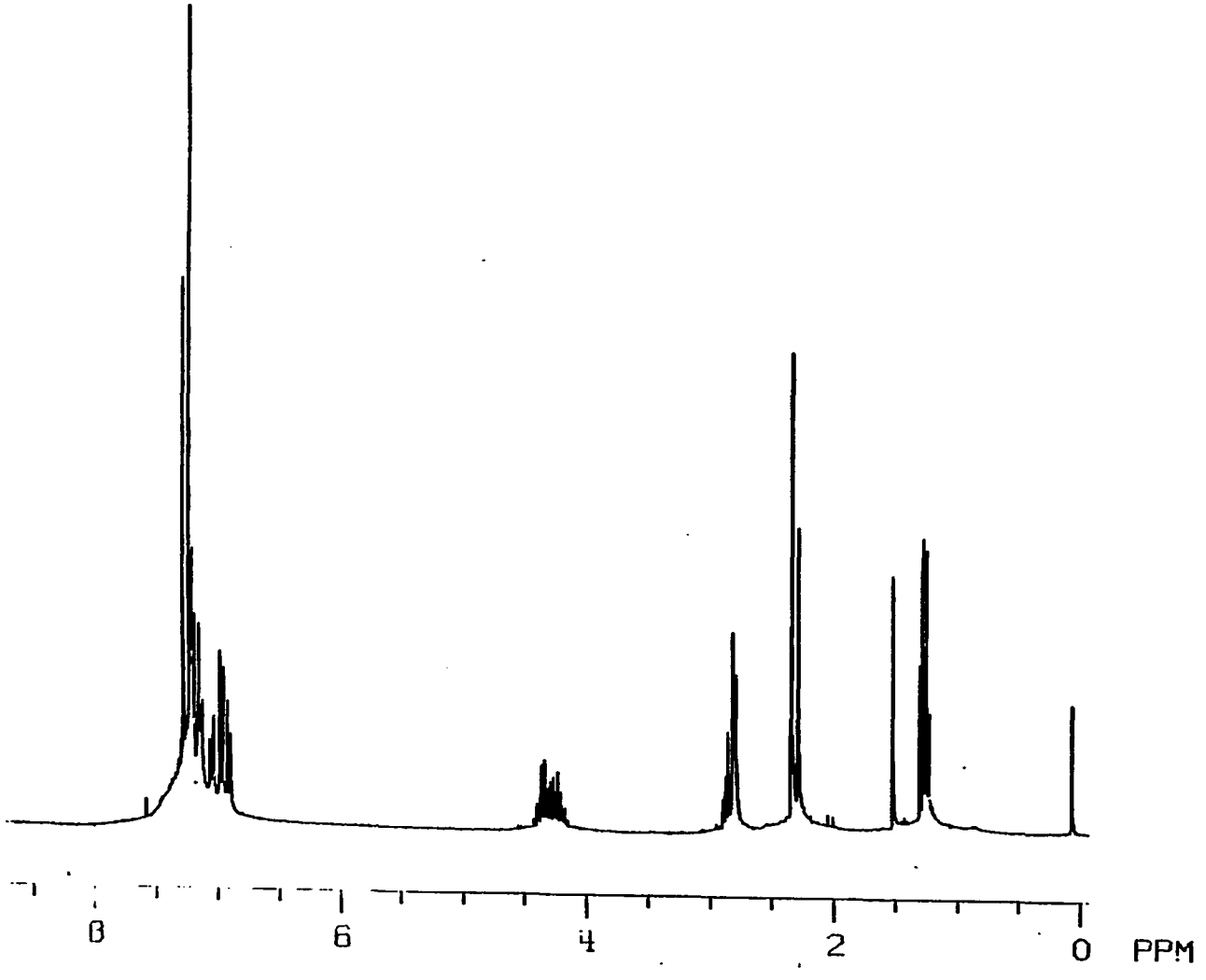

Figure 115. ^{1}H NMR of 18i in $CDCl_3$

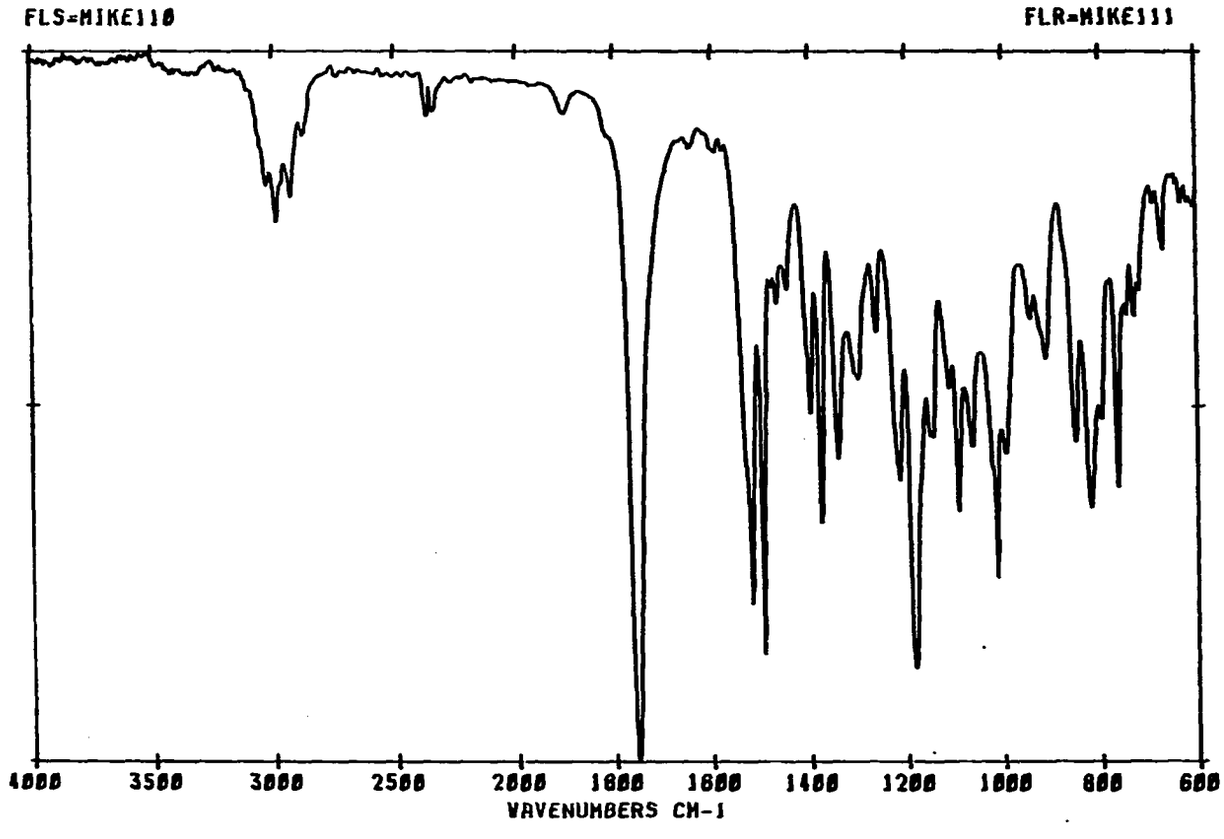

Figure 116. FT-IR of 18i in $CDCl_3$

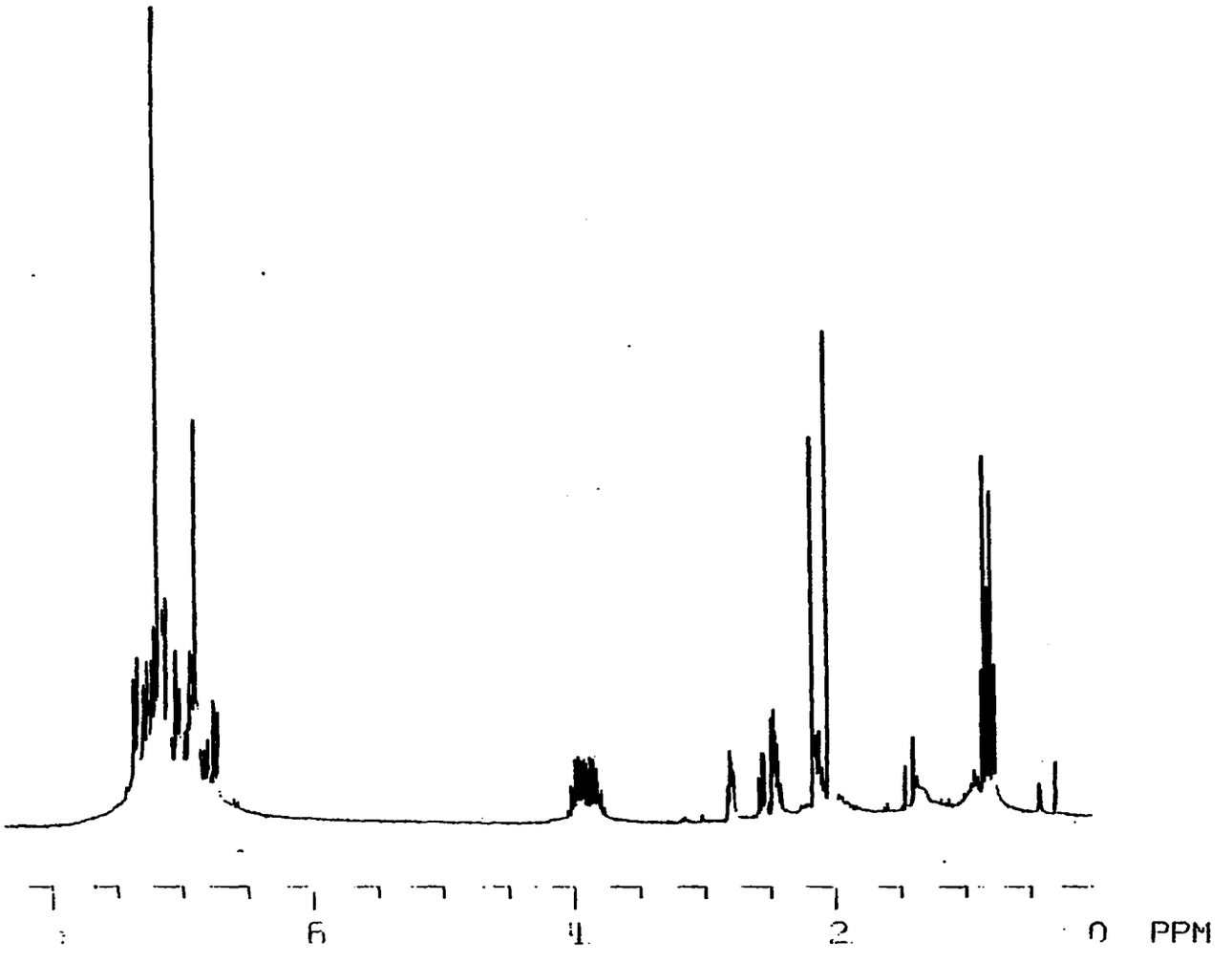

Figure 117. ^{1}H NMR of 18j in $CDCl_3$

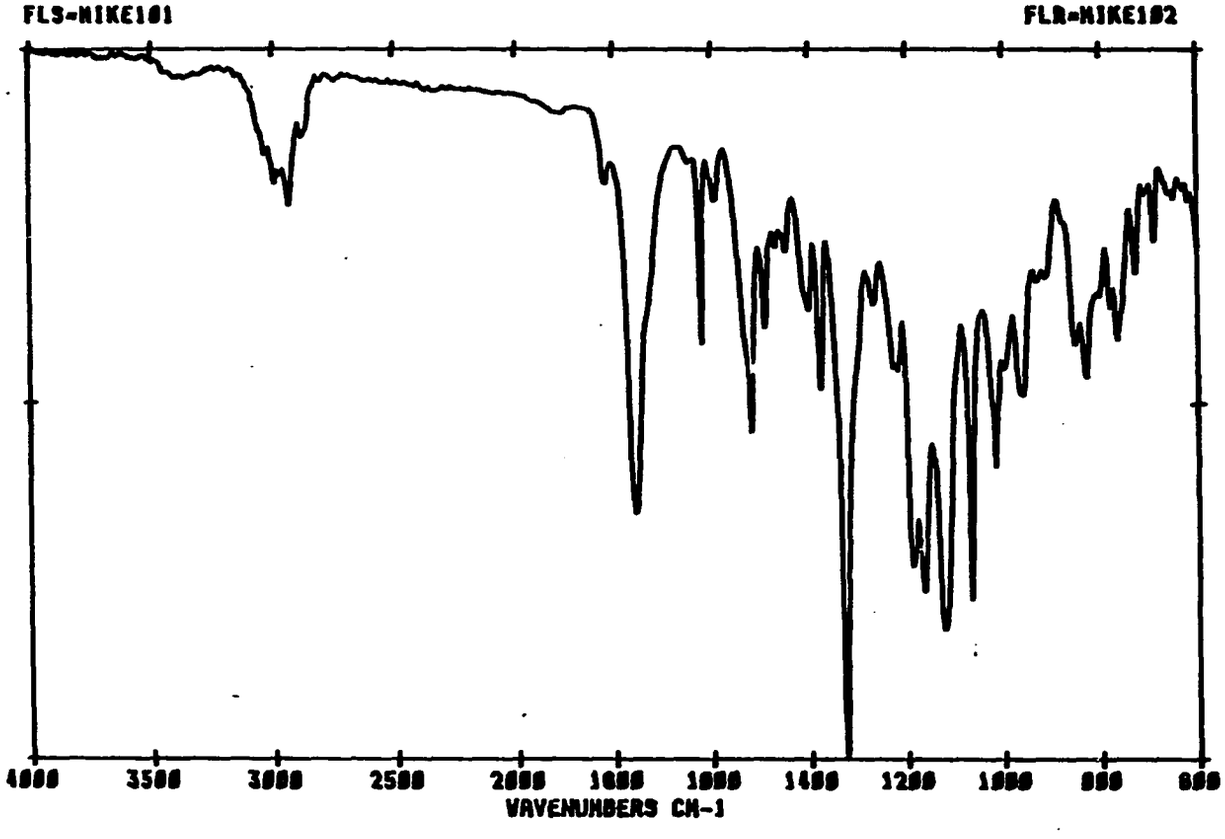

Figure 118. FT-IR of 18j in $CDCl_3$

(m), δ 2.45 (m), δ 2.15 (s), δ 2.04 (s), δ 0.80 (m).

FT-IR ($CDCl_3$): 3000 (w), 1770 (m), 1500 (m), 1350 (s), 1100 (s) cm^{-1}.

General reactions of 18 (a-j) in toluene/methanol solutions

Reaction of 18a in toluene/methanol solution (Figures 119-121) A 1 dram vial was charged with 0.5 ml of toluene/methanol solution (concentrations of 20-100% methanol were used), and 2-3 mg of 18a. The stirred solution was immersed in a constant temperature bath (temperatures of 271k, 297k and 313k were used) and treated with 10 mg of sodium methoxide. Evolution of nitrogen began immediately and stopped within 30 seconds, the reactions were stirred for 3 minutes to insure complete reaction. The mixture was quenched with 1 ml of 50% ammonium chloride solution and 0.5 ml of either was used to extract the organic products. The products 19a and 20a were analyzed rapidly by capillary GLPC. The response factor ratio of 20a/19a = 0.76 was used to correct the data to mole ratios.

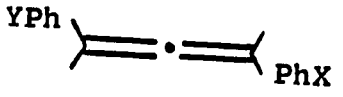

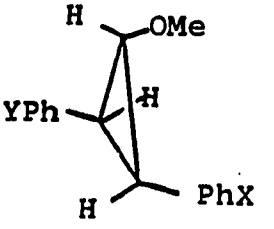

19 (a-j) 20 (a-j)

X/Y = H/H (a), CH_3/CH_3 (b), OCH_3/OCH_3 (c), Cl/Cl (d), H/CH_3 (f), H/Cl (g), H/CF_3 (h), CH_3/Cl (i), CH_3/CF_3 (j)

GC-HRMS: 19a: Calculated $C_{15}H_{12}$ m/3 192.09390
measured m/e 192.09490 error 5.2 ppm

20a: Calculated $C_{16}H_{16}O$ m/e 224.12012
measured m/e 224.12065 error 2.4 ppm

^1H NMR ($CDCl_3$): 19a: δ 7.2 (m), δ 6.7 (s)

20a: δ 7.2 (m), δ 3.7 (dd), δ 3.26 (s), δ 2.5 (dd), δ 2.37 (dd)

GC-FT-IR: 19a: 3030 (s), 1945 (m), 1600 (m), 1494 (m) cm^{-1}

20a: 3030 (s), 1608 (s), 1500 (s), 1220 (s), 1140 (s) cm^{-1}

Reaction of 18b in toluene/methanol solution (Figures 122-124) The response factor ratio for 20b/19b = 0.45.

GC-HRMS: 19b: Calculated $C_{17}H_{16}$ m/e 220.12520
measured m/e 220.12475 error 2.0 ppm

20b: Calculated $C_{18}H_{20}O$ m/e 252.15142
measured m/e 252.15043 error -3.9 ppm

^1H NMR

(acetone-d6): 19b: δ 7.2 (m), δ 6.64 (s), δ 2.24 (s)

20b: δ 7.2 (m), δ 3.65 (dd), δ 3.19 (s), δ 2.8 (s), δ 2.5 (m)

GC-FT-IR: 19b: 3030 (m), 1954 (w), 1500 (s), 1090 (s) cm^{-1}

20b: 3030 (m), 1580 (m), 1100 (s) cm^{-1}

Reaction of 18c in toluene/methanol solution (Figures 125, 126) The response factor ratio for 20c/19c = 0.13.

GC-HRMS: 19c: Calculated $C_{17}H_{16}O_2$ m/e 252.11503
measured m/e 252.11557 error 2.1 ppm

20c: Calculated $C_{18}H_{20}O_3$ m/e 284.14125
measured m/e 284.14233 error 3.8 ppm

^1H NMR ($CDCl_3$): 19c: δ 7.2 (m), δ 6.47 (s), δ 3.28 (s)

20c: δ 7.2 (m), δ 3.40 (dd), δ 3.35 (s), δ 3.34 (s), δ 3.1 (s), δ 2.50 (dd), δ 2.16 (dd)

FT-IR: 19c and 20c: 2960 (m), 2050 (w), 1932 (w), 1886 (w), 1720 (m), 1606 (m), 1514 (s), 1464 (m), 1248 (s), 1175 (m), 1034 (m), 833 (m) cm^{-1}

Reaction of 18d in toluene/methanol solution (Figures 127-128) The response factor ratio for 20d/19d = 0.48.

GC-HRMS: 19d: Calculated $C_{15}H_{10}Cl_2$ m/e 260.01596
measured m/e 260.01614 error 0.7 ppm

20d: Calculated $C_{16}H_{14}Cl_2O$ m/e 292.04218
measured m/e 292.03680 error 5.9 ppm

^1H NMR ($CDCl_3$): 19d: δ 7.2 (m), δ 6.54 (s)

20d: δ 7.2 (m), δ 3.63 (dd), δ 3.24 (s), δ 2.44 (dd), δ 2.29 (dd)

FT-IR: 19d and 20d: 2925 (m), 1940 (w), 1900 (w), 1726 (m), 1591 (s), 1495 (m), 1261 (m), 1217 (m), 1094 (s), 1012 (s), 827 (s) cm^{-1}

Reaction of 18f in toluene/methanol solution (Figures 129, 130) The response factor ratio for 20f/19f = 0.58.

GC-HRMS: 19f: Calculated $C_{16}H_{14}$ m/e 206.10955
measured m/e 206.10857 error -4.8 ppm

20f: Calculated $C_{17}H_{18}O$ m/e 238.13577
measured m/e 238.13664 error 3.7 ppm

^1H NMR ($CDCl_3$): 19f: δ 7.2 (m), δ 6.44 (q), δ 2.05 (s)

20f: δ 7.2 (m), δ 3.45 (dd), δ 3.00 (s), δ 2.98 (s), δ 2.55 (m), δ 2.1 (m)

FT-IR: 19f and 20f: 3030 (m), 2926 (m), 1933 (w), 1900 (w), 1514 (s), 1495 (s), 1454 (m),

1191 (w), 1024 (m), 823 (s), 689 (s) cm^{-1}

Reaction of 18g in toluene/methanol solution (Figures 131-133) The response factor ratio for 20g/19g = 0.77.

GC-HRMS: 19g: Calculated $C_{15}H_{11}Cl$ m/e 226.05493
measured m/e 226.05300 error -8.5 ppm

20g: Calculated $C_{16}H_{15}ClO$ m/e 258.08115
measured m/e 258.08154 error 1.5 ppm

^1H NMR ($CDCl_3$): 19g: δ 7.2 (m), δ 6.55 (q)

20g: δ 7.2 (m), δ 3.65 (dd), δ 3.23 (s), δ 2.47 (dd), δ 2.30 (dd)

GC-FT-IR: 19g: 3030 (s), 1955 (w), 1630 (m), 1500 (m), 1210 (s), 670 (s) cm^{-1}

20g: 3000 (w), 1500 (s), 1105 (s) cm^{-1}

Reaction of 18h in toluene/methanol solution (Figures 134-136) The response factor ratio for 20h/19h = 1.01.

GC-HRMS: 19h: Calculated $C_{16}H_{11}F_3$ m/e 260.08129
measured m/e 260.08125 error -0.2 ppm

20h: Calculated $C_{17}H_{15}F_3O$ m/e 292.10751
measured m/e 292.10803 error 1.8 ppm

^1H NMR ($CDCl_3$): 19h: δ 7.2 (m), δ 6.27 (q)

20h: δ 7.2 (m), δ 3.4 (m), δ 2.9 (s), δ 2.8 (s), δ 2.4 (m), δ 2.05 (m)

GC-FT-IR: 19h: 3000 (w), 1952 (w), 1320 (s), 1190 (m) cm^{-1}

20h: 3000 (w), 1640 (w), 1320 (s), 1180 (m) cm^{-1}

Reaction of 18i in toluene/methanol solution (Figures 137, 138) The response factor ratio for 20i/19i = 0.20.

GC-HRMS: 19i: Calculated $C_{16}H_{13}Cl$ m/e 240.07058
measured m/e 240.06992 error -2.8 ppm

20i: Calculated $C_{17}H_{17}CLO$ m/e 272.09680
measured m/e 272.09492 error -6.9 ppm

^1H NMR ($CDCl_3$): 19i: δ 7.2 (m), δ 6.32 (q), δ 2.07 (s)

20i: δ 7.2 (m), δ 3.34 (dd), δ 3.25 (dd), δ 2.92 (s), δ 2.90 (s), δ 2.4 (m), δ 2.2-2.0 (m)

Reaction of 18j in toluene/methanol solution (Figures 139-141) The response factor ratio for 20j/19j = 0.70.

GC-HRMS: 19j: Calculated $C_{17}H_{13}F_3$ m/e 274.09694
measured m/e 274.09668 error -1.0 ppm

20j: Calculated $C_{18}H_{17}F_3O$ m/e 306.12316
measured m/e 306.12104 error -6.9 ppm

^1H NMR ($CDCl_3$): 19j: δ 7.2 (m), δ 6.32 (q), δ 2.05 (s)

20j: δ 7.2 (m), δ 3.31 (m), δ 3.00 (s), δ 2.87 (s), δ 2.40 (m), δ 2.42 (m), δ 2.16 (s), δ 2.13 (s)

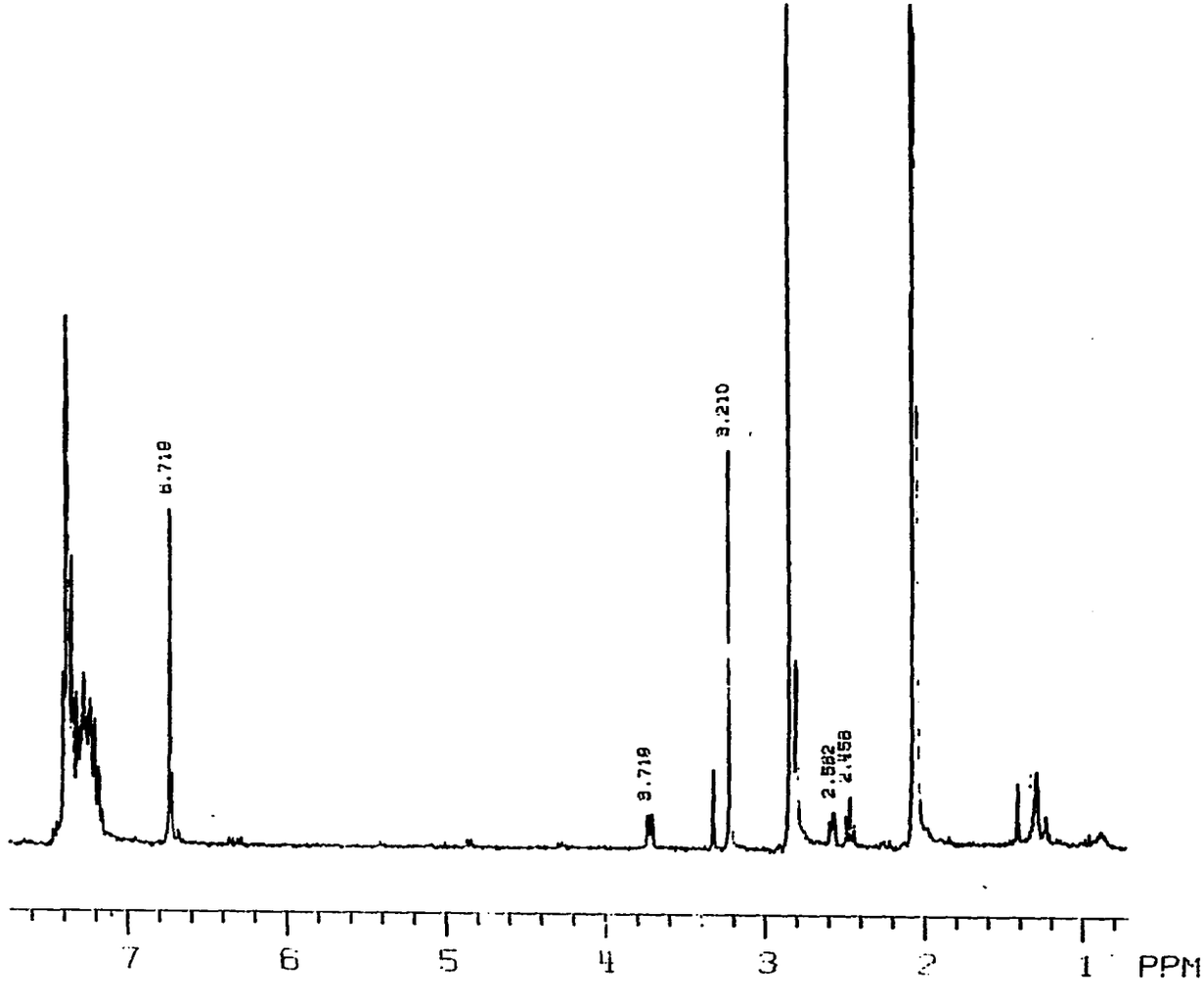

Figure 119. ^{1}H NMR of 19a and 20a in $CDCl_3$

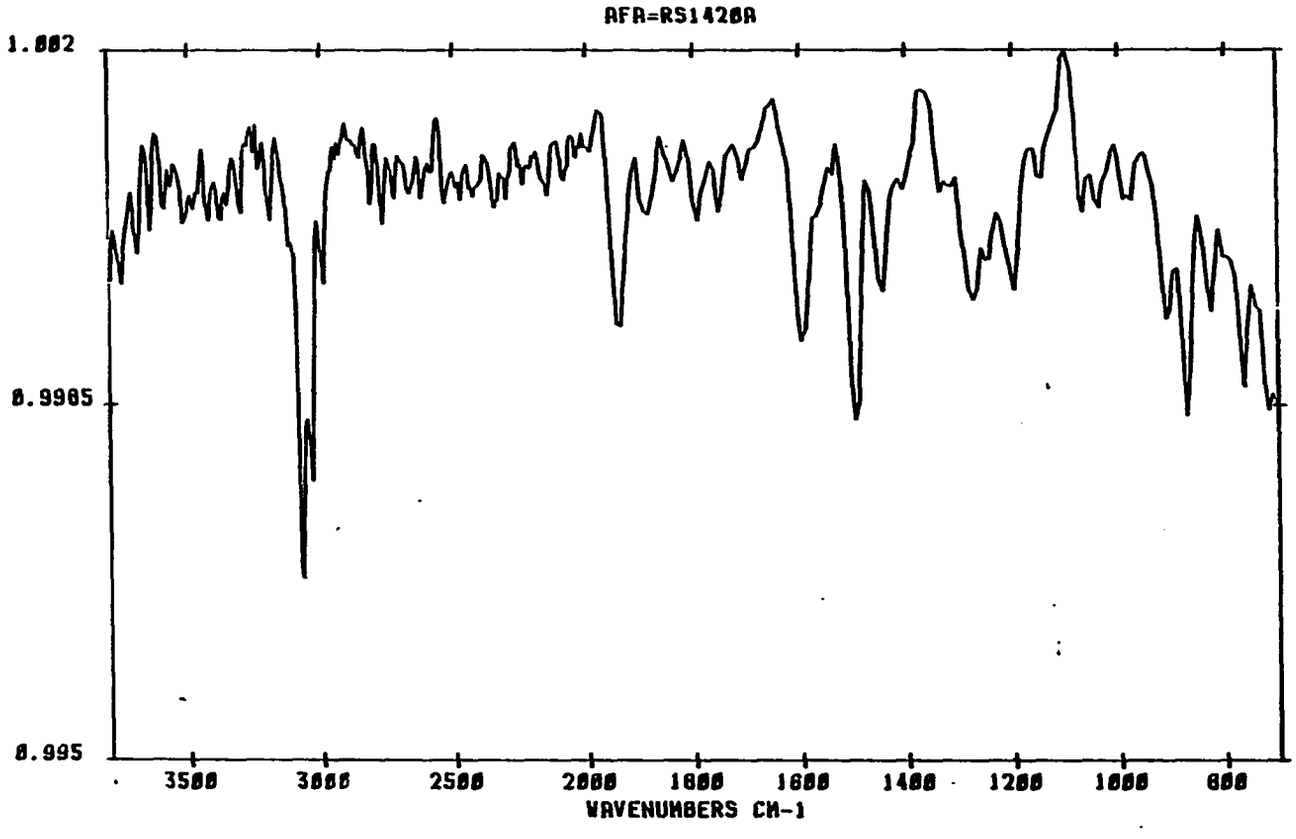

Figure 120. GC-FT-IR of 19a

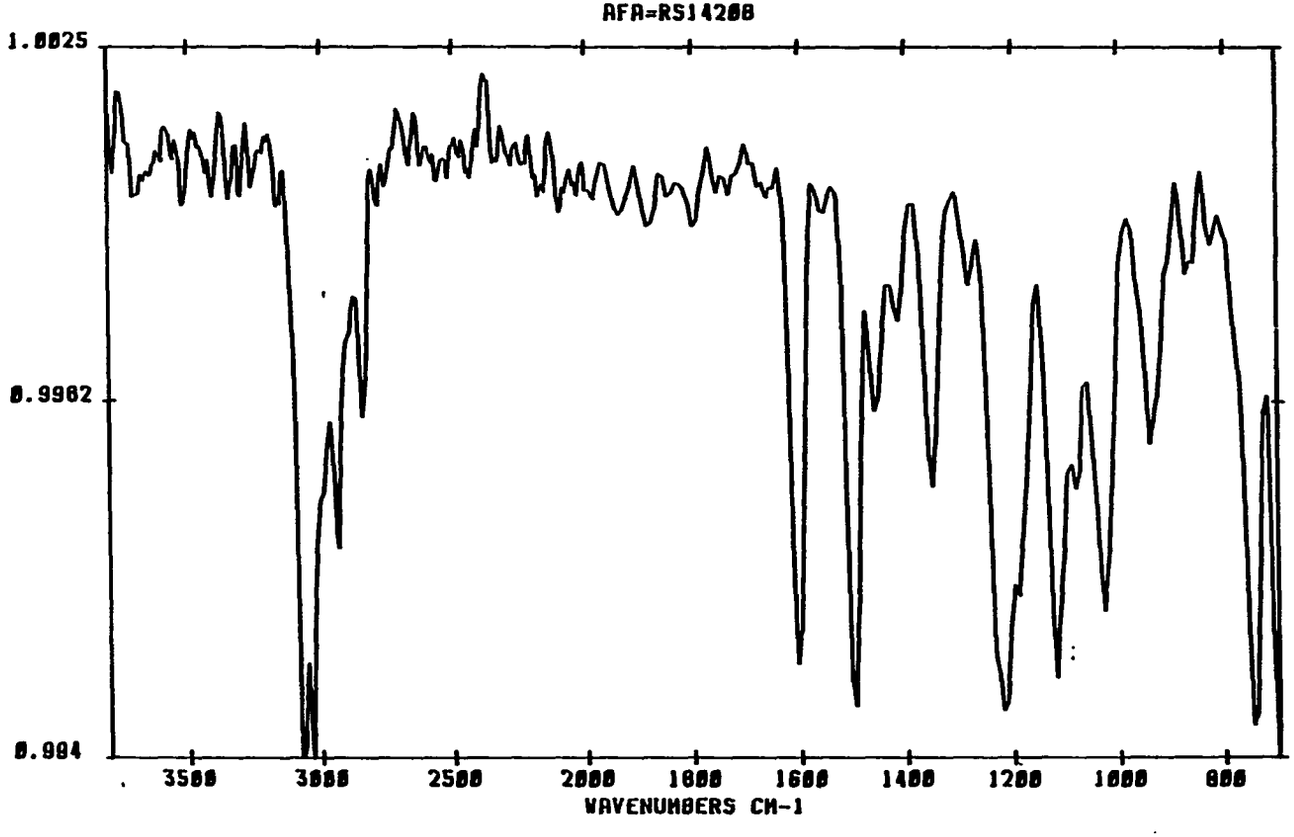

Figure 121. GC-FT-IR of 20a

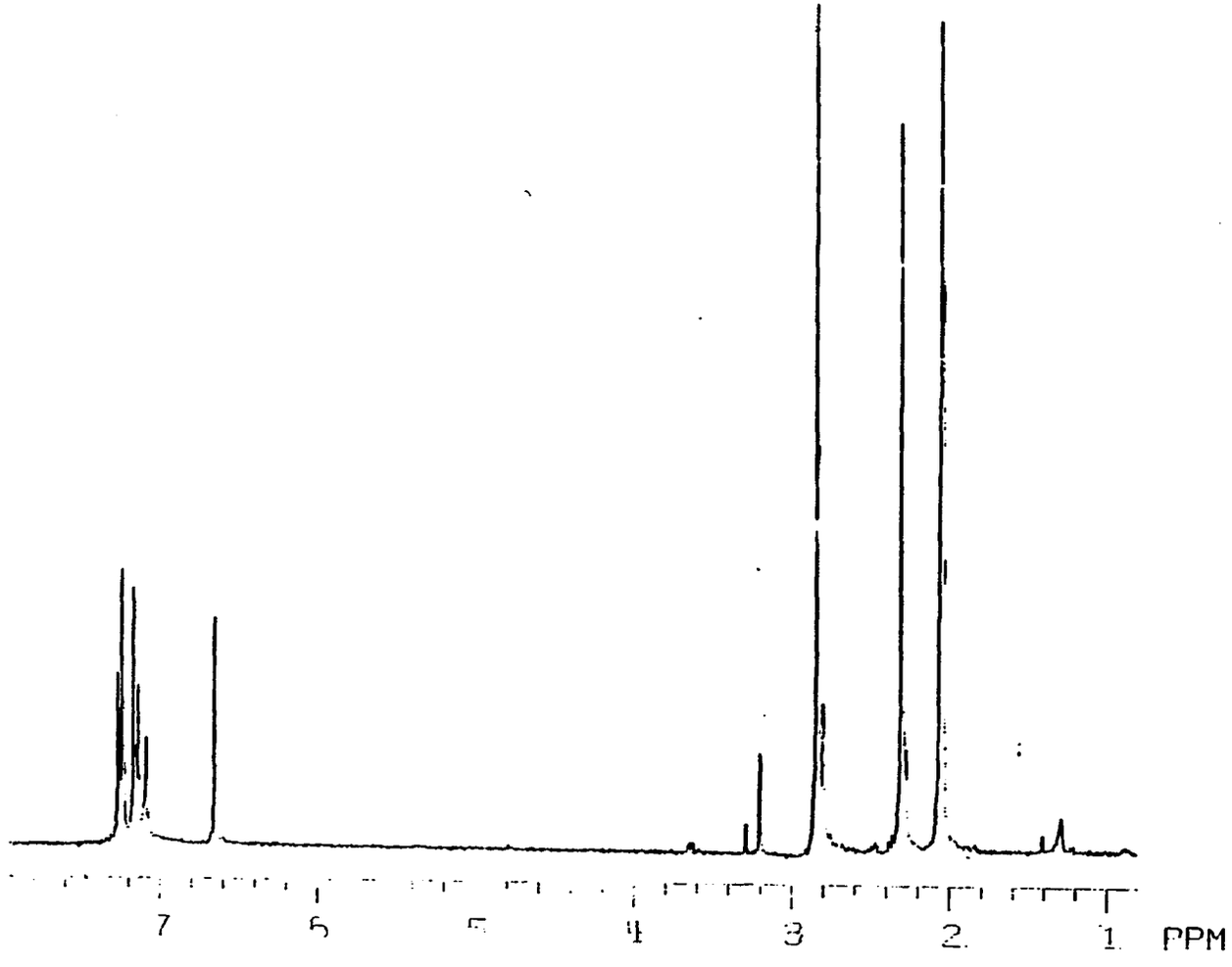

Figure 122. ^{1}H NMR of 19b and 20b in acetone-d6

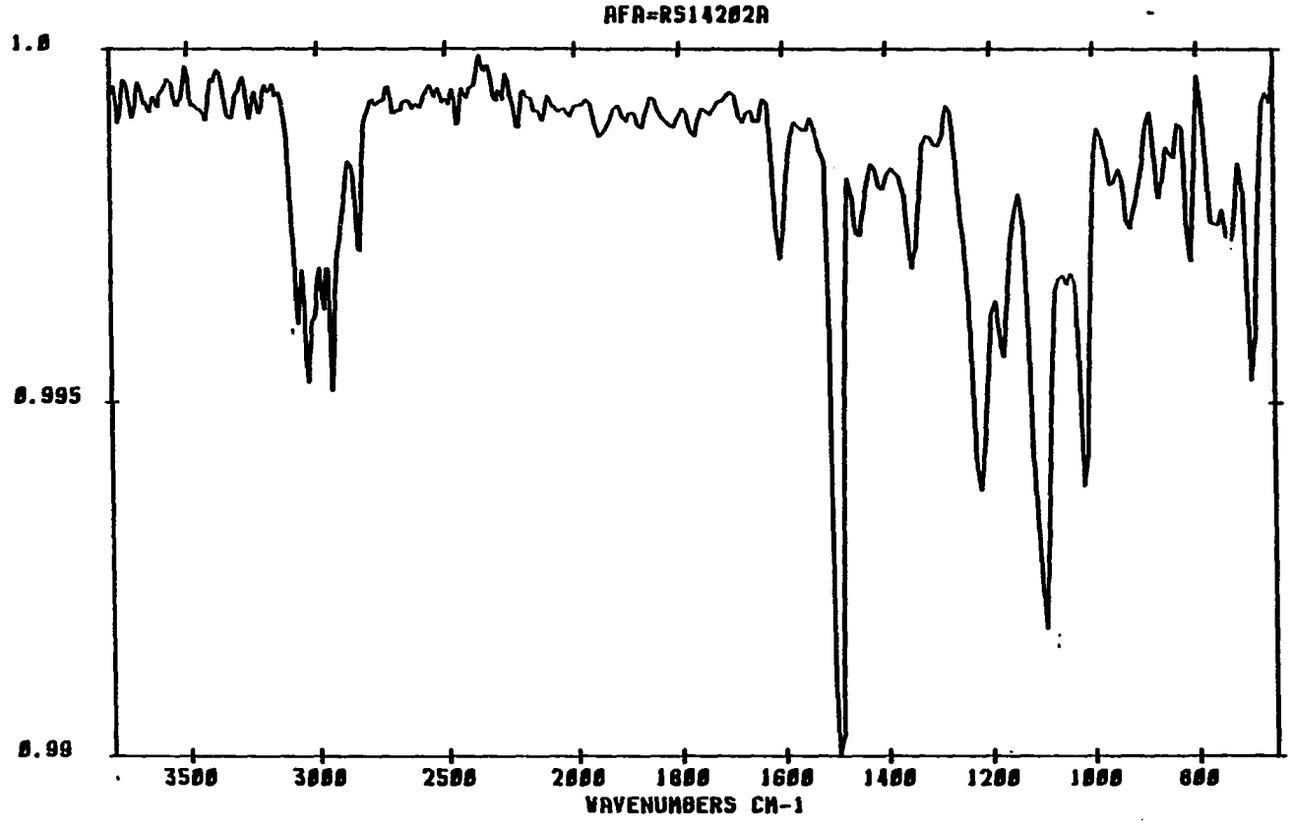

Figure 123. GC-FT-IR of 19b

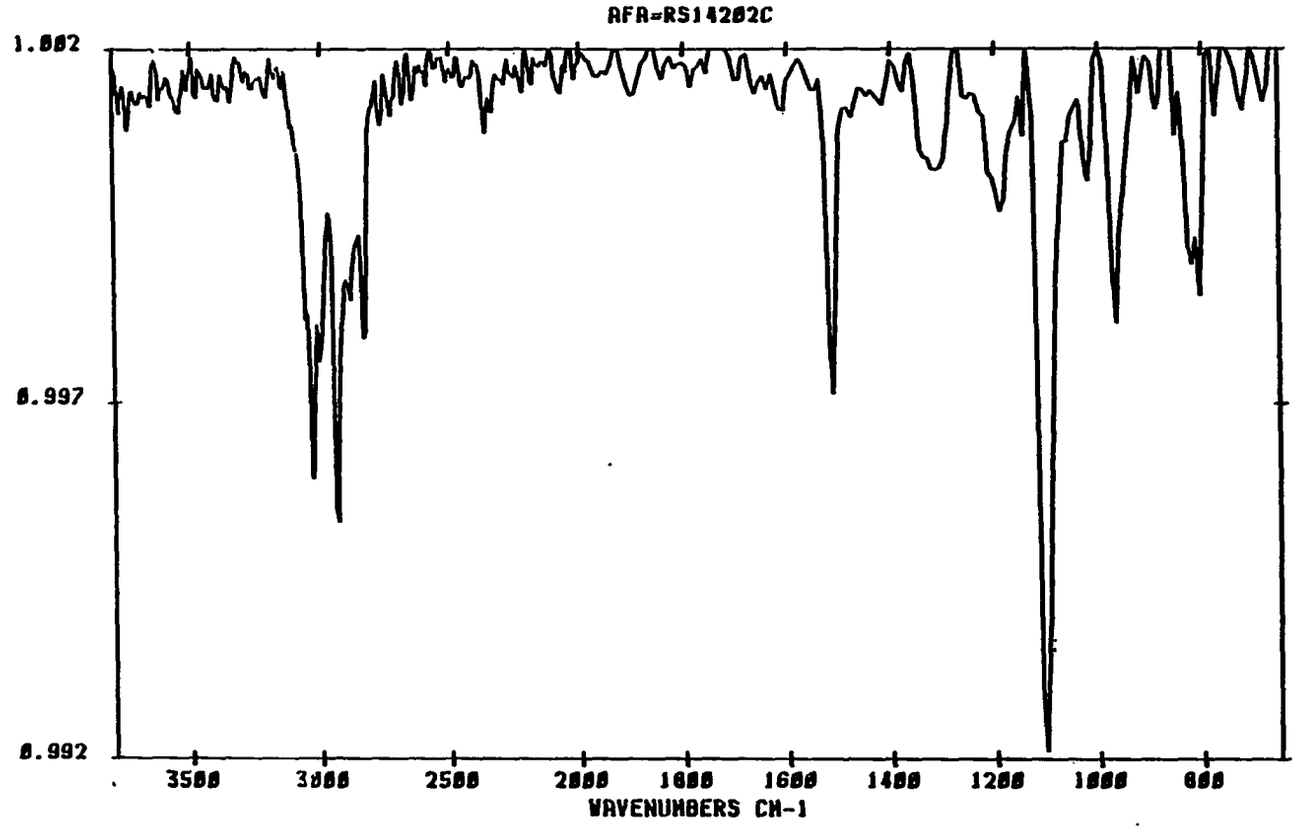

Figure 124. GC-FT-IR of 20b

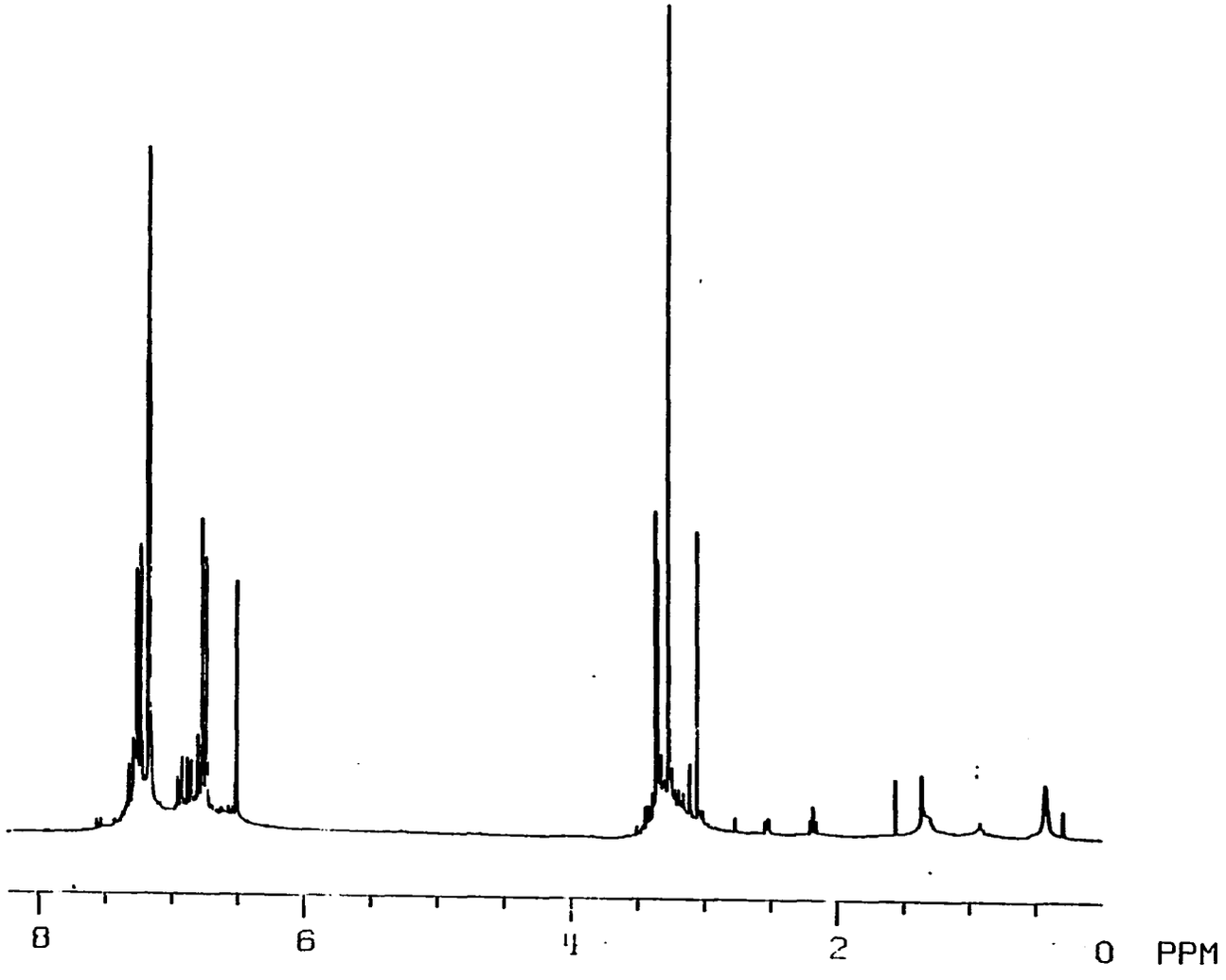

Figure 125. ^{1}H NMR of 19c and 20c in $CDCl_3$

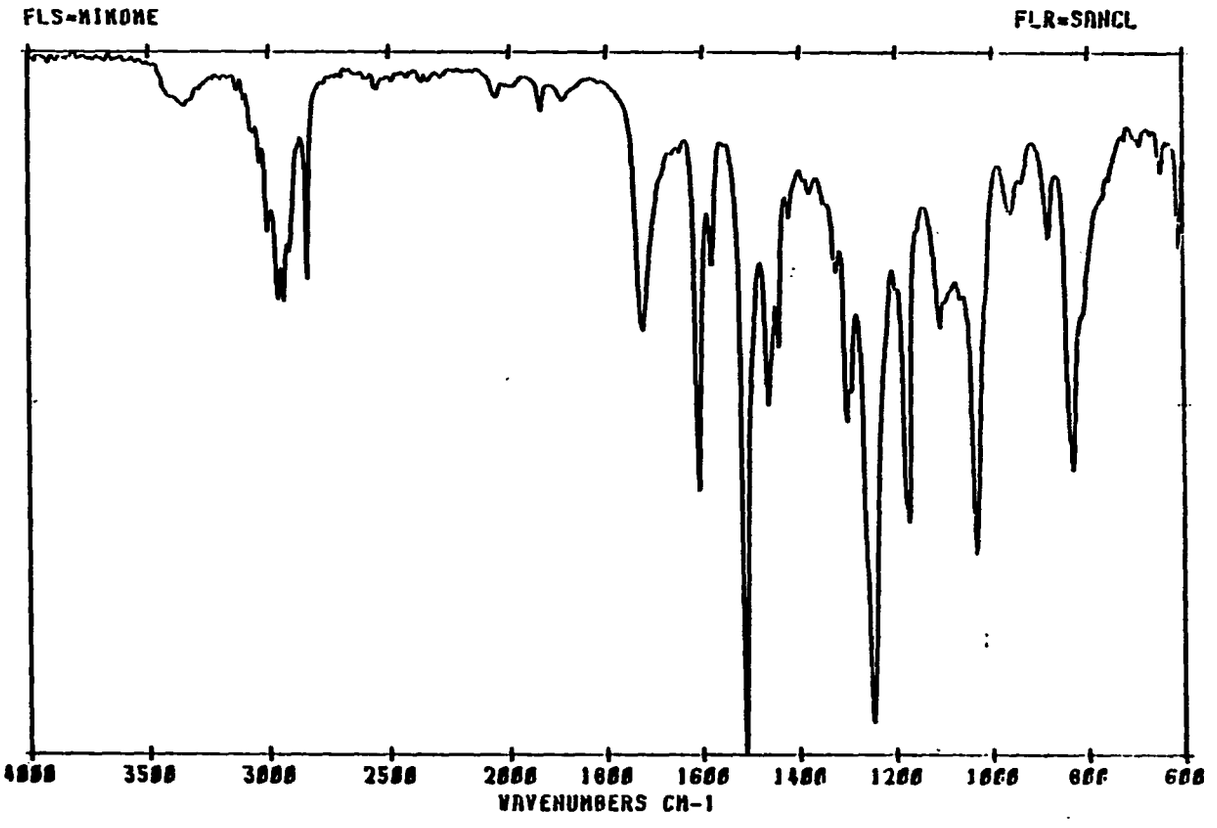

Figure 126. Ft-IR of 19c and 20c neat

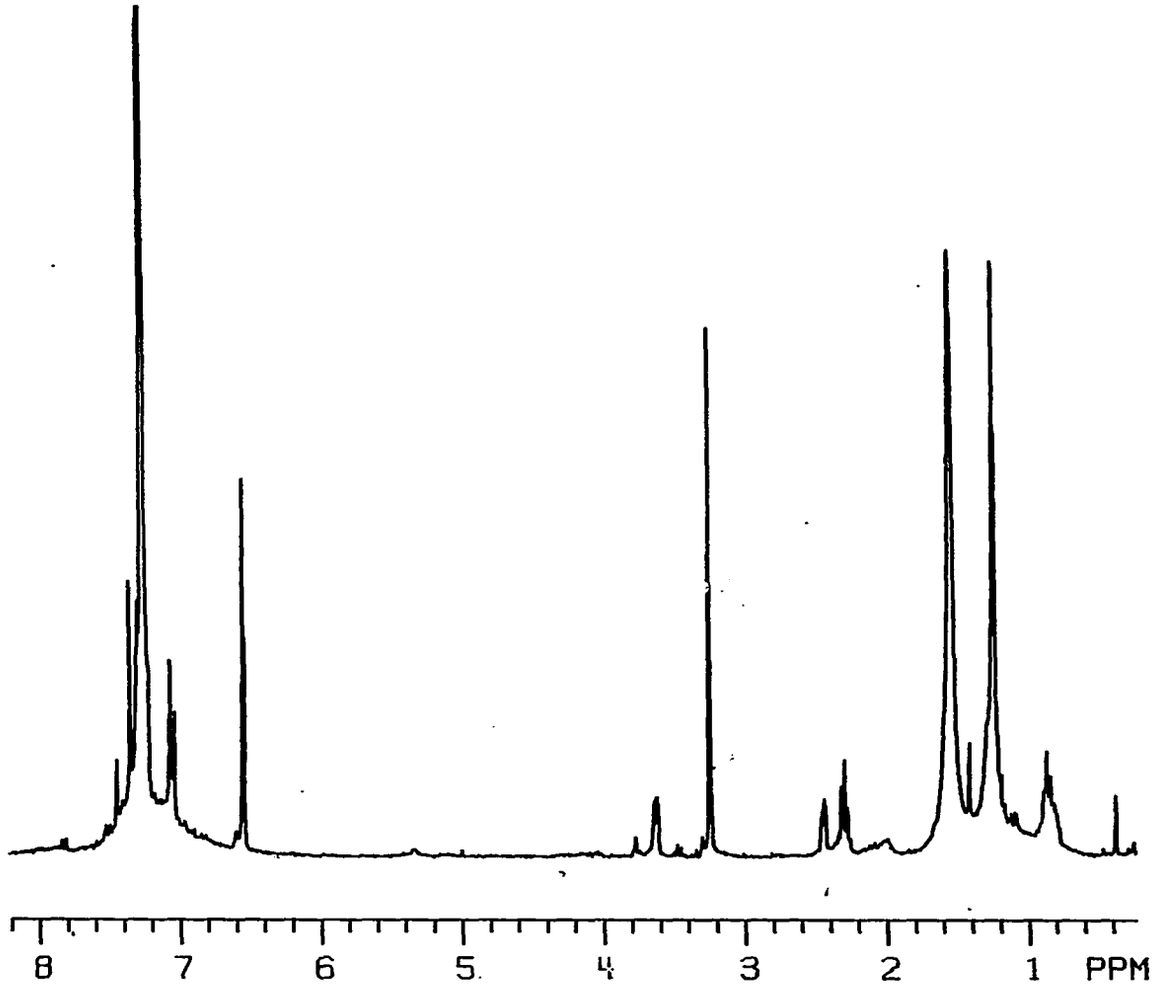

Figure 127. ^{1}H NMR of 19d and 20d in $CDCl_3$

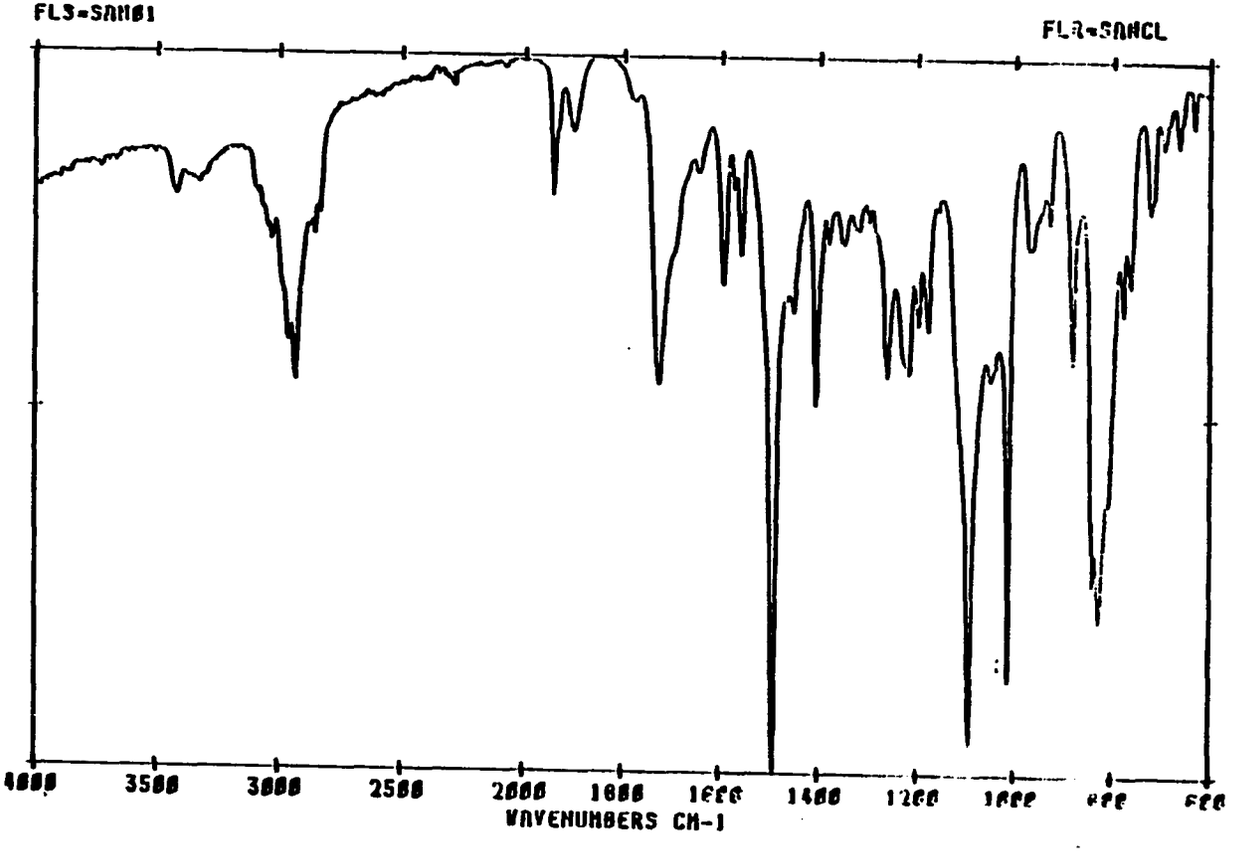

Figure 128. FT-IR of 19d and 20d neat

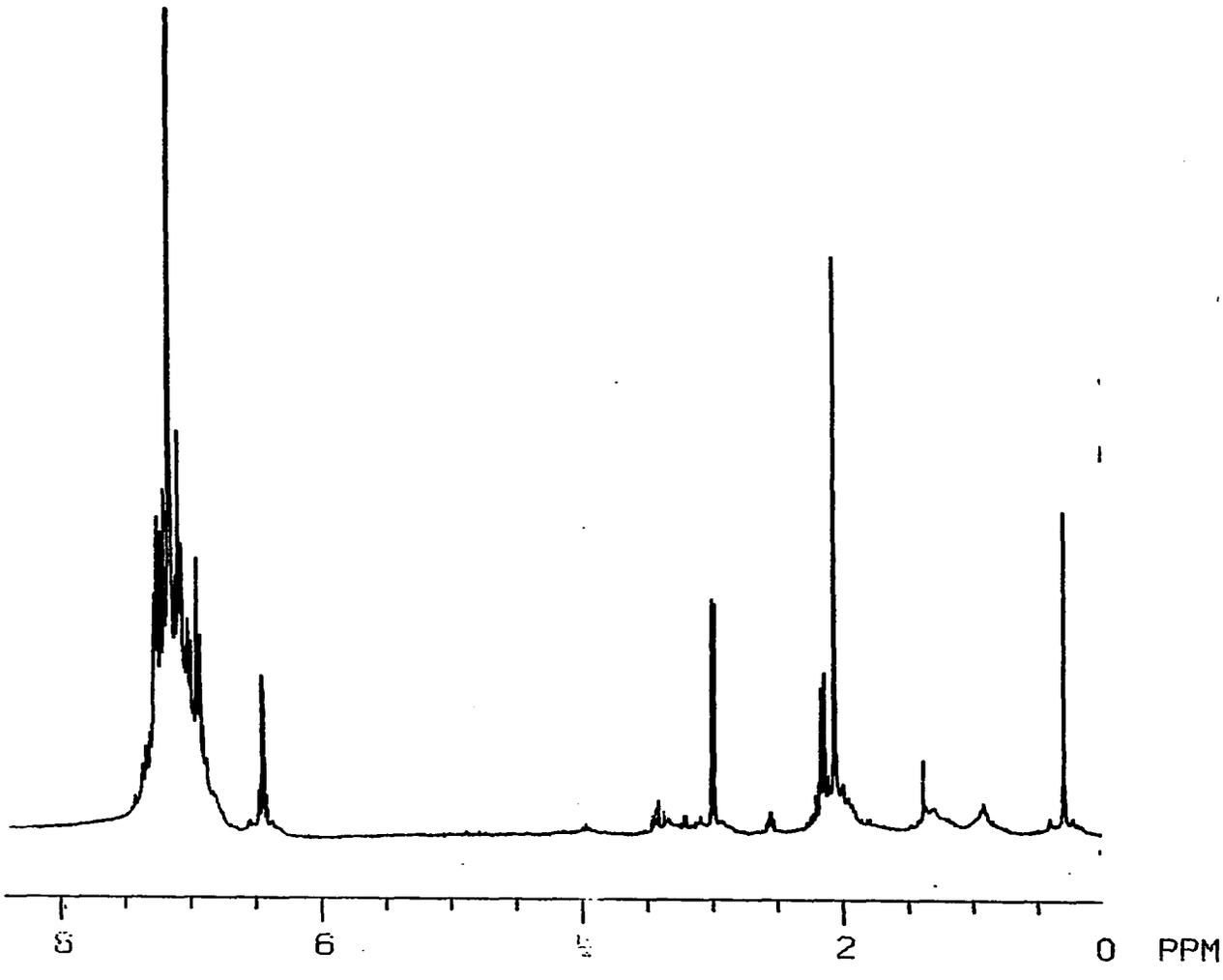

Figure 129. ^{1}H NMR of 19f and 20f in $CDCl_3$

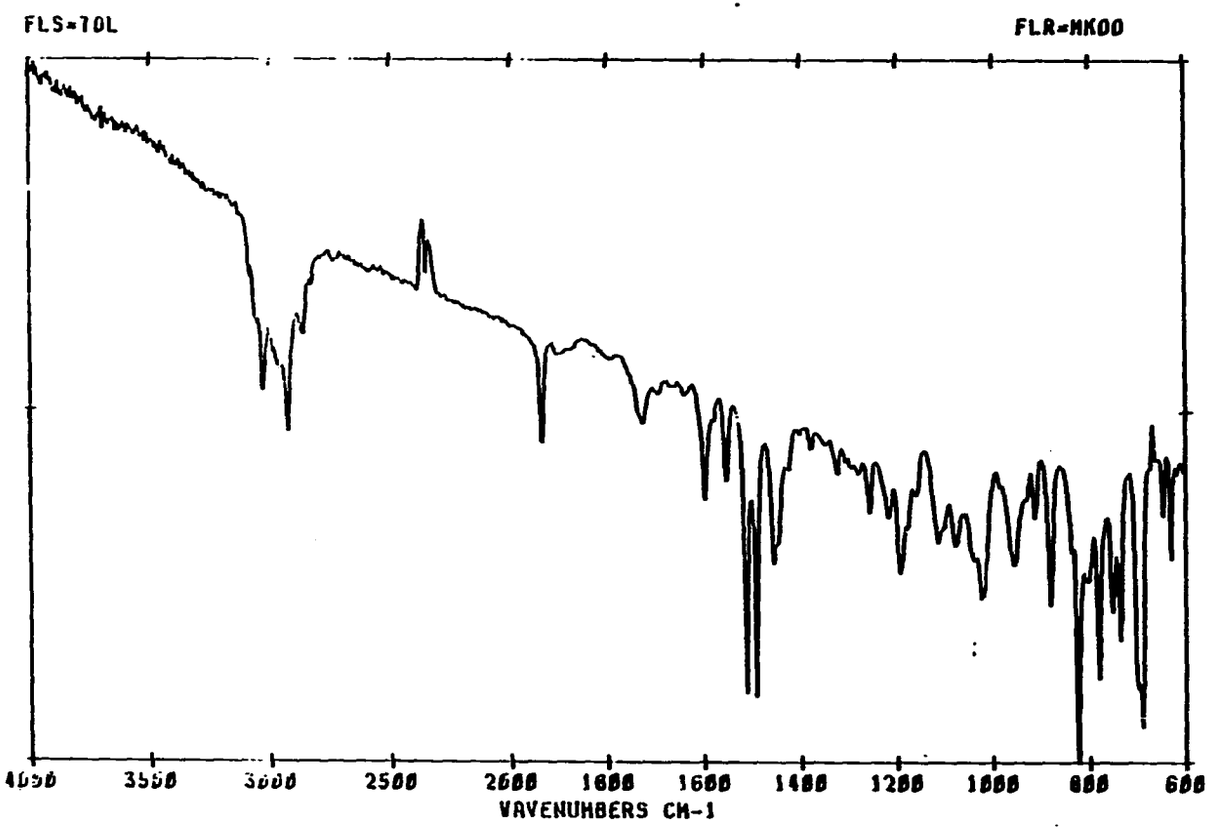

Figure 130. FT-IR of 19f and 20f neat

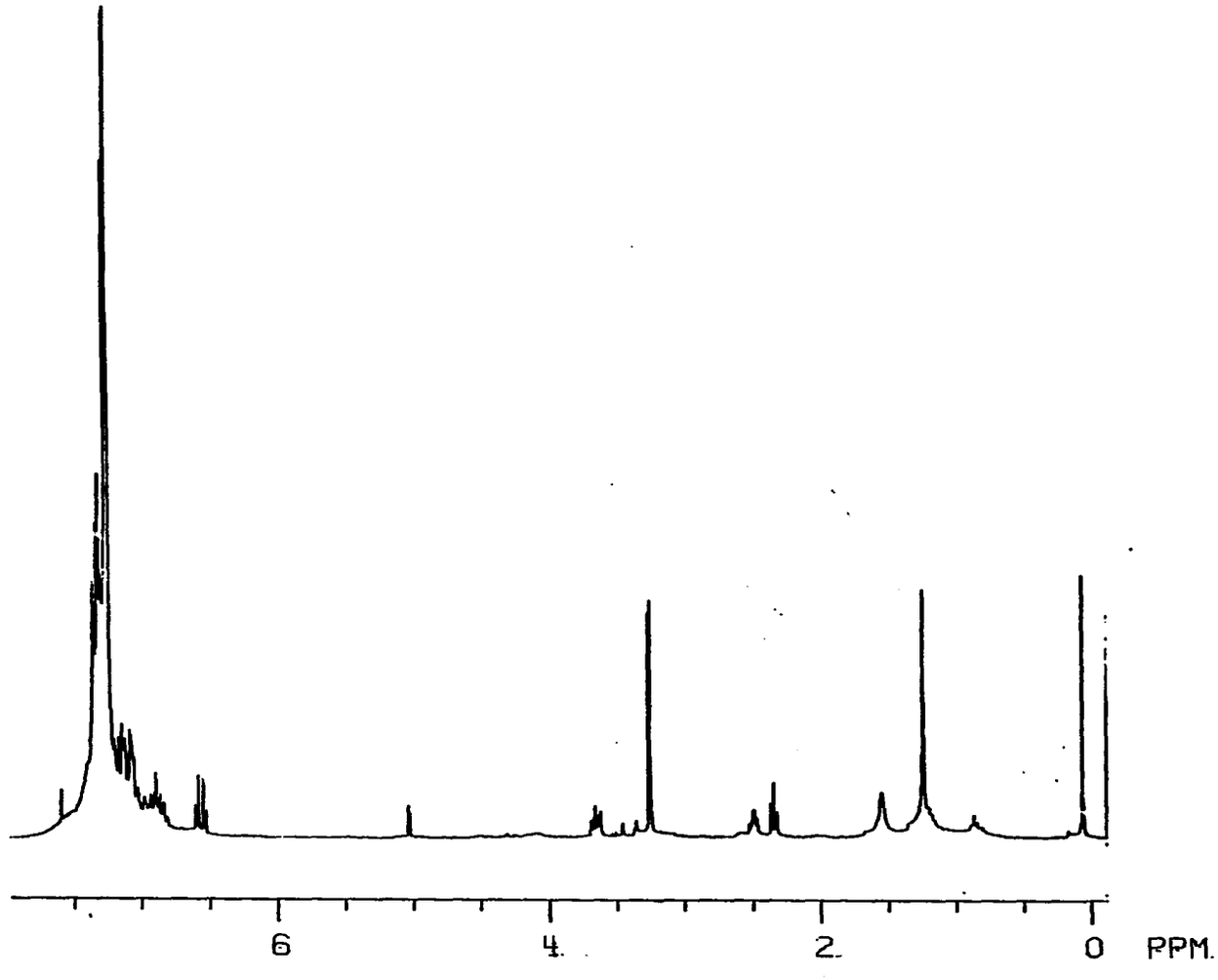

Figure 131. ^{1}H NMR of 19g and 20g in $CDCl_3$

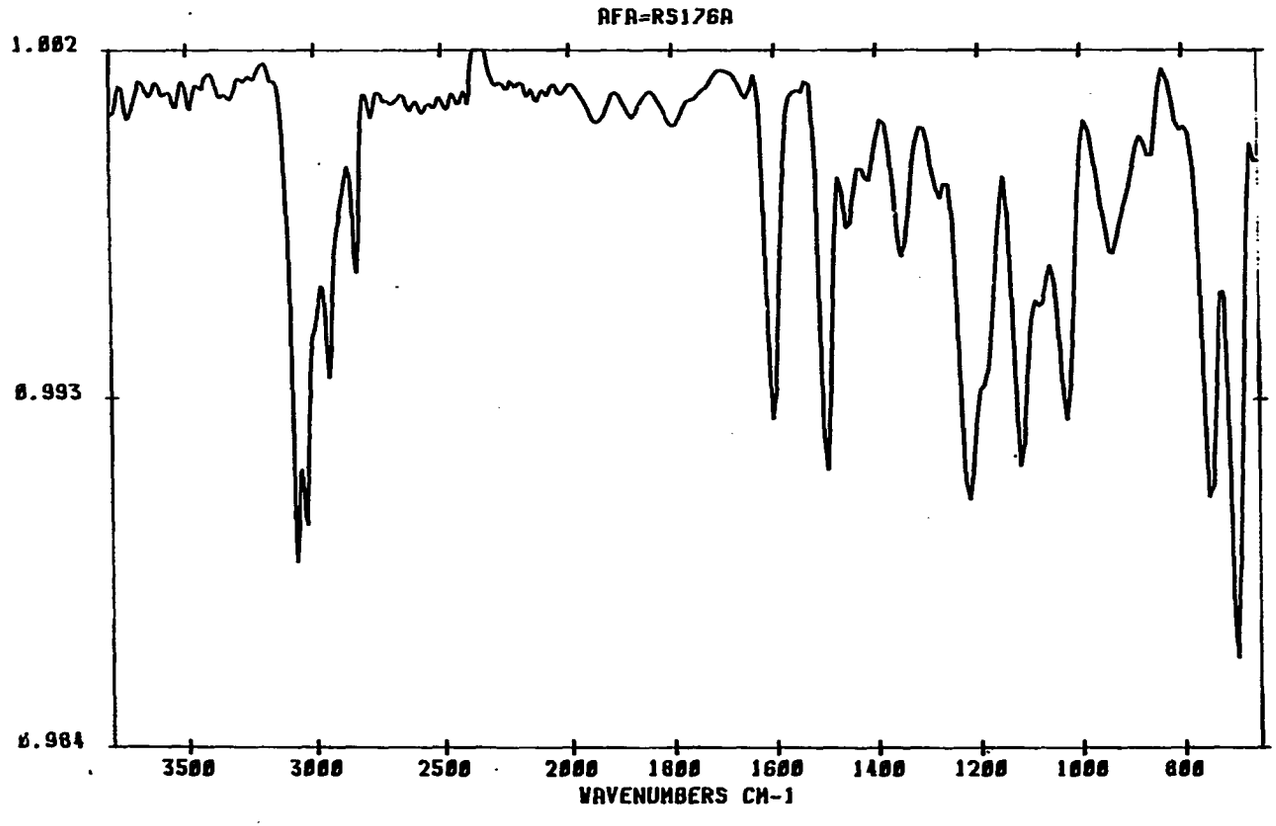

Figure 132. GC-FT-IR of 19g

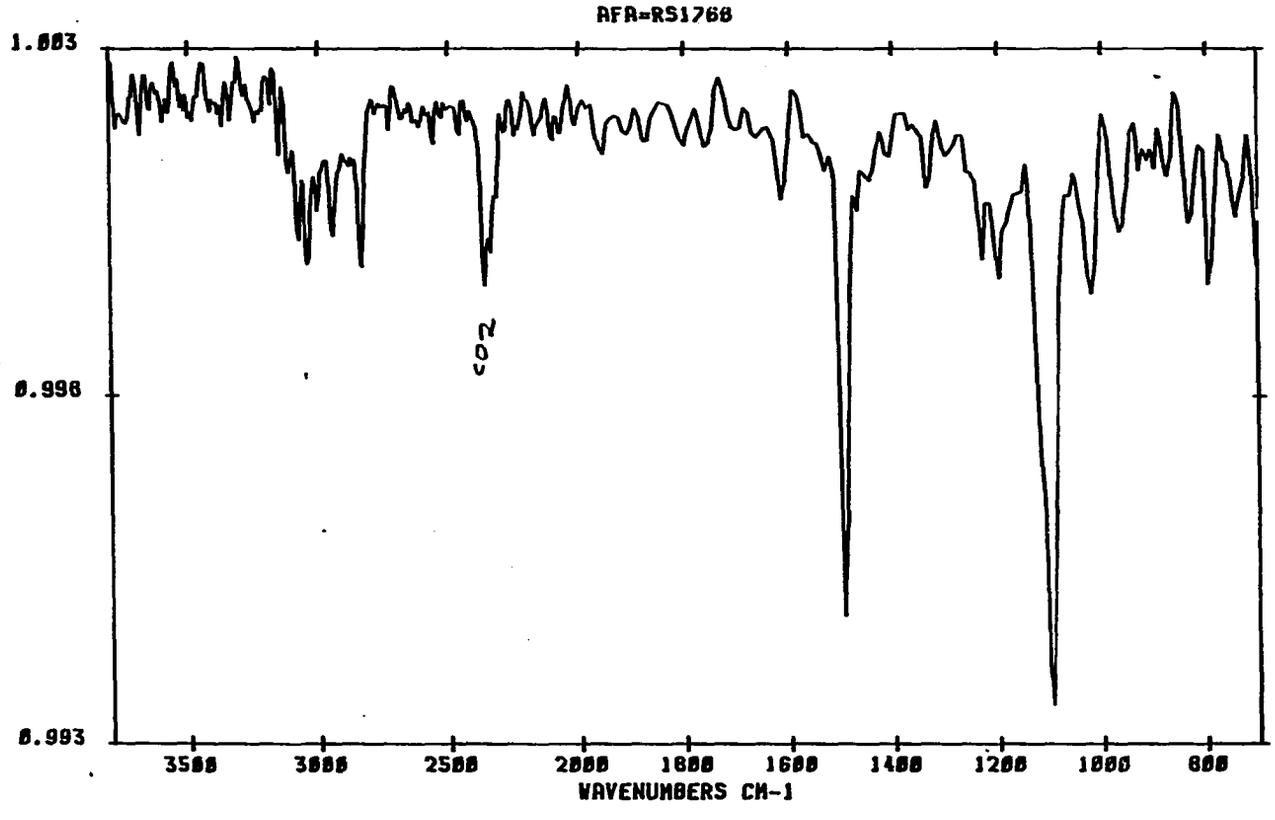

Figure 133. GC-FT-IR of 20g

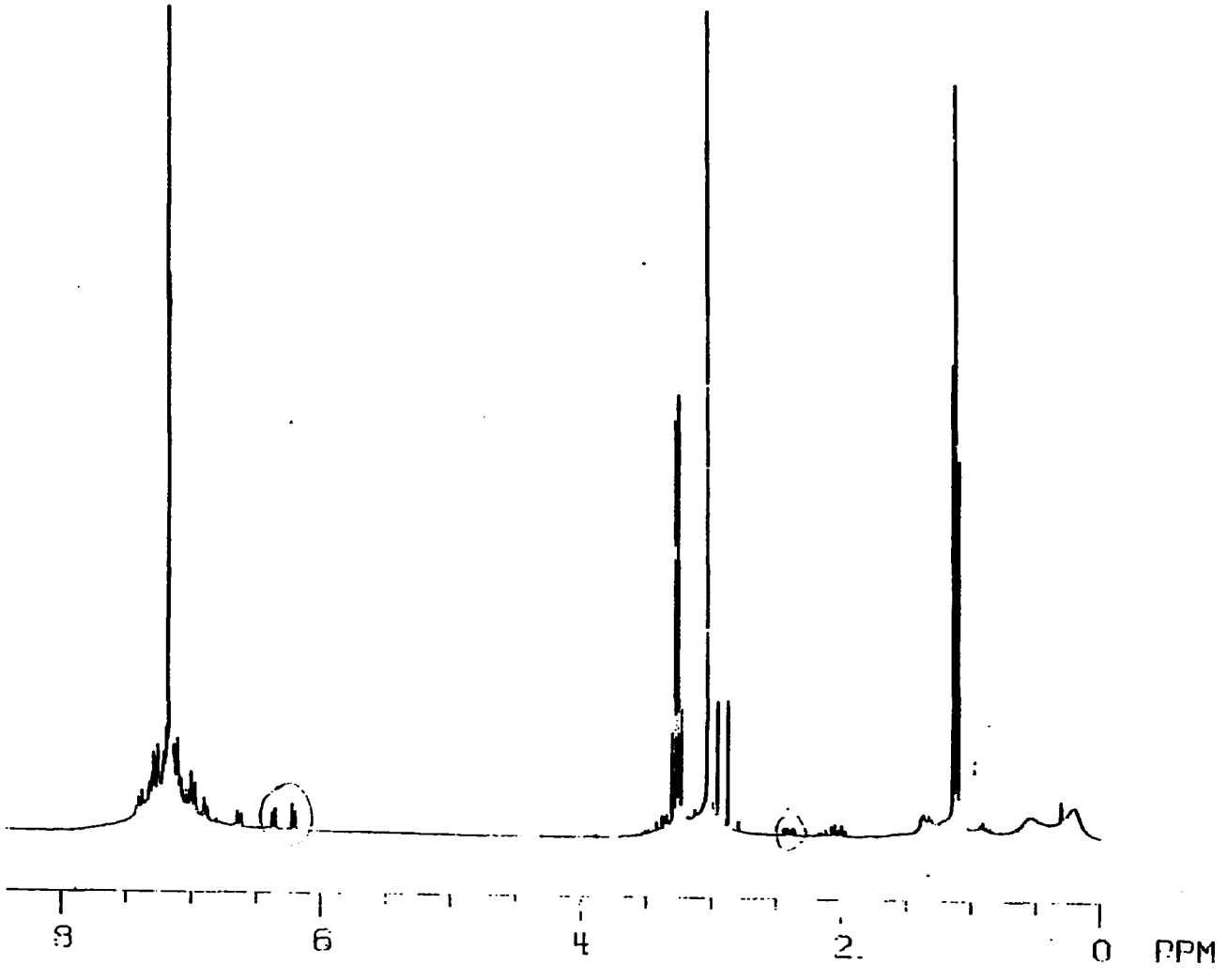

Figure 134. ^{1}H NMR of 19h and 20h in $CDCl_3$

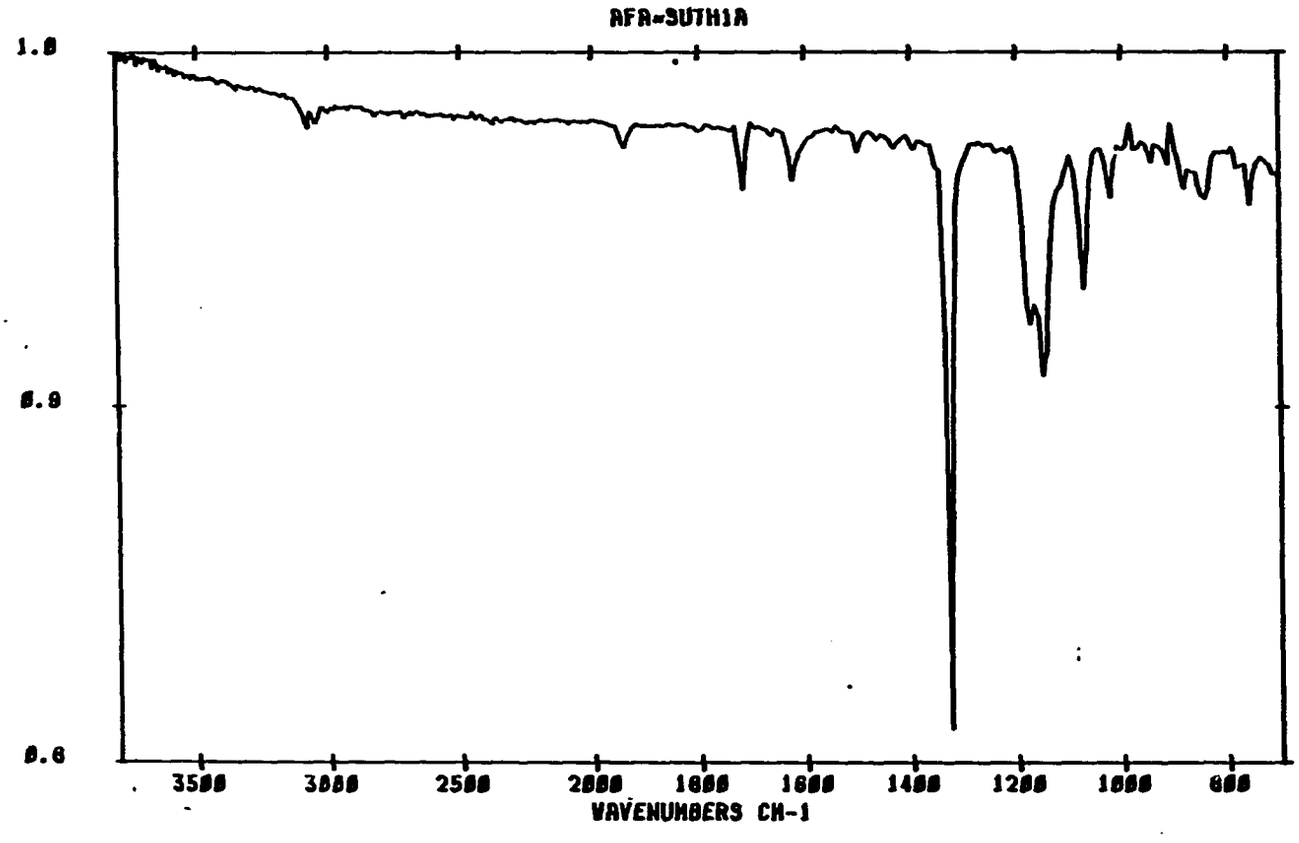

Figure 135. GC-FT-IR of 19h

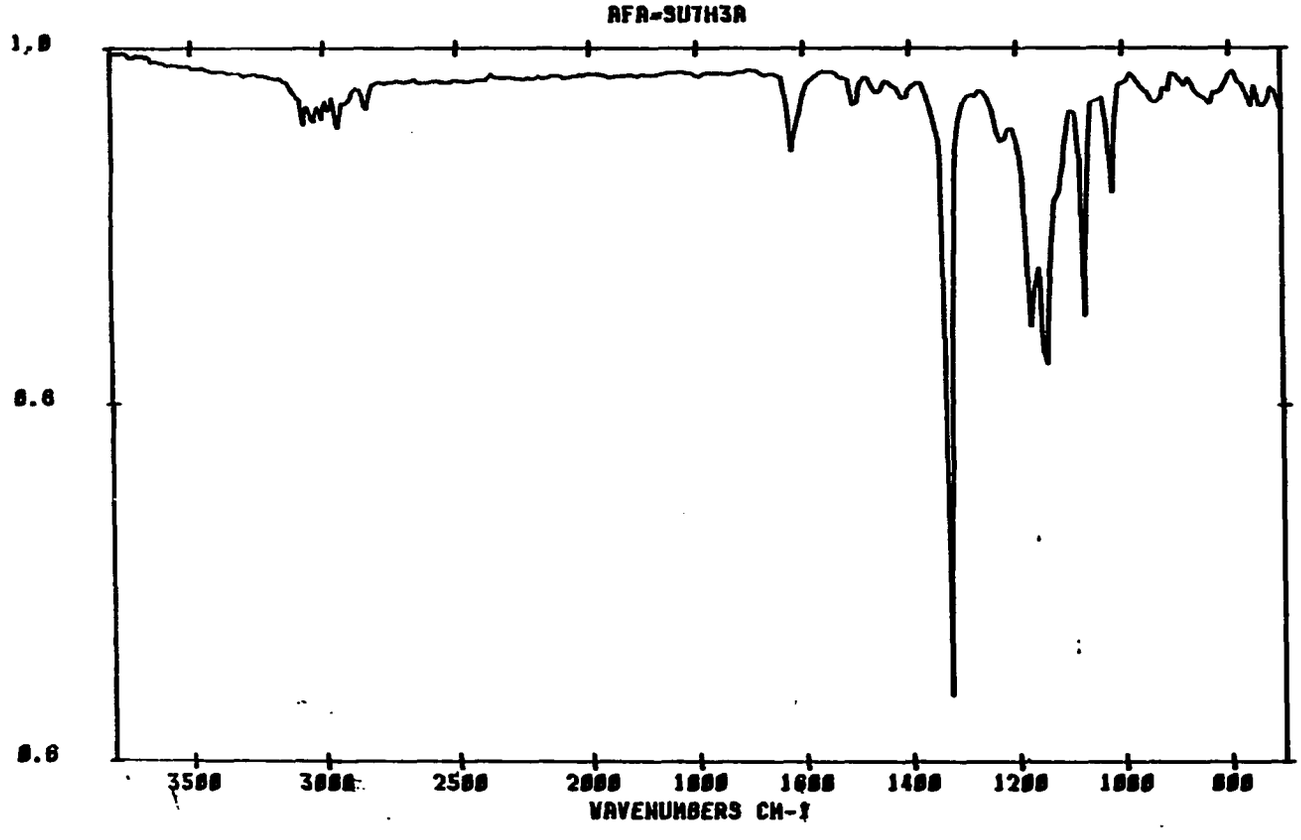

Figure 136. GC-FT-IR of 20h

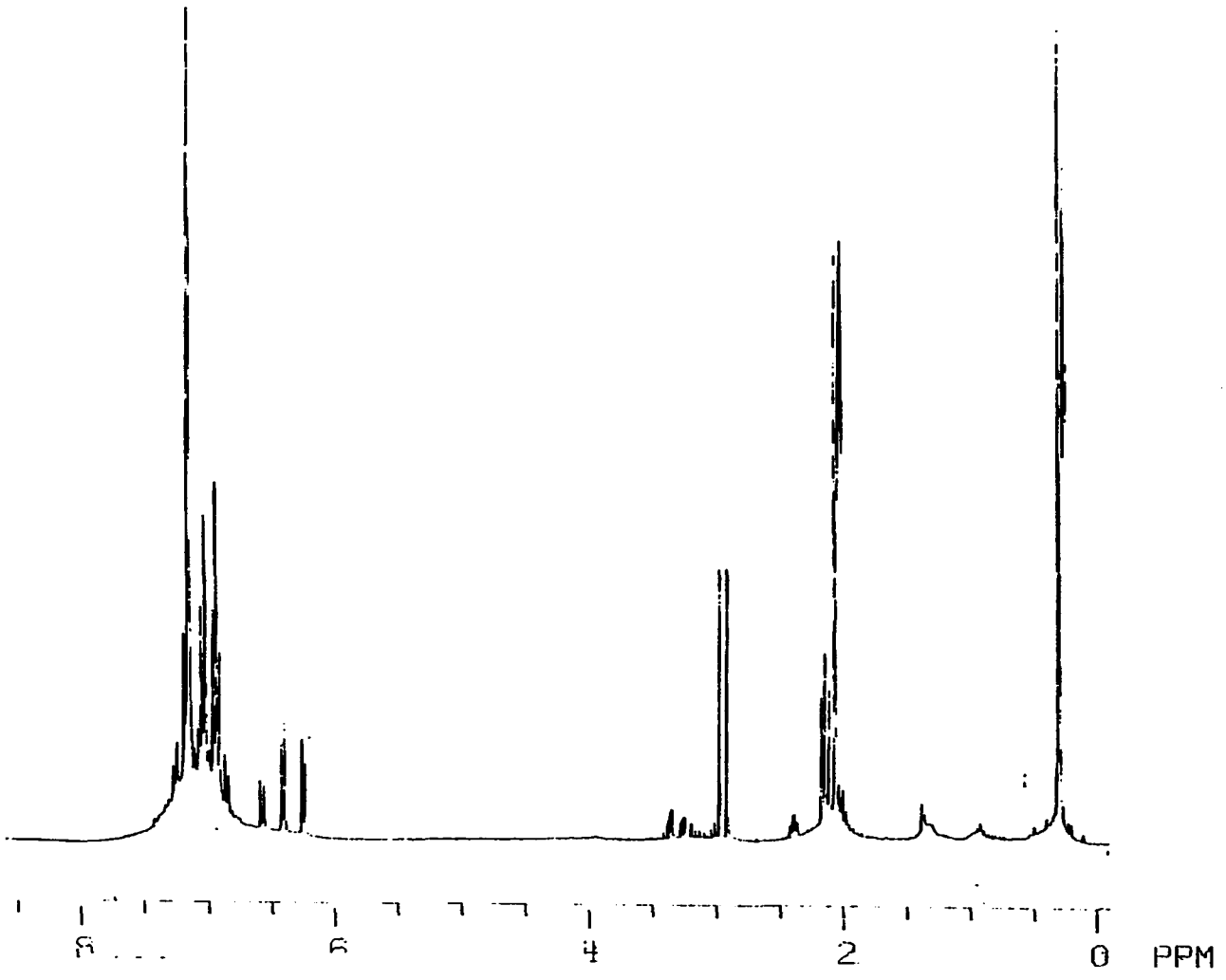

Figure 137. ^{1}H NMR of 19i and 20i

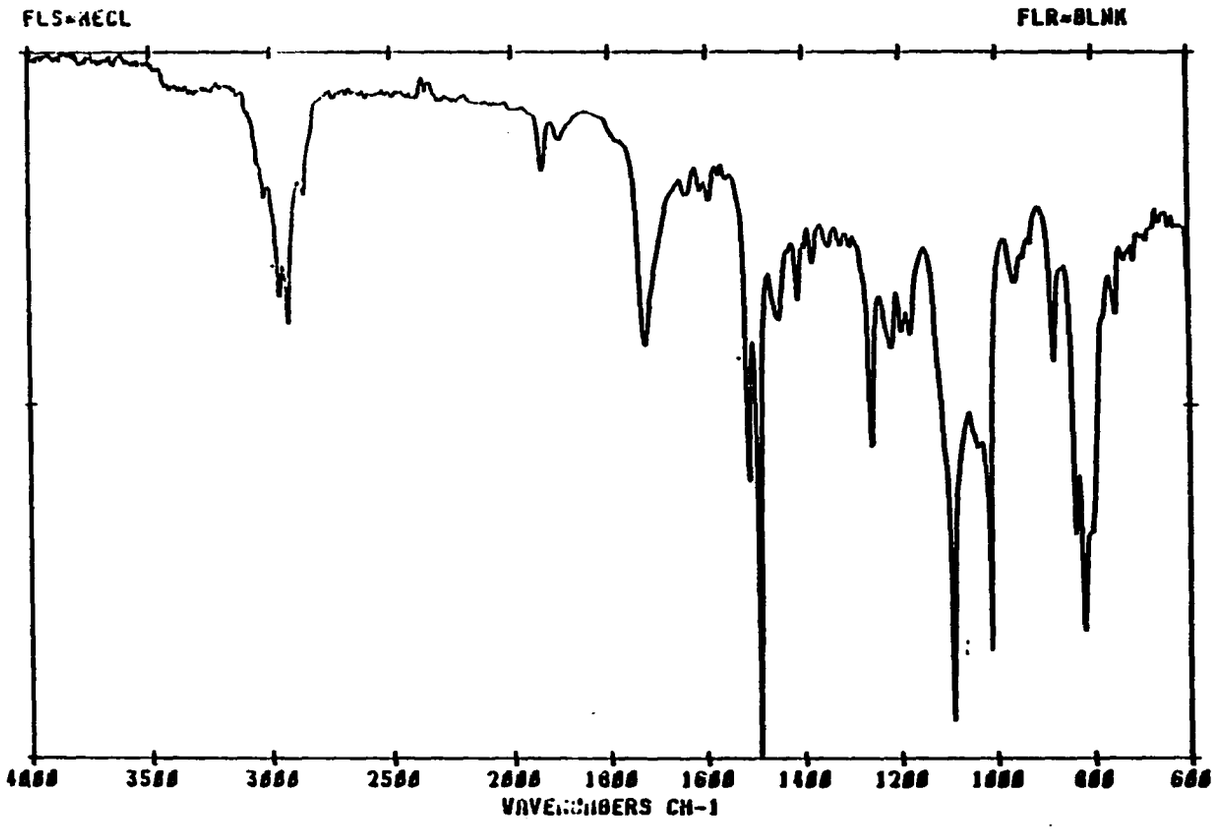

Figure 138. FT-IR of 19i and 20i neat

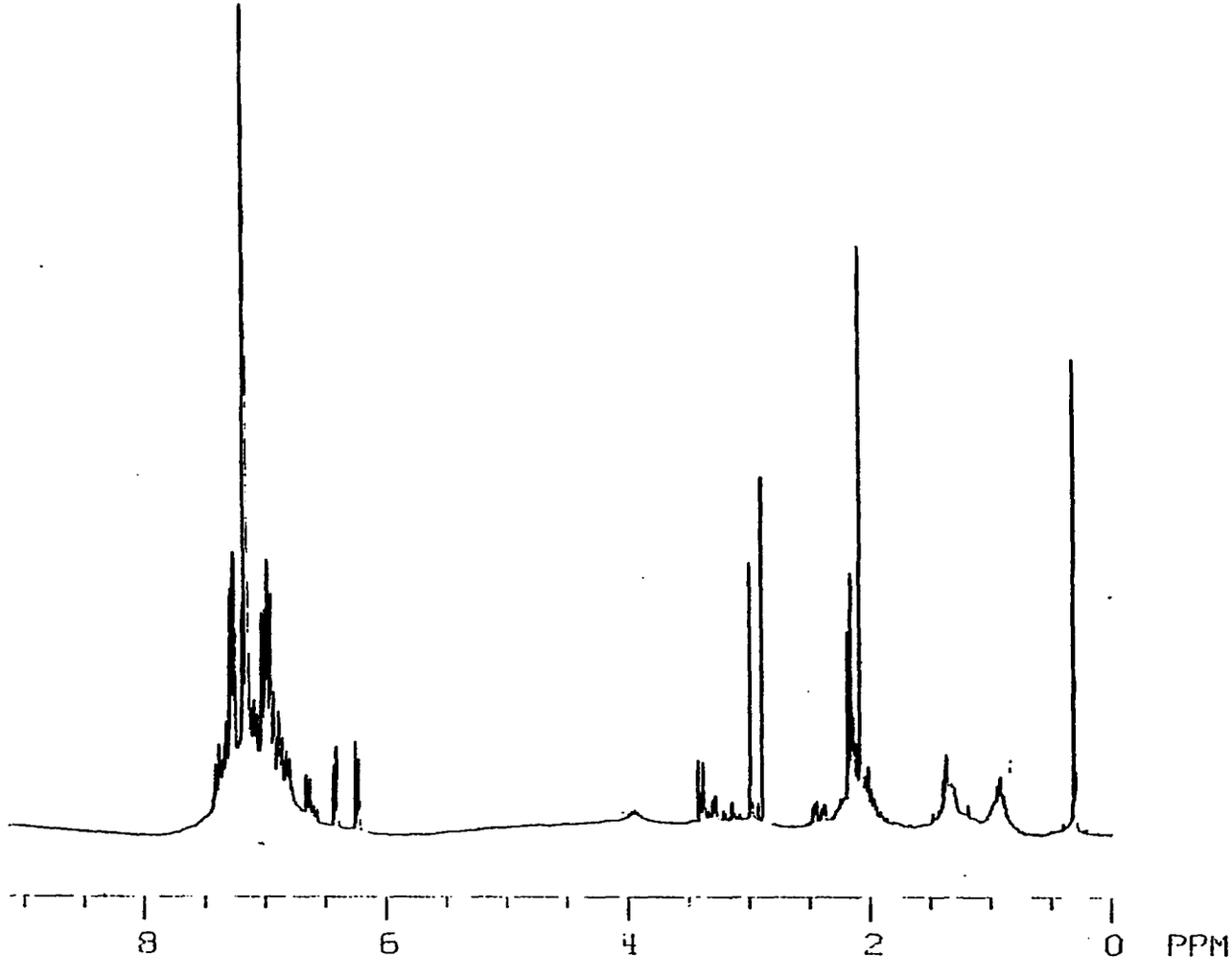

Figure 139. ^{1}H NMR of 19j and 20j in $CDCl_3$

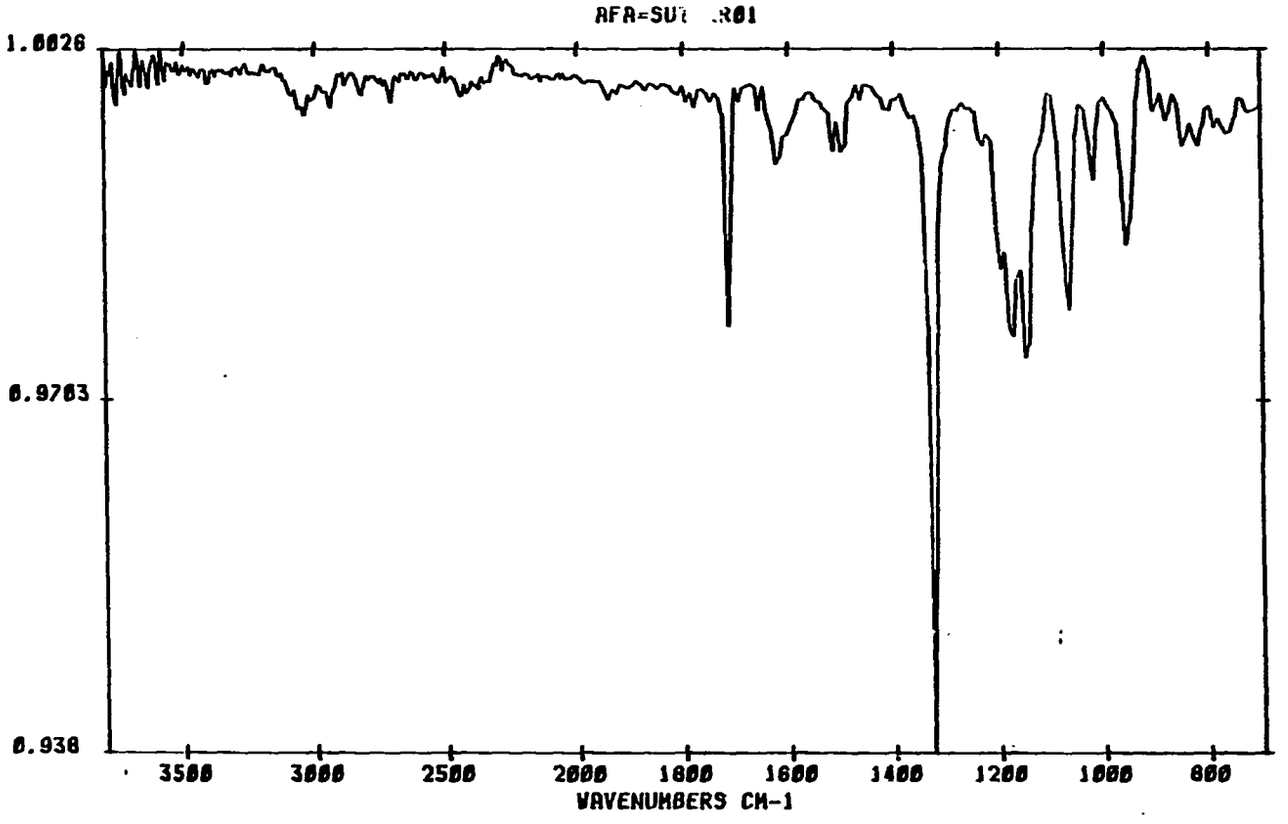

Figure 140. GC-FT-IR of 19j

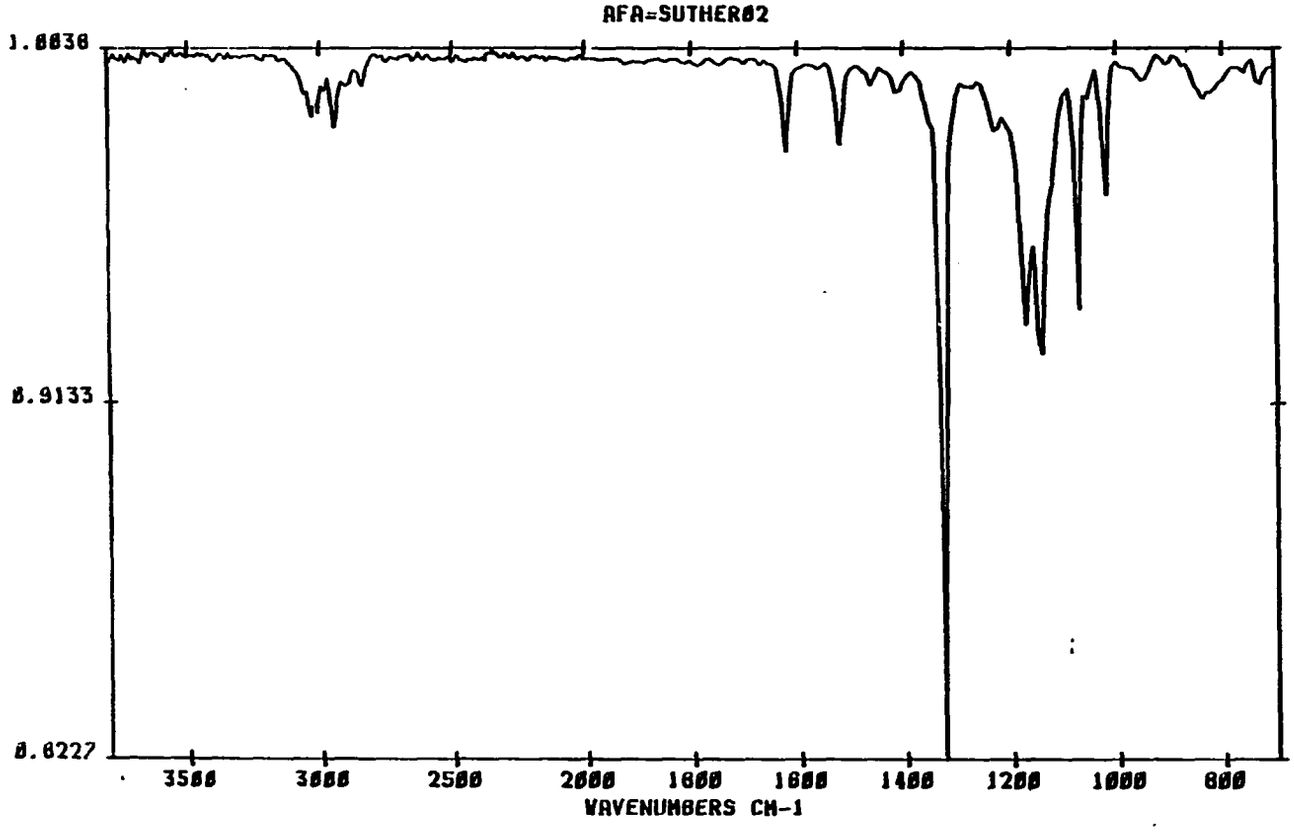

Figure 141. GC-FT-IR of 20j

REFERENCES

1. Doering, N. von E.; LaFlamme, P. M. Tetrahedron 1958, 75.

2. Kirmse, W. Carbene Chemistry, 2nd ed.; Academic Press: New York, 1971.

3. Jones, M., Jr. Carbenes; Wiley: New York, 1973.

4. Honjou, N.; Pacansky, J.; Yoshimine, M. J. Am. Chem. Soc. 1984, 106, 5361.

5. Doering, W. von E.; Hoffmann, A. K. J. Am. Chem. Soc. 1954, 76, 6162.

6. Skatteböl, L. Tetrahedron Lett. 1961, 167.

7. Skatteböl, L. Tetrahedron Lett. 1970, 2361.
Skatteböl, L. Acta Chem. Scand. 1963, 17, 1683.

8. Moore, W. R.; Hill, J. B. Tetrahedron Lett. 1970, 4343.
Moore, W. R.; Hill, J. B. Tetrahedron Lett. 1970, 4553.

9. Jones, W. M.; Grasley, M. H.; Brey, W. S. J. Am. Chem. Soc. 1963, 85, 2754.

10. Walborsky, H. M.; Hornyak, F. M. J. Am. Chem. Soc. 1955, 77, 6026.

11. Jones, W. M.; Wilson, J. W.; Tutwiler, F. B. J. Am. Chem. Soc. 1963, 85, 3309.

12. D'yakonov, L. A.; Komenclantov, M. J.; Gui-siya, F.; Korichev, G. L. J. Gen. Chem. USSR 1962, 32, 917.

13. Jones, W. M.; Muck, D. L.; Tandy, J. K. J. Am. Chem. Soc. 1966, 88, 68.

14. Muck, D. L.; Jones, W. M. J. Am. Chem. Soc. 1966, 88, 74.

15. Jones, W. M.; Walbrick, J. M. J. Org. Chem. 1969, 34, 2217.

16. Jones, W. M.; Krause, D. L. J. Am. Chem. Soc. 1971, 93, 551.

17. Miller, R. J.; Shechter, H. J. Am. Chem. Soc. 1978, 100, 7920.

18. Woodward, R. B.; Hoffmann, R. J. Am. Chem. Soc. 1965, 87, 395.

19. Magrane, J. K.; Cottle, D. L. J. Am. Chem. Soc. 1942, 64, 484.

20. Roberts, J. D.; Chambers, V. C. J. Am. Chem. Soc. 1951, 73, 5034.

21. DePuy, C. H.; Dappen, G. M.; Eilers, K. L.; Klein, R. A. J. Org. Chem. 1964, 29, 2813.

22. Kirmse, W.; Schütte, H. J. Am. Chem. Soc. 1967, 89, 1284.

23. Casas, F.; Kerr, J. A.; Trotman-Dickenson, A. F. J. Chem. Soc. 1964, 3655.

24. Hausser, J. W.; Pinkowski, N. J. J. Am. Chem. Soc. 1967, 89, 6981.

25. Parham, W. E.; Yong, K. S. J. Org. Chem. 1968, 33, 3947.

26. Hoffman, R.; Woodward, R. B. Accounts of Chemical Research 1968, 1, 17.

27. Honjou, N.; Pacansky, J.; Yoshimine, M. J. Am. Chem. Soc. 1984, 106, 5361.

28. Pasto, D. J.; Haley, M.; Chipman, D. M. J. Am. Chem. Soc. 1978, 100, 5272.

29. Baird, N. C.; Taylor, K. F. J. Am. Chem. Soc. 1978, 100, 1333.

30. Honjou, N.; Pacansky, J.; Yoshimine, M. J. Am. Chem. Soc. 1985, 107, 5332.

31. Dillon, P. W.; Underwood, G. R. J. Am. Chem. Soc. 1977, 99, 2435.

32. Bordon, W. T. Tetrahedron Lett. 1967, 447.

33. Dewar, M. J. S.; Haselbach, E.; Shanshal, M. J. Am. Chem. Soc. 1970, 92, 350.

34. Clark, D. T.; Smale, G. Tetrahedron 1969, 13.

35. Rauk, A.; Bouma, W. J.; Radom, L. J. Am. Chem. Soc. 1985, 107, 3780.

36. Ruedenberg, K.; Elbert, S. T.; Xantheas, S.; Valtazanos, P. Chemistry Department, Iowa State University of Science and Technology, unpublished results, 1988.

37. Ruedenberg, K.; Sunberg, K. R.; Quantum Science; Plenum Press: New York, 1976, p. 505.

38. Dunning, T. H.; Hay, P. J.; In Methods of Electronic Structure Theory, edited by Schaefer, H. F.; Plenum Press: New York, 1977, p 1.

39. Feller, D. F.; Ruedenberg, K. Theor. Chim. Acta 1979, 52, 231.

40. Griller, D.; Nazran, A. S.; Scaiano, J. C. J. Am. Chem. Soc. 1984, 106, 198.

41. Walbrick, J. M.; Wilson, J. W.; Jones, W. M. J. Am. Chem. Soc. 1968, 90, 2895.

42. Ninomiya, K.; Shioiri, T.; Yamada, S. Tetrahedron 1974, 30, 2151.

43. Griller, D.; Liu, M. T. H.; Scaiano, J. C. J. Am. Chem. Soc. 1982, 104, 5549.

44. Chu, I.-S. Ph.D. Dissertation, Iowa State University, 1986.

45. Shorter, J. Correlation Analysis in Organic Chemistry; Claredon Press, Oxford University Press, 1973, p. 14, p. 64.

46. Christian, S. D.; Tucker, E. E. Am. Lab. 1982, 14, 36.

47. Drefahl, G.; Plotner, G. Chem. Ber. 1958, 91, 1274.

48. Laarhoven, W. H.; Nivard, R. J. F.; Havinga, E. Recl. Trav. Chim. Pays-Bas. 1961, 80, 775.

49. Stanfield, J. A.; Reynolds, L. B. J. Am. Chem. Soc. 1952, 74, 2878.

50. Novotny, J.; Collins, C. H.; Starks, F. W. J. Pharm. Sci. 1967, 62, 910.

51. Tashchuk, K. G.; Dombrovoskii, A. V. J. Org. Chem. URSS 1965, 1, 2034.

52. House, H. O. J. Am. Chem. Soc. 1955, 77, 3070.

53. Wood, C. S.; Mallory, F. B. J. Org. Chem. 1964, 29, 3373.

54. Linn, W. J. Am. Chem. Soc. 1965, 87, 3665.

ACKNOWLEDGMENTS

I would like to express my sincere gratitude to Professor Philip M. Warner, without whose patience, encouragement and guidance this thesis would not have been possible.

I am grateful to the members of the research group for providing many insightful exchanges as well as unforgettable friendships. I would also like to thank Professor James H. Espenson for assisting with the analysis of kinetic data.

Special thanks are due my parents and in-laws for their love and support. I am deeply indebted to my wife, Sandra, for her love and understanding. My children, Megan and Michael, born during the course of this work, have been a source of much pleasure, and have provided a welcome diversion from my graduate studies.